

---

# **Energy Landscape Investigations of Chemical Matter and Structure Prediction of Binary Inorganic Solids**

Von der Fakultät Chemie der Universität Stuttgart  
zur Erlangung der Würde eines  
Doktors der Naturwissenschaften (Dr. rer. nat.)  
genehmigte Abhandlung

Vorgelegt von

**Dejan Zagorac**

aus Sisak, Kroatien

Hauptberichter:	<b>Prof. Dr. Martin Jansen</b>
Mitberichter:	<b>Priv. Doz. Dr. Klaus Doll</b>
Prüfungsvorsitzender:	<b>Prof. Dr. Thomas Schleid</b>

Tag der mündlichen Prüfung: 23.07.2012

Max-Planck-Institut für Festkörperforschung, Stuttgart  
Universität Stuttgart  
**2012**



"To my little princess, prince and queen of my heart, to my father, who faithfully watched on me from the kingdom of heaven, to my family, friends and colleagues from the far kingdoms of Earth, who kept me standing in the times without hope, and the most important, to the Lord, whose kingdom, goodness and grace is forever."

---

# Preface

*"Even the book can be bad when it is written superficially ... once the books were sacred, paper was small and rare, so only the important things were written down on paper..."*

(Father Justin Tasić (1936-2005), Serbian orthodox monk)

*"A new scientific truth does not triumph by convincing opponents and making them see the light, but rather because its opponents eventually die, and a new generation grows up that is familiar with it."*

(Max Planck (1858-1947), German physicist)

*"If I have seen further than others, it is by standing upon the shoulders of giants."*

(Isaac Newton (1642-1727), English mathematician and physicist)

*"Any intelligent fool can make things bigger and more complex... It takes a touch of genius - and a lot of courage to move in the opposite direction."*

(Albert Einstein (1879-1955), German-born theoretical physicist)

*"First they ignore you, then they laugh at you, then they fight you, then you win."*

(Mahatma Gandhi (1869-1948), Indian leader and peacemaker)

*"The scientists of today think deeply instead of clearly. One must be sane to think clearly, but one can think deeply and be quite insane."*

(Nikola Tesla (1856-1943), Serbian-Croatian inventor and engineer)

*"Ask, and you will receive. Search, and you will find. Knock, and the door will be opened to you."* (Matthew 7:7, Common English Bible (CEB))

---

# Acknowledgements

This thesis would not be possible without the support from many people. Therefore, I would like to thank first the three most important people without whom I would not exist in the scientific world and without whom this thesis would never have existed. The first is **Prof. Dr. Dr. h.c. Martin Jansen**, who gave me the opportunity to join his team, provided me with the necessary financial support and in numerous situations helped me with scientific and non-scientific problems. Next, I would like to express my greatest thanks to my mentor **Prof. Dr. J. Christian Schön**, for the intensive support, patience, enthusiasm and constant readiness for discussion. I certainly learned a lot from him and just can hope that he stays as he is - truly the best supervisor one can have. Finally, I sincerely appreciate the help and support provided by **PD. Dr. Klaus Doll**, who had enough patience to teach me quantum mechanics, *ab initio* methods, and many other aspects of theoretical chemistry from scratch. His comments and ideas were of vital importance in several of our projects and in finalizing the thesis. Although, all of these people have different attitudes towards science and unique personalities, I can say that these are some of the best people I have met, with profound scientific knowledge which they know how to pass on, and that I was really lucky to collaborate with them. In addition, I would also like to thank **PD. Dr. Klaus Doll** and **Prof. Dr. Thomas Schleid** for being co-examiners and agreeing to take on the responsibility of the final doctoral examination.

The members of the Jansen group have greatly contributed to my personal and professional time at MPI, since the group has been a source of friendships and collaboration and in this way I would especially like to thank to: **Dr. U. Wedig**, **Dr. P. Dasari**, **Dr. Z. Čančarević**, **Dr. N. Toto**, **Dr. I. Pentin**, **J. Zagorac**, **M. Sultania**, **A. Kulkarni** and **S. Neelamraju** from our theoretical group, and **Prof. Dr. R. Dinnebier**, **Dr. D. Fischer**, **Dr. J. Nuss**, **Dr. T. Bräuniger**, **Dr. K. Amsharov**,

---

**Dr. D. Shopova-Gospodinova, Dr. N. Kozhemyakina, Dr. V. Todorova, Dr. H. and Dr. G. Čakmak, J. Curda, K. Đuriš, T. Runčevski, V. Saltykov, and M. Kabdulov**, from our experimental department.

Similarly, I have found the environment outside my group as very friendly and supportive, including various departments of the Max-Planck Institute for Solid State research and the neighboring Max-Planck Institute for Intelligent Systems, and therefore I would especially like to acknowledge several people who were important during my research here: **Dr. J. Köhler, Dr. G. Bester, Dr. L. Vilčiauskas, Dr. Ž. Burghard, Dr. V. Damljanović, Dr. C. Husemann, Dr. P.Y. Prodhomme, Dr. J. Bauer, M. Fonović and A. Eberlein**. Needless to say that the MPI service group helped me in many ways during my research, and therefore, I would like to especially acknowledge the computer service group (FKF-EDV) and **A. Schuhmacher** and **K. Rössman**, the supply service and **S. Maksić**, and the graphical service and **R. Noack**.

I should not forget collaborations coming from outside MPI. Therefore, I would like to thank **A. A. Rempel** (Institute of Solid State Chemistry, Yekaterinburg, Russia) for valuable discussions about the lead sulfide system, and of course, **K. Friese** (Universidad del Pais Vasco, Bilbao, Spain) for providing measurement data of a possible intermediary monoclinic phase of PbS. When going away from MPI in order to present and discuss results, I have found various lectures, conferences and workshops of great importance for my scientific carrier and which were supported by my supervisors. In that respect, I would like to express my gratitude especially to the organizers of the Energy Landscape workshops in Chemnitz (Germany) in 2010 and in Telluride (USA) in 2011, as well as the CSSC-11 conference in Belgrade (Serbia) in 2011, and separately to several people: **Prof. Dr. P. Salamon** (San Diego State University, USA), **Prof. Dr. S. Bošković** (INN Vinča, Belgrade, Serbia), **Prof. Dr. P. Sibani** (University of Southern Denmark, Odense, Denmark), **Prof. Dr. K.-H. Hoffmann** (TU Chemnitz, Germany), **Prof. Dr. B. Matović** (INN Vinča, Belgrade, Serbia), **Prof. Dr. D. Wales** (Cambridge, UK), **Prof. Dr. T. Komatsuzaki** (RIES, Hokkaido University, Japan), **Prof. Dr. A. Rečnik** (Jožef Stefan Institute, Ljubljana, Slovenia), **PD Dr. A. Möbius** (IFW Dresden, Germany), **Dr. S. Woodley** (University College London, UK), **Dr. M.-C. Marinica** (CEA, Paris, France), **Dr. J. Dieterich** (Georg-August-University, Göttingen, Germany) and **C. Heard** (University of Birmingham, UK).



---

My time at Stuttgart was made enjoyable in large part due to the many friends that became a part of my life. I will never forget the basketball divisions of MPI, Winnenden and TV89 Zuffenhausen and I would like to thank for the support of all of the people there, especially **D. Boljanić, I. Bešlić, M. Tovirac, J. Piening, K. Minier, H. Neuffer, C. Goold, C. Ferguson, A. Smailović, M. Buchholz**, and many others from my coaching and playing days.

There is an old saying that the best is saved for the end. Of course, my work would not be possible without the strong support of my family. My wife **Jelena**, was always there in science or non-science matters, and my children **Jasna** and **Simon** were a fountain of youth, joy and inspiration in every day. My sister **Emina**, mother **Vasvija**, and stepfather **Esad** gave me support at each stage of my journey and I will always be grateful. Furthermore, I would like to thank the families that were separated from me by a distance barrier, but kept me warm, as if we were physically close. First of all I like to thank to my aunt **Bojana Zagorac**, without whose support most likely I would not be here, and then to families **Koprivca, Đakov, Milovanović, Mirjanić, Rakas, Savić, Jadžić, Đurašinov**, and, of course, **Dukić** and **Zagorac**. Usually at the very end, one remembers his beginnings and the important people on the road that brought me here. In this respect I would like to especially thank to my high school professors **Biljana Jereminov** and **Milutin Marković** as well as my university professor **Dr. Radule Tošović**, who planted the seed of knowledge, and which has become a strong tree with the branches pointing out to many different fields of science. The most important person, who watered my seed with knowledge and love all the time during my growth, is my father **Branislav**, who is not anymore with us, but continues to live through the strong roots that he gave me.

I gratefully acknowledge the funding from the Max-Planck Society which made my Ph.D. work possible. Finally, I would like to thank everybody who was important to the successful realization of thesis, as well as expressing my apology that I could not mention personally one by one.

Thank you,  
Dejan Zagorac

---

# Abstract

Recent developments in experimental solid state chemistry have offered us new possibilities in controlling synthesis routes, especially by varying the pressure and temperature. Similarly, the development of new theoretical methods and tools makes it worthwhile to reinvestigate apparently well-known systems. In this thesis several binary systems, in particular PbS and ZnO, have been investigated using several different theoretical methods.

Since lead sulfide is an important semiconductor, it is of great interest to identify possible (meta)stable modifications, both at standard and elevated pressures. To predict such structures, global optimizations on the energy landscape of PbS were performed for several pressures, using simulated annealing followed by local optimizations of the candidates found. In order to be able to take the effect of the non-bonding valence electrons of Pb into account, *ab initio* energies were employed for both the global and local optimization. Besides the experimentally known modifications (NaCl structure type at standard pressure and the CsCl structure type at high pressure), several additional promising structures, which might be accessible synthetically, were found; exhibiting e.g. the TII type (*Cmcm*), the FeB type (*Pnma*), and the  $\alpha$ -GeTe-type (*R3m*).  $E(V)$  curves and  $H(p)$  curves were calculated and analyzed, and further properties of the new modifications were investigated by performing band structure and phonon calculations.

In order to gain new insights in the ZnO system, we have performed global explorations of the energy landscape using simulated annealing with an empirical potential, both at standard and elevated pressure (up to 100 GPa). Besides the well-known structure types (wurtzite, sphalerite and rock-salt), many new interesting modifications were found in different regions of the energy landscape, e.g. the  $\check{5}\check{5}$  type, the GeP, the NiAs type, and the  $\beta$ -BeO type. Furthermore, we observed many distorted varia-

---

tions of these main types, in particular new structures built-up from various combinations of structure elements of these types, exhibiting a variety of stacking orders.

Furthermore, a search with the threshold algorithm for different numbers of formula units was performed. For each relevant structure type and number of formula units, the local energy landscape was analyzed. In addition to the threshold algorithm runs, we also performed prescribed path studies where we analyzed pairs of structures and the barriers separating them on the landscape as function of pressure and temperature. Additionally, we employed newly developed methods for the energy landscape representation. Energy landscapes are used to understand the behaviour of a chemical system, but problems exist with the visualization of high-dimensional spaces and the complexity of the structures. Therefore, finding low-dimensional representations of the energy landscape in order to analyze specific properties would be a significant step. Here, we present multidimensional representations of the energy landscapes of PbS and ZnO with various approximations.

Finally, in order to find a suitable  $AB$  compound for synthesis of the "5-5" structure type, we performed constrained explorations for binary compounds with elements from groups V, IV - VI, and III - VII. Among others, TlF, SnO, SnS, SnSe, GeS, GeSe, PbO, PbS, ZnO and ZnS, were chosen for the study. For all compounds a local optimization on *ab initio* level with LDA functional was performed for the 5-5 structure type and other experimentally known or promising structure types. Afterwards, the results were compared with earlier theoretical work involving the 5-5 structure type in the earth alkaline metal oxides and the alkali metal halides. We suggest the GeSe and the ZnO systems as the most suitable ones for synthesizing the 5-5 structure type. In both cases, the synthesis of this 5-fold coordinated structure might be possible in a small pressure range between the 6-fold coordinated NaCl and the 4-fold coordinated wurtzite structure type.

# Zusammenfassung

Neue Entwicklungen in der experimentellen Festkörperchemie bieten neue Möglichkeiten zur Kontrolle von Syntheserouten, vor allem durch Variation des Druck und Temperatur. Gleichermassen führt die Entwicklung neuer theoretischer Verfahren zu einer Neubetrachtung von scheinbar wohlbekanntem chemischen Systemen. In dieser Dissertation wurden mehrere binäre Systeme, insbesondere PbS und ZnO, unter Verwendung verschiedener theoretischer Methoden untersucht.

Da Bleisulfid ein wichtiger Halbleiter ist, wäre es von grossem Interesse, mögliche (meta)stabile Modifikationen sowohl unter Normalbedingungen als auch bei erhöhtem Druck zu identifizieren. Um solche Strukturen vorherzusagen, wurden für verschiedene Drücke globale Optimierungen mit Simulated Annealing auf der Energielandschaft von PbS durchgeführt, und die gefundenen Strukturkandidaten mithilfe von lokalen Optimierungen verfeinert. Um den Einfluss von nicht-bindenden Elektronenpaaren des Pb berücksichtigen zu können, wurden sowohl bei der globalen Suche als auch bei der lokalen Nachoptimierung *ab initio* Energien verwendet. Neben den experimentell bekannten Modifikationen (NaCl Strukturtyp bei Normaldruck und der CsCl Strukturtyp bei hohem Druck) wurden mehrere vielversprechende Strukturen gefunden, die synthetisch zugänglich sein könnten. Diese wiesen unter anderem den TII Typ ( $Cmcm$ ), den FeB Typ ( $Pnma$ ), und den  $\alpha$ -GeTe Typ ( $R3m$ ) auf. Die  $E(V)$  und  $H(p)$  Kurven wurden berechnet und analysiert, und weitere Eigenschaften der neuen Modifikationen wie die Bandstruktur und das Phononenspektrum wurden untersucht.

Um neue Einblicke in das ZnO System zu erhalten, wurden globale Untersuchungen der Energielandschaft sowohl bei Normaldruck als auch bei erhöhtem Druck durchgeführt, wobei Simulated Annealing mit einem empirischem Potential zur Energieberechnung verwendet wurde. Neben den wohlbekanntem Strukturtypen (Wurtzit, Sphalerit

---

und Kochsalz) wurden viele neue interessante Modifikationen in verschiedenen Bereichen der Energielandschaft gefunden, darunter der 5-5 Typ, der GeP und der NiAs Typ, and der  $\beta$ -BeO Typ. Des weiteren wurden viele verzerrte Varianten dieser Haupttypen beobachtet, insbesondere neue Strukturen, die durch verschiedene Kombinationen von Strukturelementen der Wurtzit- und Sphaleritstruktur generiert werden und eine Vielzahl von Stapelvarianten ergeben.

Weiterhin wurde eine Untersuchung mit dem Threshold Algorithmus für verschiedene Zahlen von Formeleinheiten durchgeführt. Für jeden relevanten Strukturtyp und Zahl der Formeleinheiten wurde die lokale Energielandschaft analysiert. Zusätzlich zu den Threshold Runs wurden Prescribed Path Untersuchungen durchgeführt, bei denen Paare von Strukturen und die sie trennenden Barrieren als Funktion von Druck und Temperatur studiert wurden. Hierbei wurden neu entwickelte Verfahren zur Darstellung von Energielandschaften eingesetzt. Energielandschaften werden dazu benutzt, um das Verhalten chemischer Systeme zu verstehen, aber es gibt Probleme mit der Visualisierung von hochdimensionalen Räumen und der Komplexität der Strukturen. Daher ist die Generierung von niedrigdimensionalen Darstellungen von Energielandschaften, welche die Analyse spezifischer Eigenschaften erlaubt, ein signifikanter Schritt. In dieser Dissertation werden multidimensionale Darstellungen der Energielandschaft von PbS und ZnO in verschiedenen Näherungen gezeigt.

Im letzten Teil der Dissertation wurden eingeschränkte spezifische Erkundungen für binäre Verbindungen aus Elementen der Gruppen V, IV-VI und III-VII durchgeführt, um passende AB-Verbindungen zu identifizieren die im 5-5 Strukturtyp synthetisiert werden könnten. Unter anderem wurden TlF, SnO, SnS, SnSe, GeS, GeSe, PbO, PbS, ZnO und ZnS für diese Untersuchung ausgewählt. Für alle diese Verbindungen wurden lokale Optimierungen des 5-5 Typs und anderer experimentell bekannter oder vielversprechender Strukturtypen auf *ab initio* Ebene mit dem LDA Funktional durchgeführt. GeSe und ZnO wurden als die Systeme identifiziert, die am besten für eine Synthese des 5-5 Typs geeignet erscheinen. In beiden Fällen könnte die Synthese dieser fünffach koordinierten Struktur in einem kleinen Druckbereich zwischen dem sechsfach koordinierten NaCl und dem vierfach koordinierten Wurtzit Typ möglich sein.

# Contents

<b>Preface</b>	<b>iii</b>
<b>Acknowledgements</b>	<b>v</b>
<b>Abstract</b>	<b>ix</b>
<b>Zusammenfassung</b>	<b>xi</b>
<b>List of Figures</b>	<b>xix</b>
<b>List of Tables</b>	<b>xxxix</b>
<b>Glossary</b>	<b>xxxiii</b>
<b>I Introduction</b>	<b>1</b>
<b>1 Introduction and Outline</b>	<b>3</b>
1.1 Introduction . . . . .	3
1.2 Outline . . . . .	7
<b>II Theoretical and computational background in solid state re- search</b>	<b>11</b>
<b>2 Energy landscape and structure prediction</b>	<b>13</b>
2.1 Energy Landscape . . . . .	13
2.2 Structure prediction and synthesis planning . . . . .	19

## CONTENTS

---

<b>3</b>	<b>Crystal structures</b>	<b>23</b>
3.1	Crystal lattice and symmetry . . . . .	24
3.2	Crystal structure types . . . . .	26
3.3	Phase transitions and polymorphism . . . . .	28
3.4	Bonding in solids . . . . .	30
<b>4</b>	<b>Electronic structure calculations</b>	<b>31</b>
4.1	General remarks . . . . .	31
4.2	Hartree-Fock . . . . .	33
4.3	Density Functional Theory (DFT) . . . . .	36
<b>III</b>	<b>Methods</b>	<b>39</b>
<b>5</b>	<b>Methods and software available in the research group</b>	<b>41</b>
5.1	Global and local optimization . . . . .	41
5.2	Choice of the energy (cost) function . . . . .	43
5.2.1	Simple and high quality empirical potentials . . . . .	44
5.2.2	Pseudopotentials and basis sets used in the <i>ab initio</i> methods . . . . .	45
5.3	Simulated annealing . . . . .	47
5.4	Monte-Carlo methods . . . . .	48
5.5	Gradient-based methods . . . . .	49
5.6	Genetic algorithms . . . . .	50
5.7	The threshold-algorithm . . . . .	51
5.8	The prescribed path algorithm . . . . .	51
5.9	Structure refinement software . . . . .	53
<b>6</b>	<b>New methods and techniques developed or applied during this research</b>	<b>55</b>
6.1	New modifications and applications of the prescribed path algorithm . . . . .	55
6.1.1	Stability analysis via constant temperature Monte Carlo simulations . . . . .	56
6.2	Phonon "supercell" technique in CRYSTAL09 . . . . .	58
6.3	New visualization techniques developed and applied in energy landscape representation . . . . .	60
6.4	Scripts for structure analysis . . . . .	67



---

<b>IV</b>	<b>Application of structure prediction and energy landscape investigation to specific chemical systems</b>	<b>69</b>
<b>7</b>	<b>Structure prediction for lead sulfide (PbS) at various pressures on ab initio level</b>	<b>71</b>
7.1	Introduction . . . . .	71
7.2	Optimization procedure . . . . .	73
7.2.1	Statistical analysis of the optimization process . . . . .	78
7.3	Results and Discussion . . . . .	79
7.3.1	Phase transitions and modifications stable at elevated pressure . . . . .	79
7.3.2	Low-density modifications stable in the negative pressure region . . . . .	85
7.3.3	New modifications found exhibiting unknown structure types . . . . .	88
7.4	Electronic aspects at standard and elevated pressures . . . . .	90
7.5	Conclusion . . . . .	95
<b>8</b>	<b>Investigation of kinetic stability, electronic and vibrational properties of PbS and BaS as a function of pressure</b>	<b>97</b>
8.1	Introduction . . . . .	97
8.2	Optimization procedure . . . . .	99
8.3	Results and Discussion . . . . .	100
8.3.1	Electronic properties . . . . .	101
8.3.2	Vibrational properties . . . . .	110
8.4	Conclusion . . . . .	115
<b>9</b>	<b>Structure prediction in the zinc oxide (ZnO) system for various pressures</b>	<b>119</b>
9.1	Introduction . . . . .	119
9.2	Optimization procedure . . . . .	121
9.3	Results and Discussion . . . . .	122
9.3.1	Statistical analysis of the optimization process . . . . .	122
9.3.2	Phase transitions and modifications found in the high pressure region . . . . .	124
9.3.3	Investigations of the new stacking variants of ZnO . . . . .	126
9.3.4	Negative pressure region and low-density modifications . . . . .	129
9.4	Conclusion . . . . .	131

## CONTENTS

---

<b>10 Energy landscape investigation in ZnO</b>	<b>133</b>
10.1 Introduction . . . . .	133
10.2 Optimization procedure . . . . .	134
10.2.1 Analysis methods in the prescribed path explorations . . . . .	136
10.3 Results and Discussion . . . . .	136
10.3.1 The threshold algorithm calculations . . . . .	136
10.3.1.1 Energy landscape of ZnO for different number of formula units . . . . .	136
10.3.2 The Prescribed Path Algorithm calculations . . . . .	141
10.3.2.1 Energy landscape of ZnO for different temperatures (0 - 1000 K) . . . . .	141
10.3.2.2 Procedure I . . . . .	141
10.3.2.3 Procedure II . . . . .	143
10.3.2.4 Procedure III . . . . .	147
10.3.2.5 Thermal stability analysis (TSA) via constant tempera- ture Monte Carlo simulations . . . . .	159
10.4 Conclusion . . . . .	161
<b>11 Structure prediction as a guide in synthesis planning: investigation of systems exhibiting the 5-5 structure type</b>	<b>165</b>
11.1 Introduction . . . . .	165
11.2 Optimization procedure . . . . .	166
11.3 Results and Discussion . . . . .	168
11.4 Conclusion . . . . .	172
<b>V Summary</b>	<b>173</b>
<b>12 Summary</b>	<b>175</b>
<b>VI Appendix</b>	<b>179</b>
<b>13 Appendix A: Software available in the research group</b>	<b>181</b>
13.1 Computational software . . . . .	181
13.1.1 G-42 program . . . . .	181

---

13.1.2	CRYSTAL-program . . . . .	181
13.1.3	VASP program . . . . .	182
13.1.4	GULP program . . . . .	182
13.2	Visualizational software . . . . .	183
13.2.1	KPLOT program . . . . .	183
13.2.2	VESTA program . . . . .	183
13.2.3	MATLAB program . . . . .	184
13.2.4	J-ICE program . . . . .	184
13.2.5	XCRYSDEN program . . . . .	184
13.2.6	XMGRACE program . . . . .	184
<b>14</b>	<b>Appendix B: Structure prediction for PbS at various pressures on <i>ab initio</i> level</b>	<b>187</b>
<b>15</b>	<b>Appendix C: Investigation of kinetic stability, electronic and vibrational properties of PbS and BaS as a function of pressure</b>	<b>191</b>
<b>16</b>	<b>Appendix D: Energy landscape investigation in ZnO</b>	<b>197</b>
16.1	The threshold algorithm calculations . . . . .	197
16.2	The prescribed path calculations . . . . .	200
	<b>References</b>	<b>209</b>
<b>VII</b>	<b>Formalia</b>	<b>221</b>

## CONTENTS

---

# List of Figures

2.1	3D-projection of the energy landscape . . . . .	16
2.2	2D-projection of a 3N-dimensional energy landscape . . . . .	17
3.1	Diamond is an allotrope of carbon, where the carbon atoms are arranged in a variation of the face-centered cubic crystal structure . . . . .	25
3.2	Graphite has a layered, planar structure, where each layer is separated and the carbon atoms are arranged in a hexagonal lattice . . . . .	27
5.1	A simplified model of the prescribed path algorithm . . . . .	52
6.1	Flowchart of the prescribed path (PP) algorithm . . . . .	57
6.2	3D-Model of the energy landscape as function of $a$ , $V$ , and $E$ in the ZnO system based on the threshold algorithm runs, using sphalerite as initial configuration with 1 formula unit per simulation cell . . . . .	61
6.3	3D-Model of the energy landscape as function of $a$ , $V$ , and $E$ in the ZnO system based on the prescribed path algorithm runs, using sphalerite/wurtzite as initial/ final configurations with 2 formula unit per simulation cell . . . . .	62
6.4	3D-Model of the energy landscape as function of $r$ , $V$ , and $E$ in the ZnO system based on the prescribed path algorithm runs, using sphalerite/wurtzite as initial/ final configurations with 2 formula unit per simulation cell . . . . .	63
6.5	2D-Model of the energy landscape as function of $\%$ and $V$ (while $E$ is defined by the color) in the PbS system based on the <i>ab initio</i> calculations with 4 formula unit per simulation cell . . . . .	65

## LIST OF FIGURES

---

6.6	3D-Model of the energy landscape as function of $\%$ , $V$ , and $E$ in the PbS system based on the <i>ab initio</i> calculations with 4 formula unit per simulation cell . . . . .	66
7.1	Galena mineral (PbS) from Devon, England, UK . . . . .	72
7.2	Mineral galena (PbS) from Savoie, Rhone-Alpes, France . . . . .	73
7.3	Visualization of the experimentally observed structures . . . . .	74
7.4	Visualization of the calculated structure types . . . . .	78
7.5	$E(V)$ curves at LDA level for the most relevant structure types in PbS .	80
7.6	$H(p)$ curves at LDA level in the PbS system . . . . .	80
7.7	$E(V)$ curves at LDA level for the most relevant structure types in PbS .	81
7.8	$H(p)$ curves at LDA level in the PbS system . . . . .	82
7.9	Visualization of the experimentally observed thallium iodide (TII) structure type: a) TII-type in a periodically repeated unit cell; b) 7-fold coordination of the Pb-atom by S-atoms. . . . .	83
7.10	Visualization of the experimentally observed germanium sulfide (GeS) structure type: a) GeS-type in a periodically repeated unit cell; b) 7-fold coordination of the Pb-atom by S-atoms in the GeS type (often depicted as 6-fold coordination as in previous figure). The similarity of these structure types becomes clear when the distant S-atom is included in the coordination sphere of the Pb-atom in the GeS type. . . . .	83
7.11	Visualization of the experimentally observed iron boride (FeB) structure type: a) FeB-type in a periodically repeated unit cell; b) 7-fold coordination of the Pb-atom by S-atoms in the FeB type. . . . .	84
7.12	Visualization of the experimentally observed germanium telluride ( $\alpha$ -GeTe) structure type: a) $\alpha$ -GeTe in a periodically repeated unit cell; b) 6-fold (3+3) coordination of the Pb-atom by S-atom in the $\alpha$ -GeTe type. . . . .	85
7.13	Visualization of the calculated structure types . . . . .	86
7.14	Visualization of the additionally calculated high-pressure structures . . .	87
7.15	Visualization of the additional calculated high-pressure structures . . . .	89
7.16	Visualization of the additional calculated high pressure structures . . . .	90

**LIST OF FIGURES**

---

7.17 Band structure calculation of the NaCl type structure in PbS at equilibrium volume showing a tiny gap . . . . .	91
7.18 Density of states (DOS) of the NaCl type modification in the PbS system at equilibrium . . . . .	91
7.19 Band structure calculation of the CsCl type structure at equilibrium volume exhibiting metallic properties . . . . .	92
7.20 Density of states (DOS) of the CsCl type modification in the PbS system at equilibrium . . . . .	92
7.21 Band structure of the TII type at the computed equilibrium volume in the PbS system using LDA . . . . .	94
7.22 Band structure of the FeB type at the computed equilibrium volume in the PbS system using LDA . . . . .	94
8.1 Visualization of the experimentally observed and calculated structure types in PbS calculated using the LDA functional: a) Rock salt (NaCl) structure type ( $Fm - 3m$ ) in a periodically repeated unit cell; b) $\alpha$ -germanium telluride structure type ( $R3m$ ) in a periodically repeated unit cell; c) Six-fold coordination of the Pb-atom by the S-atoms in the $\alpha$ -GeTe type, often depicted as three-fold coordination as in figure b). . . . .	98
8.2 Visualization of coordination polyhedra of the experimentally observed and calculated structure types in PbS calculated using the LDA functional: a) $PbS_6$ octahedron with six-fold coordination of the Pb-atom by the S-atoms in the NaCl type; b) $PbS_6$ octahedron with six-fold coordination (3 short and 3 long distances) of the Pb-atom by the S-atoms in the $\alpha$ -GeTe type. Note that when the $\alpha$ -GeTe modification is represented with six-fold coordination of the Pb-atom by the S-atoms, the distortion from perfect NaCl type becomes obvious. . . . .	98
8.3 At equilibrium, PbS is found in the NaCl modification, shown with the standard cubic and the primitive rhombohedral unit cell (a). This results in a distortion of the perfect rock salt type structure at expanded volumes to the rhombohedral $\alpha$ -GeTe type of structure, which exhibits a larger cell parameter but smaller rhombohedral angle than in the NaCl type of modification (b). . . . .	100

## LIST OF FIGURES

---

8.4	The figures show phonon modes corresponding to vibrations in the [100], [010] and [001] direction (figures a, b and c). The phonon modes are degenerate at the $\Gamma$ -point and their combination produces a vibration in the [111] direction. . . . .	101
8.5	Charge density plot of NaCl modification in PbS calculated on LDA level	102
8.6	Charge density plot of selected layers of the NaCl and $\alpha$ -GeTe type modifications of PbS (on LDA level) along the (1 1 1) planes for the Pb atom layer in the NaCl type modification (left) at equilibrium and $\alpha$ -GeTe type (right) at expanded volume . . . . .	102
8.7	Charge density plot of selected layers of the NaCl and $\alpha$ -GeTe type modifications of PbS (on LDA level) along the (1 1 1) planes for the S atom layer in the NaCl structure type (left) at equilibrium and $\alpha$ -GeTe structure type (right) at expanded volume . . . . .	103
8.8	Electron charge density difference map of selected layers of the NaCl and the $\alpha$ -GeTe type modifications of PbS using LDA along the (1 1 1) planes for the Pb atom layer in the NaCl modification (left) at equilibrium and $\alpha$ -GeTe type (right) at expanded volume . . . . .	103
8.9	Electron charge density difference map of selected layers of the NaCl and the $\alpha$ -GeTe type modifications of PbS using LDA along the (1 1 1) planes for the S atom layer in the NaCl modification (left) at equilibrium and $\alpha$ -GeTe type of structure (right) at expanded volume . . . . .	104
8.10	Band structure calculation performed using the LDA functional in the NaCl type of structure at equilibrium volume ( $V = 50.30 \text{ \AA}^3$ , $a = 5.86 \text{ \AA}$ ) in the PBS system . . . . .	105
8.11	Electronic density of states (DOS) in the NaCl type of structure at equilibrium volume ( $V = 50.30 \text{ \AA}^3$ , $a = 5.86 \text{ \AA}$ ) . . . . .	105
8.12	Band structure calculation performed using the LDA functional in the NaCl type of structure at expanded volume ( $V = 61.48 \text{ \AA}^3$ , $a = 6.24 \text{ \AA}$ in the PbS sytem), which corresponds to the pressure greater then 10GPa	106
8.13	Electronic density of states (DOS) in the NaCl type of structure at expanded volume ( $V = 61.48 \text{ \AA}^3$ , $a = 6.24 \text{ \AA}$ ), which corresponds to the pressure greater then 10GPa . . . . .	106



## LIST OF FIGURES

---

8.14 Band structure calculation performed using the LDA functional in the $\alpha$ -GeTe type of structure at expanded volume ( $V = 61.48 \text{ \AA}^3$ , $a=4.56 \text{ \AA}$ , $\alpha = 56.32^\circ$ ) in the PbS system, which corresponds to the pressure greater than 10GPa . . . . .	107
8.15 Electronic density of states (DOS) performed in the $\alpha$ -GeTe type of structure at expanded volume ( $V = 61.48 \text{ \AA}^3$ , $a=4.56 \text{ \AA}$ , $\alpha = 56.32^\circ$ ), which corresponds to the pressure greater than 10GPa . . . . .	108
8.16 Band structure calculation performed using the LDA functional in the $\alpha$ -GeTe type of structure at equilibrium volume ( $V = 50.30 \text{ \AA}^3$ , $a = 4.13 \text{ \AA}$ , $\alpha = 60^\circ$ ), in the PbS system . . . . .	108
8.17 Electronic density of states (DOS) performed using the LDA functional in the $\alpha$ -GeTe type of structure at equilibrium volume ( $V = 50.30 \text{ \AA}^3$ , $a = 4.13 \text{ \AA}$ , $\alpha = 60^\circ$ ) . . . . .	109
8.18 Band structure calculation performed using the LDA functional in the NaCl type of structure at equilibrium volume in barium sulfide system .	109
8.19 Electronic density of states (DOS) calculation performed in the NaCl type of structure at equilibrium volume . . . . .	110
8.20 Phonon-dispersion relation of the NaCl type modification using the LDA functional . . . . .	111
8.21 Phonon-dispersion relation of the NaCl type modification using the LDA functional . . . . .	111
8.22 Phonon-dispersion relation of the NaCl type modification using the LDA functional . . . . .	112
8.23 Phonon-dispersion relation of BaS (NaCl structure) using the LDA functional . . . . .	112
8.24 Phonon-dispersion relation of the NaCl type modification in PbS using the B3LYP functional . . . . .	113
8.25 Phonon-dispersion relation of the NaCl type modification in PbS using the B3LYP functional . . . . .	114
8.26 Phonon-dispersion relation of the NaCl-type modification in PbS using the Hartree-Fock approximation . . . . .	114
8.27 Phonon-dispersion relation of the $\alpha$ -GeTe type modification using the LDA functional . . . . .	116

## LIST OF FIGURES

---

8.28	Phonon-dispersion relation of the $\alpha$ -GeTe type modification using the LDA functional . . . . .	116
9.1	Zincite mineral (ZnO) from Franklin Hill Mine in New Jersey, USA . . .	120
9.2	Small embedded zincite mineral (ZnO) from Franklin Hill Mine in New Jersey, USA . . . . .	121
9.3	Visualization of the experimentally observed structure types in the ZnO system: a) wurtzite ( <i>B4</i> ) type; b) rock salt ( <i>B1</i> ) type; c) sphalerite ( <i>B3</i> ) type. Note that the small light spheres and large dark spheres correspond to O and Zn atoms, respectively. . . . .	122
9.4	$E(V)$ curves at LDA level for the most relevant structure types in ZnO .	125
9.5	$H(p)$ curves at LDA level in the ZnO system . . . . .	125
9.6	Visualization of the calculated structure types in the ZnO system participating in the high-pressure region: a) germanium phosphide (GeP); and b) nickel arsenide (NiAs) structure types. Note that the small light spheres and large dark spheres correspond to O and Zn atoms, respectively.	126
9.7	$H(p)$ curves at B3LYP level in the ZnO system . . . . .	127
9.8	$H(p)$ curves at Hartree-Fock level in the ZnO system . . . . .	127
9.9	Visualization of the new stacking variants of ZnO: a) 5H ; and b) 9R polytypes. Note that the small light spheres and large dark spheres correspond to O and Zn atoms, respectively. . . . .	128
9.10	$E(V)$ curves at LDA level for the new stacking variants of ZnO . . . . .	129
9.11	$E(V)$ curves at B3LYP level for the new stacking variants of ZnO . . . . .	130
9.12	$E(V)$ curves at Hartree-Fock level for the for the new stacking variants of ZnO . . . . .	130
9.13	Visualization of the calculated structure types in the ZnO system participating in negative pressure region: a) $\beta$ -beryllium oxide (BeO); and b) "5-5" structure types. Note that the small light spheres and large dark spheres correspond to O and Zn atoms, respectively. . . . .	131
9.14	$H(p)$ curves at Hartree-Fock level in the ZnO system . . . . .	132
10.1	TA probability graph in ZnO system with 1 formula unit per simulation cell with sphalerite structure as a starting point . . . . .	137

10.2 Model using all relevant local minima as initial/final configuration (the sphalerite, the wurtzite, the "5-5", the NaCl, the NiAs and the $\beta$ -BeO type) . . . . .	142
10.3 Results of the crystallographic analysis in the prescribed path runs using the wurtzite type as initial configuration ( $x = 0$ ) and the sphalerite type cell as final configuration ( $x = 100$ ), performed with constant temperature Monte Carlo simulations within the prescribed path procedure II . . . . .	144
10.4 Results of the crystallographic analysis in the prescribed path runs using the wurtzite type as initial configuration ( $x = 0$ ) and the sphalerite type cell as final configuration ( $x = 100$ ), performed with constant temperature Monte Carlo simulations within the prescribed path procedure II . . . . .	145
10.5 Results of the crystallographic analysis in the prescribed path runs using the wurtzite type as initial configuration ( $x = 0$ ) and the NaCl type cell as final configuration ( $x = 100$ ), performed with constant temperature Monte Carlo simulations within the prescribed path procedure II . . . . .	146
10.6 Results of the crystallographic analysis in the prescribed path runs using the wurtzite type as initial configuration ( $x = 0$ ) and the NaCl type cell as final configuration ( $x = 100$ ), performed with constant temperature Monte Carlo simulations within the prescribed path procedure II . . . . .	146
10.7 Results of the energy landscape analysis in the prescribed path runs between the wurtzite ( $x = 0$ ) and the sphalerite type ( $x = 100$ ), performed with constant temperature MC simulations within the prescribed path procedure III at low temperatures (comparing results from 50 K, 100 K, and 250 K) . . . . .	149
10.8 Results of the crystallographic analysis in the prescribed path runs using the wurtzite type as initial configuration ( $x = 0$ ) and the sphalerite type cell as final configuration ( $x = 100$ ), performed with constant temperature Monte Carlo simulations within the prescribed path procedure III . . . . .	149

## LIST OF FIGURES

---

10.9 Results of the energy landscape analysis in the prescribed path runs using the wurtzite type as initial configuration ( $x = 0$ ) and the sphalerite type cell as final configuration ( $x = 100$ ), performed with constant temperature Monte Carlo simulations within the prescribed path procedure III at high temperatures (comparing results from 50 K, 500 K, and 1000 K) . . . . .	150
10.10 Results of the crystallographic analysis in the prescribed path runs using the wurtzite type as initial configuration ( $x = 0$ ) and the sphalerite type cell as final configuration ( $x = 100$ ), performed with constant temperature Monte Carlo simulations within the prescribed path procedure III at high temperatures (comparing results from 50 K, 500 K, and 1000 K)	150
10.11 Group-subgroup relation graph of subgroups for the group-subgroup pair	151
10.12 Group-subgroup relation graph of subgroups for the group-subgroup pair	152
10.13 Results of the energy landscape analysis in the prescribed path runs using the wurtzite type as initial configuration ( $x = 0$ ) and the rock salt (NaCl) type cell as final configuration ( $x = 100$ ), performed with constant temperature Monte Carlo simulations within the prescribed path procedure III at low temperatures (comparing results from 50 K, 100 K, and 250 K) . . . . .	153
10.14 Results of the crystallographic analysis in the prescribed path runs using the wurtzite type as initial configuration ( $x = 0$ ) and the rock salt (NaCl) type cell as final configuration ( $x = 100$ ), performed with constant temperature Monte Carlo simulations within the prescribed path procedure III . . . . .	153
10.15 Results of the energy landscape analysis in the prescribed path runs using the wurtzite type as initial configuration ( $x = 0$ ) and the rock salt (NaCl) type cell as final configuration ( $x = 100$ ), performed with constant temperature Monte Carlo simulations within the prescribed path procedure III at high temperatures (comparing results from 50 K, 500 K, and 1000 K) . . . . .	154

10.16	Results of the crystallographic analysis in the prescribed path runs using the wurtzite type as initial configuration ( $x = 0$ ) and the rock salt (NaCl) type cell as final configuration ( $x = 100$ ), performed with constant temperature Monte Carlo simulations within the prescribed path procedure III at high temperatures (comparing results from 50 K, 500 K, and 1000 K) . . . . .	154
10.17	Group-subgroup relation graph of subgroups for the group-subgroup pair	155
10.18	Results of the energy landscape analysis in the prescribed path runs using the sphalerite type as initial configuration ( $x = 0$ ) and the rock salt (NaCl) type cell as final configuration ( $x = 100$ ), performed with constant temperature Monte Carlo simulations within the prescribed path procedure III at low temperatures (comparing results from 50 K, 100 K, and 250 K) . . . . .	156
10.19	Results of the crystallographic analysis in the prescribed path runs using the sphalerite type as initial configuration ( $x = 0$ ) and the rock salt (NaCl) type cell as final configuration ( $x = 100$ ), performed with constant temperature Monte Carlo simulations within the prescribed path procedure III . . . . .	156
10.20	Results of the energy landscape analysis in the prescribed path runs using the sphalerite type as initial configuration ( $x = 0$ ) and the rock salt (NaCl) type cell as final configuration ( $x = 100$ ), performed with constant temperature Monte Carlo simulations within the prescribed path procedure III at high temperatures (comparing results from 50 K, 500 K, and 1000 K) . . . . .	157
10.21	Results of the crystallographic analysis in the prescribed path runs using the sphalerite type as initial configuration ( $x = 0$ ) and the rock salt (NaCl) type cell as final configuration ( $x = 100$ ), performed with constant temperature Monte Carlo simulations within the prescribed path procedure III at high temperatures (comparing results from 50 K, 500 K, and 1000 K) . . . . .	157
10.22	A short summary of our prescribed path investigations in the ZnO system	158

## LIST OF FIGURES

---

11.1	Visualization of the: a) <i>h</i> -BN-structure type. Note the 3-fold coordination of this structure and a longer bond length in <i>c</i> -direction, compared to the 5-5 type; b) and c) 5-5 structure type in a primitive and a periodically repeated cell. . . . .	166
11.2	Corelation diagram for <i>AB</i> systems with the 5-5 structure type between the ratio of the ionic radii and the transition pressure . . . . .	170
11.3	Corelation diagram for <i>AB</i> systems with the 5-5 structure type between the ratio of the ionic radii and the energy . . . . .	171
11.4	Corelation diagram for the <i>AB</i> systems with the 5-5 structure type, using energies and transition pressures . . . . .	171
15.1	Projected density of states (DOS) performed using the LDA functional in the NaCl type of structure at equilibrium volume ( $V = 50.30 \text{ \AA}^3$ , $a = 5.86 \text{ \AA}$ ) . . . . .	193
15.2	Projected density of states (DOS) performed using the LDA functional in the NaCl type of structure at equilibrium volume ( $V = 50.30 \text{ \AA}^3$ , $a = 5.86 \text{ \AA}$ ) . . . . .	193
15.3	Projected density of states (DOS) performed using the LDA functional in the NaCl type of structure at expanded volume ( $V = 61.48 \text{ \AA}^3$ , $a = 6.24 \text{ \AA}$ ), which corresponds to the pressure greater then 10GPa. . . . .	194
15.4	Projected density of states (DOS) performed using the LDA functional in the NaCl type of structure at expanded volume ( $V = 61.48 \text{ \AA}^3$ , $a = 6.24 \text{ \AA}$ ), which corresponds to the pressure greater then 10GPa. . . . .	194
15.5	Projected density of states (DOS) performed using the LDA functional in the in the $\alpha$ -GeTe type of structure at expanded volume ( $V = 61.48 \text{ \AA}^3$ , $a=4.56 \text{ \AA}$ , $\alpha = 56.32^\circ$ ), which corresponds to the pressure greater then 10GPa. . . . .	195
15.6	Projected density of states (DOS) performed using the LDA functional in the in the $\alpha$ -GeTe type of structure at expanded volume ( $V = 61.48 \text{ \AA}^3$ , $a=4.56 \text{ \AA}$ , $\alpha = 56.32^\circ$ ), which corresponds to the pressure greater then 10GPa. . . . .	195

16.1 Group - subgroup relation graph of maximal subgroups. The starting group is  $Fm - 3m$  (no. 225), where the ideal rock salt ( $B1$ ) structure appears, and the final subgroup is  $F - 43m$  (no. 216), where the ideal sphalerite ( $B3$ ) structure appears . . . . . 203

16.2 Group - subgroup relation graph of maximal subgroups. The starting group is  $Fm - 3m$  (no. 225), where the ideal rock salt ( $B1$ ) structure appears, and the final subgroup is  $I4mm$  (no. 107), where the ideal GeP structure appears . . . . . 204

16.3 Group - subgroup relation graph of maximal subgroups. The starting group is  $P6_3/mmc$  (no. 194), where the ideal 5-5 structure appears, and the final subgroup is  $P6_3mc$  (no. 186), where the ideal wurtzite structure appears . . . . . 205

16.4 Group - subgroup relation graph of maximal subgroups. The starting group is  $P6_3mc$  (no. 186), where the ideal wurtzite structure appears, and the final subgroup is  $Cm$  (no. 8), where different distortions of experimentally observed structures appear . . . . . 206

## LIST OF FIGURES

---



# List of Tables

1	Fundamental Physical Constants . . . . .	xxxiv
2	Unit conversions . . . . .	xxxiv
3	Acronyms . . . . .	xxxv
9.1	Results of the crystallographic analysis of the global optimization calculations in ZnO for different number of formula unit $Z$ and radius scale factor $R$ . . . . .	123
9.2	Overview of the crystallographic analysis of the global optimization calculations performed at various pressures in ZnO for different number of formula unit $Z$ and radius scale factor $R$ . . . . .	124
10.1	Thermal stability analysis (TSA) for the wurtzite type of structure in the ZnO system . . . . .	159
10.2	Thermal stability analysis (TSA) for the sphalerite type of structure in the ZnO system . . . . .	160
10.3	Thermal stability analysis (TSA) for the rock salt (NaCl) type of structure in the ZnO system - Part I . . . . .	160
10.4	Thermal stability analysis (TSA) for the rock salt (NaCl) type of structure in the ZnO system - Part II . . . . .	161
11.1	Stability and cell parameters of the 5-5 structure in different systems calculated with the LDA functional . . . . .	169

## GLOSSARY

---

# Glossary

## GLOSSARY

---

Symbol	Meaning	Unit
$\epsilon_0$	electric constant	$8.854187817\dots\times 10^{-12}$ Fm <sup>-1</sup>
$e$	elementary charge (of proton)	$1.60217733(49)\times 10^{-19}$ C
$eV$	electron Volt	$1.60217653(14)\times 10^{-19}$ J
$a_0$	Bohr radius	$5.29177249(24)\times 10^{-11}$ m $\approx 0.53$
$k_B$	Boltzman constant	$1.380658(12)\times 10^{-23}$ J/K
$h$	Planck constant	$6.6260755(40)\times 10^{-34}$ Js
$N_A$	Avogadro constant	$6.0221367(36)\times 10^{23}$ mol <sup>-1</sup>
$R$	molar gas constant	$8.314510(70)$ J/K mol

**Table 1: Fundamental Physical Constants**

Symbol	Meaning	Unit
$E_h$	Hartree energy = $\frac{e^2}{4\pi\epsilon_0 a_0}$	$4.3597482(26)\times 10^{-18}$ J $2.6255000\times 10^6$ J/mol $27.211652$ eV
$eV$	electron Volt	$627.51\times 10^3$ Calories/mol (US Calorie) $96.485333\times 10^3$ J/mol $23.060548\times 10^3$ Calories/mol $8056.394763434$ cm <sup>-1</sup>
$\frac{eV}{k_B}$	$eV$ divided by Boltzman's constant	$11605.505(20)$ K
$\frac{eV}{3}$	Electronvolt per cubic angstrom	$160.2176487$ GPa
$cal$	Calorie (USA - definition)	$4.18400$ J
	Mean Calorie	$4.19002$ J
	15°C Calorie	$4.1890$ J
1 GPa	GigaPascal	10 Kbar
1 atm	Atmosphere	$1.01325$ bar $101325$ Pa

**Table 2: Unit conversions**

Symbol	Meaning
AO	Atomic Orbital
AEBS	All Electron Basis Set
BZ	Brillouin Zone (first)
B3LYP	Becke-Lee-Yang-Paar (hybrid)
CMPZ	"CoMPare Zellen" (= Compare Cells)
DFT	Density Functional Theory
DOS	Density of States
ECP	Effective Core Potential
GA	Genetic Algorithm
GGA	Generalized Gradient Approximation
GO	Global Optimization
GTO	Gaussian Type Orbital
HF	Hartree-Fock
LCAO	Linear Combination of Atomic Orbitals
LDA	Local Density Approximation
LO	Local optimization
MC	Monte Carlo
MD	Molecular Dynamics
NEB	Nudged Elastic Band
PCA	Principal Coordinate Analysis
PP	Prescribed Path
PPBS	Pseudopotential Basis Set
PW	Plane Wave
PWGGA	Perdew-Wang GGA
QM	Quantum Mechanics
RGS	"RaumGruppenSucher" (= Space Group Searcher)
RHF	Restricted HF
ROHF	Restricted Open-shell HF
SA	Simulated Annealing
SCF	Self-Consistent-Field
SFND	"SymmetrieFiNDer" (= Symmetry Finder)
STO	Slater Type Orbital
TA	Threshold Algorithm
VBH	Von Barth-Hedin
VSEPR	Valence Shell Electron Pair Repulsion

Table 3: Acronyms

## GLOSSARY

---

# Part I

## Introduction





# 1

## Introduction and Outline

### 1.1 Introduction

Through out history people have always been interested in the future. If someone could know the future, or would be able to predict some event, he would be in a better position than others who cannot do so. The act of predicting, via reasoning about the future in a logical manner, by extrapolating from past observations, is especially close to the scientist. Through history many famous scientists have struggled with the issue of prediction; e.g. the famous Danish physicist Niels Bohr (1885-1962), who was one of the first to develop and apply quantum theory and has won the Nobel Prize for Physics in 1922, said: *"Prediction is very difficult, especially if it's about the future."*

In the past centuries, solid state chemistry was based on the experimental synthesis and various observations, which would provide information about the possible compounds in a chemical system. Afterwards, different phenomenological models were employed to rationalize the possibility of a compound's existence. However, as the famous Australian-born British physicist and X-ray crystallographer William Lawrence Bragg (1890-1971), inventor of the law of the diffraction, later named after him, and the winner of the Nobel Prize for Physics in 1915, said: *"The important thing in science is not so much to obtain new facts as to discover new ways of thinking about them"*.

Therefore, we see that the idea of modeling solids and predicting synthesis routes is an ancient one, and many modern concepts in solid state research can relate to ideas going back to the beginning of the last century. However, the connection to modern concepts of structure prediction, modeling of solids and energy landscapes developed

## 1. INTRODUCTION AND OUTLINE

---

in the past thirty years is rather difficult, since the modern methods demand high computational power, which was quite small or completely lacking before the eighties.

The first attempts of the structure prediction in chemical systems started over forty years ago with work on retrosynthesis [1, 2], protein sequence prediction [3–5] and structure prediction of clusters [6–8]. However, the first consideration of a structure prediction concept in solid state chemistry came only in the nineteen-eighties. [9, 10] Afterwards, first attempts of crystal structure prediction and energy landscape exploration of solids emerged in the 1990's [11–17], and systematic structure prediction of experimentally observed or totally unknown chemical systems has especially progressed in the past decade with the rapid increase of computer power and the development of more efficient exploration methods. [8, 18–22] The attitude of the general public and scientists also began to change during these two decades to take predictions of new compounds much more serious and as testable propositions, which can be best described in the words of Milton Friedman (1912-2006), a famous American economist who won the Nobel Prize in Economics in 1976, who said : *"The only relevant test of the validity of a hypothesis is comparison of prediction with experience"*.

Today, scientists have successfully synthesized many new materials and studied their properties, but the purely experimental approach is no longer the only route to discover new compounds. There are several alternatives, which nowadays, one could say sometimes even give priority to the theory compared to the experiment, especially in the field of molecular chemistry: First, the theoretical prediction of new compounds and new (meta)-stable modifications of already existing molecules and solids, followed by their experimental synthesis, and second, the purely theoretical prediction of new compounds and new (meta)-stable modifications of unknown systems where there is no comparison to an experimental result is possible or where an experiment is not feasible at all. [8, 10, 11, 16, 17, 23–27] One might even say that we have come to the point where it is increasingly necessary for the presentation and discussion of experiments in solid state research to verify or combine the experiment with theoretical calculations.

Although structure prediction and the investigation of the energy landscape of solids is nowadays highly developed, there are still several problems a scientist in solid state theory has to face, and maybe the biggest problem is the increasingly multidisciplinary approach to the problem. In order to produce a valuable high-quality result, it is

necessary to apply knowledge from many areas of chemistry (structural-, inorganic-, quantum- etc.), physics (solid state-, quantum mechanics, etc.) physical-chemistry (equilibrium thermodynamics, phase transitions, etc), crystallography (crystal lattice, symmetry relations) and computer programming (programming languages, applications, visualizations, etc.). Clearly, obtaining equal expertise in all of these fields is almost impossible. What usually happens, in order to have good theoretical results, instead of having one person dealing with a multidisciplinary problem, we have several specialists from different fields jointly attacking the problem.

Reflecting this large variety of fields where structure prediction is applied and which contribute to such prediction, numerous computational methods for simulating and predicting structures of inorganic solids have emerged in the past two decades, combined with the development of sophisticated simulation tools, ranging from minimization techniques, molecular dynamics, simulated annealing to first principles energy calculations. One of the main principles in these calculations is that structure prediction does not only consist of simulating the existing structures, but also identifies unknown modifications in experimentally observed or not-yet-synthesized chemical systems, their relationship, and their possible properties. In this context, the most important observation is that (meta)stable compounds are kinetically stable local minima of the free energy on the energy landscape.

If we consider the needs of industry over the last decades, there is an enormous demand for new materials, possibly only accessible via chemical synthesis routes, e.g. via high pressure synthesis, leading to the study of materials under high pressure [28], both on the theoretical and experimental basis. Experiments at high pressures exceeding 10 GPa [29, 30] have enormously increased the number of new high-pressure phases discovered in different chemical systems. However, there are limitations to the experimental methods, since the in-situ measurements are still far from trivial, and in many cases the only information obtained are the cell parameters of the investigated modification. This is the moment when theoretical calculations can be used as a supplement to the experimental results, and help identify newly generated phases. As a consequence, in the last two decades a vast number of structure prediction calculations has been performed on chemical systems, focusing on the high-pressure phases. [31–45]

Besides the high-pressure investigation, there have been parallel developments in the area of new experimental synthesis techniques, which can lead to metastable compounds

## 1. INTRODUCTION AND OUTLINE

---

thermodynamically stable at effective negative pressures, e.g. via the growth of crystalline compounds in an amorphous matrix of the same atomic composition that had been deposited at very low temperatures (liquid nitrogen or liquid helium temperature) using atom beams [46, 47]. In many cases, the modification formed when employing this method has proven to be a low density phase that would be the thermodynamically preferred one only at high temperatures or negative pressures [46–49]. This puts new challenges to the theoretical calculations, since one can no longer expect that all structure candidates at high or negative pressures are also local minima of the potential energy, i.e. of the enthalpy at zero pressure and temperature. Instead, it is necessary to study the enthalpy surface for many different pressures, in order to determine as many candidates as possible for the pressure of interest. However, this procedure poses no additional difficulties, since it is completely analogous to structure prediction of solids at low (zero) pressure via the determination of local minima of the potential energy of the specific chemical system. [17, 22, 24, 25, 50]

Although natural sciences are highly developed at the present moment, only a very small part of the world around us has been studied experimentally. For example, the deepest holes in the earth explored so far are about 12 km deep, while the approximate radius of the earth is 6371 km, which means that the deepest drilled hole, and therefore the available observed data, reaches only 0.19 % of the earth radius<sup>1</sup>. If we go to other planets, then our knowledge from direct observations is even smaller. Since most elements and compounds in the universe exist under conditions of extremely high pressures and temperatures, deep within the planets and stars, this large important part of our world has been out of reach for conventional science. However, using new theoretical techniques one can address this unexplored world and ask fascinating questions, e.g. how materials behave under these extreme conditions? Can we compute and/or observe new high-density crystal modifications? What is the effect of extreme conditions on their physical properties? Some of these questions will be addressed in this thesis.

---

<sup>1</sup>Even while drilling the holes, the temperatures and pressures observed were much higher than predicted.

## 1.2 Outline

The thesis itself is divided into several parts: (I) **Introduction**, (II) **Theoretical background**, (III) **Methods**, (IV) **Application of structure prediction and energy landscape investigation to specific chemical system**, and (V) **Summary**, followed by an VI **Appendix**.

In **Part(II) Theoretical background**, we review some aspects of the theoretical approaches to energy landscape and structure prediction, electronic structure calculations, crystal structures and physical properties of solids.

**Part(III) Methods**, is separated into two chapters. First, in the Chapter: *Methods and software available* (Chapter 5), we describe the methods and software employed in this thesis that were available to us at the beginning of the work. Next, in the Chapter: *New methods and techniques developed or applied during this research* (Chapter 6), we describe new modifications and applications of the prescribed path algorithm, the phonon "supercell" technique in the CRYSTAL09 code, new visualization techniques applied in the representation of energy landscape, and newly developed scripts for structure analysis.

**Part(IV) Applied structure prediction and energy landscape investigation of specific chemical systems**, describes 5 different studies:(1) "*Structure prediction for lead sulfide (PbS) at standard and high pressures on ab initio level*", (2) "*Investigation of kinetic stability, electronic and vibrational properties of PbS and BaS as a function of pressure*", (3) "*Structure prediction in the zinc oxide (ZnO) system for various pressures*", (4) "*Energy landscape investigation in ZnO*", and (5) "*Structure prediction as a guide in synthesis planning: investigation of systems exhibiting the 5-5 structure type*". This is followed by a summary of work on additional systems of interest.

In **Chapter 7**: "*Structure prediction for lead sulfide (PbS) at standard and high pressures on ab initio level*", we performed structure prediction by global optimizations on the energy landscape of PbS for various pressures, using simulated annealing followed by local optimization of the candidates found. In order to be able to take the effect of the

## 1. INTRODUCTION AND OUTLINE

---

nonbonding valence electrons of Pb into account, *ab initio* energies were employed for both the global and local optimization. As lead sulfide is an important semiconductor, it is of great interest to identify possible (meta)stable modifications, both at standard and elevated pressures. Besides the experimentally known modifications (NaCl structure type at standard pressure and the CsCl structure type at high pressure), several additional promising structures, which might be accessible synthetically, were found; exhibiting, e.g., the TII type ( $Cmcm$ ), the FeB type ( $Pnma$ ), and the  $\alpha$ -GeTe type ( $R3m$ ) of modification.

In **Chapter 8**: “*Investigation of kinetic stability, electronic and vibrational properties of PbS and BaS as a function of pressure*”, we investigate the possible reasons for the existence of the metastable modification  $\alpha$ -GeTe type in the PbS system; in particular, we address the question, whether the  $\alpha$ -GeTe type modification might be stabilized (and conversely the rock salt modification destabilized) by steric effects of the non-bonding electron pair. We have investigated the electronic and vibrational properties of PbS and calculated then for the BaS system, for comparison.

In **Chapter 9**: “*Structure prediction in the zinc oxide (ZnO) system for various pressures*”, we performed structure prediction by global optimizations on the energy landscape of zinc oxide for various pressures, using simulated annealing with empirical potentials followed by local optimization on the *ab initio* level. We have found the observed structure types (wurtzite, sphalerite and rock-salt), in agreement with experiment and in addition, many new interesting modifications were calculated in different regions of the energy landscape.

In **Chapter 10**: “*Energy landscape investigation in ZnO*”, the energy landscape of the zinc oxide system was investigated by performing a number of calculations using the threshold algorithm, where the number of atoms in the simulation cell ( $Z$ ) was varied from 1 Zn and 1 O atom to 6 Zn and 6 O atoms. Starting from results of the global optimizations and threshold calculations in the ZnO system, we performed prescribed path explorations, in order to investigate the features of the energy landscape of ZnO that connect the major minimum basins of the system. We present here the prescribed path algorithm, a new method for exploring transition routes and barriers between even

distant minima, as well as learning about aspects of the structural stability and possible synthesis processes as function of temperature and pressure, and making contact with experimental observations. Finally, for each relevant structure, thermal stability was separately analyzed.

In **Chapter 11**: “*Structure prediction as a guide in synthesis planning: investigation of systems exhibiting the 5-5 structure type*”, we performed data exploring for binary compounds with elements from groups V, IV - VI, and III - VII. Next, local optimization on *ab initio* level with LDA functional was performed. Furthermore, the results are compared with earlier theoretical work involving the 5-5 structure type in the earth alkaline metal oxides and the alkali metal halides.

## 1. INTRODUCTION AND OUTLINE

---



## Part II

# Theoretical and computational background in solid state research



## 2

# Energy landscape and structure prediction

*"The best way to predict the future is to invent it."*

(Alan Curtis Kay (1940-), an American computer scientist) [51]

The prediction of crystalline structures on the atomic level is one of the biggest challenges in condensed matter science. [7, 8, 17, 18, 25] In order to find possible new (meta)stable compounds in a chemical system which have not yet been synthesized, it is very important to have a collaboration between theory and experiment. Similarly, in many chemical systems, the information obtained from experiments is not sufficient to allow a structure determination of a new compound, describe phase transitions among various (meta)stable modifications or investigate their properties. This is the point where the theoretical explanations can play a key role and especially the energy landscape approach, which considers a chemical system and its dynamics on the energy landscape as a function of the ionic degrees of freedom [7, 18, 52].

## 2.1 Energy Landscape

The description of the energy landscape depends primarily on the intended application, e.g. general scientific models (chemistry, physics, etc), specific systems (molecules, proteins, solids, etc.) or even outside of the natural sciences and engineering (economics,

## 2. ENERGY LANDSCAPE AND STRUCTURE PREDICTION

---

energetics, ecology, etc). The term "energy landscape" was most probably introduced for the first time in terms of potential energy surfaces or energy hypersurface of glasses and as the cost function of the non-linear optimization problem in mathematics [7, 52–54]. The IUPAC definition of the energy hypersurface (synonymous with potential energy surface, PES) gives :

*"The notion of hypersurface is used to stress the multidimensionality of PESs. In a molecular system consisting of  $N$  atomic nuclei, the number of the independent coordinates that fully determine the PES is equal to  $3N - 6$  (or  $3N - 5$  if the system is linear)." [52]*

From the physical point of view the energy landscape of a molecule or a system of molecules is defined as a mapping of all possible conformations of a molecular entity, or the spatial positions of interacting molecules in a system, to their corresponding energy (usually the potential energy), with the pictures typically shown of landscapes corresponding to a projection on a two- or three-dimensional Cartesian coordinate system. In a purely mathematical approach, an energy landscape can be defined as a pair  $(X, f)$  consisting of a  $n$ -dimensional space  $X$  representing the physical states or parameters of a system together with a continuous function  $f : X \rightarrow R$  representing the energies associated with these states or parameters such that the image of  $f$  represents a hypersurface embedded in  $R^{n+1}$ . [7].

An analogous definition is used in solid state research, where the chemical system is represented as a collection of  $N$  atoms via a  $3N$ -dimensional position vector,  $\vec{X} = (\vec{X}_1, \dots, \vec{X}_N)$ , plus a  $3N$ -dimensional momentum vector,  $\vec{P} = (\vec{p}_1, \dots, \vec{p}_N)$ , or its velocity vector,  $\vec{V} = (\vec{v}_1, \dots, \vec{v}_N)$ , and its (potential) energy  $E(\vec{X})$ . Therefore, for both molecules and solids, the energy hypersurface over the  $3N$ -dimensional space of all atom arrangements is known as the energy landscape of the chemical system. [7, 16–19, 25, 53–55]<sup>1</sup>

The energy of such a classical system  $E = E(\vec{X}, \vec{V})$  can be split into two parts:

$$E = E(\vec{X}, \vec{V}) = E_{pot}(\vec{X}) + E_{kin}(\vec{V}), \quad (2.1)$$

---

<sup>1</sup>For a full quantum mechanical description, we also need to take into account additional electronic and spin degrees of freedom. In order to have a concise summary, we only discuss the classical system without electric and magnetic fields, and for the more complex cases, we point the reader to the Energy Landscape literature.

where  $E_{pot}(\vec{X})$  is the potential energy and  $E_{kin}(\vec{V}) = 1/2 \sum_i m_i \vec{v}_i^2$  is the kinetic energy, respectively. The time evolution of such a system is governed by Newton's equations:

$$\frac{d \vec{x}_i}{dt} = \frac{\vec{p}_i}{m_i} = \vec{v}_i \quad (2.2)$$

$$\frac{d \vec{p}_i}{dt} = \vec{F}_i = - \frac{\partial E_{pot}(\vec{X})}{\partial \vec{x}_i} \quad (2.3)$$

In principle these equations can be solved and yield a unique solution (trajectories  $(\vec{X}(t), \vec{V}(t))$ ) for every physically valid choice of initial conditions  $(\vec{X}_0, \vec{V}_0)$ .

We could also view the energy landscape in a slightly simplified way as the union of the large number of local minima (regions) separated by energy barriers of different sizes and shapes (see figs. 2.1 and 2.2). The minima represent stable structures found at zero temperature, and the height of the barriers around them are a measure of the kinetic stability of those configurations at non-zero temperatures. The energy landscape explorations provide us with the information which structures are associated with (meta)stable compounds of the chemical system under investigation. Once the local minima on the energy landscape are known, one can investigate their stability and properties, and finally plan synthesis routes [17, 55–57].

In order to mathematically define an energy landscape, we need a configuration space of states (or solutions of an optimization problem), energy (or cost) function given as a real function over configuration space, and a neighborhood relation (topology). Energy landscapes of atomic configurations (i.e. inorganic structures) usually have "natural" neighborhoods given by the topology of  $\mathfrak{R}^{3N}$ , but for optimization problems we have to explicitly define such a neighborhood relation called a moveclass.

The next step in going from the classical mechanical description above to the thermodynamic one is the determination of the so-called locally ergodic regions on the energy landscape [55, 58–60]. For a given temperature  $T$ , a subset  $\mathfrak{R}$  of the configuration space is called locally ergodic on the observation time scale  $t_{obs}$ , if the time  $t_{eq}(\mathfrak{R}, T)$  it takes for the system to equilibrate within  $\mathfrak{R}$  is much shorter than  $t_{obs}$ , while the time  $t_{esc}(\mathfrak{R}, T)$  it takes for the system to leave the region  $\mathfrak{R}$ , the so-called escape time, is much larger than  $t_{obs}$ ,

## 2. ENERGY LANDSCAPE AND STRUCTURE PREDICTION

---

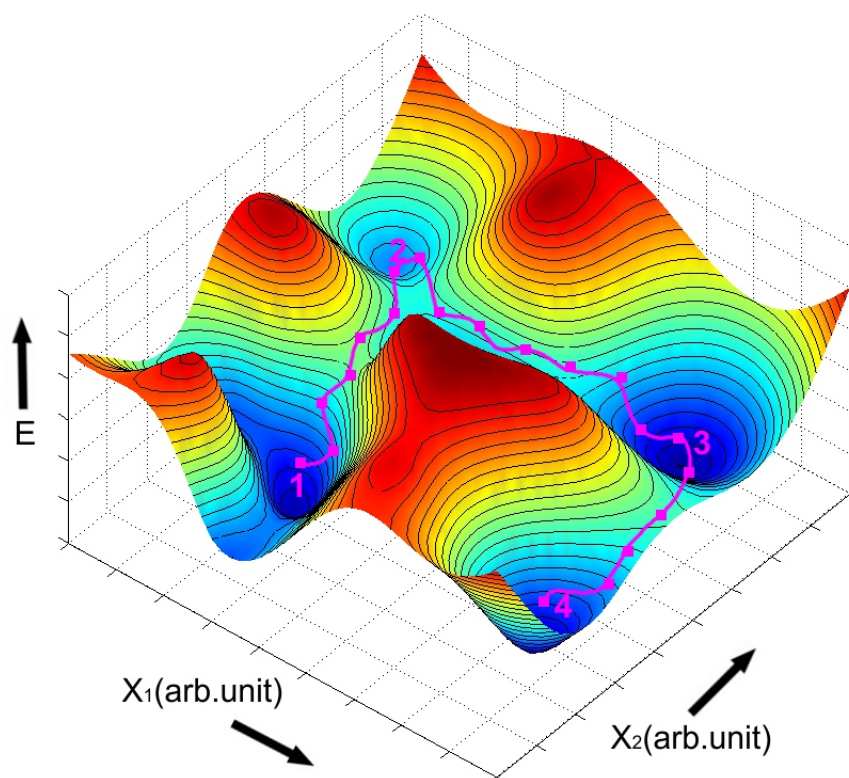


**Figure 2.1: 3D-projection of the energy landscape** - Schematic representation of a cut through a configuration space for a single-component system with fictive coordinates  $X_1$  and  $X_2$ . Local minima, labeled 1 – 4, are separated by high energy barriers. If we assume that minimum no. 1 is the global minimum (stable structure which is lowest in energy) in this chemical system, then we can see that minimum no. 3 is another big low-energy valley, which is usually a sign for a good structure candidate. However, the picture also shows that with increase of pressure and/or temperature, direct transition between minima nos. 1 and 3, will probably not occur. What is likely to happen is that the global minimum (no. 1), transforms to the metastable structure (no. 2), which is higher in energy than the structure (minimum) no. 3, and therefore not stable enough not to convert to structure (minimum) no. 3. Note that a good structure candidate is also minimum no. 4, which is separated by a high energy barrier from the global minimum (no. 1), and therefore the most favorable path to experimentally reach structure (minimum) no. 4, may be to follow a rather complicated transition route via minima nos. 2 and 3.

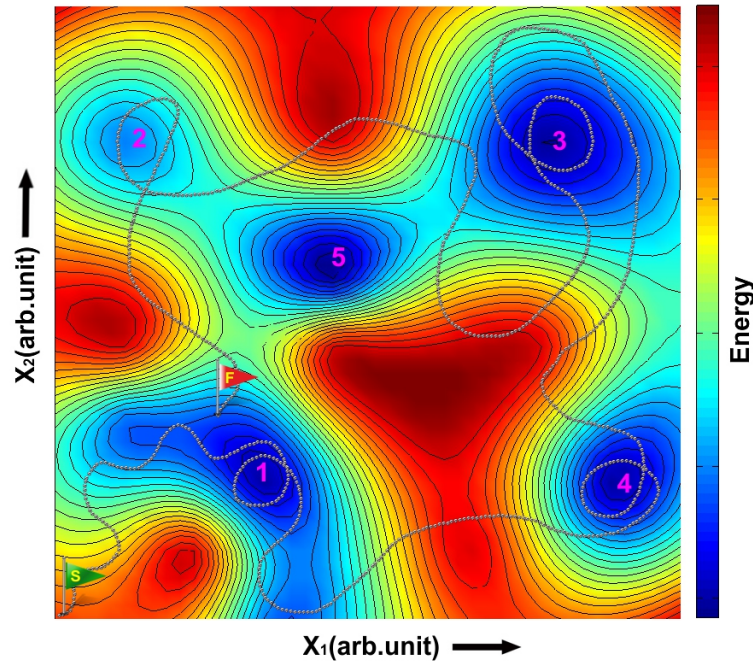


**Figure 2.2:** 2D-projection of a 3N-dimensional energy landscape - The silver dotted line shows the trajectory of time evolution of a system on the energy landscape, where  $s$  stands for start, and  $f$  for finish of the trajectory. This applies both to a trajectory of a real system and a simulated one on the computer. Silver dots indicate equal time steps, e.g. two dots might be separated in time by one minute in a real system or one nanosecond in a simulation. Measurements correspond to time averages of observables along the trajectory over a time interval (e.g. 5 minutes). Note that the trajectory spends more time in certain regions than in other. In particular, some regions are 'explored' rather thoroughly, i.e. one could replace the time average along the trajectory in such a region by an average over all states in the region. When this is possible, one says that this region of the energy landscape is "locally ergodic". The regions around minima nos. 1, 3 and 4 are locally ergodic regions on the time scale of observation encountered during the simulation. The 2D-projection allows us to see that minimum no. 5 exists also on the landscape, and that the region around it is even lower in energy than minimum no. 2, but has not been found during this particular simulation run. Note also from the picture that all local minima and barriers are found in random order, so if one wants to analyze (structure) relations between minima, a complex analysis needs to be performed at a later stage.

## 2. ENERGY LANDSCAPE AND STRUCTURE PREDICTION

---

$$t_{esc}(\mathfrak{R}, T) \gg t_{obs} \gg t_{eq}(\mathfrak{R}, T). \quad (2.4)$$

If this holds true, then the ergodic theorem tells us that we can replace the time averages of observables  $O[\vec{R}(t), \vec{P}(t)]$  over a time interval  $[t_1, t_2]$  of length  $t_{obs} = t_2 - t_1$  along this trajectory,

$$\langle O \rangle = \frac{1}{t_{obs}} \int_{t_1}^{t_2} O(\vec{R}(t'), \vec{P}(t')) dt' \quad (2.5)$$

inside the locally ergodic region  $\mathfrak{R}$  by the so-called (Boltzmann) ensemble average,

$$\langle O \rangle_{ens}(T) = \frac{\int O(\vec{P}, \vec{R}) e^{-\frac{E(\vec{P}, \vec{R})}{k_B T}} d\vec{P} d\vec{R}}{\int e^{-\frac{E(\vec{P}, \vec{R})}{k_B T}} d\vec{P} d\vec{R}} \quad (2.6)$$

restricted to the region  $\mathfrak{R}$ . However, this "equality" holds only within an accuracy  $a_m$  of the measurements process,

$$\left| \langle O \rangle_{t_{obs}} - \langle O \rangle_{ens}(T) \right| < a_m$$

since only local ergodicity is reached. In the next step we can compute the local free energy for every locally ergodic region  $\mathfrak{R}_i$

$$F(\mathfrak{R}_i, (T)) = -k_B T \ln Z(\mathfrak{R}_i, (T)) \quad (2.8)$$

and apply the usual laws of thermodynamics to the system as long as it remains within the region  $\mathfrak{R}_i$ . A simplified representation of the locally ergodic regions on the energy landscape is shown in Figure 2.2.

As a result, for any given observation time scale  $t_{obs}$ , the configuration space of the chemical system is split into a large number of disjoint locally ergodic regions which are connected by transition regions. Each such locally ergodic region corresponds to a kinetically stable compound of the chemical system on the time scale of observation. It



## 2.2 Structure prediction and synthesis planning

---

is important to note that the set of all locally ergodic regions on an energy landscape depends not only on the observation time chosen, but also on temperature (since the escape time in particular tends to vary strongly with temperature). As long as the probability of being found in one of these locally ergodic regions is much larger than the probability of being found in a transition region, the system can be considered to be in (meta)stable thermodynamic equilibrium on the timescale  $t_{obs}$  at temperature  $T$ .

Thermodynamic parameters (e.g. temperature, pressure, electric  $\vec{E}$  or magnetic  $\vec{B}$  external fields, etc.) can influence the energy landscape in different ways. Temperature, for example, changes the dynamics of the landscape in a stochastic fashion via the average kinetic energy ( $\langle E_{kin} \rangle = 3/2Nk_B T$ ). The pressure  $p$  modifies the energy function itself, but as long as these external parameters are time-independent, these influences do not pose any real difficulties in energy landscape investigations. We can perform the exploration of this modified landscape  $E(\vec{p} \neq 0, \dots)$  analogously to the one of the potential energy landscape  $E(\vec{p} = 0, \dots)$ .

To summarize, the first step is the determination of the locally ergodic regions on the energy landscape. At low temperatures escape times are controlled by energy barriers, and will increase exponentially according to the Arrhenius law [52],

$$t_{esc} \propto e^{\frac{E_{barrier}}{k_B T}}. \quad (2.9)$$

We observed many examples where these barriers are actually high enough for local ergodicity to hold even at high temperatures [55, 61, 62].

## 2.2 Structure prediction and synthesis planning

The crystal structure prediction and rational planning of syntheses, i.e. the search for new crystalline compounds followed by their synthesis has been an important topic of solid state chemistry in the past two decades. [7, 8, 17, 18, 24, 25, 63] Two separate lines of investigation have developed which we should distinguish: structure modeling and structure prediction [8]. Modeling of structures is nowadays to some extent routine using either lattice energy minimization (with appropriate interatomic potentials) or electronic structure techniques [8, 11, 18, 63, 64]. Usually the procedure is simple: structure parameters are taken from experiment (e.g. from the Inorganic Crystal Structure Database (ICSD) [65, 66], Pearson’s Crystal Data (PCD) [67], Cambridge

## 2. ENERGY LANDSCAPE AND STRUCTURE PREDICTION

---

Structural Database (CSD) [68], etc) and standard minimization methods are applied, which result in minor displacements from the experimental structure. This procedure may help to validate the methods and potentials by comparison with experimentally observed structures in the chemical system, but it is not a structure prediction.

Crystal structure prediction we can define as the procedure which starts with no empirically based information on the positions of the atoms in the unit cell. The goal of structure prediction is the determination of as many of the low-lying local minima as possible. Both identifying the energetically favored candidate for a given set of thermodynamic parameters and finding the candidates that represent metastable modifications requires the use of a global optimization method, where in general we permit free variation of atom positions, cell parameters, ionic charges and composition.

In this initial phase of structure prediction, called the global optimization, many different classes of structure prediction methods can be distinguished. Beside the pure methods of structure modeling and structure prediction, many different classes exist which combine them without a strict boundary, e.g. determining the structures of already synthesized compounds, where only powder diffraction data are available but no successful structural model has been found or in crystal structure refinement, where an approximate structure is known and the energy is then minimized, in order to generate a more accurate model. [69]. There are many global optimization methods available, e.g. simulated annealing [24, 70–72], genetic algorithm [8, 73–75], basin hopping [7, 63, 76], thermal cycling [77, 78], etc., and this is discussed in more detail in **Part(III)**.

Alternatively, the structure of a compound could be guessed from information obtained from past experiments. This approach essentially consists of correlating chemically similar compounds and proposing unknown structures in analogy with experimentally observed ones. Usually, such suggestions are based on electronegativity differences, size mismatch between the constituent elements, or simply the location in the periodic table (e.g. data mining, structure mapping, etc). [79–83] One of the latest combinations of methods with a high prediction rate consists of merging data mining with quantum mechanics, the so-called "Data mining structure prediction" [84, 85]. Then there are many other methods ranging from topological modeling methods [8, 63], which have shown to be especially precise in analyzing and predicting frameworks, especially microporous structures, including zeolites, [86–89], molecular packing approaches, which

## 2.2 Structure prediction and synthesis planning

---

explore in a systematic and efficient way, the different modes of packing of the component molecules, including the use of molecular dynamics (MD) simulations [8, 27, 90], to the metadynamics approach [8, 63, 91, 92] and the ergodicity search algorithm used in our group, which uses Monte Carlo simulations at constant temperature and stochastic quenches.[8, 17–19, 24, 63]

A detailed description of our methods is presented in **Chapter 4** and in **Part(III)**. The examples of modern structure predictions performed in the PbS and ZnO system are presented in **Chapters 7** and **9**. In **Chapter 11** we use a similar approach as in modern data mining structure prediction techniques. Finally, we use a completely new approach in **Chapter 10** where we combine the results of the structure prediction with Monte Carlo simulations, and employ the prescribed path algorithm presented in **Part(III)**, in order to correlate landscape features with actual synthesis routes.

## **2. ENERGY LANDSCAPE AND STRUCTURE PREDICTION**

---

# 3

## Crystal structures

*"A good decision is based on knowledge and not on numbers."*

(Plato (423-347 BC), Greek philosopher and mathematician) [93]

In order to perform a qualitative and quantitative structure prediction and energy landscape investigation, one needs to have deep insight into structural chemistry and crystallography. Synthesis planning as well as investigation of chemical and physical properties of a compound can only be understood when its structure is known. In the simple example of graphite and diamond one can see the great influence of materials structure on its properties (see figs. 3.1 and 3.2) : both of them consist only of carbon, but their physical and chemical properties are totally different (graphite is one of the softest and diamond the hardest material on earth. [94–96])

There are several definitions of crystal structure; one of the most frequently used in mineralogy and crystallography describes a crystal structure as a unique arrangement of atoms, ions or molecules in a solid. A crystal structure is composed of a pattern, a set of atoms (ions or molecules) arranged in a particular way called structural motif, and a crystal lattice, exhibiting periodic long-range order and symmetry. [97, 98] There are many ways to describe the crystal structure. For example, many crystal structures show similarities, so they can be described and classified using the so-called structure types (see later). Crystal structures can also be discussed in terms of the simple packing of spheres (see figs. 3.1 and 3.2). In order to fill space in the most economical way with spheres of equal size, we arrange them in a closest-packing of spheres. There

### 3. CRYSTAL STRUCTURES

---

are different abbreviations for the stacking sequence according to Hagg, Zhdanov or Jagodzinski. [99–101] We address this question especially in the ZnO system.

The coordination number and the coordination polyhedron serve to characterize the surroundings of an atom (see figs. 3.1 and 3.2). The coordination number of a central atom in a crystal is the number of its nearest neighbors, which is derived by simply counting the other atoms to which it is bonded (by either single or multiple bonds). Therefore, the coordination number specifies the number of coordinated cations by the closest neighboring anions, and conversely. Assigning a coordination number appears to be a simple task in many compounds; however, it is not always clear how to define a "closest neighboring atom". The coordination polyhedron appears when the centers of the adjacent coordinated atoms are connected with each other. For every coordination number, there are usually several typical coordination polyhedra. However, there are cases where two of the coordination polyhedra for a given coordination number differ only slightly, and can be converted into one another by minor displacements of atoms. For example, a trigonal bipyramid can be converted into a tetragonal pyramid by displacements of four of the coordinated atoms.[99, 100] We address this question especially in the PbS and ZnO system, as well as in the investigations of the 5-5 modification.

#### 3.1 Crystal lattice and symmetry

In order to describe and compare the many thousands of crystal structures that are known, one needs to define the shape and symmetry of each unit cell as well as its size and the positions of the atoms within it. In a crystal, atoms are joined to form a larger network with a periodic order in three dimensions. The crystal lattice has been constructed when one connects the periodically repeated atoms of one kind in three space directions to a 3D- grid, e.g. by periodically repeating a small parallelepiped in three dimensions without gaps. This parallelepiped is called the unit cell, and a unit cell having the smallest possible volume is called a primitive cell. [99–103] We address this question especially in the investigations of the electronic and vibrational properties of PbS.

One of the most characteristic features of any crystal is its symmetry. The space groups (in 3D) are generated from combinations of the 32 crystallographic point groups and the 14 Bravais lattices, which can be divided into 7 crystal lattice systems. This

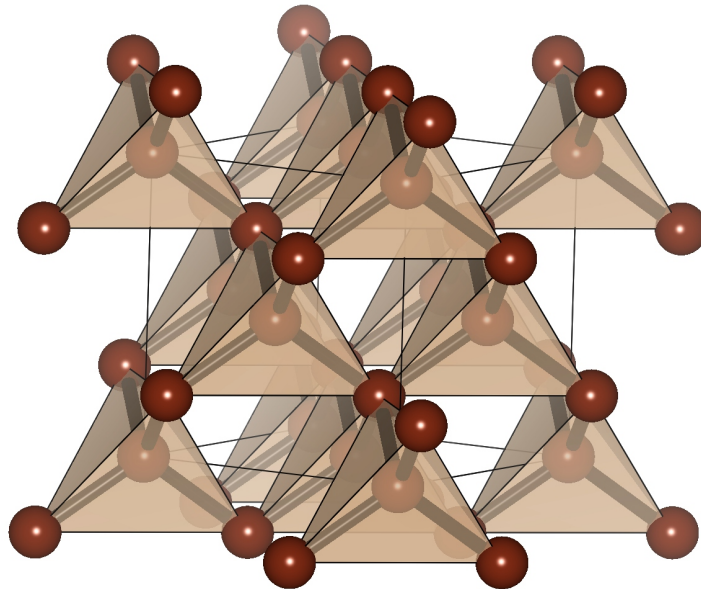


**Figure 3.1:** Diamond is an allotrope of carbon, where the carbon atoms are arranged in a variation of the face-centered cubic crystal structure - This cubic form of diamond has a stacking sequence  $ABCABCABC\dots$ , and a 4-fold coordination. Diamond has the highest hardness and thermal conductivity of any bulk material and therefore its major industrial application is in cutting and polishing tools. [95, 96, 100]

### 3. CRYSTAL STRUCTURES

---

results in a space group being the combination of the translational symmetry, the point group symmetry operations of reflection, rotation and rotoinversion, and the screw axis and glide plane symmetry operations. The combination of all these symmetry operations results in a total of 230 unique space groups describing all possible crystal symmetries. The concept of symmetry is extremely useful in describing the shapes of both individual molecules and periodic structures, since it provides a way of describing similar features in different structures so that they can become unifying features. The Bravais lattice is of vital importance when interpreting the results of the electronic structure calculations.[100, 102] The knowledge of the crystal symmetry is also of special importance in crystal structure analysis, e.g. in unit cell transformations, group-subgroup relations of the space groups, choice of the  $\vec{k}$ -vectors subsets and Brillouin zones of space groups when calculating properties of a compound, etc. Qualitative and quantitative tools in crystal structure analysis are offered on the Bilbao Crystallographic Server [104], Crystal Impact web page [105], etc. Crystal structure analysis will be of particular importance in the prescribed path investigations.

#### 3.2 Crystal structure types

In the past there have always been debates about how to properly define and classify crystal structures. One approach is to classify a structure using the so-called structure types derived from observations, e.g. lead sulfide crystallizes in the rock salt structure type, which we could describe as a distribution of Pb and S atoms in PbS corresponding to that of Na and Cl atoms in the NaCl structure. According to the definitions used here, every structure type is characterized by its space group, Wyckoff sequence, Pearson number and cell parameters ( $c/a$  ratio). A structure prototype is a freely chosen representative of a sequence of crystal structures which are identical (isopointal). Usually this is one of the first published structures, and so far there are more than 6.000 prototypes among more than 100.000 crystal structures known. In our example, the rock salt (NaCl) structure is a prototype of PbS, but there are many other compounds which crystallize in the rock salt prototype, e.g. PbSe, PbTe, SnTe, ZnO (at high pressures), etc. [97, 100, 106–108] There are many structural data bases containing both crystal structures and their prototypes, e.g. the Inorganic Crystal Structure Database (ICSD) [65, 66], the Pearson's Crystal Data (PCD) [67], the Cambridge



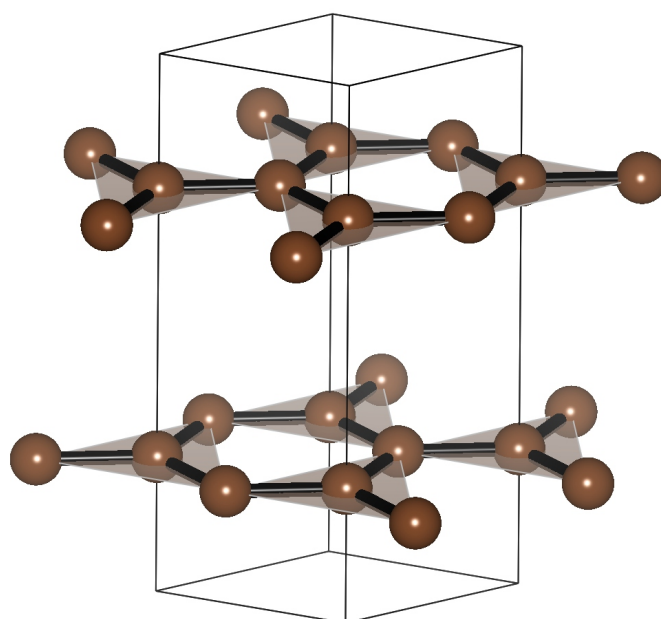


**Figure 3.2:** Graphite has a layered, planar structure, where each layer is separated and the carbon atoms are arranged in a hexagonal lattice - This hexagonal form of graphite has a stacking sequence  $ABABAB\dots$ , and a 3-fold coordination. Graphite is the most stable form of carbon under standard conditions and, unlike diamond, is an electrical conductor. Therefore, graphite is used in thermochemistry as the reference state for defining the heat of formation of carbon compounds. [94, 96, 100]

### 3. CRYSTAL STRUCTURES

---

Structural Database (CSD) [68], etc. Visualization of structures and useful information about some important prototypes can be obtained using e.g. internet pages such as (<http://cst-www.nrl.navy.mil/lattice/index.html> [109]), which currently contains links to 286 structure prototypes in 98 of the 230 space groups. Since the focus of this work was especially structures of binary compounds, more background information can be found in ref. [110].

The crystal structure types can be indexed in different ways: Strukturbericht designation symbols, where symbols  $A$  and  $B$  are used for monoatomic and diatomic structure types, symbols  $C$  and  $D$  for  $AB_2$  and  $A_nB_m$  compounds, respectively, symbols  $E, F, G, \dots, K$  specify more complex compounds, symbols  $L, O,$  and  $S$  specify alloys, organic compounds and silicates; the Pearson symbol which indicates the crystal symmetry and the number of atoms in the conventional unit cell; the prototype index which is an index of the various crystal structures by prototype compound; or symmetry, which shows the space group index of a structure, and in this case one needs in addition the atom positions, of course, in order to have a complete description of the structure. [103, 109] Furthermore, when describing the crystal structure in order to perform a calculation, one needs to give the value of  $Z$ , which represents the number of formula units in the simulation cell (conventional or primitive unit cell). One should note that in order to represent all the crystalline modifications of a system in one plot (e.g. the  $E(V)$  curves, the  $H(p)$  curves, etc.), one needs to perform the calculation for the same number of formula units for all modifications, preferably in the primitive unit cell. We address this issue especially in the ZnO system when using the TA and the PP algorithm. [101, 103]

### 3.3 Phase transitions and polymorphism

In order to explain structure transformations, first we need to define thermodynamic stability. When the Gibbs free energy of the reaction ( $\Delta G$ ) in the structure transformation of a compound from structure A to another structure B is positive, then structure A is thermodynamically stable compared to structure B.

$\Delta G$  depends on the changes in the enthalpy ( $\Delta H$ ) and entropy ( $\Delta S$ ), and both of them depend on pressure and temperature, which are kept constant, when the system is described in the Gibbs ensemble. This means that a structure can be stable only within a certain range of pressures and temperatures and by variation of the pressure

### 3.3 Phase transitions and polymorphism

---

and/or the temperature,  $\Delta G$  will eventually become negative with respect to some other structure, and a phase transition will occur. This may be a solid - solid phase transition or a transition to another aggregate state, such as a liquid or a liquid crystal. From the definition of the change in the Gibbs free energy ( $\Delta G$ ):

$$\Delta G = \Delta H - T\Delta S \quad (3.1)$$

with,

$$\Delta H = \Delta U + p\Delta V \quad (3.2)$$

we can draw conclusions for the temperature and pressure dependence of thermodynamically stable structures. First, that with the increase of temperature ( $T$ ), structures with a low degree of order, but usually with more symmetry (on average), will be favored. Their formation involves a positive entropy ( $\Delta S$ ), while the value  $\Delta G$  then depends mainly on the  $T\Delta S$  term. With further rapid increase of temperature, melting will occur, where microscopic order is even lower, but the symmetry is maximal (a perfectly isotropic and homogeneous phase), and finally to the evaporation of the substance. Second, higher pressures ( $p$ ) favor structures that occupy a lower volume, i.e. that have a higher density. As their formation involves a decrease in the volume (negative  $\Delta V$ ),  $\Delta H$  will have a negative value. In our example, diamond (with density  $3.51 \frac{g}{cm^3}$ ) is more stable than graphite (density  $2.26 \frac{g}{cm^3}$ ) at high pressures. [99, 100]

A phase transition is by definition: *"A change in the nature of a phase or in the number of phases as a result of some variation in externally imposed conditions, such as temperature, pressure, activity of a component or a magnetic, electric or stress field."* [52]

As we see from this definition, a phase transition is triggered by an external parameter which most commonly is a change in temperature or pressure, which results in changes in at least one property of a material and often involves a structural change from one to another modification. Solid-state phase transitions can be divided according to Buerger into reconstructive phase transitions (first-order transitions), displacive phase transitions (second-order transition), and order - disorder transitions (second-order transition). We note that a thermodynamically unstable structure can also exist

### 3. CRYSTAL STRUCTURES

---

at ambient conditions when its conversion to some other structure proceeds at a negligible rate. Such modifications are usually called metastable, inert or kinetically stable. Many of the crystalline modifications can be stabilized kinetically at sufficiently low temperatures. [99, 100, 111]

The definition of isomers is: *"One of several species (or molecular entities) that have the same atomic composition (molecular formula) but different line formulae or different stereochemical formulae and hence different physical and/or chemical properties."* [52]

The corresponding phenomenon for crystal structures is called polymorphism and different structures are called modifications or polymorphic forms. Modifications differ not only in the structure type, but also in their physical and chemical properties (see figs. 3.1 and 3.2).

*"A reversible transition of a solid crystalline phase at a certain temperature and pressure (the inversion point) to another phase of the same chemical composition with a different crystal structure is called polymorphic transition"*. [52]

Polymorphic forms with structures having different stacking sequences are called polytypes. [99, 100] We encounter such polytypes especially in the ZnO system.

#### 3.4 Bonding in solids

Finally we turn to the description of the bonding in solids, which basically means in our case moving from the explanations of the crystal structure to the electronic structure. In crystal structures we meet several important types of bonding: ionic, covalent, metallic, and molecular. Besides these, hydrogen-bonded solids (e.g. ice) constitutes another category that is also important in solid state chemistry. These are many examples of solids that have a single bonding type, but there are also many solids that exhibits a mixture of bonding types (e.g. covalent and metallic or covalent and ionic). Here we will deal mostly with cases that range from purely covalent type of bonding to purely ionic bonding, with degree of ionic or covalent character largely depending on the difference between the electronegativity of the atoms. To understand the bonding in solids beyond just the overall cohesive energy, one also needs to take into account lattice energy, molecular orbital theory, Lewis structures, VSEPR theory and orbital hybridization theory. [100, 102, 106, 111–116] We address this issue especially in the investigations of electronic and vibrational properties of PbS.

## 4

# Electronic structure calculations

*"Your theory is crazy, but it's not crazy enough to be true."*

(Niels Bohr (1885-1962), Danish physicist) [117]

### 4.1 General remarks

The aim of the first-principles approaches in quantum chemistry is to calculate the properties of molecules and crystals without the use of any experimental data. [17–19, 24] This calculation involves all atomic particles (the electrons and the nuclei), and the solution is simplified through the Born-Oppenheimer approximation. First, the electronic system is studied for different atomic configurations in order to calculate the potential energy surface and to find the optimized atomic positions corresponding to the minimal total energy per primitive cell. Quantum chemistry of solids concerns mainly those physical and chemical properties of solids that depend on the electronic structure, and they are always connected with the choice of the electronic Hamiltonian. In the case of crystal structures, the approximate electronic Hamiltonians are usually chosen in such a way that the translational and point symmetry of a crystal is maintained. In this chapter we present two of the most popular approximate methods for the description of many-electron systems, the Hartree-Fock method and the density functional theory (DFT). [101, 103, 118, 119]

Which atom arrangement will correspond to a stable or metastable modification depends mostly on the distribution of the electrons. Single atoms of a noble gas are such that the atoms are only weakly interacting, so that the gas phase is thermodynamically

## 4. ELECTRONIC STRUCTURE CALCULATIONS

---

stable at ambient conditions. For all other elements the interaction is strong enough to result in a condensed phase. Only at very high temperatures, single atoms appear and the vapor phase is formed. At ambient conditions atoms have to be linked to produce stable structures. The electrons in a group of atoms (cluster/bulk solid) can only exist in particular states, just as in a single atom. The energies of those states are expressed mathematically as the eigenvalues of the Hamiltonian of the chemical system, and the corresponding wave functions are found as theoretical solutions of the Schrödinger equation [120]:

$$H\Psi = E\Psi \quad (4.1)$$

where  $H$  is the Hamiltonian of a chemical system,  $\Psi$  is the wave function, and  $E$  is the energy of the system.

It is very hard (usually impossible) to find exact mathematical solutions of this equation for a multi-atom system, but we can nevertheless learn much about the wave functions  $\psi$ , and therefore about the electrons in the atomic systems, from experimental data and calculations that employ mathematical approximations. [99–101] Crystals are complex quantum-mechanical systems consisting of a large number of atomic nuclei ( $N_a$ ) and electrons ( $N_e$ ), which can be modeled by the nonrelativistic Hamiltonian ( $H$ )<sup>1</sup>:

$$H_{total} = -\frac{1}{2} \sum_{i=1}^{N_e} \Delta_{\vec{r}_i} - \frac{1}{2} \sum_{j=1}^{N_a} \frac{1}{M_j} \Delta_{\vec{R}_j} + V(\vec{r}_i, \vec{R}_j) \quad (4.2)$$

where,

$$V(\vec{r}_i, \vec{R}_j) = \sum_{j_1 < j_2} \frac{Z_{j_1} Z_{j_2} e^2}{|\vec{R}_{j_1} - \vec{R}_{j_2}|} + \sum_{i_1 < i_2} \frac{e^2}{|\vec{r}_{i_1} - \vec{r}_{i_2}|} - \sum_{i,j} \frac{Z_j e^2}{|\vec{R}_j - \vec{r}_i|} \quad (4.3)$$

and where  $\vec{r}_i$  are the coordinates of the electrons ( $i = 1, 2, \dots, N_e$ ),  $\vec{R}_j$  are the coordinates of the nuclei ( $j = 1, 2, \dots, N_a$ ),  $Z_j$  is the charge of the nucleus  $j$ , and  $V(\vec{r}_i, \vec{R}_j)$  is the energy of the Coulomb interaction of electrons and nuclei (see also section 5.2.1). [101, 103, 118, 119]

---

<sup>1</sup>given in atomic units ( $\hbar = 1, m_e = 1, \dots$ )

Furthermore, by applying the Born-Oppenheimer approximation [121–123] to the wave function  $\psi$ , we separate the electronic and the ionic degrees of freedom:

$$\Psi_{Total} = \Psi_{Electronic} \times \Psi_{Nuclear} \quad (4.4)$$

Next, we solve the equation for the electrons in a static lattice potential of fixed ions. Afterwards we determine the movement of the nuclei around constant average positions and finally take the electron-phonon interaction into account employing perturbative methods. However, usually, the first major approximation when dealing with the electrons is the one-electron approximation, which leads to the Hartree- and the Hartree-Fock approximations. This results in  $N$  coupled one-particle equations, where each electron sees a different average potential generated by the other  $N - 1$  electrons, so we just need to solve this set of one-particle equations iteratively until self-consistency has been reached. For the historical development and detailed reviews of electronic structure calculation, we refer to refs. [101, 103, 118, 119, 124].

## 4.2 Hartree-Fock

The nonrelativistic Hamiltonian  $H$  (4.2) is already an approximation since it does not take into account the spin-orbit interaction and other relativistic effects. Furthermore, the solution to the time-independent Schrödinger equation (4.1) is possible only after applying some additional approximations. The Hartree-Fock (HF) method is such an approximate method for the determination of the ground-state wave function and ground-state energy of a quantum many-body system.[103]

It all started at the end of the 1920's, when D.R. Hartree introduced a procedure, which he called the self-consistent field (SCF) method, to calculate approximate wavefunctions as a product of single electron wavefunctions. His main idea was to solve the many-body time-independent Schrödinger equation (4.1) from fundamental physical principles without use of empirical data, i.e. *ab initio*. At the beginning of the 1930's, Slater and Fock independently pointed out that the Hartree method did not respect the principle of antisymmetry of the wavefunctions. The Hartree method used the Pauli exclusion principle in its older formulation, forbidding the presence of two electrons in the same quantum state. However, this was shown to be fundamentally incomplete in its neglect of quantum statistics. [124–129]

## 4. ELECTRONIC STRUCTURE CALCULATIONS

---

Then, it was shown that the Slater determinant<sup>1</sup>:

$$\Psi_{HF} = \frac{1}{\sqrt{N!}} \begin{bmatrix} \Psi_1(x_1) & \Psi_2(x_1) & \cdots & \Psi_N(x_1) \\ \Psi_1(x_2) & \Psi_2(x_2) & \cdots & \Psi_N(x_2) \\ \vdots & \vdots & \ddots & \vdots \\ \Psi_1(x_N) & \Psi_2(x_N) & \cdots & \Psi_N(x_N) \end{bmatrix} = \frac{1}{\sqrt{N!}} \det [ \Psi_1 \quad \Psi_2 \quad \cdots \quad \Psi_N ] \quad (4.5)$$

satisfies the antisymmetric property of the exact solution and is therefore a suitable Ansatz for applying variational principles. Then the original Hartree method can be looked at as an approximation to the Hartree-Fock method by neglecting exchange.[103, 119, 126, 127, 130] Expressed in a Slater-type or Gaussian-type basis set, the Hartree-Fock equation can be transformed into matrix form called Roothaan equations.<sup>2</sup> Here, we will discuss only the Restricted Hartree-Fock (RHF) method, where the solid is a closed-shell system with all orbitals doubly occupied (two spin states are possible for each electron). The open shell systems, where some of the electrons are not paired, can be dealt with using the Restricted Open-shell Hartree-Fock (ROHF) or Unrestricted Hartree-Fock (UHF) method.[101, 103, 118, 119, 131]

Usually, the Hartree-Fock method is used to solve the time-independent Schrödinger equation for a multi-electron atom, molecule or solid described in the fixed-nuclei approximation by the electronic Hamiltonian  $H$ . However, because of the complexity of the differential equations, the problem is usually impossible to solve analytically, so a numerical technique (usually employing iteration) is applied. The method makes several major simplifications in order to deal with this task: the Born-Oppenheimer approximation is inherently assumed, the effects of electron correlation and relativistic

---

<sup>1</sup>A Slater determinant (named after the physicist John C. Slater) is an expression in quantum mechanics for the wavefunction of a many-fermion system, which by construction satisfies the Pauli principle. The Slater determinant arises from the consideration of a wavefunction for a collection of electrons. A determinant of one-particle orbitals was first used by Heisenberg and Dirac in 1926 [125]

<sup>2</sup>The Roothaan equations are a representation of the Hartree-Fock equation in a non-orthonormal basis set which applies to closed-shell molecules, atoms or solids where all orbitals are doubly occupied. This is generally called Restricted Hartree-Fock theory (RHF). The method was developed independently by Clemens C. J. Roothaan and George G. Hall in the early 1950s [128, 129], and the equations are sometimes called the Roothaan-Hall equations. The Roothaan equations can be written in the form of a generalized eigenvalue problem  $FC = SC\epsilon$ , where  $F$  is the so-called Fock matrix,  $C$  is a matrix of coefficients,  $S$  is the overlap matrix of the basis functions, and  $\epsilon$  is the (diagonal, by convention) matrix of orbital energies. In the case of an orthonormalised basis set the overlap matrix,  $S$ , reduces to the identity matrix. [123, 128, 129]



effects are completely neglected, the wave function is approximated by a single Slater determinant, and the basis set is composed of a finite number of functions.

The Hartree-Fock method is based on the set of approximated one-electron orbitals. For a Hartree-Fock calculation performed for a simple atom, the orbitals are usually set as in the hydrogen atom (an atom with one electron, but the appropriate nuclear charge). However, for more complicated calculations in molecules or bulk crystals, one needs to start from linear combinations of atomic orbitals (LCAO)<sup>1</sup>. At this point, a new approximate Hamiltonian operator, called the Fock operator ( $F$ ), is constructed. Next, the system of equations for one-electron functions in the Hartree-Fock method (also known as the one-electron approximation or self-consistent field (SCF) method as explained below) is obtained from the variational principle minimizing the next functional [101, 103, 119, 131, 132]:

$$\langle E \rangle = \int \psi^* H \psi d \vec{x} \quad (4.6)$$

with the conditions that only anti-symmetric wave functions are admissible, because of the Pauli-principle, and that these wave functions are normalized,

$$\int |\psi|^2 d \vec{x} = 1 \quad (4.7)$$

Then the one-electron functions satisfy the following system of Hartree-Fock equations:

$$F \varphi_i = \varphi_i \varepsilon \quad (4.8)$$

with the Fock operator  $F$  defined as:

$$F = H_0 + J - K \quad (4.9)$$

where  $\varphi$  is a row of functions  $\varphi_i$  and  $\varepsilon$  is the eigenvalue-matrix. In the Fock operator  $F$ , the term  $H_0$  is the one-electron operator,  $J$  is the Coulomb operator and  $K$  is the exchange operator. [103, 119, 130, 132]

---

<sup>1</sup>This gives a collection of one electron orbitals that, due to the fermionic nature of electrons, must be antisymmetrized. In order to deal with this problem, Fock and Slater introduced the anti-symmetry from the outset, by using a Slater-determinant instead of a single product.

## 4. ELECTRONIC STRUCTURE CALCULATIONS

---

Initially, the  $\varphi_i^{(0)}$ , that are used to construct  $J$  and  $K$ , are an educated guess, but the solutions  $\varphi_i^{(1)}$  are already a better approximation to the true Hartree-Fock wave function, and can be used to construct a new Fock-operator. This operator is then used in equation 4.8 and by solving the equation, a new set of approximate one-electron orbitals is obtained, which one then uses to construct a new Fock operator, etc. The procedure is stopped when the change in total electronic energy is negligible between two iterations. In this way, a set of so-called "self-consistent" one-electron orbitals is calculated. The Hartree-Fock electronic wavefunction is then equal to the Slater determinant of these approximate one-electron wavefunctions. In modern Hartree-Fock calculations, the one-electron wavefunctions are approximated by a linear combination of atomic orbitals (LCAO) or so-called Slater-type orbitals. It is very common for the atomic orbitals (AO) to be composed of a linear combination (LC) of one or more Gaussian-type orbitals, rather than Slater-type orbitals, in the interest of saving considerable computational time. Various basis sets are used in practice, most of which are composed of Gaussian functions. [103, 118, 119, 131]

The simplifications in the Hartree-Fock algorithm, especially because of neglecting electron correlations, can lead to large deviations from experimental results. A number of approaches has been developed to deal with this issue (e.g. post-Hartree-Fock methods, MP2 theory, etc). [103, 119, 132] A common alternative to Hartree-Fock calculations is density functional theory (DFT), [130, 132] which includes both exchange and correlation energies, although only approximately. It is also common to use calculations that are a hybrid of the two methods; the popular B3LYP scheme is one such hybrid functional method. [133, 134]

### 4.3 Density Functional Theory (DFT)

The starting point of density functional theory (DFT) is present in the Thomas-Fermi model of a uniform electron gas [135, 136] and the Slater local exchange approximation [125]. However, a real proof for the viability of DFT came much later with the Hohenberg-Kohn theorems [137, 138]. Traditional methods in electronic structure theory, in particular Hartree-Fock theory and its descendants, are based on the complicated many-electron wavefunction. The main objective of DFT is to replace the many-body

### 4.3 Density Functional Theory (DFT)

---

electronic wavefunction with the electronic density as the basic quantity, so DFT can be summarized by the sequence:

$$\rho(r) \rightarrow \Psi(r_1, r_2, \dots, r_N) \rightarrow V(r) \quad (4.10)$$

where knowledge of  $\rho(r)$  implies knowledge of the wavefunction and the potential, and therefore of all other observables.<sup>1</sup> [103, 130, 132]

Hohenberg and Kohn tried to formulate DFT as an exact theory of a many-body system. The formulation applies to any system of interacting particles in an external potential  $V(r)$ , including any problem of electrons and fixed nuclei, where the Hamiltonian for the electrons can be written:

$$H\Psi = [T + V + U]\psi = \left[ -\frac{1}{2} \sum_{i=1}^N \Delta_i + \sum_{i=1}^N V(r_i) + \sum_{i<j} U(r_i, r_j) \right] \Psi = E\Psi \quad (4.11)$$

where  $H$  is the electronic Hamiltonian,  $N$  is the number of electrons and  $U$  is the electron-electron interaction. The operators  $T$  and  $U$  are so-called universal operators as they are the same for any system, while  $V$  is system dependent (non-universal). The potential  $V$  is called the external potential. This may be not only that of nuclei but also include electrostatic or magnetic fields.

DFT is based upon two theorems first proven by Hohenberg and Kohn [137]:

- Theorem I: In a system of interacting particles, the external potential ( $V(r)$ ) can be uniquely determined (except for a constant) by the ground state density  $n_0(r)$ .
- Theorem II: A universal functional for the energy  $E[n]$  in terms of density  $n(r)$  can be defined for any external potential  $V(r)$ . Then the exact ground state energy of the system for a potential  $V(r)$  is the global minimum of this functional, and the density  $n(r)$  that minimizes the functional is the exact ground state density  $n_0(r)$ . [130, 132]

The most common implementation of DFT is through the Kohn-Sham equations obeying the initial Hamiltonian. [138] By solving the equations one finds the ground

---

<sup>1</sup>This also represents the fact that ultimately the electron density and not a wavefunction is the observable.

## 4. ELECTRONIC STRUCTURE CALCULATIONS

---

state density and energy of the original interacting system with accuracy limited only by the approximations in the exchange-correlation functional. The major problem with DFT is that the exact functionals for exchange and correlation are not known except for the free electron gas, and that they cannot be constructed in a systematic fashion. [118, 132, 139–141].

In the last fifty years, DFT has been one of the most popular methods for calculations in the materials sciences. In many cases, DFT with the local-density approximation (LDA) gives satisfactory results for solid-state calculations in comparison to experimental data, at relatively low computational costs when compared to other ways of solving the quantum mechanical many-body problem. Using the generalized gradient approximations (GGA), very good results for molecular geometries and ground state energies have been achieved. However, it was not considered accurate enough for calculations in quantum chemistry until the 1990s, when the approximations used in the theory were greatly refined to better model the exchange and correlation interactions. Today, DFT is one of the leading methods for electronic structure calculations. [118, 131, 139–141]

As we mentioned in the previous section (4.2), it is common to use calculations that are a hybrid of the two methods. A popular functional is known as BLYP.<sup>1</sup> Even more widely used is B3LYP [134, 142, 143], which is a hybrid method in which the DFT exchange functional, in this case from BLYP, is combined with the exact exchange functional from Hartree-Fock theory. Unfortunately, although the results obtained with these functionals are usually sufficiently accurate for most applications, there is no systematic way of improving them. Therefore in the current DFT approach it is not possible to estimate the error of the B3LYP calculations without comparing them to the calculations obtained with another method or with experimental data [118, 123, 131, 139–141].

---

<sup>1</sup>from the names Becke, Lee, Yang and Parr.

Part III  
Methods



## 5

# Methods and software available in the research group

*"Et ipsa scientia potestas est."/"And knowledge itself, is power."*

(Francis Bacon (1561-1626), English philosopher, statesman, scientist, lawyer, jurist, author and pioneer of the scientific method) [144]

### 5.1 Global and local optimization

Theoretical structure prediction in solid state chemistry can be addressed in terms of searching for a minimum of an energy (cost) function defined over a space of acceptable solutions. A variety of methods have been developed to deal with this issue and they can generally be divided into the global and the local optimization stage. [24, 145, 146]

The local optimization explores only a limited region of the energy landscape, usually by following some downhill route from a starting point, locating one or more local minima along the way, while the global optimization approach can, in principle, locate the global minimum. Sometimes, local optimization procedures are used as a global optimization tool, since by a multiple application of the algorithm from many different starting points one should eventually hit upon the global minimum. This approach is pretty successful if only very few widely separated minima are present on the energy landscape. However, in many cases, the landscape possesses a large number of minima, so the local optimizations usually get stuck in the high energy region of the landscape. Usually, multiple local optimizations instead of a global optimization are not very effec-

## 5. METHODS AND SOFTWARE AVAILABLE IN THE RESEARCH GROUP

---

tive, unless one has an efficient way of choosing starting points based on e.g. chemical or physical intuition.[17, 18, 24]

Therefore, global optimization methods have to be employed, in order to obtain a good sample of the low-lying minima, and in many cases the global minimum. There are several global optimization approaches: deterministic (the most successful are branch and bound methods and methods based on real algebraic geometry), stochastic (several Monte-Carlo-based algorithms exist such as simulated annealing (SA), direct Monte-Carlo sampling, stochastic tunneling, parallel tempering, Monte-Carlo with minimization, etc) and heuristics (or metaheuristics). Heuristic strategies include evolutionary algorithms (e.g., genetic algorithms), swarm-based optimization algorithms (e.g., particle swarm optimization and ant colony optimization), memetic algorithms, and algorithms combining global and local search strategies [63, 70–72, 123, 145, 147–151]. Usually for structure prediction and energy landscape investigations we use simulated annealing (implemented in the G-42 code - see Appendix). Once we have chosen simulated annealing as our GO method, in the following procedure one defines the system as a set of  $N$  atoms located inside a periodically repeated unit cell, where the atom positions, electric charges, and the cell parameters can be varied. <sup>1</sup> In this way we obtain a large set of several hundreds or thousands of structural configurations that correspond to local minima on the energy landscape. [18, 24]

In the next step, these configurations are refined (also by automated structure refinement programs [131, 152, 153]) in order to remove duplicates and to sort them in structure families. For the remaining set of structure candidates, two successive minimizations are performed: a quench (using the G-42 code), using the same moveclass and the same level of accuracy for the energy calculations as in simulated annealing, and subsequently a local optimization, usually on the *ab initio* level (using the CRYSTAL09 code) at a high level of accuracy. The local optimizations employed analytical gradients with respect to the atom positions [154, 155], and the cell parameters [156, 157], and a local optimizing routine [158], sometimes combined with a heuristic algorithm that employs an automated nested minimization scheme and structure refinement. [131, 152, 153] The local optimization is usually performed both with the Hartree-Fock approximation

---

<sup>1</sup>When the GO is performed in order to calculate clusters, usually one employs a fixed large simulation cell, and varies only the atomic positions.



and on the DFT level, using several density functionals (e.g. LDA, B3LYP).<sup>1</sup> Finally, the E(V)-curves for all structure candidates are computed, which allows us to decide which of the possible modifications is thermodynamically stable and which of them are close in energy but metastable, at a given pressure and temperature. [17, 18, 24, 131]

## 5.2 Choice of the energy (cost) function

In order to perform structure prediction calculations or energy landscape investigations, one needs to define the energy (cost) function and the neighborhood structure, i.e. the moveclass that controls the dynamics. In the ideal case one should try to perform as much as possible of the calculation on the *ab initio* level, but a major problem is the computational time required for each energy evaluation. This means that approximations are necessary, and the degree of simplification is chosen dependent on the purpose of the calculation. Generally, we consider the following aspects of the energy function: computational time, global/local accuracy/applicability, transferability, representation, robustness, availability. [17, 18, 24, 131]

In some cases (e.g. structure determination), various kinds of external constraints or final optimization goals need to be taken into account. Usually, these are most effectively implemented by modifying the energy landscape through addition of penalty terms or replacing it by some cost function landscape. Similarly, the optimal neighborhood structure (moveclass) will also depend on the problem under investigation, e.g. stochastic investigations give more freedom in the choice of moveclass. For example, in the stability analysis using the threshold algorithm, only physically valid moves should be used, since the details of the barrier structure must be preserved. However, in the global optimizations one can employ moves that allow jumps between widely separated regions of the energy landscape, as long as the physically relevant minima remain unchanged.[17, 18, 24]

---

<sup>1</sup>This final comparison of the results for different *ab initio* methods is very important, especially for structure prediction in chemical systems where no experiments have been performed, so the only way to gain some insight into the quality and robustness of the results is the comparison of the results obtained from different theoretical methods.

## 5. METHODS AND SOFTWARE AVAILABLE IN THE RESEARCH GROUP

---

### 5.2.1 Simple and high quality empirical potentials

There exist a large number of empirical potentials that have been used in structure prediction and modeling of ionic compounds. These range from two-body potentials like the Buckingham-potential [159], the Born-Huggins-Meyer-potential [160], or a refined version with environment dependent radii [161, 162], over dipole [163] and quadrupole [164] shell models, to various kinds of breathing potentials [33, 165–178] of increasing levels of refinement. The latter ones are discussed in more detail in refs. [179–181].

It is an open question which potential is best to use; if one wants to compute at least some properties of a given material with relatively high accuracy, then one should, in principle, use the more refined potentials. However, usually they are quite complicated, computationally expensive and they need good experimental background for fitting the parameters. Since we are performing calculations in unknown systems with high complexity and without any experimental data, these complex potentials are not always suitable. It was also observed that many of these potentials strongly favor the structure(s) to which they have been fitted, and even successfully reproduce their properties, but at the same time, these potentials often weaken or even eliminate the minima representing important alternative modifications on the landscape of the chemical system. In the following part, we will describe the energy function and empirical potentials used in our group.

The energy function used for calculating the potential energy is a combined Coulomb and Lennard-Jones potential for non-covalent and partly covalent bonds. The long-range forces are calculated by Ewald summation in the formulation of De Leeuw [182], that also contains the dipole correction to the total energy, which needs to be included in some special cases. [183, 184] The repulsion between neighboring ions is controlled by the  $r^{-12}$  term in the Lennard-Jones part while the attraction due to the polarization of the ions is expressed by the van der Waals  $r^{-6}$  term. The energy function for  $N$  atoms takes the form:

$$E = \frac{E_{(total)}}{N} = \frac{E_{(Coulomb)}}{N} + \frac{E_{(Lennard-Jones)}}{N} \quad (5.1)$$

where

$$E_{(Coulomb)} = \frac{q_i q_j}{4\pi\epsilon\epsilon_0 r_{ij}} = k_e \frac{q_i q_j}{r_{ij}} \quad (5.2)$$

## 5.2 Choice of the energy (cost) function

---

with

$$k_e = \frac{1}{4\pi\epsilon\epsilon_0} \quad (5.3)$$

and

$$E_{(Lennard-Jones)} = 4 \epsilon_{ij} \left[ \left( \frac{\sigma_{ij}}{r_{ij}} \right)^6 - \left( \frac{\sigma_{ij}}{r_{ij}} \right)^{12} \right] \quad (5.4)$$

with  $\sigma_{ij} = (R_i + R_j) r_s$ . [17, 18, 24, 52]

Here  $\mathbf{r}_{ij}$  is the vector between the ions  $i$  and  $j$ ,  $R_i$  and  $R_j$  are the radius of the ions  $i$  and  $j$ , while  $r_s$  is the radius scale factor. Variables  $q_i$  and  $q_j$  correspond to the effective charges, and  $\epsilon_{ij}$  is the Lennard-Jones parameter, which is usually fitted to experimental data.  $\epsilon_0$  is the permittivity of a vacuum, and  $k_e$  is the Coulomb constant. The specific dielectric constant  $\epsilon$  is usually set equal to 1, since we deal with atom-atom interactions. [17, 18, 24, 52]

The Lennard-Jones potential contributes usually about 10% of the total energy [185], while the order of magnitude for  $\epsilon_{ij}$  has been chosen accordingly.<sup>1</sup> The parameters are usually varied over a relatively wide range of physically reasonable values in order to study their influence on the resulting landscape [15].

The ionic radii, which are taken from the literature [186], in the sum  $\sigma_{ij} = (R_i + R_j) r_s$  are scaled by altering the radius scale factor parameter ( $r_s$ ) in the Lennard-Jones part of the potential. The charge is always the formal charge of the ion corresponding to the point charge model for lattice energy calculations. In order to overcome the limitations of the simple potential as much as possible while still retaining its advantages, we repeat our global explorations for slightly varied values of the parameters  $r_s$  and  $\epsilon_{ij}$ .<sup>2</sup> [15]

### 5.2.2 Pseudopotentials and basis sets used in the *ab initio* methods

Quantum chemical calculations are usually performed using a finite set of basis functions. The choice of the basis set becomes very important in periodic systems with a variety of chemical bonding. Three basic types of basis sets define three types of

---

<sup>1</sup>In this work, the parameters  $\epsilon_{ij}$  and  $r_s$  in the potential have not been fitted to experimental values, since the necessary data are not available for every relevant structure candidate.

<sup>2</sup>For the same reason, the Lennard-Jones parameters  $\epsilon_{ij}$  are usually chosen to be independent of the ion types, so that the ions present in the system are only characterized by the ionic charge and ionic radii of the potential.

## 5. METHODS AND SOFTWARE AVAILABLE IN THE RESEARCH GROUP

---

methods of the electronic structure calculations in crystals: atomic-sphere (AS) methods, plane-wave (PW) methods, and linear combination of atomic orbitals (LCAO) methods. Each of these methods has its advantages and disadvantages. [103, 132]

In this work a basis composed of a finite number of atomic orbitals, centered at each atomic nucleus within the solid (LCAO) was used.<sup>1</sup> Initially, these atomic orbitals have typically been Slater-type orbitals, which corresponded to a set of functions which decayed exponentially with distance from the nuclei like the hydrogen wave function. However, later it was realized that these Slater-type orbitals could in turn be approximated as linear combinations of Gaussian orbitals, which led to huge computational savings [103, 118, 131, 132, 139–141, 187]. In molecular quantum chemistry two types of atomic like basis sets are used: Slater-type orbitals (STO) and Gaussian-type orbitals (GTO).<sup>2</sup> [188]

There are many types of basis sets composed of Gaussian-type orbitals. They are typically composed of the minimum number of basis functions required to represent all of the electrons on each atom. Polarization functions can be added in order to achieve some flexibility within the basis set. A common naming convention for minimal basis sets is STO-XG, where X is an integer. This X value represents the number of Gaussian primitive functions. In these basis sets, the same number of Gaussian primitives comprise core and valence orbitals. Minimal basis sets typically give rough results but are much cheaper than their larger counterparts [118, 139–141, 188, 189]. The valence electrons usually contribute most of the bonding in molecules and solids. Due to this fact, it is common to represent valence orbitals by more than one basis function, (each of which can in turn be composed of a fixed linear combination of primitive Gaussian functions). The notation for these split-valence basis sets is typically X-YZg, where X represents the number of primitive Gaussians comprising each core atomic orbital basis function, and Y and Z indicate that the valence orbitals are composed of two basis functions each. The first one is composed of a linear combination of Y primitive Gaussian functions, and the other is composed of a linear combination of Z primitive Gaussian functions. Basis sets in which there are multiple basis functions

---

<sup>1</sup>A number of electronic structure calculation programs (e.g. WIEN, VASP) employ very large plane-wave sets. Those are often combined with pseudopotentials, since the wave functions of the inner electrons are very expensive to describe using only plane waves.

<sup>2</sup>It is not really correct to call them orbitals. They are better described as basis set functions, since they are Slater-type or Gaussian-type functions used to approximate the shapes of the orbitals defined as one-electron wavefunctions.

corresponding to each atomic orbital, including both valence orbitals and core orbitals or just the valence orbitals, are called double, triple, or quadruple-zeta basis sets. [103, 131, 132, 188].

The idea behind effective core potentials (ECPs), also known as pseudopotentials (PP), is to treat the core electrons as creating effective averaged potentials rather than actual particles. Effective core potentials are based on the frozen-core approximation and serve to represent the potential generated by core electrons. Application of the ECP is computationally efficient, as it allows formulation of a theoretical method for dealing only with the valence electrons, while retaining the accuracy of all-electron methods. [103, 127, 132]

Useful links for the pseudopotentials and basis sets, which have been used in this work, can be found on the following web pages: CRYSTAL [190–192], Stuttgart/Cologne group [193–195], EMSL [196–198], etc. The energy-consistent pseudopotentials are semi-local pseudopotentials adjusted to reproduce atomic valence-energy spectra. The adjustment of the pseudopotential parameters has been done in fully numerical calculations, and the valence basis sets have been generated *a-posteriori* via energy optimization. The complete set of potentials includes one-component (non-relativistic and scalar-relativistic) effective-core potentials (ECP), spin-orbit (SO) and core-polarization potentials (CPP). [190, 193, 196]

### 5.3 Simulated annealing

The simulated annealing approach is based on simple concepts of physical annealing. When we heat a metal high enough for it to melt, the atoms become disordered. With slow cooling, the atoms may crystallize in an ordered state, with the energy reaching the global minimum. If the temperature is decreased too rapidly (the system is "quenched") or if the initial temperature is too low, then the system may freeze into a glassy state or a crystalline structure with defects such as vacancies and dislocations.[8, 19, 63, 72]

In the computational simulated annealing method the atom configuration is continually changed at each temperature using either molecular dynamics or a Monte Carlo scheme, where move class operators are applied to move a random number of ions within the current structure candidate, and the Metropolis criterion is used to

## 5. METHODS AND SOFTWARE AVAILABLE IN THE RESEARCH GROUP

---

determine whether the Monte Carlo move is accepted or rejected. The initial temperature within the molecular dynamics simulation (or Metropolis criterion) is chosen such that the kinetic energy is high enough to allow the system to easily overcome energy barriers between local minima. The temperature reduction permits a configuration with lower potential energy to be obtained and decreases the probability of jumps between local minima. If the annealing process is continued and carried out slowly enough, the final structure is most likely to be the global minimum of the investigated system.[8, 19, 24, 63, 72]

In this work, the global optimizations were performed employing the stochastic simulated annealing algorithm [70–72], which is based on random walks on the energy landscape (see below). Each step from configuration  $x_i$  to a neighbor  $x_{i+1}$  is accepted according to the Metropolis criterion [199], with a temperature schedule  $T_n = T_0\gamma^n$  ( $\gamma = 0.95, \dots, 0.995$ ). The moveclass usually consisted of atom movement (80% of all the moves), atom exchange (5% of all the moves), and random variations of the cell parameters (15% of all the moves), keeping the ionic charges fixed. The global optimization simulated annealing procedure is implemented in the program package **G42** with the possibility of using the *ab initio* **CRYSTAL09** or the **VASP** code for energy calculations (see Appendix and refs. [16, 17, 190–192, 200, 201]).

### 5.4 Monte-Carlo methods

In a Monte Carlo simulation, we attempt to follow the "time dependence" of a model for which change does not proceed in some rigorously predefined fashion<sup>1</sup>, but rather in a stochastic manner which depends on a sequence of random numbers which are generated during the simulation one after another. With a second (different) sequence of generated random numbers, the simulation will not give identical results but will produce values which agree with those obtained from the first sequence within "statistical error". Considering problems of statistical mechanics, we may attempt to sample a region of phase space, in order to estimate certain properties of the model, although we may not be moving in phase space along the same path which an exact solution to the physical dynamics of the model would produce. [202, 203]

---

<sup>1</sup>e.g. according to Newton's equations of motion.

Monte Carlo (MC) methods are used for simulating the behavior of a system (e.g. chemical, physical, mathematical, etc.), and this is performed in a stochastic fashion, i.e. by using random numbers in the moveclass that produce next configuration, which is the main difference to the deterministic methods such as molecular dynamics. [204]. The MC algorithm works as following: one (or many) walker at configuration  $i$  at time step  $t$  chooses one of the neighbor configurations as test configuration  $j$ . If this configuration fulfills an acceptance criterion, the walker moves to  $j$ ; otherwise, it remains at  $i$ . The classical MC usually employs the ratio of the Boltzmann-factors of configurations  $i$  and  $j$  as acceptance criterion (the so-called Metropolis criterion [199]). If the energy of state  $j$  is equal or below the one of state  $i$ , the move is accepted. If  $E(j) > E(i)$ , the move is only accepted with probability  $\exp(-(E(j) - E(i))/C)$ , where  $C$  is a control parameter. Such a weighted random walk can be used in order to simulate the ensemble average of the chemical system at temperature  $T = C/k_B$ . When a stochastic quench is employed, only downhill moves are accepted ( $T = C = 0$ ). [19, 24, 63, 131]

If we now combine simulated annealing as a global optimization method [70–72] with Monte Carlo methods using the Metropolis criterion, then each points of the search space would correspond to a state of some physical system, and the function  $E(s)$  as the internal energy of the system in that state. Thus, the aim is to bring the system, from an arbitrary initial state, to a state with the lowest possible energy. At each step, the SA moveclass considers some neighbor  $s'$  of the current state  $s$ , and, as in the MC simulations described above, decides between moving the system to state  $s'$  or staying in state  $s$ . Upon lowering the temperature, the calculated ensemble becomes more concentrated at low energies. The sequence of temperatures is chosen such that the system ultimately tends to move to states with lower energy. If one decreases the control parameter  $C$  slow enough, the random walk will end up in the global minimum of the system. Usually, this step is repeated until the system reaches a state which is good enough for the particular application. [19, 24, 63, 131] Various stochastic Monte Carlo and quench procedures are implemented in the program package **G42** [16, 17].

## 5.5 Gradient-based methods

The simple stochastic (or random search) methods described here are very general and they can be applied to both discrete and continuous landscapes [19, 24, 63]. On the other

## 5. METHODS AND SOFTWARE AVAILABLE IN THE RESEARCH GROUP

---

hand, these algorithms do not take available local information such as the derivatives of the cost function into account. Such information is used in those classes of algorithms that follow the gradient downhill (such as gradient descent, line search) or take, in addition, second derivatives into account (conjugated gradient, Newton-Raphson, etc. [123, 131, 149, 151]). A simple gradient-based method is implemented in the program package **G42**, and more refined local minimizations are accessible by calling the **GULP** code [205–207] from the **G42** program [16, 17].

### 5.6 Genetic algorithms

Another big class of global optimization methods are the so-called genetic algorithms [8, 19, 24, 63, 73–75], but since this method was not used in this work, we will give just a short outline. A genetic algorithm (GA) is a search technique used in computer science to find approximate solutions to optimization and search problems. Genetic algorithms are a particular class of evolutionary algorithms that use techniques inspired by evolutionary biology such as inheritance, mutation, natural selection, and recombination (or crossover) [75, 208].

Typically, different random arrangements of atoms make up each candidate structure in the initial population of structures. The algorithm works by mimicking Darwinian evolution<sup>1</sup>, the basic tenets of which are that offspring resemble their parents and that procreation is a reward for success. Applied in the framework of the exploration of the energy landscapes this means that an ensemble of configurations with the lowest energy survives preferentially from one generation to the next. The selection criteria can vary between two extremes: only those configurations with the lowest energy survive, or all new configurations always survive (at least for one generation). Between these two extremes one uses probabilistic criteria analogous to the Metropolis criterion. [8, 19, 24, 63, 131, 208] Software available in our group for performing calculations with the genetic algorithm is the **GULP** program. [205–207]

---

<sup>1</sup>or in some cases Lamarckian evolution.



## 5.7 The threshold-algorithm

The threshold algorithm was originally developed as an implementation of the lid algorithm for the study of the barrier structure of continuous landscapes.<sup>1</sup> [16, 17, 19, 24, 210–212]

The threshold algorithm performs an exploration of subregions of the landscape: A subregion is defined as all the states that can be reached from some starting minimum without crossing the energy lid (threshold). The exploration of the region below the lid is performed using random walks with a simple acceptance criterion: The move is accepted, if the energy of the new configuration is below the current lid; otherwise, the move is rejected. The moveclass consisted of atom movements (85% of all moves) and random variation of the cell parameters (15% of all moves), keeping the ionic charges fixed. The periodically repeated quench runs were typically performed every 50.000 steps. The energy difference between successive lids was 0.1 eV/atom. By connecting the results of the explorations of many subregions, one gains a detailed overview over the connectivity of the whole landscape, including the energetic and entropic barriers, which allows us to construct the tree graph of the investigated system. [16, 17, 19, 24, 131] The threshold algorithm is implemented in the program package **G42** [16, 17].

## 5.8 The prescribed path algorithm

The prescribed path method allows us to explore transition routes and barriers between even distant minima, as well as gain more insights into the temperature dependence of the synthesis and transformation processes in the system. Transition state structures can be determined by searching for first-order saddle points on the potential energy surfaces or, in other words, on the energy landscapes (see chapter 2.1). In the past decades, many new methods were developed in order to search for transition states, e.g. the nudged elastic band method [213] and its variants [214, 215], the dimer method [216] and its variants [217], adaptive kinetic Monte Carlo [218], Bader charge density analysis [219], the string method [220] and its variants [221], transition path sampling [222] and its variants [223], transition networks [224], and others. However, locating transition

---

<sup>1</sup>There are others examples, e.g. a lid-based global optimization technique such as the deluge algorithm, where the energy lid that must not be crossed during the random walk is slowly lowered from very high lid values, squeezing the walker into a low energy minimum [209].

## 5. METHODS AND SOFTWARE AVAILABLE IN THE RESEARCH GROUP

---

states is often quite difficult and none of the methods developed can guarantee to find the right transition state. Each method has its advantages and disadvantages depending on the particular investigation, and very often methods are combined, so there is no strict border where one method ends and another begins (an overview of some of the main methods can be found in refs. [7, 62, 225, 226]).

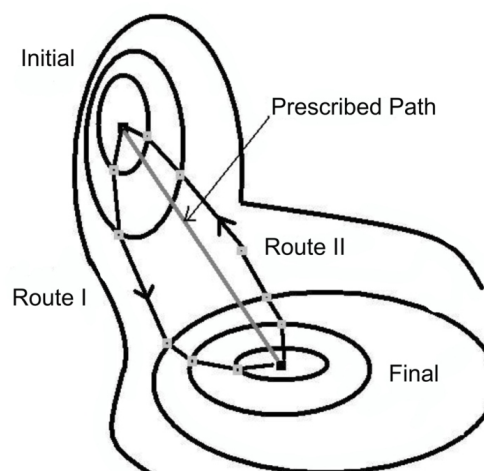


**Figure 5.1: A simplified model of the prescribed path algorithm** - Two separate minima, representing initial and final atom configuration, are connected in a high dimensional space via a prescribed path, where they can relax to different transition routes.

Similarly, the prescribed path (PP) algorithm, which we present here, is related to the nudged elastic band (NEB) method. [213] The method works by optimizing the atom arrangement at a number of intermediate steps along a "reaction path" (see figure 5.1). In contrast to e.g. the classical NEB-method, the stochastic relaxation and/or Monte Carlo simulation during the PP-runs can yield several relaxed paths, competing with each other. In particular, the simulations at finite temperature allow us to cross small barriers in the direction orthogonal to the reaction coordinate (see chapter 6.1). Therefore the transition route associated with one given prescribed path can consist of a bundle of similar but different individual transition paths [62].<sup>1</sup>

---

<sup>1</sup>Note that in order to avoid differences in the number of atoms/number of formula units of the initial and final structure, these structures must be appropriately enlarged or reduced to the same size while keeping their structure type fixed. For this, we employ several tools and algorithms implemented in the KPLLOT program, such as MTRI, TZ, and RPSY; for details see the **KPLLOT** manual [227].

## 5.9 Structure refinement software

When performing global and local optimizations in a chemical system, one encounters several problems related to structure prediction and determination. First, we note that the large number of structure candidates will usually not exhibit any obvious symmetries (they are given in space group  $P1$ , due to the unrestricted optimization procedure), which is especially the case when using a simple empirical potential as a cost function. To deal with this issue, we use several algorithms SFND [228], RGS [229] and CMPZ [230] that have been implemented in the program **KPLOT**. [227] SFND [228], short for "SymmetrieFiNDer" (= symmetry finder), identifies all symmetries of a periodic structure, where only the atomic coordinates are given as input. RGS [229], short for "RaumGruppenSucher" (= space group searcher), determines for a given set of symmetries the space group of the structure. Finally, CMPZ [230], short for "CoMPare Zellen" (= compare cells), performs a comparison of a given pair of periodic structures, and determines, whether these structures are the same within some given set of tolerances. With the help of these algorithms we can determine the symmetries and space groups of all minimum configurations of the enthalpy landscapes we have identified, eliminate duplicates and group these structures into families. For more details on the working of these algorithms, we refer to the references given.

Second, if one uses empirical parameters for the ionic radii and Lennard-Jones-interaction strengths, the nearest-neighbor distances among the atoms are not necessarily in agreement with those one would observe in experiment. Both the size of the unit cell and the relative atom positions might differ somewhat from the experimental values, making a comparison between predicted and subsequently synthesized compounds difficult.[131]

Third, our calculations produce large numbers of structure candidates. Since this number can vary between several hundreds and several thousands in one chemical system, it is very hard to manually perform the structure analysis. In order to bypass this problem, we perform an automated determination of the symmetries and space groups of the structures using the **LOAD** program [131], and eliminate duplicate structures using the **FILTER** program [131].

## 5. METHODS AND SOFTWARE AVAILABLE IN THE RESEARCH GROUP

---

## 6

# New methods and techniques developed or applied during this research

*"All truths are easy to understand once they are discovered; the point is to discover them."* (Galileo Galilei (1564-1642), Italian physicist, mathematician, astronomer, and philosopher) [231]

### 6.1 New modifications and applications of the prescribed path algorithm

For the first time the prescribed path algorithm was used for stability estimates of different modifications, the analysis of the barriers separating them on the landscape and to connect theoretical results to real experimental observations. We employ this algorithm for finding transition regions and minimum energy paths between various locally ergodic regions. In its most simple version (see figure 6.1), the prescribed path algorithm performs a set of local minimizations (e.g. via a gradient descent or stochastic quench) starting from points along a well-defined route on the energy landscape or within a well-defined set of points on the energy landscape. These points are generated by varying atom positions, e.g. by atom displacements, rotation of groups of atoms or atom exchange, and / or by variation of cell parameters. Typically, such a route is defined by selecting a path (often essentially a straight line) between a pair of starting-

## 6. NEW METHODS AND TECHNIQUES DEVELOPED OR APPLIED DURING THIS RESEARCH

---

and end-point configurations, or via the free (rotational) movement of a group of atoms (e.g. in structures with rotating complex anions [26]), or by the change of the cell parameters from one unit cell to another one, while keeping the relative atom positions fixed. [56] Another available option works by using atom exchange moves for generating points along the path; this allows the exploration of large multi-minima regions on the landscape such as those involved in chemical order-disorder transitions (see figure 6.1 and refs. [26, 40]).

In addition to local minimizations, the prescribed path algorithm allows us to perform Monte Carlo (MC) simulations (see section 5.4) at a given (set of) temperature(s) starting from the points along the path, with the option of performing a subsequent local minimization. During the random quenches and the MC simulations, the (random) choice of moves can be completely free or restricted to some coordinates and/or cell parameters. A special case of the prescribed path explorations are those, where the constant temperature explorations and minimizations are confined to the plane orthogonal to the line connecting two structures in the cell parameter-plus-atom position space. Note that this is only possible for those prescribed paths that are defined via a straight-line connection of two configurations (or at least a piece-wise straight line), otherwise one cannot define an orthogonal plane. Of course, we can again perform stochastic quenches, simulated annealing or Monte Carlo runs at constant temperature, in order to explore the cross sections of the landscape orthogonal to the prescribed path. [56, 62]

### 6.1.1 Stability analysis via constant temperature Monte Carlo simulations

In a preliminary study, short stochastic constant temperature Monte Carlo walks on the energy landscape were used to gain information about the thermal stability of the minimum structures that served as starting and final points of the prescribed path investigations.

For example in the ZnO system, in each run 8 atoms (4 Zn, 4 O) per cell were used, and as starting points we chose the wurtzite, the sphalerite, the rock salt, the "5-5", the nickel arsenide and the  $\beta$ -BeO structure type. The temperatures selected varied from 50 - 1000 K, and for each temperature and starting structure, 100 runs consisting of 10000 MC steps at the given temperature followed by 5000 quench steps were performed. Both

## 6.1 New modifications and applications of the prescribed path algorithm

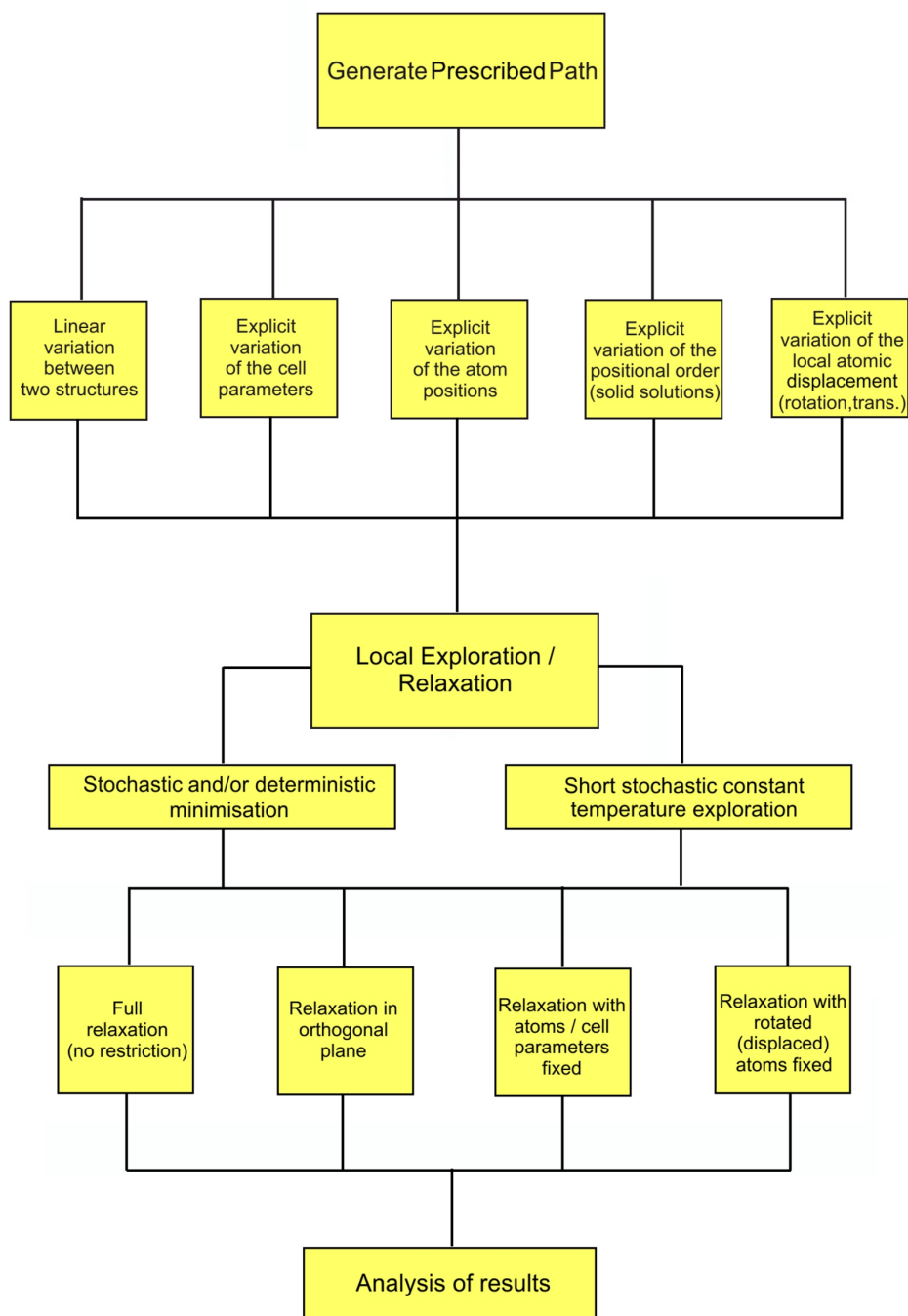


**Figure 6.1: Flowchart of the prescribed path (PP) algorithm** - The flowchart shows a variety of possible modules or procedures in the prescribed path algorithm, from the beginning stage, when a prescribed path between two structures is generated, through different optimization routines, until the final stage of analysis.

## 6. NEW METHODS AND TECHNIQUES DEVELOPED OR APPLIED DURING THIS RESEARCH

---

the atom positions (90% of all Monte Carlo steps shift an individual atom, 5% swap the positions of two atoms) and the parameters of the periodically repeated simulation cell (5% of all Monte Carlo steps) were freely varied during the random walks [62].<sup>1</sup>

### 6.2 Phonon "supercell" technique in CRYSTAL09

We present here the procedure for the calculation of the phonon spectra (new in the **CRYSTAL09** code) via a supercell technique, where the supercells are defined by a matrix that multiplies the cell vectors in direct space. The straightforward way would be to employ a huge supercell, e.g. with a matrix:

$$\begin{bmatrix} N & 0 & 0 \\ 0 & N & 0 \\ 0 & 0 & N \end{bmatrix} \quad (6.1)$$

with e.g.  $N = 5$ . However, this is prohibitively expensive for the *ab initio* calculations at present time. Therefore, we computed the phonon dispersion in the most important directions of the reciprocal lattice, where specific smaller matrices can be used. [57]

For example, the  $\Gamma$ -X direction [232] in the reciprocal *fcc* lattice corresponds to the line from  $(0, 0, 0)$  to  $(\frac{1}{2}, 0, \frac{1}{2}) = \frac{1}{2}\vec{b}_1 + \frac{1}{2}\vec{b}_3$  where the vectors  $\vec{b}_1$ ,  $\vec{b}_2$ , and  $\vec{b}_3$  are the reciprocal lattice vectors corresponding to the primitive vectors of the direct lattice. To obtain the dispersion in this direction, a supercell derived from the reciprocal lattice vectors  $\vec{b}_1$ ,  $\vec{b}_2$ , and  $\frac{\vec{b}_1 + \vec{b}_3}{N}$  is chosen, where  $N$  is proportional to the number of points along the given direction. According to the usual transformation between reciprocal and direct lattice [101];

$$\vec{a}_1 = \frac{2\pi(\vec{b}_2 \times \vec{b}_3)}{(\vec{b}_1)(\vec{b}_2 \times \vec{b}_3)}; \vec{a}_2 = \frac{2\pi(\vec{b}_3 \times \vec{b}_1)}{(\vec{b}_1)(\vec{b}_2 \times \vec{b}_3)}; \vec{a}_3 = \frac{2\pi(\vec{b}_1 \times \vec{b}_2)}{(\vec{b}_1)(\vec{b}_2 \times \vec{b}_3)}, \quad (6.2)$$

the corresponding direct cell is then obtained as  $\vec{a}_1 - \vec{a}_3$ ,  $\vec{a}_2$  and  $N\vec{a}_3$ . As a whole, the supercell matrix is therefore:

$$\begin{bmatrix} 1 & 0 & -1 \\ 0 & 1 & 0 \\ 0 & 0 & N \end{bmatrix} \quad (6.3)$$

---

<sup>1</sup>We note that this method for analyzing the stability of a given minimum configuration is complementary to the threshold runs starting from this structure, where the temperature of the random walker is set to infinity but only moves to states below a sequence of energy lids are allowed. [62]



## 6.2 Phonon "supercell" technique in CRYSTAL09

---

For example, with  $N = 2$ , we obtain the X-point in addition to the  $\Gamma$ -point.

Further important directions in the reciprocal lattice corresponding to the direct *fcc* lattice are:

$\Gamma$ -L: from  $(0, 0, 0)$  to  $(\frac{1}{2}, \frac{1}{2}, \frac{1}{2})$  in reciprocal space; use as reciprocal lattice vectors:  $\vec{b}_1$ ,  $\vec{b}_2$ , and  $\frac{\vec{b}_3}{N}$  with the corresponding supercell matrix:

$$\begin{bmatrix} 1 & 0 & 0 \\ 0 & 1 & 0 \\ 0 & 0 & N \end{bmatrix} \quad (6.4)$$

$\Gamma$ -K-X: from  $(0, 0, 0)$  to  $(\frac{1}{2}, 1, \frac{1}{2})$  in reciprocal space; use  $\vec{b}_1$ ,  $\vec{b}_2$ , and  $\frac{(\vec{b}_1 + 2\vec{b}_2 + \vec{b}_3)}{N}$  with the corresponding matrix:

$$\begin{bmatrix} 1 & 0 & -1 \\ 0 & 1 & -2 \\ 0 & 0 & N \end{bmatrix} \quad (6.5)$$

In case of the rhombohedral lattice, the directions in the Brillouin zone are obtained according to ref. [232].

$\Gamma$ -Z: from  $(0, 0, 0)$  to  $(\frac{1}{2}, \frac{1}{2}, \frac{1}{2})$  in the reciprocal space; use  $\frac{(\vec{b}_1 + \vec{b}_2 + \vec{b}_3)}{N}$ ,  $\vec{b}_2$ ,  $\vec{b}_3$  as reciprocal lattice vectors, with the corresponding matrix:

$$\begin{bmatrix} N & 0 & 0 \\ -1 & 1 & 0 \\ -1 & 0 & 1 \end{bmatrix} \quad (6.6)$$

$\Gamma$ -L: from  $(0, 0, 0)$  to  $(0, \frac{1}{2}, 0)$  in the reciprocal space; use as reciprocal lattice vectors:  $\vec{b}_1$ ,  $\frac{\vec{b}_2}{N}$ ,  $\vec{b}_3$  with the corresponding matrix:

$$\begin{bmatrix} 1 & 0 & 0 \\ 0 & N & 0 \\ 0 & 0 & 1 \end{bmatrix} \quad (6.7)$$

$\Gamma$ -F: from  $(0, 0, 0)$  to  $(\frac{1}{2}, \frac{1}{2}, 0)$  in reciprocal space; use as reciprocal lattice vectors:  $\frac{(\vec{b}_1 + \vec{b}_2)}{N}$ ,  $\vec{b}_2$ ,  $\vec{b}_3$  with the corresponding matrix:

$$\begin{bmatrix} N & 0 & 0 \\ -1 & 1 & 0 \\ 0 & 0 & 1 \end{bmatrix} \quad (6.8)$$

This procedure is as efficient as possible, as we require only supercells with size  $N$ ,

## 6. NEW METHODS AND TECHNIQUES DEVELOPED OR APPLIED DURING THIS RESEARCH

---

and not  $N^3$ , as would be necessary if we were to compute the phonon dispersion for all the directions at the same time. [62]

### 6.3 New visualization techniques developed and applied in energy landscape representation

The use of graphs in order to represent some numbers is a quite recent invention, dating from the middle of the XVIII century, when first quantities, time series, scatterplots, and multivariate displays appeared. [233–235] Modern graphs are able to do much more than just to replace statistical data and tables. In order to reach graphical excellence one should: show the original data without distortions, focus the viewer on the substance (rather than on the methodology, design, etc.), use the smallest space possible, make large data sets coherent, when possible give different perspectives, and give a good and clear explanation and description. [233–235] However, it is not trivial to achieve this excellence in the graphical visualization in different fields of sciences, e.g. the data interpretation can be addressed differently in social sciences [233–235], chemistry [236–238], quantum mechanics [239, 240], etc .

In the graphical visualization of the energy landscape, one encounters several problems, such as the high-dimensional space, complicated barrier structures, etc. Therefore, finding a low-dimensional representation of the energy landscape and analyzing its features would be a significant step forward and provide us with new insights about the specific system. There are two basic approaches to this subject in molecules so far: for a small molecule or molecules consisting of a few building blocks, one can employ low-dimensional projections of the landscape to highlight important features (e.g. the transition path during a conformational change or a chemical reaction [241]), and for larger molecules, the search for reduced coordinates has led to the application of the so-called principal coordinate analysis (PCA) [242–245] to the configurations that represent local minima.<sup>1</sup> [56]

In the field of solid state chemistry there exist several closely related graph based methods in the visualization of the energy landscape: the tree graph, the disconnectivity graph, the lumped graph or the 1d-projection. [7, 246–248] All of these methods

---

<sup>1</sup>For solids, this approach appears to be most suited for amorphous or glassy compounds, where large classes of similar dynamically relevant minima exist.

### 6.3 New visualization techniques developed and applied in energy landscape representation

---

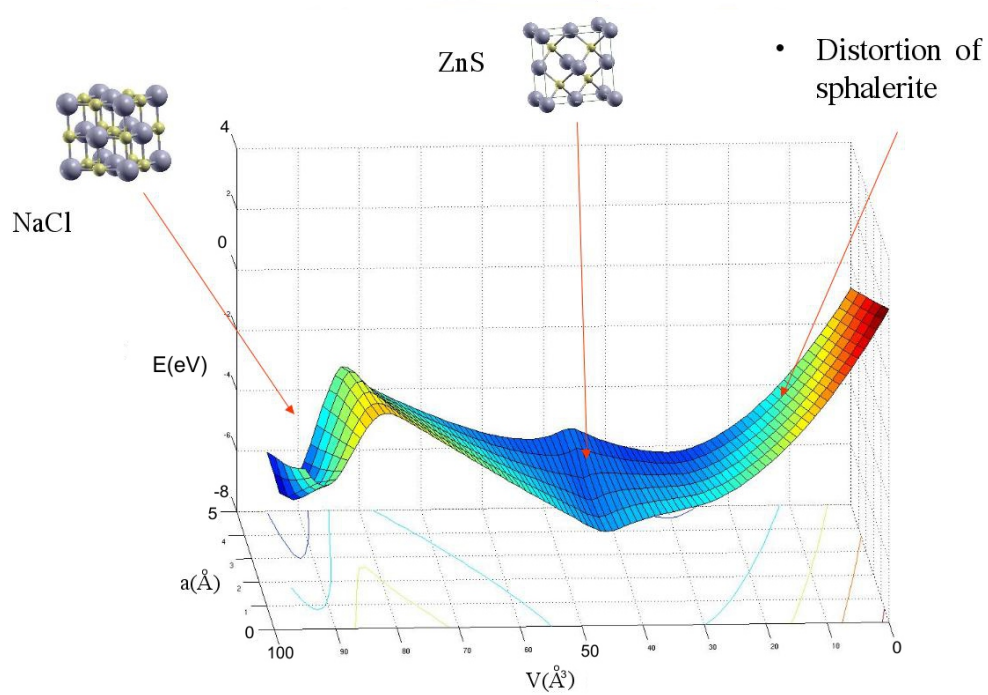


**Figure 6.2:** 3D-Model of the energy landscape as function of  $a$ ,  $V$ , and  $E$  in the ZnO system based on the threshold algorithm runs, using sphalerite as initial configuration with 1 formula unit per simulation cell - Note that the  $x$ -coordinate represents volume  $V$  ( $\text{\AA}^3$ ), the  $y$ -coordinate the  $a$ - cell parameter ( $\text{\AA}$ ), and the  $z$ -coordinate the energy  $E$  (eV), respectively.

## 6. NEW METHODS AND TECHNIQUES DEVELOPED OR APPLIED DURING THIS RESEARCH

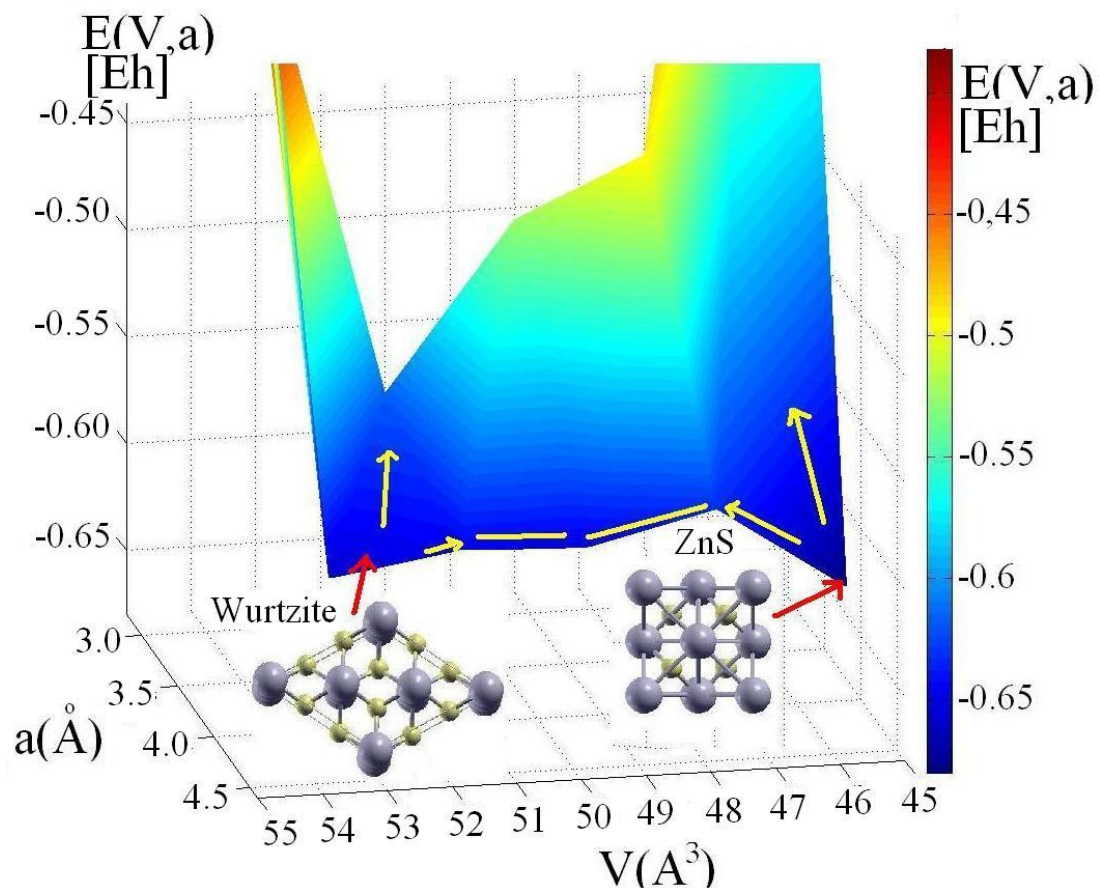
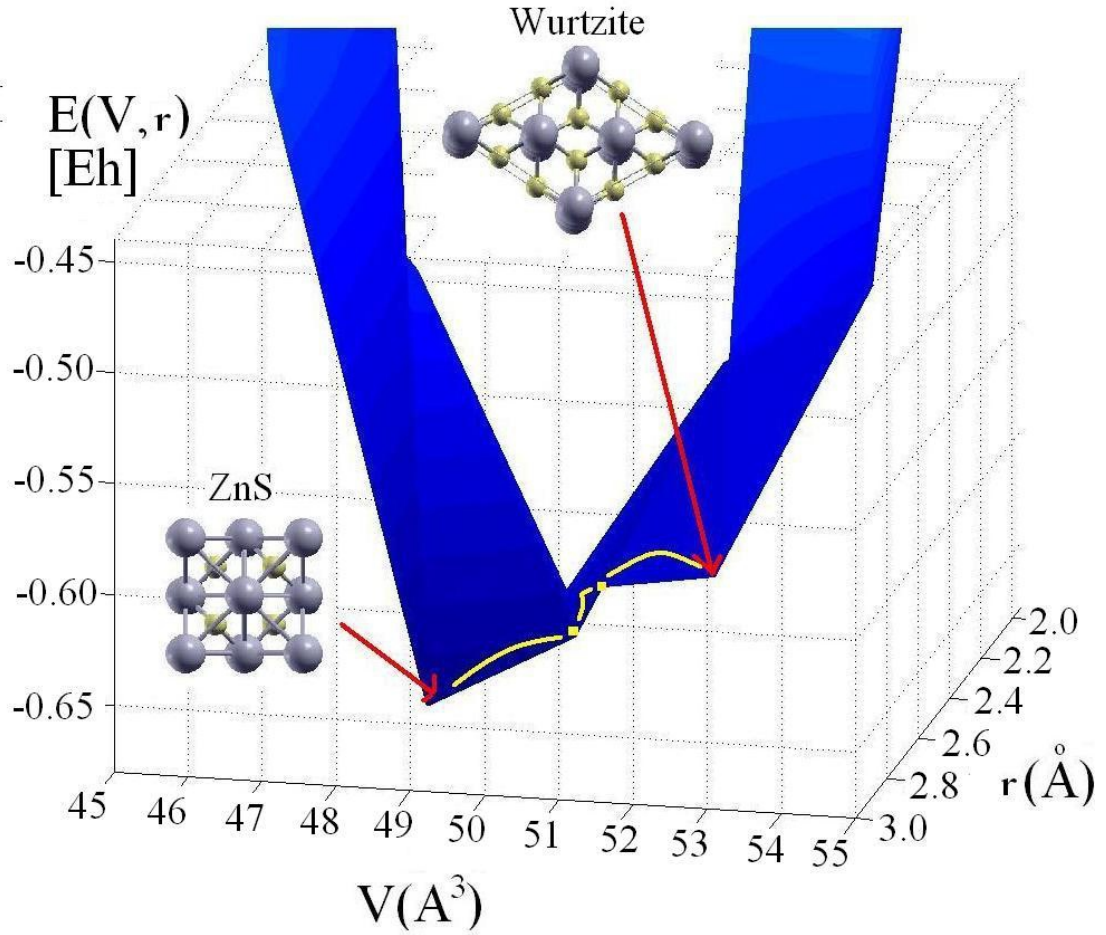


Figure 6.3: 3D-Model of the energy landscape as function of  $a$ ,  $V$ , and  $E$  in the ZnO system based on the prescribed path algorithm runs, using sphalerite/wurtzite as initial/ final configurations with 2 formula unit per simulation cell - Note that the  $x$ -coordinate represents the volume  $V$  ( $\text{\AA}^3$ ), the  $y$ -coordinate the  $a$ -cell parameter ( $\text{\AA}$ ), and the  $z$ -coordinate the energy  $E$  ( $E_h$ ), respectively.

### 6.3 New visualization techniques developed and applied in energy landscape representation



**Figure 6.4:** 3D-Model of the energy landscape as function of  $r$ ,  $V$ , and  $E$  in the ZnO system based on the prescribed path algorithm runs, using sphalerite/wurtzite as initial/ final configurations with 2 formula unit per simulation cell - Note that the  $x$ -coordinate represents the volume  $V$  ( $\text{\AA}^3$ ), the  $y$ -coordinate the average atom-atom nearest neighbor distances  $r$  ( $\text{\AA}$ ), and the  $z$ -coordinate the energy  $E$  ( $E_h$ ), respectively.

## 6. NEW METHODS AND TECHNIQUES DEVELOPED OR APPLIED DURING THIS RESEARCH

---

yield a one dimensional picture of the energy landscape and have the same basic idea.<sup>1</sup> Recent variations take some additional information into account (e.g. the alternative disconnectivity graph [249] or topology networks [250]. [56])

Here, we present our new 2D and 3D projections of the energy landscape. In figure 6.2 we present in a simple way the results of the threshold algorithm for 1 atom per simulation cell ( $Z = 1$ ) using sphalerite as initial structure in the ZnO system. We can see that sphalerite is the most dominant minimum, with distortions lying close by on the energy landscape, while the NaCl basin is clearly separated by the high energy barrier (for more details see chapter 10). In figures 6.3 and 6.4 we focus on a subregion containing two minima of the landscape. Both of these models show us that the wurtzite and the sphalerite structure are big basins on the energy landscape of ZnO (with 2 formula unit per simulation cell), with high energy barriers between them and a small unique energy path connecting these basins. In all the figures the  $x$ -coordinate corresponds to the volume  $V$  per unit cell of ZnO ( $Z = 1, 2$ ), and  $z$ -coordinate to the energy (in  $eV$  or  $E_h$ ). In figures 6.2 and 6.3, the  $y$ -coordinate is the cell parameter  $a$ , and in figure 6.4,  $y$  corresponds to the average distance value ( $r$ ), which is calculated as the mean of all distances within the first neighbor sphere of the atoms in the configurations represented in the model. The models are based on the data points calculated with the threshold algorithm and the prescribed path algorithm (see chapter 10, where a 2D model is also presented). One could say that we reached a moment of desired graphical excellence, since we managed to show the large amount of the original data (see chapter 10 and Appendix) without distortions in the multi-dimensional space by using only one graph and by using different perspectives.

Another very important aspect of the landscape are the probability flows between the minima which directly reflect the relaxation and transformation dynamics. While the actual flows will depend on the temperature, of course, important information is already contained in the observed transition probabilities as function of energy lid during the threshold runs. These probabilities can be represented in a transition map [251], where the major basins of the energy landscape are depicted, together with connections showing the amount of probability flow as function of energy range. In **chapter 10** we show one of the threshold algorithm probability graphs for the flow emanating from the

---

<sup>1</sup>They all start from one local minimum, select an energy lid, observe allowed transitions between minima, and then repeat with a higher lid, until all the minima on the landscape are connected.

### 6.3 New visualization techniques developed and applied in energy landscape representation

---

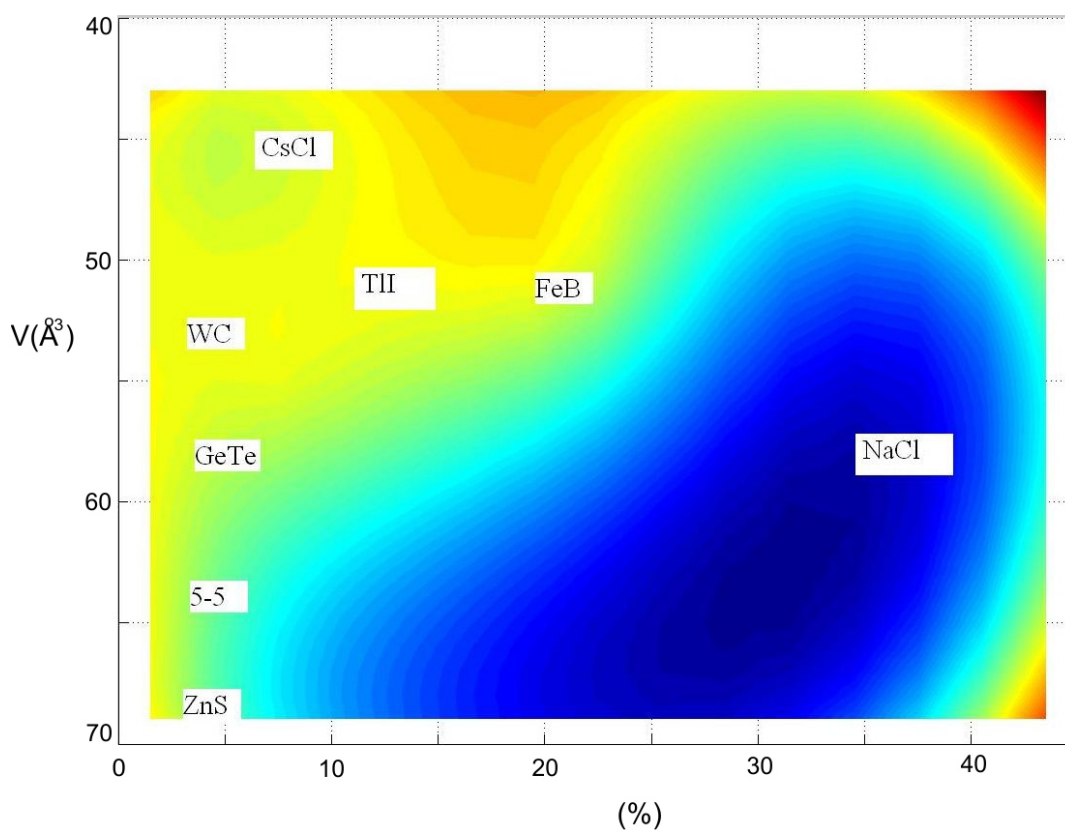


**Figure 6.5:** 2D-Model of the energy landscape as function of % and  $V$  (while  $E$  is defined by the color) in the PbS system based on the *ab initio* calculations with 4 formula unit per simulation cell - Note that the  $x$ -coordinate represents the percentage of occurrence of a certain minimum (%), the  $y$ -coordinate the volume  $V$  ( $\text{\AA}^3$ ), and the  $z$ -coordinate the energy  $E$  ( $E_h$ ), respectively, using a biharmonic spline interpolation scheme implemented in MATLAB as in previous cases.

## 6. NEW METHODS AND TECHNIQUES DEVELOPED OR APPLIED DURING THIS RESEARCH

---

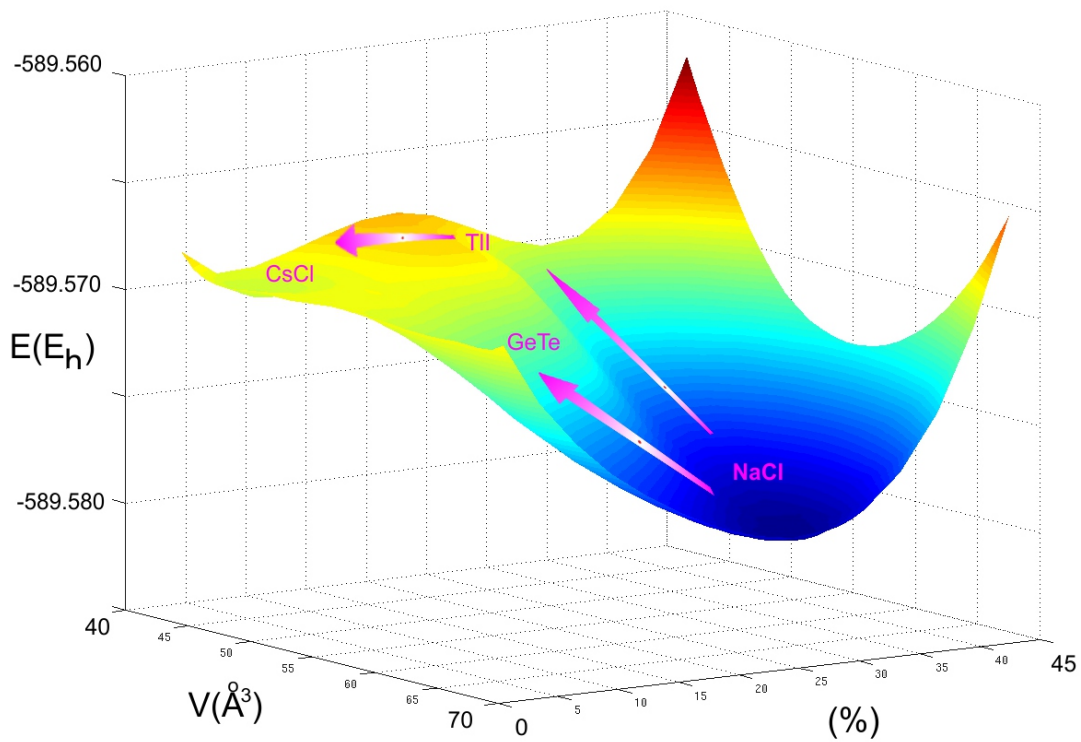


**Figure 6.6:** 3D-Model of the energy landscape as function of %,  $V$ , and  $E$  in the PbS system based on the *ab initio* calculations with 4 formula unit per simulation cell - Note that the  $x$ -coordinate represents the percentage of occurrence of a certain minimum (%), the  $y$ -coordinate the volume  $V$  ( $\text{\AA}^3$ ), and the  $z$ -coordinate the energy  $E$  ( $E_h$ ), respectively.



sphalerite minimum (denoted ZnS) as function of energy lid. [56] Finally by combining the probability graphs with the  $E(V)$  curves, we obtained new 2D- and 3D-models represented in figures 6.5 and 6.6. In figure 6.5 we present a 2D-model of the energy landscape as function of occurrence (%), volume ( $V$ ), and energy ( $E$ ) in the PbS system based on the *ab initio* calculations with 4 formula unit per simulation cell, where the major difference to the previous models is introducing the percentage of occurrence of a specific minimum on the  $x$ -coordinate. In this 2D-model we can see the rock salt structure as the greatest basin on the energy landscape, with many small minima lying close by, e.g. the  $\alpha$ -GeTe type, the 5-5 type etc. However, there is another minimum (CsCl), separated by a high energy barrier, which is possible to bypass via the TII (FeB) structure type (for more details see **chapters 7 and 8**). If we use now a 3D-model (see figure 6.6), then this situation is even easier to understand and, furthermore, one can see that there are some unique paths which one can follow in the synthesis process, e.g. the transition path NaCl-TII(FeB)-CsCl is clearly separated from the NaCl- $\alpha$ -GeTe transition path.

## 6.4 Scripts for structure analysis

The following scripts/programs were developed during this work:

- VolDis.v1.0 - Program written as (c)shell script for analyzing cell parameters, volumes and distances from KPLOT program [227].
- Cellvector.v1.0 - Program written in Perl language for calculating the primitive cell parameters.
- Volume cacl.v1.0 - Program written in Perl language for calculating the volumes of the structures (in radians or degrees, any symmetry, etc.).

The following scripts/programs were updated during this work:

- LOAD.V-4.8 - Modified to fit the threshold and prescribed path algorithm results [131].
- FILTER.V-3.8 -Modified to fit the multiple high pressure calculations [131].

**6. NEW METHODS AND TECHINQUES DEVELOPED OR APPLIED  
DURING THIS RESEARCH**

---

## Part IV

# Application of structure prediction and energy landscape investigation to specific chemical systems



# 7

## Structure prediction for lead sulfide (PbS) at various pressures on *ab initio* level

*"And no, we don't know where it will lead. We just know there's something much bigger than any of us here."*

(Steve Jobs (1955-2011), American businessman, designer and inventor)

### 7.1 Introduction

Lead sulfide (PbS) is known as an important semiconductor, and therefore, it is of great interest to identify possible stable and metastable modifications, both at standard and elevated pressures. In order to predict such structures, global optimizations on the energy landscape of PbS were performed for several pressures, using simulated annealing (SA) followed by local optimization of the candidates found. In order to be able to take the effect of the non-bonding valence electrons of  $\text{Pb}^{2+}$  into account, *ab initio* energies were employed at each step of optimization procedure. [56, 252]

The natural mineral form of lead sulfide is galena (see figures 7.1 and 7.2). Galena is one of the most abundant and widely distributed sulfide minerals. It is the most important lead ore mineral, and the first use dates back to 3000 BC. Usually it is found widely distributed in hydrothermal veins or in sedimentary rocks as beds or impregnations, associated with sphalerite, pyrite, chalcopyrite, barite, quartz, fluorite,

## 7. STRUCTURE PREDICTION FOR LEAD SULFIDE (PbS) AT VARIOUS PRESSURES ON AB INITIO LEVEL

---

and calcite. The crystals are soft, grey in color, bright when fresh, but often receive a dull tarnish after exposure to air. [253–256]



**Figure 7.1: Galena mineral (PbS) from Devon, England, UK** - The picture shows common galena's appearance in nature (grey color), i.e. as distributed through the quartz vein material (white color). The mineral size is 30mm x 50mm. [256]

PbS has been used as a detection material in infrared sensors (e.g. photon detectors) [257] or in quantum-confinement studies in nanocrystals. [258, 259] However, the high dielectric constant of PbS usually leads to relatively slow detectors, compared to silicon, germanium, InSb, or HgCdTe. [260] Thus, identifying (and eventually synthesizing) a new PbS modification would be very interesting from the viewpoint of structural chemistry.

Theoretical studies of the electronic structure of PbS have been performed by many groups.<sup>1</sup> These calculations identified a direct band gap at the  $L$  point of the Brillouin zone. Furthermore, it was found that the NaCl modification in the lead sulfide system undergoes a metal-insulator transition under pressure, on the level of the generalized gradient approximation (GGA). [267] However, recent careful investigations showed that this issue is much more subtle, and that the LDA gives an incorrect description of the gap, with an inverted character of the band: The valence band maximum has

---

<sup>1</sup>The band structure has been calculated using the Green function method,[261] orthogonalized plane waves,[262] local basis sets,[263, 264] empirical pseudopotentials,[265, 266] augmented or linear augmented plane waves (APW),[267–270] and the projector augmented wave method.[270].



**Figure 7.2: Mineral galena (PbS) from Savoie, Rhone-Alpes, France** - The picture shows mineral association of galena (grey color), quartz (transparent color), pyrite (gold color) and dolomite (white color). One can see nice cubic crystals of galena. The specimen is in the collection of the Smithsonian Institute (Washington, USA) from 1973 and the scale at the bottom of the image is one inch long (with a mark at 1 cm). [256]

Pb  $p$  character, and the conduction band minimum has S  $p$  character. [270, 271] These calculations might be improved with hybrid functionals or the GW approach. [270, 271]

There are also many experiments performed in lead sulfide system by various groups. The NaCl ( $B1$ ) structure is the most common form observed in this experiments at standard conditions. [272] PbS undergoes a pressure-induced phase transition from the NaCl ( $B1$ ) type to an intermediate orthorhombic phase (suggested to belong to the  $B16$  [273, 274] or  $B33$  [275–277] structure types) at 2.2 GPa, with more recent results supporting the TII structure type. A further pressure-induced phase transition from the orthorhombic phase to the CsCl type ( $B2$ ) phase takes place at 21.5 GPa. [56, 252] Furthermore, there have been suggestions that additional modifications might exist in nanocrystalline PbS films. [278, 279]

## 7.2 Optimization procedure

In this study, stochastic simulated annealing, based on random Monte Carlo walks on the energy landscape with decreasing temperature parameter, was used as a global optimization algorithm. Each simulated annealing run consisted of eight atoms (four

## 7. STRUCTURE PREDICTION FOR LEAD SULFIDE (PBS) AT VARIOUS PRESSURES ON AB INITIO LEVEL

---

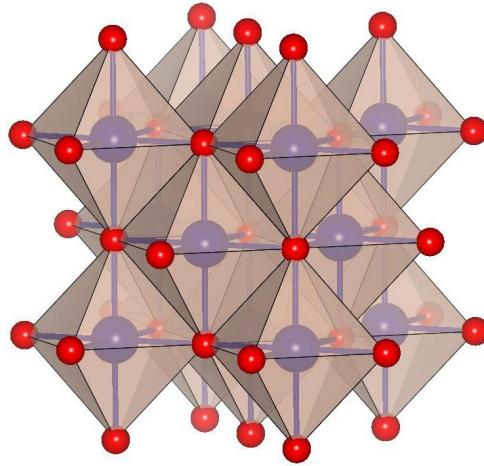


**Figure 7.3:** Visualization of the experimentally observed structures - The rock salt (NaCl) structure type in a periodically repeated unit cell.

Pb, four S) per unit cell. The initial cell was much larger than the estimated cell size for a solid phase (based on atomic and ionic radii) in order to be able to position the atoms at random places and allow sufficient freedom for rearrangement. Both the atom positions (70% of all Monte Carlo steps move an individual atom, 10% swap the positions of two atoms) and the parameters of the periodically repeated simulation cell (20% of all Monte Carlo steps) were freely varied during the random walks. Each simulated annealing run consisted of 5000 steps, followed by 10000 quench steps. [56, 252]

All the total energy calculations were performed on the *ab initio* level, using **CRYSTAL09** program. [191, 192] During the global search, for Pb, a large-core pseudopotential [280] was used, together with a [2s2p] basis set (the first *s* contraction consisted of the first three primitives as in Ref. [280]; the first *p* contraction consisted of the first two primitives as in Ref. [280] and an additional *sp* shell with exponent 0.15). Similarly, a large-core pseudopotential [281] was used for S, with a [2s2p] basis set (the first *s* and *p* contraction consisted of the first three primitives as in Ref. [281] and an additional *sp* shell with exponent 0.15). An overview of the basis sets is given in the Appendix. A 4 x 4 x 4 k-point sampling net was employed.<sup>1</sup>. [56, 252]

---

<sup>1</sup>Note that spin-orbit coupling is not implemented in the code and thus could not be included in the calculations.



## 7.2 Optimization procedure

Table 7.1. Structural data of the energetically most favorable modifications found after local optimization (at a pressure of 0 GPa) on Hartree-Fock, DFT-B3LYP and DFT-LDA level.

Space group and modification	Cell parameters and fractional coordinates		
	HF	B3LYP	LDA
<i>Fm-3m</i> (225) NaCl type	a=6.18 Å Pb (0 0 0) S (½, ½, ½)	a=6.08 Å Pb (0 0 0) S (½, ½, ½)	a=5.86 Å Pb (0 0 0) S (½, ½, ½)
<i>Cmcm</i> (63) TII type	a=4.34 Å, b=12.88 Å, c=4.42 Å Pb (0 0.6381 ¾) S (0 0.8434 ¾)	a=4.24 Å, b=12.51 Å, c=4.33 Å Pb (0 0.6337 ¾) S (0 0.8507 ¾)	a=4.06 Å, b=11.33 Å, c=4.18 Å Pb (0 0.6207 ¾) S (0 0.8579 ¾)
<i>Pnma</i> (62) FeB type	a=9.48 Å, b=4.28 Å, c=6.31 Å Pb (0.6396 ¾ 0.7541) S (0.3273 ¼ 0.6875)	*	a=7.92 Å, b=4.14 Å, c=5.93 Å Pb (0.5926 ¾ 0.7947) S (0.3334 ¼ 0.6515)
<i>Pm-3m</i> (221) CsCl type	a= 3.75 Å Pb (0 0 0) S (½, ½, ½)	a= 3.70 Å Pb (0 0 0) S (½, ½, ½)	a=3.54 Å Pb (0 0 0) S (½, ½, ½)
<i>R3m</i> (160) $\alpha$ -GeTe type	a=4.59 Å, $\alpha$ =56.11° Pb (0 0 0) S (0.4556, 0.4556, 0.4556)	a=4.37 Å, $\alpha$ =58.80° Pb (0 0 0) S (0.4741, 0.4741, 0.4741)	*
<i>P6<sub>3</sub>/mmc</i> (194) NiAs type	a=4.29 Å, c=7.50 Å Pb (0 0 0) S (½ ⅓ ¼)	a=4.22 Å, c=7.39 Å Pb (0 0 0) S (½ ⅓ ¼)	a=4.00 Å, c=7.17 Å Pb (0 0 0) S (½ ⅓ ¼)
<i>P6-m2</i> (187) $\alpha$ -WC type	a=4.22 Å, c=3.89 Å Pb (0 0 0) S (½ ⅓ ½)	a=4.14 Å, c=3.81 Å Pb (0 0 0) S (½ ⅓ ½)	a=3.92 Å, c=3.72 Å Pb (0 0 0) S (½ ⅓ ½)
<i>P2<sub>1</sub>/m</i> (11) PbS-I	a=6.08 Å, b=4.11 Å, c=11.18 Å, $\beta$ =95.78° Pb (0.6868 ¾ 0.6275) Pb (0.2485 ¾ 0.9018) S (0.7288 ¾ 0.9354) S (0.3905 ¼ 0.6291)	a=5.99 Å, b=4.10 Å, c=10.65 Å, $\beta$ =91.42° Pb (0.8174 ¾ 0.8686) Pb (0.2515 ¾ 0.5980) S (0.7553 ¾ 0.5791) S (0.1240 ¼ 0.8535)	a=5.76 Å, b=3.96 Å, c=9.55 Å, $\beta$ =98.97° Pb (0.2640 ¾ 0.4053) Pb (0.7764 ¾ 0.0993) S (0.2741 ¾ 0.1067) S (0.9459 ¼ 0.3391)
<i>Pma2</i> (28) PbS-II	a=7.31 Å, b=6.04 Å, c=6.43 Å Pb (¾ 0.6906 0) Pb (¼ 0.8386 0.5571) S (½ 0 0.8646) S (¾ 0.7574 0.3982)	a=7.27 Å, b=5.64 Å, c=6.51 Å Pb (¾ 0.6679 0) Pb (¼ 0.8262 0.5592) S (½ 0 0.8644) S (¾ 0.7324 0.3972)	a=6.68 Å, b=5.64 Å, c=5.85 Å Pb (¾ 0.6442 0) Pb (¼ 0.8193 0.5532) S (½ 0 0.8910) S (¾ 0.7171 0.4384)
<i>Amn2</i> (38) PbS-III	a=3.98 Å, b=12.78 Å, c=12.11 Å Pb (0 0.6555 0) Pb (½ ½ 0.6405) Pb (0 ½ 0.3401) S (½ 0.7911 0.9709) S (0 ½ 0.7870) S (½ ½ 0.1951)	a=4.12 Å, b=11.55 Å, c=11.28 Å Pb (0 0.6621 0) Pb (½ ½ 0.6378) Pb (0 ½ 0.3226) S (½ 0.8284 0.9478) S (0 ½ 0.8100) S (½ ½ 0.1382)	a=3.83 Å, b=10.34 Å, c=9.80 Å Pb (0 0.7100 0) Pb (½ ½ 0.6529) Pb (0 ½ 0.2942) S (½ 0.7730 0.8068) S (0 ½ 0.8314) S (½ ½ 0.0829)
<i>P6<sub>3</sub>mc</i> (186) PbS-IV (distorted NiAs)	a=4.23 Å, c=8.35 Å Pb (0 0 0) S (⅔ ⅓ 0.1792)	a=4.20 Å, c=7.76 Å Pb (0 0 0) S (⅔ ⅓ 0.1924)	a=4.04 Å, c=7.27 Å Pb (0 0 0) S (⅔ ⅓ 0.2261)

\*When the structure is optimized on this corresponding level of theory, it becomes the NaCl structure type (cell parameters and fractional coordinates correspond to the NaCl structure).

## 7. STRUCTURE PREDICTION FOR LEAD SULFIDE (PBS) AT VARIOUS PRESSURES ON AB INITIO LEVEL

---

During the global optimization, the Hartree-Fock approximation was used, which is usually easier and faster to converge for random structures than the calculations performed with density functional theory (DFT), due to the larger band gaps. [282, 283] After the global optimization and after the subsequent local minimization, the symmetries and space groups of the configurations found are determined using the algorithms SFND [228], and RGS [229], respectively, that are implemented in the program **KPLOT**. [227]

The local optimizations used are based on the analytical gradients [154–156] and are performed both on the Hartree-Fock and the DFT level, employing the B3LYP functional<sup>1</sup> in combination with the correlation functional of Lee, Yang, and Parr) and the local density approximation (LDA). It is usually reasonable to choose at least two different *ab initio* methods, in order to make qualitative and quantitative validity of the results. [56, 252]

These local optimizations are much less time consuming than the global search, but they should be performed with a higher accuracy. Thus, a small-core pseudopotential [284] together with a [4s4p3d1f] basis set (i.e., consisting of four *s*, four *p*, three *d*, and one *f* function), was used for Pb (the inner [2s2p3d] as in Ref. [284], plus *sp* 0.37, *sp* 0.17, *f* 0.3). For *S*, a [5s4p1d] all-electron basis set was used. The inner [3s2p] shells were chosen as in Ref. [263], together with three additional exponents (*sp* 0.2413, *sp* 0.106, *d* 0.383) (see Appendix). The k-net sampling was enlarged to 8 x 8 x 8 points. A smearing temperature of 0.001  $E_h$  was applied during the local optimization and the calculation of the  $E(V)$  curves, in order to facilitate the numerical integration. [56, 252]

---

<sup>1</sup>Becke's three-parameter functional [134]

## 7.2 Optimization procedure

Table 7.2. Structural data of additional unknown modifications found after local optimization on the Hartree-Fock level (at a pressure of 0 GPa). In brackets, we list known structure types which show the greatest similarity to the new modifications.

Space group and modification	Cell parameters and fractional coordinates
<i>Pc</i> (7) PbS-V	a=6.99Å, b=5.39Å, c=7.74Å, $\beta=92.77^\circ$ Pb (0 0.7008 0) Pb (0.4481 0.2079 0.1602) S (0.3026 0.5664 0.3689) S (0.8238 0.3205 0.1642)
<i>C222<sub>1</sub></i> (20) PbS-VI (distorted NiAs)	a=4.63Å, b=7.48Å, c=7.31Å Pb (0.6262 0 0) S (0 0.8334 ¼)
<i>Pmn2<sub>1</sub></i> (31) PbS-VII (distorted WC)	a=4.26Å, b=4.81Å, c=6.30Å Pb (0 0.7893 0) S (0 0.8401 0.5503)
<i>P2<sub>1</sub>3</i> (198) PbS-VIII (distorted NaCl)	a=6.38Å Pb (0.2323 0.7676 0.2676) S (0.3007 0.8007 0.6993)
<i>Pmma</i> (51) PbS-IX (distorted PbO)	a=6.96Å, b=3.50Å, c=3.55Å Pb (¾ 0 0.5829) S (½ ½ 0)

Table 7.3. Energies (in hartree ( $E_n$ ) per formula unit, at a pressure of 0 GPa) and number of occurrences of the energetically most favorable structures for various pressures. The entry "Number of times found" corresponds to the combined outcomes of the local optimizations with Hartree-Fock and DFT at the corresponding pressure.

Name of Modification	Energy			Number of times found			
	HF	B3LYP	LDA	0 GPa	4 GPa	8 GPa	24 GPa
<b>NaCl type</b>	-589.4566	-591.1171	-589.5851	32	29	14	9
<b>TlI type</b>	589.4591	-591.1139	-589.5832	1	-	-	18
<b>FeB type</b>	-589.4044	*	-589.5830	4	6	21	9
<b>CsCl type</b>	-589.4286	-591.0929	-589.5683	-	-	-	4
<b><math>\alpha</math>-GeTe type</b>	-589.4587	-591.1170	*	4	-	-	-
<b>NiAs type</b>	-589.4472	-591.1121	-589.5798	1	-	4	-
<b><math>\alpha</math>-WC type</b>	-589.4422	-591.1067	-589.5763	2	1	3	-
<b>PbS-I</b>	-589.4569	-591.1105	-589.5748	-	-	4	10
<b>PbS-II</b>	-589.4514	-591.1036	-589.5660	-	-	3	-
<b>PbS-III</b>	-589.4467	-591.1039	-589.5651	-	-	-	3
<b>PbS-IV</b>	-589.4564	-591.1136	-589.5795	3	-	-	-

\*When the structure was optimized on this specific level of theory, it changed to the NaCl structure type.

## 7. STRUCTURE PREDICTION FOR LEAD SULFIDE (PBS) AT VARIOUS PRESSURES ON AB INITIO LEVEL

---

### 7.2.1 Statistical analysis of the optimization process

The global optimizations at 0, 4, 8, and 24 GPa have been performed, with 100 simulated annealing (SA) runs at 0 GPa, and 50 runs at each of the three other pressures. In total 32 structure candidates were found after the global optimization at 0 GPa, exhibiting a symmetry different from  $P1$ . After eliminating duplicates, there remained 18 unique structures. At 4 GPa, we found 13 candidates (eight unique), at 8 GPa 15 candidates (ten unique), and at 24 GPa 18 candidates (11 unique), respectively. Afterwards, a local optimization was performed for each candidate using the Hartree-Fock approximation and DFT, both with B3LYP and LDA functionals. Finally, 11 promising structure candidates were obtained (table 7.1). A list of the additional structures, with structure parameters found after Hartree-Fock (HF) optimization is given in table 7.2. [252]

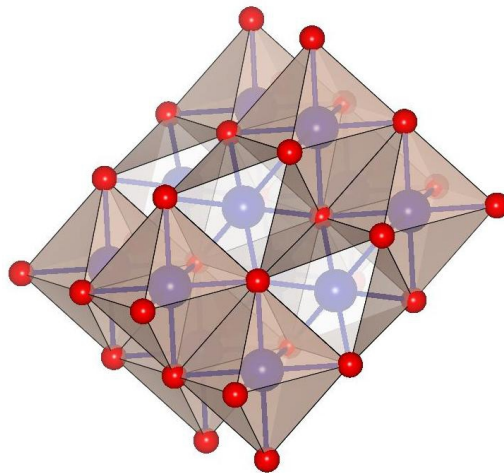


**Figure 7.4: Visualization of the calculated structure types** - The nickel arsenide (NiAs) structure type in a periodically repeated unit cell.

Naturally, we have found in most of the runs the experimentally observed NaCl structure type (see figure 7.3 and table 7.3), [272] Additionally, we have identified several promising minima, exhibiting the following structure types: thalium iodide (TII) (see figure 7.9), iron boride (FeB) (see figure 7.11, germanium telluride ( $\alpha$ -GeTe) (see figure 7.12, nickel arsenide (NiAs) (see figure 7.4), and tungsten carbide  $\alpha$ -WC (see figure 7.13). Furthermore, we have found several other stable modifications with so-far-unknown structure types denoted as PbS-I, PbS-II,..., PbS-IX, with space groups  $P2_1/m, Pma2, Amm2, P6_3mc, Pc, C222_1, Pmn2_1, P2_13,$  and  $Pmma,$  respectively. At

zero pressure, the NaCl type was the most common outcome of the global search, while at elevated pressures the FeB, the TII, and the PbS-I structures occurred in the majority of the runs. Furthermore, at 24 GPa, the experimentally observed CsCl structure type corresponded to a local minimum (see table 7.3). We have statistically analyzed all the global optimization and local optimization runs performed. All the global optimization runs reached a local minimum. The most common outcome of the global optimization runs at standard pressure were structures with  $P1$  symmetry (66%), but with an increase of pressure, the percentage of  $P1$  structures decreased (e.g. at 24 GPa it is only 36%). Apparently, the increase of pressure favors more symmetric structures in the PbS system; a similar trend has been observed in the e.g. alkali sulfides. [41] A statistical analysis of the local optimization runs is presented in table 7.3. [252]

## 7.3 Results and Discussion

### 7.3.1 Phase transitions and modifications stable at elevated pressure

We have computed the  $E(V)$  curves for the most relevant structure types (see figures 7.5 and 7.7). The pressure-driven phase transitions can be derived most easily from the enthalpy vs. pressure ( $H(p)$ ) diagram for the modifications compared (see figures 7.6 and 7.8). Since the electronic structure of PbS calculated via the LDA showed better agreement with the experiment (compared to B3LYP and HF), in the following we present only the results obtained using LDA. [56, 252]

We observe that the rock salt (NaCl) structure was the lowest in energy at standard pressure with calculations performed on the level of the local density approximation (LDA). When we performed calculations using HF or B3LYP, the  $\alpha$ -GeTe structure type was a very good structure candidate. In fact, this slightly distorted NaCl structure type is a tiny bit lower in energy than the NaCl structure at the HF level (see table 7.3). We note that in earlier phonon experiments and calculations no evidence of structural instability of the NaCl modification via a soft mode was found. [285–287]

With calculations performed at 4.5 GPa, we observe a transition to the thallium iodide (TII-B33) type (see figures 7.5, 7.6, and 7.9). This is in reasonable agreement with experiment, as the transition between the NaCl and the B33 type of structure is observed at 2.2 GPa. [275, 277] The orthorhombic TII type ( $Cmcm$ ) can be considered to be a rather distorted NaCl structure type. [288] It can be described as a chain of

## 7. STRUCTURE PREDICTION FOR LEAD SULFIDE (PBS) AT VARIOUS PRESSURES ON AB INITIO LEVEL

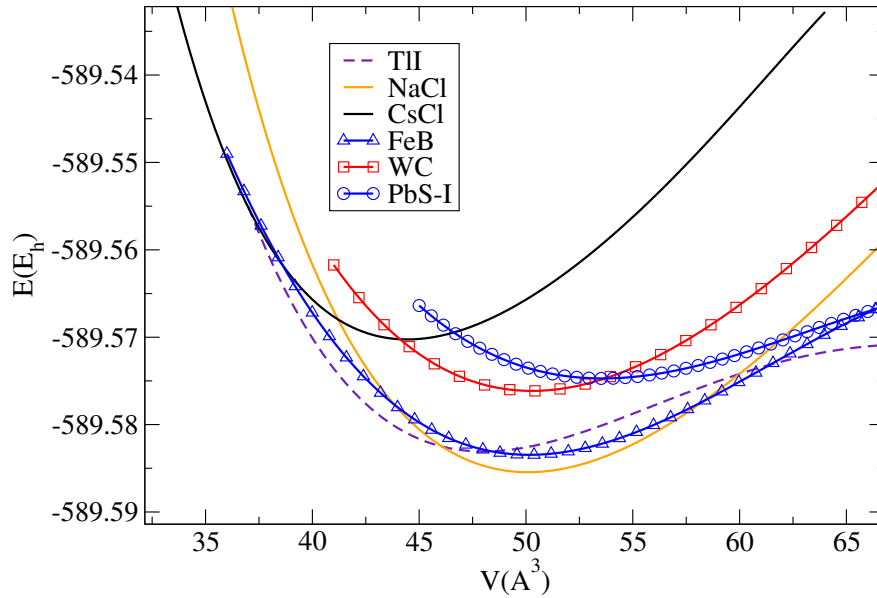


**Figure 7.5:**  $E(V)$  curves at LDA level for the most relevant structure types in **PbS** - The figure shows the high-pressure structure candidates. Energies per formula unit are given in hartrees ( $E_h$ ).

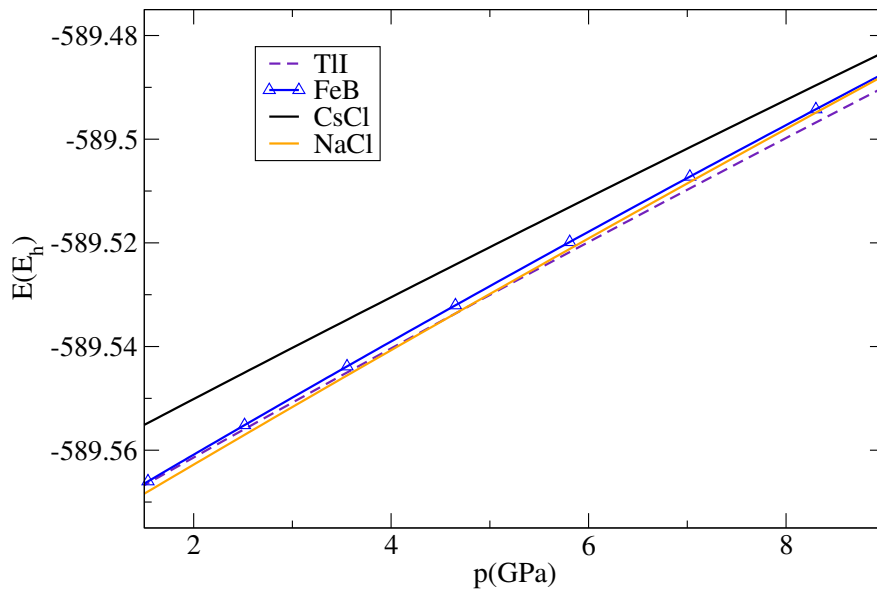


**Figure 7.6:**  $H(p)$  curves at LDA level in the **PbS** system - The figure shows relevant modifications participating in pressure-induced phase transitions from the NaCl to the TII structure type at elevated pressures. Enthalpies per formula unit are given in hartrees ( $E_h$ ).

monocapped trigonal prisms sharing common rectangular faces, with a Pb atom in the center of this  $S_7$  polyhedron. The stacking order is  $ABAB$ . In the thallium iodide system this orthorhombic modification of thallium iodide transforms to the CsCl type modification with increasing temperature. [289] The same process occurs in the lead sulfide system upon further increase of pressure. [56, 252]

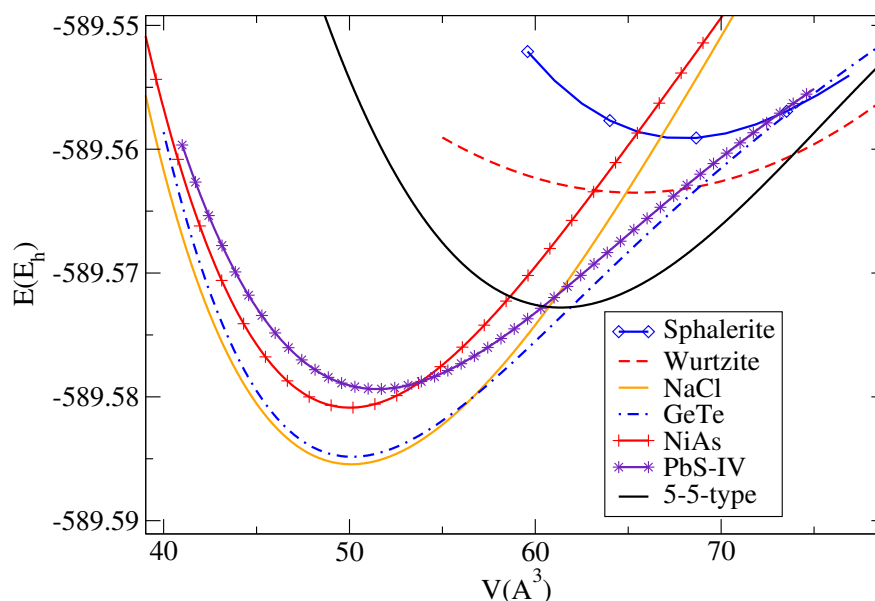


**Figure 7.7:**  $E(V)$  curves at LDA level for the most relevant structure types in **PbS** - The figure shows the low pressure structure candidates. Energies per formula unit are given in hartrees ( $E_h$ ).

In the previous investigations of lead sulfide, another orthorhombic phase has been claimed to exist at intermediary pressures (exhibiting the  $Pnma$  space group), known as the GeS (B16) type (see figure 7.9). [273, 274] However, as in other lead chalcogenides the experimental evidence favoring one or the other remains controversial. [275, 277, 290–294] In order to address this issue, we minimized the experimentally known structure of GeS in the PbS system [274] using the LDA functional. As a result we have found that PbS in the GeS type keeps the  $Pnma$  space group and coordination, but using the CMPZ algorithm, [230] one sees that it is essentially equivalent to the TII modification as far as its atom arrangement is concerned. The transition pressures (to the NaCl and the CsCl modifications) and energy levels match those of the TII type, too. In addition, we performed a series of geometrical comparisons between all

## 7. STRUCTURE PREDICTION FOR LEAD SULFIDE (PbS) AT VARIOUS PRESSURES ON AB INITIO LEVEL

---

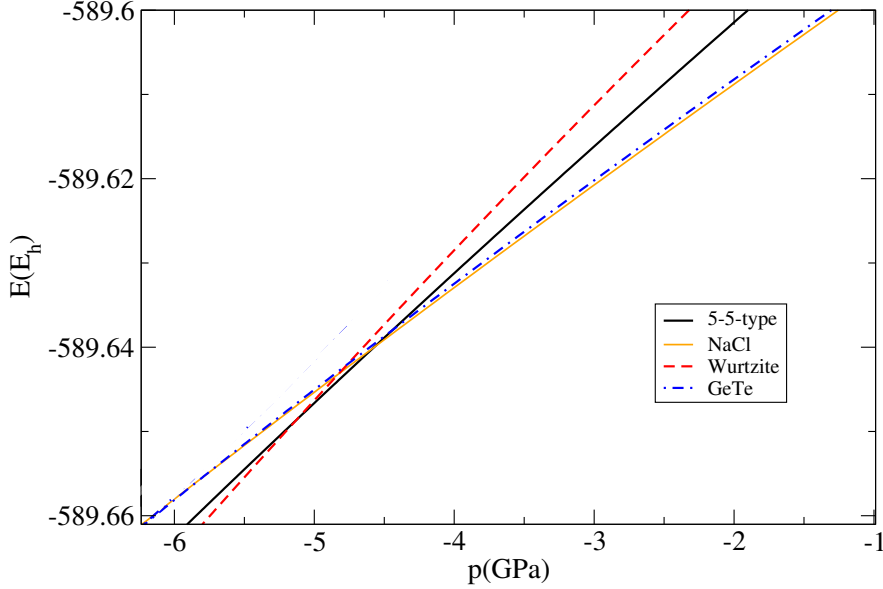


**Figure 7.8:**  $H(p)$  curves at LDA level in the PbS system - The figure shows relevant modifications participating in low density region. Enthalpies per formula unit are given in hartrees ( $E_h$ )

known experimental and suggested theoretical structures at intermediary pressures in PbS using the CMPZ algorithm implemented in the **KPLOT** program. [227] Mapping and matching the GeS type [273, 274] (with a 3 + 3 (+1) coordination of Pb by S) with the CrB type [275] (with 5 + 2 coordination) and the TII type [277] (with 1 + 4 + 2 coordination) in PbS was successfully performed. Similarly, a successful mapping was performed between all experimentally known structures in the PbS system at intermediary pressures [273–275, 277] and our calculated ones for the TII and the GeS type. We therefore conclude that all of these modifications belong to the same big valley on the energy landscape of the lead sulfide system, representing the TII type of structure at the intermediary range of pressures. [56, 252]

In our calculations, we have also identified a possible alternative for the TII structure type. This modification exhibiting the  $Pnma$  space group, and it is known as the iron boride (FeB, B27) type of structure (see figure 7.11). A comparison using CMPZ clearly showed that this structure type in the PbS system is different from the GeS type (B16) or the TII type (B33). We can describe the FeB structure type in a similar fashion as the TII type, i.e., via a chain of monocapped trigonal  $PbS_7$  prisms and



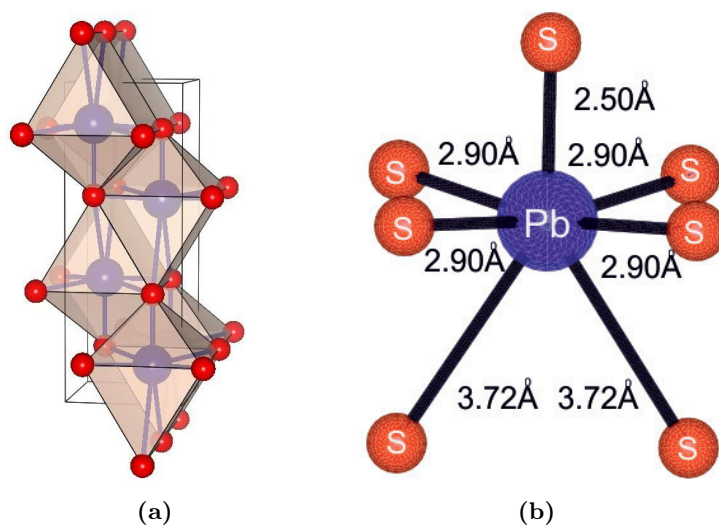


**Figure 7.9:** Visualization of the experimentally observed thallium iodide (TlI) structure type: a) TlI-type in a periodically repeated unit cell; b) 7-fold coordination of the Pb-atom by S-atoms.

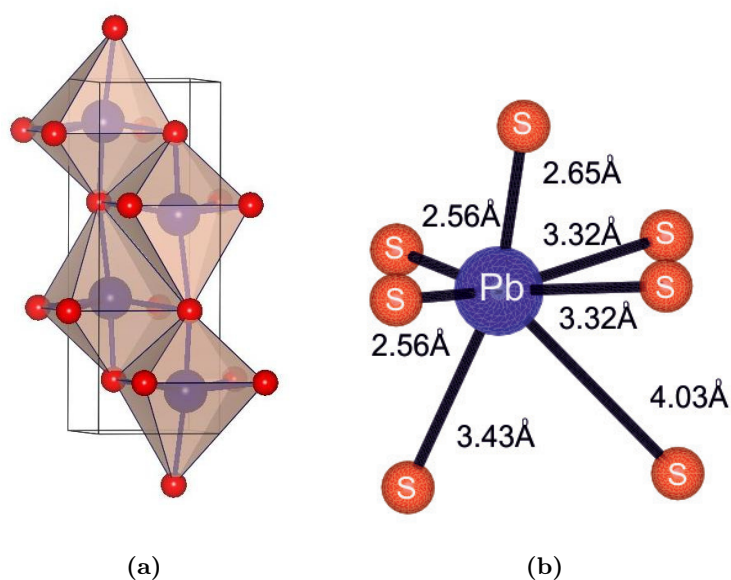


**Figure 7.10:** Visualization of the experimentally observed germanium sulfide (GeS) structure type: a) GeS-type in a periodically repeated unit cell; b) 7-fold coordination of the Pb-atom by S-atoms in the GeS type (often depicted as 6-fold coordination as in previous figure). The similarity of these structure types becomes clear when the distant S-atom is included in the coordination sphere of the Pb-atom in the GeS type.

## 7. STRUCTURE PREDICTION FOR LEAD SULFIDE (PBS) AT VARIOUS PRESSURES ON AB INITIO LEVEL

---

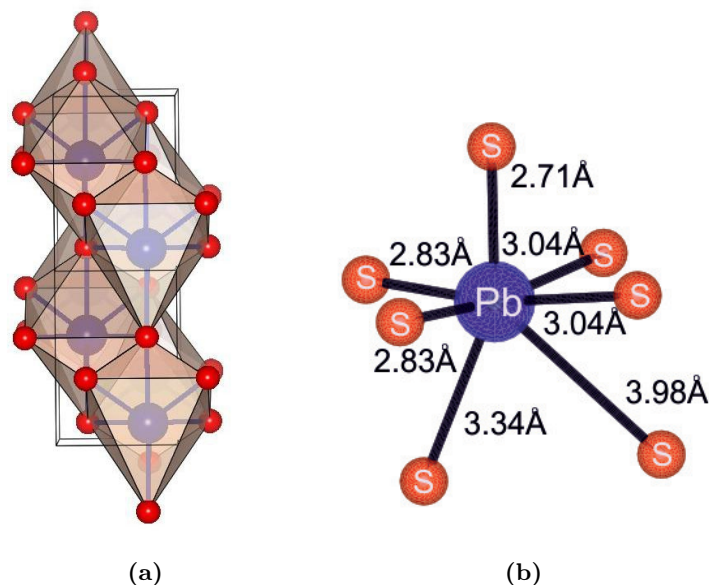


**Figure 7.11:** Visualization of the experimentally observed iron boride (FeB) structure type: a) FeB-type in a periodically repeated unit cell; b) 7-fold coordination of the Pb-atom by S-atoms in the FeB type.

with the same stacking, *ABAB*. However, there is a difference in symmetry and the atom positions. The FeB type has space group *Pnma* and contains zig-zag chains of lead atoms [295], while the TII type exhibits space group *Cmcm* and contains layered rectangular chains of Pb and S atoms. We note that in the lead telluride (PbTe) system, the FeB type is experimentally and theoretically observed for an intermediary range of pressures between the NaCl and the CsCl modification. [290, 291] According to our calculations, the FeB type is another competitive orthorhombic phase of PbS, which becomes preferable to the NaCl type at a somewhat higher pressure ( $\sim 10$  GPa) than the TII type. This is supported by the fact that the FeB modification lies very close to the NaCl-type basin on the energy landscape of PbS, such that at standard pressure it is highly metastable against a transformation back to the NaCl type. [56, 252]

A further increase of pressure causes a transition from the TII-type phase to the CsCl-type (B2) phase. The transition is calculated to occur at 25 GPa (at LDA level), which is in good agreement with the experimental data (21.5 GPa).<sup>1</sup>

---

<sup>1</sup>For comparison, the following transition pressures were found using the B3LYP functional: for NaCl to TII at 12 GPa, NaCl to CsCl at 25 GPa, TII to CsCl at 37 GPa, respectively.

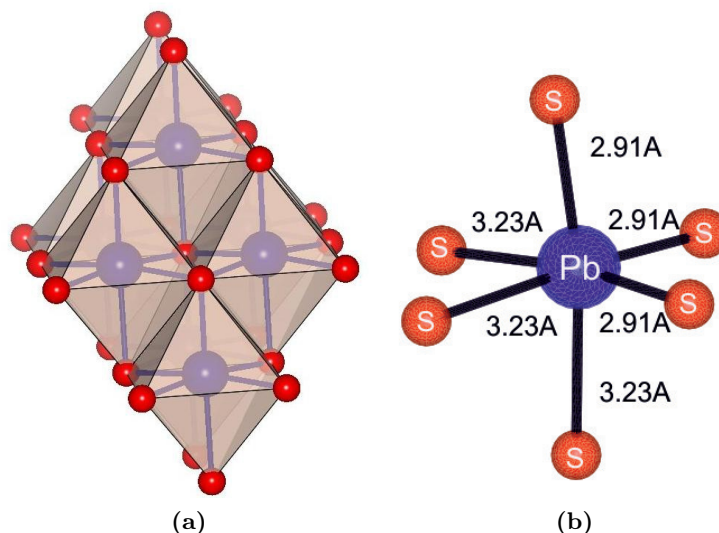


**Figure 7.12:** Visualization of the experimentally observed germanium telluride ( $\alpha$ -GeTe) structure type: a)  $\alpha$ -GeTe in a periodically repeated unit cell; b) 6-fold (3+3) coordination of the Pb-atom by S-atom in the  $\alpha$ -GeTe type.

### 7.3.2 Low-density modifications stable in the negative pressure region

Our calculations show a transition in the negative pressure region, between the NaCl and the  $\alpha$ -GeTe type modification at around -6 GPa calculated using LDA functional (see figures 7.7, 7.8, and 7.12. There exist no experimental or calculated data yet regarding a possible  $\alpha$ -GeTe structure in the PbS system. The  $\alpha$ -germanium telluride structure (hR6) can be described as a distorted rock salt structure, with 3 + 3 fold coordination of the Pb atoms by S atoms in the  $R3m$  space group. [296] Furthermore, germanium telluride is found in a high-temperature phase (cubic, NaCl) and a low-temperature phase (rhombohedral,  $\alpha$ -GeTe). The cubic-to-rhombohedral phase transition in germanium telluride has been studied experimentally [297] and theoretically [298].

In this respect, we note that  $\text{Pb}^{2+}$  ions might exhibit a stereochemically active lone pair. Recent studies on PbO and PbS [299] have tried to find evidence for a steric electron pair in the PbO ( $B10$ ) type of structure<sup>1</sup> in these two systems. However, the DFT calculations show that the distorted structure is not due to a sterically active lone pair, but results from cation-anion interactions, which produce such asymmetric electron densities. Furthermore, there is no stereochemical evidence of the lone pair in

<sup>1</sup>The PbO structure type can be described as a distortion of the CsCl structure.

## 7. STRUCTURE PREDICTION FOR LEAD SULFIDE (PbS) AT VARIOUS PRESSURES ON AB INITIO LEVEL

---

the PbS system, so far, and the thermodynamically stable modification of PbS is found in the highly symmetric rock salt crystal structure. However, the appearance of the  $\alpha$ -GeTe type in our global search could be an indication of the lone pair in lead sulfide system, and this will be discussed in greater detail in the next chapter. [56, 252]

Besides the  $\alpha$ -GeTe type as a distorted version of NaCl at standard pressure, we have also found the slightly distorted PbO type of structure ( $B10$ ) at high pressure (denoted as PbS-IX type). However, it exhibits a lower symmetry (space group  $Pmma$  (no. 51)) than the PbO type and it was stable only within the Hartree-Fock approximation.

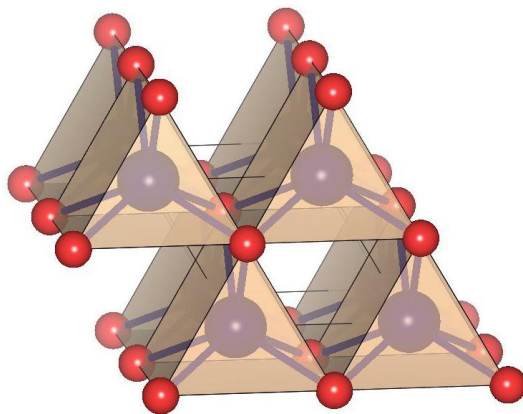


**Figure 7.13: Visualization of the calculated structure types** - The tungsten carbide ( $\alpha$ -WC) structure type in a periodically repeated unit cell.

In addition to the structures discussed previously, we have found two promising candidates that exhibit known structure types. These modifications appeared in our global searches both at standard and elevated pressures, but have not yet been observed in the experiment: the nickel arsenide ( $B8_1$ ) structure (see figure 7.4) and the so-called  $\alpha$ -WC ( $B_h$ ) type, a low-temperature modification of tungsten carbide (see figure 7.13). [300] There is an indication from the  $H(p)$  curves that the NiAs type would be easier to synthesize than the  $\alpha$ -WC type. Furthermore, our global investigations of PbS have led us to several additional minima possibly relevant in the negative pressure region which can be considered as distortions of known types. These minima, denoted as PbS-IV (space group:  $P6_3mc$ ) and PbS-VIII (space group:  $P2_13$ ) are energetically very good candidates in the low-density region of the energy landscape. Similarly, there also exists a distorted version of the NiAs type on the landscape denoted as PbS-IV (coordination

number  $3 + 3$ ), which is even lower in energy than the sixfold coordinated NiAs type for low densities. Analogously, a distorted NaCl modification was structurally located between the  $\alpha$ -GeTe and the NaCl type, denoted as a PbS-VIII modification, but it was only stable in the Hartree-Fock local optimization. If a DFT functional with LDA or B3LYP was used, the PbS-VIII type was unstable and quickly converted to the NaCl type. Therefore we have not included it as a relevant structure candidate in the negative pressure region in figures 7.7 and 7.8 and tables 7.1-7.3, as we did with PbS-IV. [56, 252]

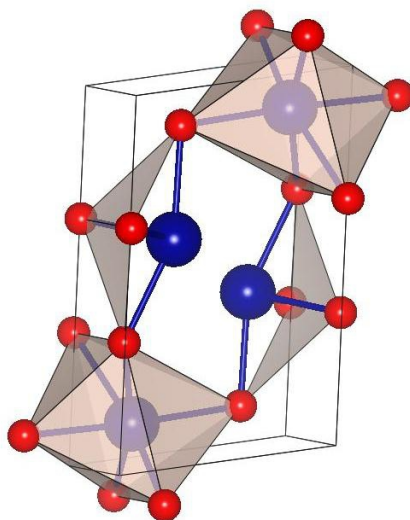


**Figure 7.14: Visualization of the additionally calculated high-pressure structures** - The PbS-I structure type found in a periodically repeated unit cell.

In our previous calculations, we have often encountered several known prototypes, such as wurtzite ( $B4$ ), sphalerite ( $B3$ ), and the so-called “5-5” structure type [15] that are possible competitors at large negative pressures. However, there were not encountered during our global optimizations at standard pressure. In order to be able to judge whether these modifications need to be considered in the negative pressure regions, we performed a series of local optimizations for these structure types using different functionals (DFT and HF). All of these candidates were found to be stable in the negative pressure region, with the “5-5” structure type as the lowest one in energy. However, when we start a random walk from the 5-5 minimum at standard pressure, we rapidly leave this region of the energy landscape for minute initial displacements indicating instability already at low temperatures. Similarly, our

## 7. STRUCTURE PREDICTION FOR LEAD SULFIDE (PBS) AT VARIOUS PRESSURES ON AB INITIO LEVEL

---

calculations show that both the sphalerite- and the wurtzite-type modification represent only small side minima, being 0.6-0.7 eV per formula unit higher in energy than the NaCl structure type, which is in good agreement with previous calculations (see figure 7.7). [267] The total energy is therefore higher than those of all the other structures listed in Table 7.2; this might explain why these modifications did not appear in our global optimizations at standard pressure. Thus, we conclude that wurtzite (*B4*), sphalerite (*B3*), and the 5-5 type of modification should be very hard to synthesize, while the  $\alpha$ -GeTe-type modification might be the most promising target for experimental synthesis at standard or small effective negative pressures, especially as it can be obtained from the rock salt type by a slight distortion. [56, 252]

### 7.3.3 New modifications found exhibiting unknown structure types

Several minima exhibiting previously unknown structure types were found during our global searches at various pressures. We have found as additional candidates with calculations performed at standard pressure the PbS-IV, PbS-V, PbS-VI, and PbS-VIII types (see table 7.2). The last three structure types were stable only on the Hartree-Fock level, however. PbS-V exhibits space group 7 (*Pc*), and has an irregular structure with sixfold coordination of Pb by S and conversely. Although the PbS-VI modification has space group  $C222_1$  (no. 20), structure analysis performed showed that it could be visualized as a strongly distorted NiAs type. Finally, PbS-IV and PbS-VIII, which were discussed earlier, are unknown PbS structure types found at standard and effective negative pressures. PbS-IV (space group:  $P6_3mc$ ) can be described as a distortion of the NiAs type with 3 + 3 coordination of Pb by S atoms, and PbS-VIII (space group:  $P2_13$ ) can be described as a distortion of the NaCl type. [56, 252]

When we performed calculations at elevated pressures, we have found structures exhibiting the PbS-I, PbS-II, PbS-III, PbS-VII, and PbS-IX types (see tables 7.2 and 7.3), which are stable at both Hartree-Fock and DFT level, except the PbS-IX type. When this slightly distorted PbO type of structure is optimized with DFT, it becomes the CsCl type modification. At 4 GPa we observed a strongly distorted version of the  $\alpha$ -WC type, denoted as PbS-VII type. This structure exhibits space group  $Pmn2_1$  (no. 31), but a successful comparison to the WC type (space group  $P\bar{6}m2$ , a supergroup of  $Pmn2_1$ ) was made with the CMPZ algorithm. [230]

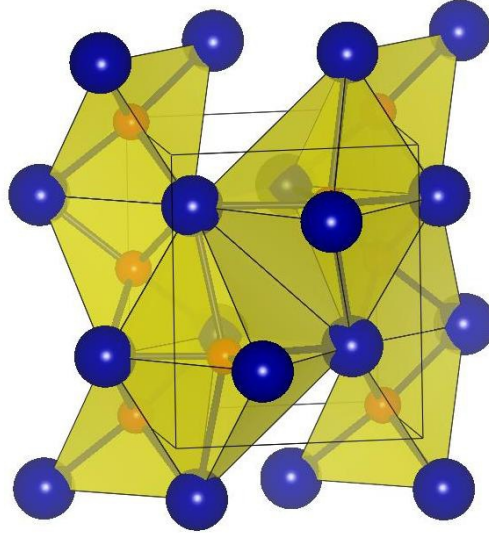


**Figure 7.15: Visualization of the additional calculated high-pressure structures** - The PbS-II structure type in a periodically repeated unit cell. Note that PbS-II structure is represented with S-atoms coordinated by 4 and 6 Pb-atoms.

Here we note a report of a monoclinic structure at intermediary pressures, which was observed in previous investigations of the PbS system. [277, 301] While performing our calculations at high pressures, we have also often encountered a monoclinic modification denoted as PbS-I (see table 7.3). PbS-I shows space group  $P2_1/m$  (no. 11) and can be described as an irregular structure with Pb and S coordinated by a total of 11 S and Pb atoms, respectively (within a distance interval of 1.7 Å). We observe that one Pb atom is in the center of an S octahedron which is corner connected to S triangles around the second Pb atom (see figure 7.14). This structure type was observed in the pressure range from 8 to 24 GPa (see table 7.3) and might be related to the TII type, as a strongly distorted version. Thus, we think that PbS-I, although having an irregular structure, could help in explaining the possible appearance of monoclinic intermediary phases in the lead sulfide system. [56, 252]

The PbS-II type of structure crystallizes in space group  $Pma2$  (nr. 28) at 8 GPa (see figure 7.15). We observe that the Pb atoms are cubic close packed and that they are coordinated by four and six sulfur atoms each. Similarly, the S atoms are coordinated by four and six Pb atoms in this unknown structure type. We note that in recent work in nanocrystalline PbS films a structure has been proposed consisting of a Pb-*fcc* lattice

## 7. STRUCTURE PREDICTION FOR LEAD SULFIDE (PbS) AT VARIOUS PRESSURES ON AB INITIO LEVEL

---

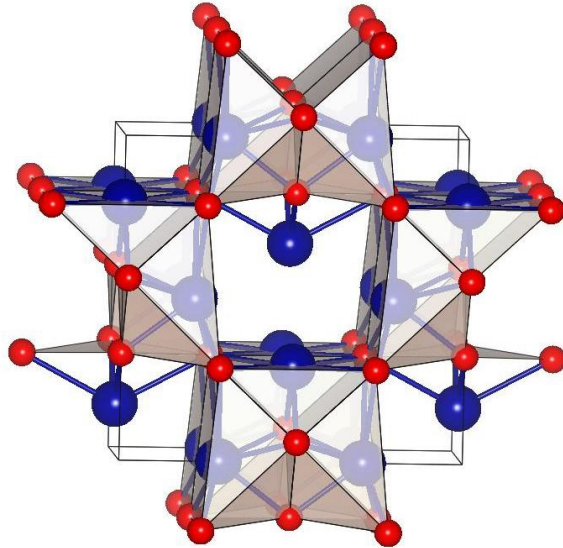


**Figure 7.16: Visualization of the additional calculated high pressure structures**  
- The PbS-III structure type in a periodically repeated unit cell.

with S located at random positions on 84% of the octahedral and 8% of the tetrahedral holes of the fcc lattice, possibly related to the  $V_{52}O_{64}$  or to the  $DO_3$  structure type. [278, 279] Our PbS-II structure appears to be related to this family of structures sharing the same underlying structure elements<sup>1</sup>.

Furthermore, we have found a high-pressure structure candidate PbS-III, which has showed the highest variation in the local coordination of all the new structure types found in the present work. This structure was found at 24 GPa and can be described as consisting of several different irregular structure elements (see figure 7.16). It exhibits space group  $Amm2$  (no. 38), and the three irreducible Pb and S atoms in the asymmetric unit cell are each fourfold, sixfold, and sevenfold coordinated, respectively. [56, 252]

### 7.4 Electronic aspects at standard and elevated pressures

We have performed band structure calculations for the most relevant structures in order to gain additional insight into the properties of the possible modifications of lead sulfide.

---

<sup>1</sup>The Pb-atom is in the *fcc* packing, and S-atom is in the octahedral and tetrahedral holes.



## 7.4 Electronic aspects at standard and elevated pressures

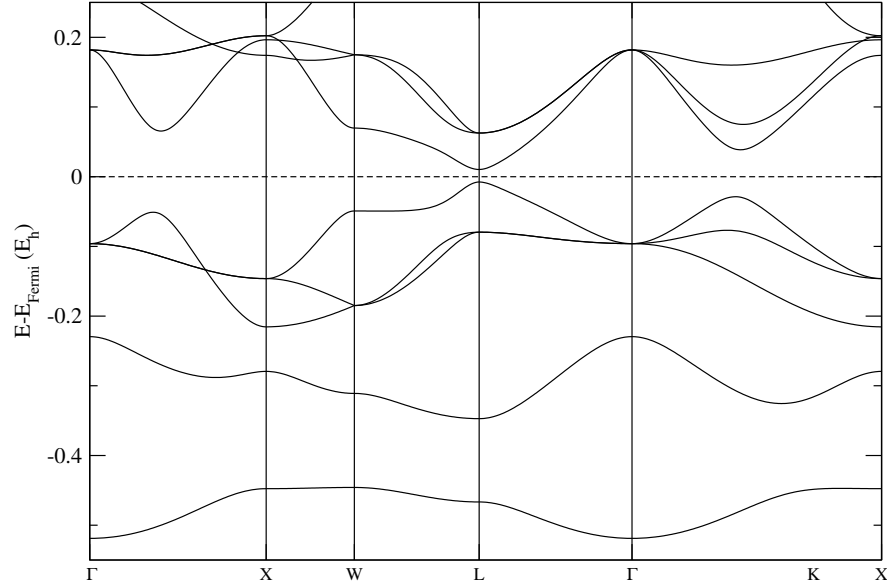


**Figure 7.17:** Band structure calculation of the NaCl type structure in PbS at equilibrium volume showing a tiny gap - Calculations performed using LDA functional.

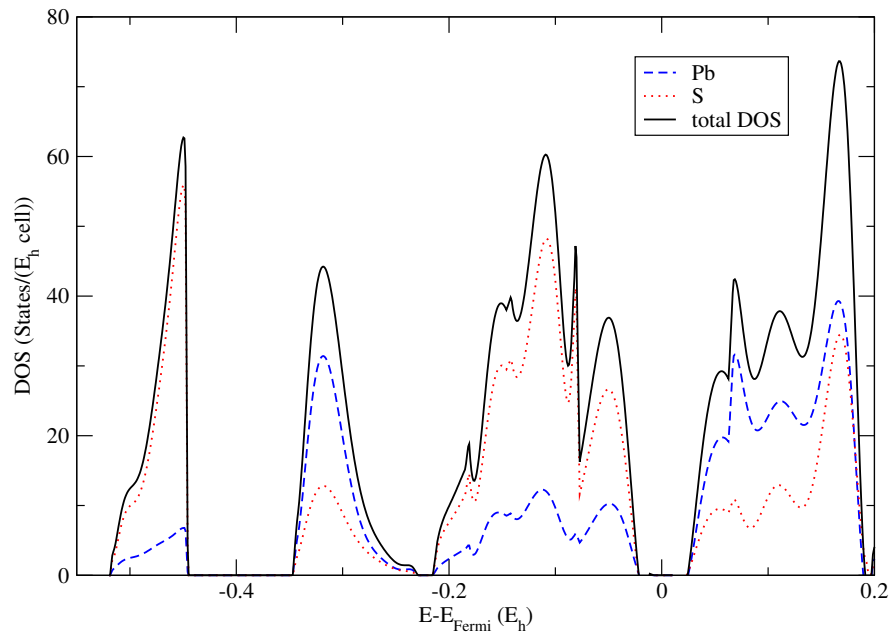


**Figure 7.18:** Density of states (DOS) of the NaCl type modification in the PbS system at equilibrium - Calculations performed using LDA functional.

## 7. STRUCTURE PREDICTION FOR LEAD SULFIDE (PBS) AT VARIOUS PRESSURES ON AB INITIO LEVEL

---

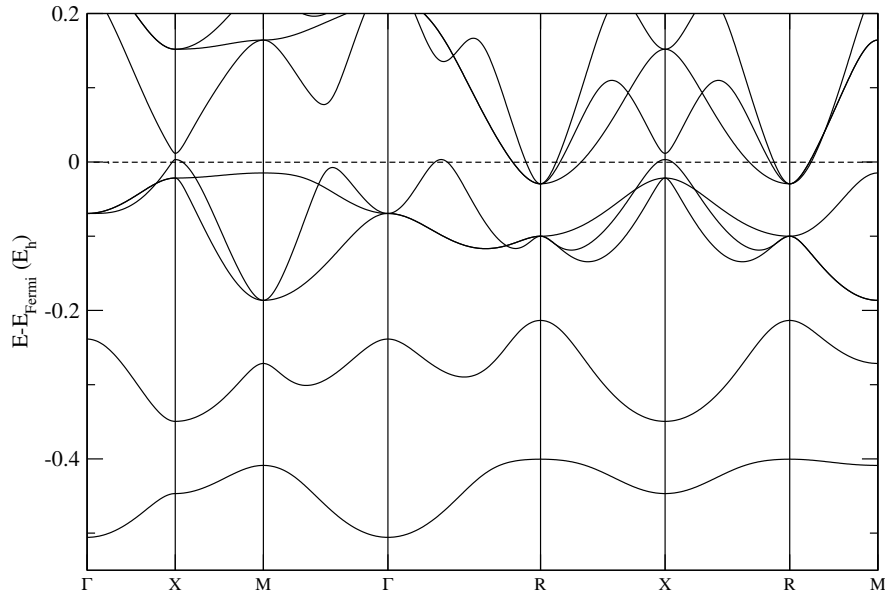


**Figure 7.19:** Band structure calculation of the CsCl type structure at equilibrium volume exhibiting metallic properties - Calculations performed using DFT-LDA.

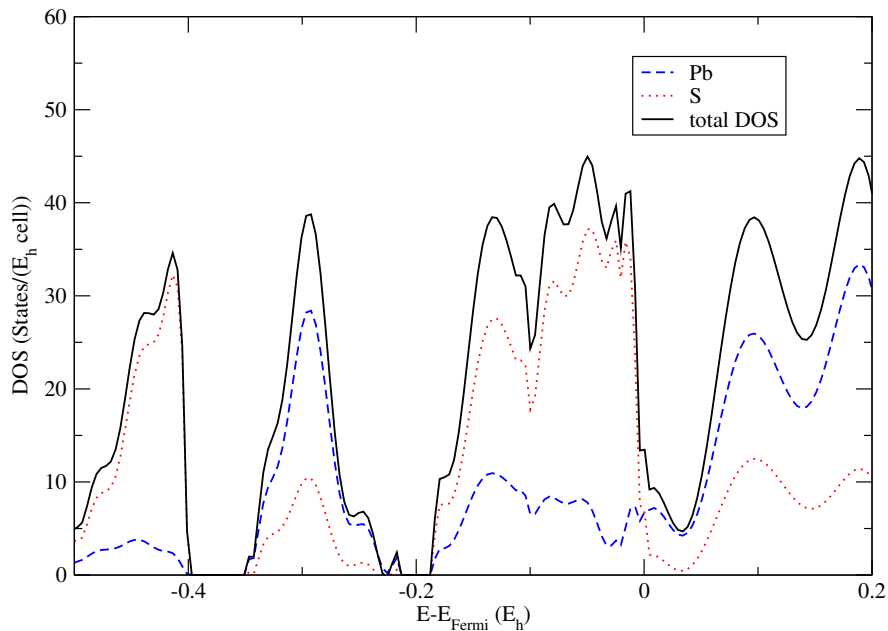


**Figure 7.20:** Density of states (DOS) of the CsCl type modification in the PbS system at equilibrium - Calculations performed using DFT-LDA.

## 7.4 Electronic aspects at standard and elevated pressures

---

Since the better agreement with experiment was found for the DFT-LDA calculations, here we present the results performed using the local density approximation.

The band structure calculations show that the NaCl-type modification has a tiny gap (for more details, see Appendix and figure 7.17). The CsCl modification is metallic for the whole pressure range, even at 0 GPa (see figure 7.19). From the total and projected density of states (DOS) calculations (see figures 7.18 and 7.20), we observe that Pb states fill the gap in the case of the CsCl structure. Compared to the NaCl structure type, the Pb-Pb distances are shorter in the CsCl structure<sup>1</sup>, and therefore we conclude that the shortening of the Pb-Pb distances is the reason for the metallic character of the CsCl modification. Both the TII and the FeB modification show an insulating state for the calculated pressure range (from 5 to 25 GPa), but we observe a smaller band gap in the FeB type at equilibrium volume:  $E_{gap}(TII) \approx 1.8$  eV and  $E_{gap}(FeB) \approx 0.7$  eV, respectively (see figures 7.21 and 7.22). [56, 252]

In order to compare the band structures calculated with LDA, we have performed band structure calculations using the B3LYP functional. However, the computed gap was too large for the NaCl-type modification ( $\approx 2$  eV; see also Ref. [302]), because the experimental data show a gap of only  $\approx 0.3$  eV [303, 304] (in good agreement with the LDA calculation). Furthermore, the  $E(V)$  and  $H(p)$  curves calculated with B3LYP indicate transition pressures that are too high compared to experiment<sup>2</sup> [252, 275–277]

In addition, the Mulliken population analyses were performed for the NaCl, the TII, and the CsCl type of structure, using the LDA functional. At the respective equilibrium volume, the computed Mulliken charge of the Pb cation/S anion is  $\pm 1.05$  in the NaCl type,  $\pm 0.91$  in the CsCl type, and  $\pm 0.92$  in the TII type of structure, respectively, and therefore far away from the ideal values ( $\pm 2$ ) in the case of a purely ionic compound. This relatively small charge transfer is consistent with the relatively small electronegativity ( $EN$ ) difference between sulfur and lead ( $EN(S) - EN(Pb) = 0.25$ ) [305]. We note that the magnitude of the Mulliken charge decreases when the volume is further reduced for all three modifications investigated.

---

<sup>1</sup>NaCl: 4.14 Å, CsCl: 3.54 Å.

<sup>2</sup>e.g., the NaCl-TII transition has been calculated to occur at 12 GPa compared to the experimentally observed one at 2.2 GPa.

## 7. STRUCTURE PREDICTION FOR LEAD SULFIDE (PbS) AT VARIOUS PRESSURES ON AB INITIO LEVEL

---

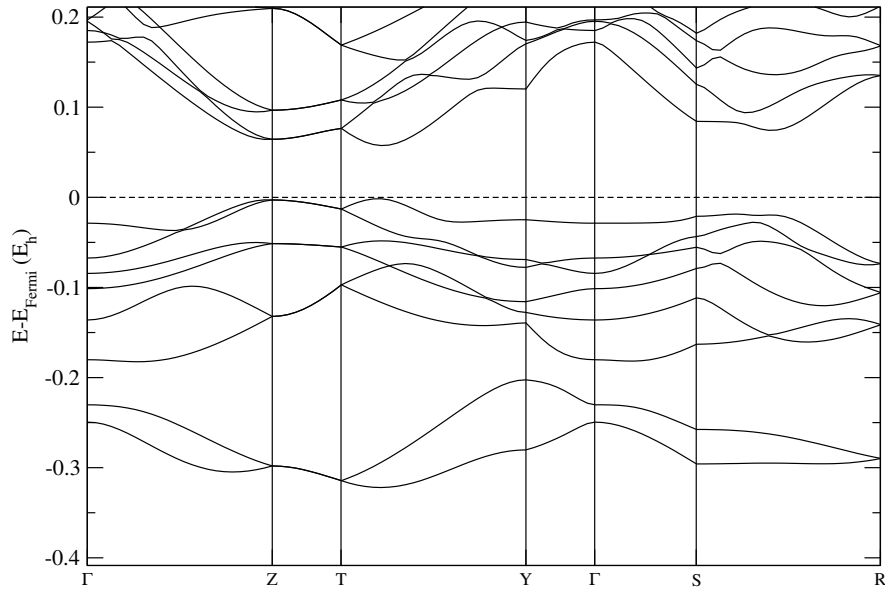


**Figure 7.21: Band structure of the TII type at the computed equilibrium volume in the PbS system using LDA** - Note that the labels of the special points in the TII type correspond to a base-centered orthorhombic lattice, respectively.

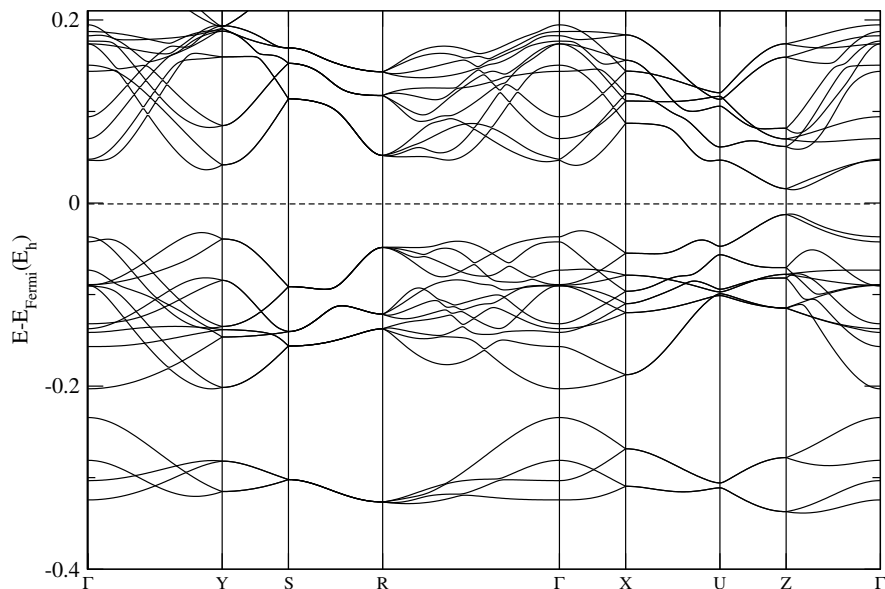


**Figure 7.22: Band structure of the FeB type at the computed equilibrium volume in the PbS system using LDA** - Both the TII and the FeB modifications should be insulators, but we observe a smaller band gap in the FeB type structure. Note that the labels of the special points in the FeB type correspond to a simple orthorhombic lattice, respectively.

## 7.5 Conclusion

A structure prediction study for bulk PbS for various pressures using *ab initio* energy calculations during both the global and local optimization was performed. According to our calculations a transition from the NaCl type to the thallium iodide (*B33*) type at 4.5 GPa was found, which is in agreement with what the experimental observations. In addition, we have discovered a new competitive orthorhombic phase, showing the iron boride (*B27*) type, which appears at a slightly higher pressure than the TII type of structure, in analogy to the PbTe system. This may help to clarify the experimental data, where several orthorhombic phases have been claimed to exist at intermediary pressures.

Furthermore, the TII (FeB) to the CsCl transition was observed at 25 GPa, and again this is in agreement with what was found in the experiment. We have found new structure candidates which have not yet been discussed theoretically or experimentally, in particular an additional modification exhibiting the  $\alpha$ -GeTe structure type, which might be stable at slightly negative pressures. Furthermore, we have investigated the electronic band structures and density of states (DOS) of the most relevant structure types which appeared to be in good agreement with the experimental data.

**7. STRUCTURE PREDICTION FOR LEAD SULFIDE (PBS) AT  
VARIOUS PRESSURES ON AB INITIO LEVEL**

---

# Investigation of kinetic stability, electronic and vibrational properties of PbS and BaS as a function of pressure

*"Nature is pleased with simplicity."*

(Isaac Newton (1642-1727), English mathematician and physicist)

## 8.1 Introduction

A fundamental goal in solid state chemistry is to understand the electronic structure of chemical compounds, since it controls many physical and chemical properties of a solid. Of particular interest is the structure directing influence of electronic features such as degeneracies in the band structure that can lead to e.g. Peierls distortions or charge density waves, and steric electron pairs that can be the cause of deviations in the symmetry of a structure from the one expected based on e.g. spherical ion models. [306] This "stereochemical activity" of lone pairs is well documented by numerous examples [112, 113, 307], and they have been theoretically addressed through the VSEPR concept [114], and subsequent quantum chemical refinements (for a review see e.g. [115]), providing a sound basis for classifying and even qualitatively predicting local geometries.

Therefore, whenever one encounters a solid compound where 'excess' valence elec-

## 8. INVESTIGATION OF KINETIC STABILITY, ELECTRONIC AND VIBRATIONAL PROPERTIES OF PBS AND BAS AS A FUNCTION OF PRESSURE

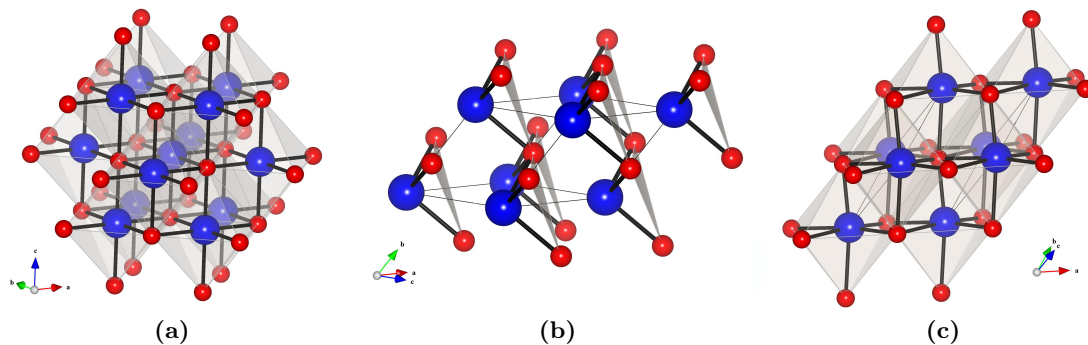


**Figure 8.1:** Visualization of the experimentally observed and calculated structure types in PbS calculated using the LDA functional: a) Rock salt (NaCl) structure type ( $Fm-3m$ ) in a periodically repeated unit cell; b)  $\alpha$ -germanium telluride structure type ( $R3m$ ) in a periodically repeated unit cell; c) Six-fold coordination of the Pb-atom by the S-atoms in the  $\alpha$ -GeTe type, often depicted as three-fold coordination as in figure b).

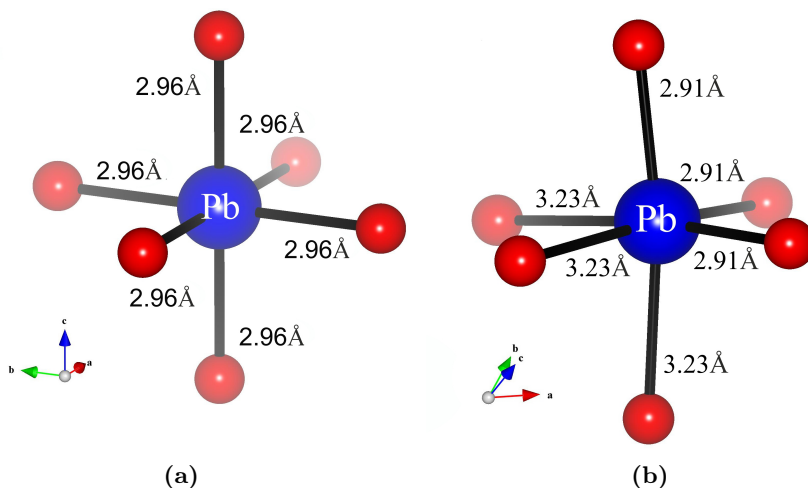


**Figure 8.2:** Visualization of coordination polyhedra of the experimentally observed and calculated structure types in PbS calculated using the LDA functional: a)  $PbS_6$  octahedron with six-fold coordination of the Pb-atom by the S-atoms in the NaCl type; b)  $PbS_6$  octahedron with six-fold coordination (3 short and 3 long distances) of the Pb-atom by the S-atoms in the  $\alpha$ -GeTe type. Note that when the  $\alpha$ -GeTe modification is represented with six-fold coordination of the Pb-atom by the S-atoms, the distortion from perfect NaCl type becomes obvious.



trons are present that are not accounted for by covalent bonds between the atoms or a (formal) charge transfer from the cationic species to the anionic one, a full understanding of the compound demands the investigation of the effect of these electrons on the compound's structural, electronic and vibrational properties. This becomes even more critical in the context of the global energy landscape view of a chemical system, [17–19] where a multitude of competing structures exist that might be stabilized or destabilized by exactly such effects, depending on the thermodynamic boundary conditions such as pressure and temperature.

In order to investigate possible stereochemical activity of PbS, we compared two modifications found after global optimization in PbS (see **chapter 7**), the experimentally observed rock salt type of structure [272, 275] and the predicted low-temperature  $\alpha$ -GeTe type of structure [296], and investigated their electronic and vibrational properties. [62] The  $\alpha$ -GeTe type of structure can be described as a rhombohedral distortion along the [111] direction of the rock salt structure and a subsequent shear relaxation along the same direction as a second order parameter [308], reducing the rhombohedral angle  $\alpha$  from the perfect fcc value of  $60^\circ$  and leading to a 3+3 fold coordination of Pb by S (see figures 8.1, 8.2, 8.3, and 8.4). [62]

## 8.2 Optimization procedure

All calculations were performed on the *ab initio* level using the CRYSTAL09 program [191, 192]. The local optimizations employed analytical gradients with respect to the atom positions [154, 155], and the cell parameters [156–158], and a local optimizing routine [309]. The subsequent phonon calculations were based on analytical first and numerical second derivatives [310]. These local optimizations were performed both on the Hartree-Fock and the DFT level, employing the B3LYP<sup>1</sup> and the LDA functional. For the calculations in the lead sulfide (PbS) system, basis sets for Pb and S were used as in ref. [252]. For the calculations in the barium sulfide (BaS) system, we used the same basis set for S as for PbS. For Ba, we used the pseudopotential by Hay and Wadt [311], in combination with the tightest *sp*-contraction from ref. [312]. In addition, we used 3 *sp* shells with exponent 0.95, 0.45, 0.17, and 2 *d* shells with exponents 0.4 and

---

<sup>1</sup>Becke's three parameter functional [134] in combination with the correlation functional of Lee, Yang and Parr

## 8. INVESTIGATION OF KINETIC STABILITY, ELECTRONIC AND VIBRATIONAL PROPERTIES OF PBS AND BAS AS A FUNCTION OF PRESSURE

---

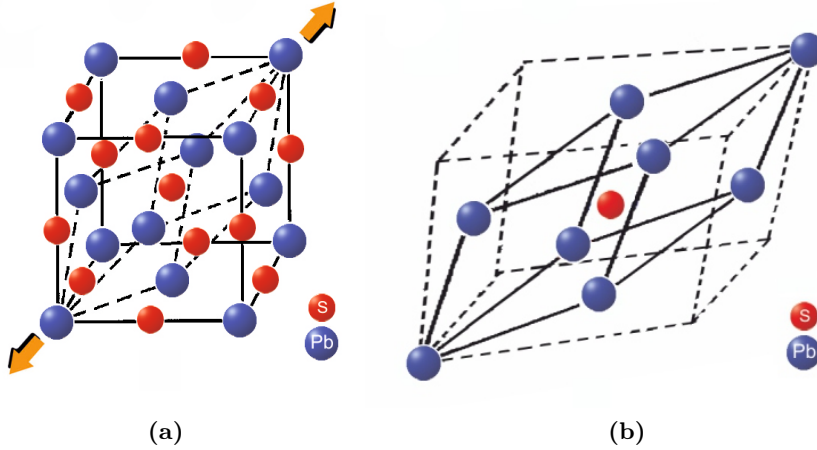


**Figure 8.3:** At equilibrium, PbS is found in the NaCl modification, shown with the standard cubic and the primitive rhombohedral unit cell (a). This results in a distortion of the perfect rock salt type structure at expanded volumes to the rhombohedral  $\alpha$ -GeTe type of structure, which exhibits a larger cell parameter but smaller rhombohedral angle than in the NaCl type of modification (b).

0.15. Therefore, in total a  $[4s4p2d]$  basis set was used for Ba. Note that especially the diffuse  $d$ -shell is crucial to obtain the proper conduction band structure and band gap of BaS. [313–315]

A supercell technique was used to obtain the frequency dependent dispersion, as implemented in the **CRYSTAL09** code. In order to achieve maximum computational efficiency and to keep the calculations tractable, selected supercells for the various directions were used (for a description see section 6.2). The LO-TO splitting at the  $\Gamma$  point was calculated using the dielectric function, which was computed within the framework of the coupled perturbed Kohn-Sham method (see Appendix). [316] Structure analysis and visualization was performed using **KPLOT** [227] and the **VESTA** [317] program, and the **J-ICE** program [318] was used for the visualization and analysis of the phonon modes (see Appendix).

### 8.3 Results and Discussion

The  $\alpha$ -GeTe modification becomes thermodynamically stable at negative pressures (-6 GPa) within the local density approximation (LDA) and already at standard pressure

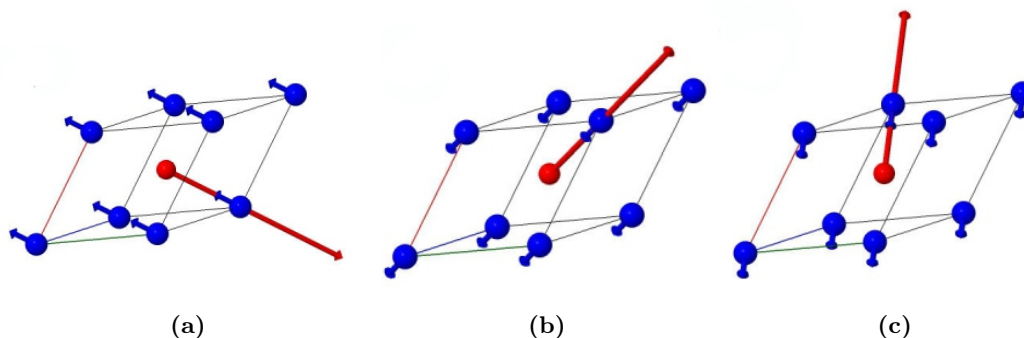


**Figure 8.4:** The figures show phonon modes corresponding to vibrations in the  $[100]$ ,  $[010]$  and  $[001]$  direction (figures a, b and c). The phonon modes are degenerate at the  $\Gamma$ -point and their combination produces a vibration in the  $[111]$  direction.

within the Hartree-Fock (HF) approximation (see **chapter 7**). [252] The analogous cubic-to-rhombohedral phase transition in germanium telluride (GeTe) system has been studied experimentally [297, 319, 320] and theoretically [298, 321], see also the overview in ref. [322]. As a reference point, we compare our results also with the corresponding ones for BaS [313–315, 323], which is in many ways an analogue to PbS, but where no unusual electronic or structural effects related to localized electron pairs are expected.

### 8.3.1 Electronic properties

At the beginning we have calculated charge density plots of the two PbS modifications in different planes in order to investigate the effects of the excess electron pair in lead sulfide (see figure 8.5). Then, we have analyzed separate layers of Pb atoms (see figure 8.6) and the S atoms (see figure 8.7) in the lead sulfide system for many cuts along the  $(1\ 1\ 1)$  planes for both the rock salt (NaCl) and the germanium telluride ( $\alpha$ -GeTe) modification. We have observed the same type of distortions for the  $\alpha$ -GeTe modification of PbS as in the analogous germanium telluride system. [297] In addition, we have computed electron charge density difference maps of selected layers of the NaCl and the  $\alpha$ -GeTe type modifications of PbS using LDA along the  $(1\ 1\ 1)$  planes for the Pb atom and S atom layer (see figures 8.8 and 8.9). We observe the slight change in the charge density between the two structures, which reflects the rhombohedral distortion and the different coordination of the Pb atoms with respect to the S neighbors<sup>1</sup>

<sup>1</sup>In the NaCl structure CN = 6, and in the  $\alpha$ -GeTe type of structure CN = 3+3.

## 8. INVESTIGATION OF KINETIC STABILITY, ELECTRONIC AND VIBRATIONAL PROPERTIES OF PBS AND BAS AS A FUNCTION OF PRESSURE

---

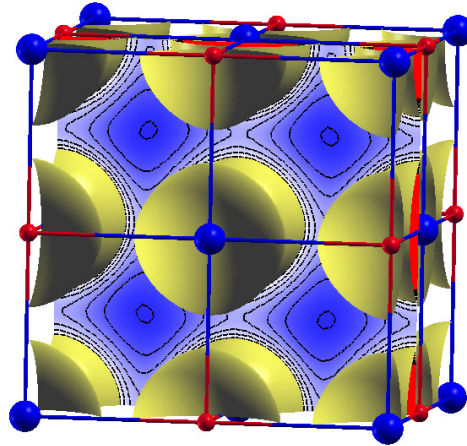


**Figure 8.5:** Charge density plot of NaCl modification in PbS calculated on LDA level - In this figure we show a charge density plot through the (0 1 0) plane, and similar results are observed for the (1 0 0), (0 0 1) and (1 1 1) plane in the equilibrium rock salt structure.

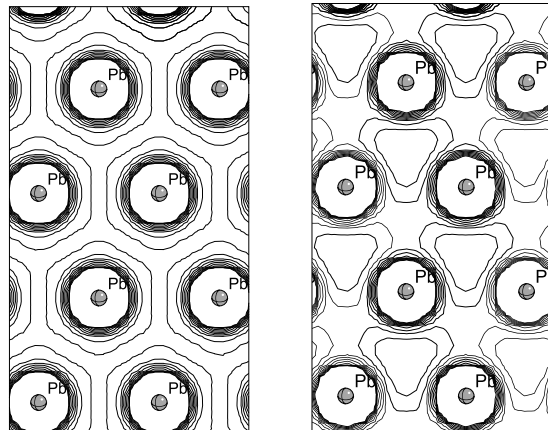


**Figure 8.6:** Charge density plot of selected layers of the NaCl and  $\alpha$ -GeTe type modifications of PbS (on LDA level) along the (1 1 1) planes for the Pb atom layer in the NaCl type modification (left) at equilibrium and  $\alpha$ -GeTe type (right) at expanded volume - Note that the Pb-Pb and S-S distances are 4.14 Å in the left figures, and 4.33 Å in the right figures and that the isolines in the figures represent density in atomic units ( $electron/bohr^3$ ), ranging up to 0.1 a.u. with a step size of 0.01 a.u.

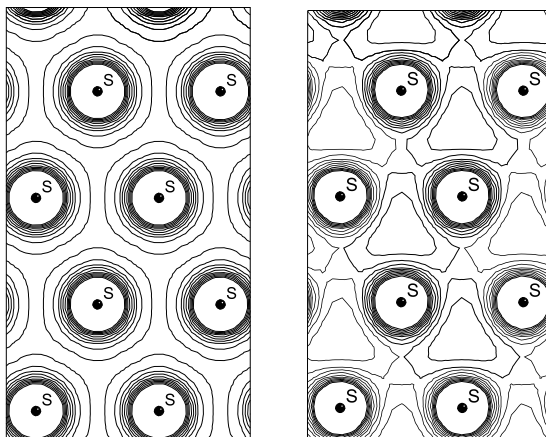


Figure 8.7: Charge density plot of selected layers of the NaCl and  $\alpha$ -GeTe type modifications of PbS (on LDA level) along the (1 1 1) planes for the S atom layer in the NaCl structure type (left) at equilibrium and  $\alpha$ -GeTe structure type (right) at expanded volume - Note that the isolines in the figures represent density in atomic units ( $electron/bohr^3$ ), ranging up to 0.1 a.u. with a step size of 0.01 a.u.

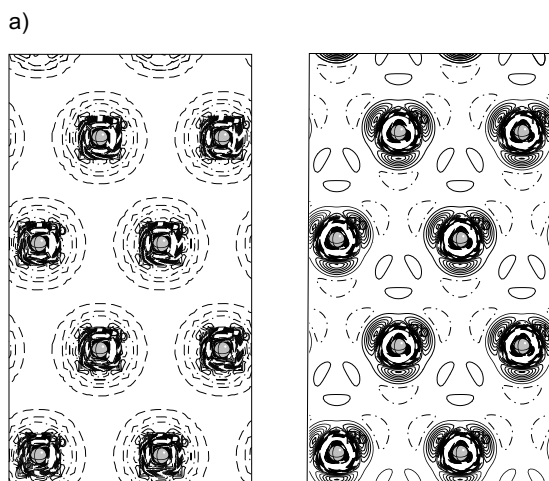
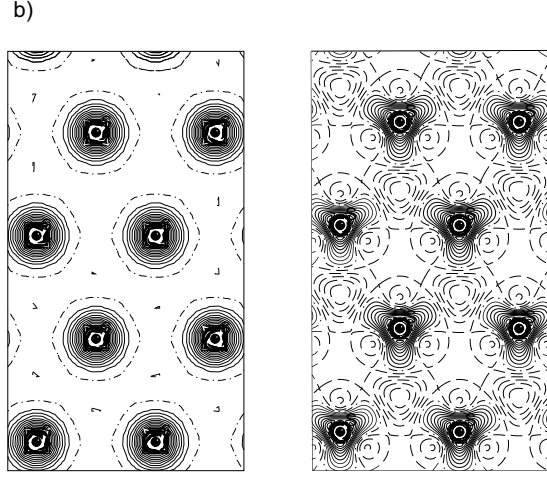


Figure 8.8: Electron charge density difference map of selected layers of the NaCl and the  $\alpha$ -GeTe type modifications of PbS using LDA along the (1 1 1) planes for the Pb atom layer in the NaCl modification (left) at equilibrium and  $\alpha$ -GeTe type (right) at expanded volume - The charge density difference is computed as the difference of the electron charge density of PbS and the charge density of free  $Pb^+$  and  $S^-$  ions at the same positions as in the respective lattices. Note that the isolines in the figures represent density in atomic units ( $electron/bohr^3$ ), ranging up to 0.1 a.u. with a step size of 0.01 a.u. Positive values are indicated with full lines, negative values with dashed lines, and zero values with a dash-dotted line.

## 8. INVESTIGATION OF KINETIC STABILITY, ELECTRONIC AND VIBRATIONAL PROPERTIES OF PBS AND BAS AS A FUNCTION OF PRESSURE

---



**Figure 8.9:** Electron charge density difference map of selected layers of the NaCl and the  $\alpha$ -GeTe type modifications of PbS using LDA along the (1 1 1) planes for the S atom layer in the NaCl modification (left) at equilibrium and  $\alpha$ -GeTe type of structure (right) at expanded volume - The slight change in the charge density between the two structures reflects the rhombohedral distortion and the different coordination of the Pb atoms with respect to the S neighbors (6 in the NaCl structure, 3+3 in the  $\alpha$ -GeTe structure).

Based on these calculations one would hesitate to point to a definite signature of a stereochemically active localized  $Pb^{2+}$  electron pair in either the NaCl or the  $\alpha$ -GeTe type modification, although, there is clearly a correlation of the structure with the charge density plots. This is in agreement with previous calculations performed in the PbS system (in the NaCl type). [270, 271, 286, 287, 324]

In the next step, we have considered the band structures and densities of states (DOS) of the NaCl and  $\alpha$ -GeTe type modifications in PbS, and the NaCl modification in BaS, calculated with LDA functional. Furthermore, all of these calculations were performed and analyzed at equilibrium and expanded volumes (see figures 8.10, 8.11, 8.12, 8.13, 8.14, 8.15, 8.16, 8.17, 8.18, and 8.19). Both PbS modifications show a typical semiconductor band structure, in agreement with experiment (for the NaCl type) and previous calculations (for the NaCl type), e.g. refs. [262, 267]. When computed in the same space group, only minute differences between the two band structures are observed.

However, both the NaCl type and the  $\alpha$ -GeTe type band structure in PbS show a clearly separated  $6s^2(\text{Pb})$ -band at about  $-0.3 E_h$  lying between the  $3s^2(\text{S})$  and  $3p^6(\text{S})$  bands at about  $-0.5 E_h$  and  $-0.1 E_h$ , respectively ( $E_F = 0.0 E_h$ ). This suggests the

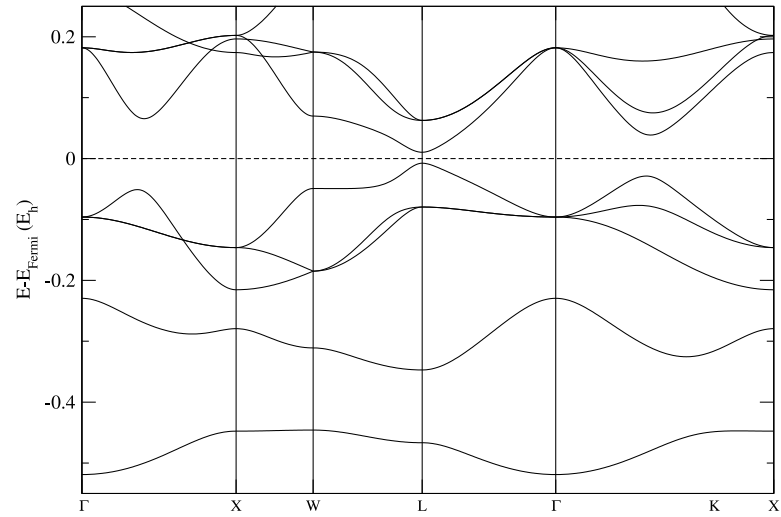


**Figure 8.10: Band structure calculation performed using the LDA functional in the NaCl type of structure at equilibrium volume ( $V = 50.30 \text{ \AA}^3$ ,  $a = 5.86 \text{ \AA}$ ) in the PBS system - Note that the labels of the special points correspond to a face-centered cubic lattice, respectively (notation according to [232]).**

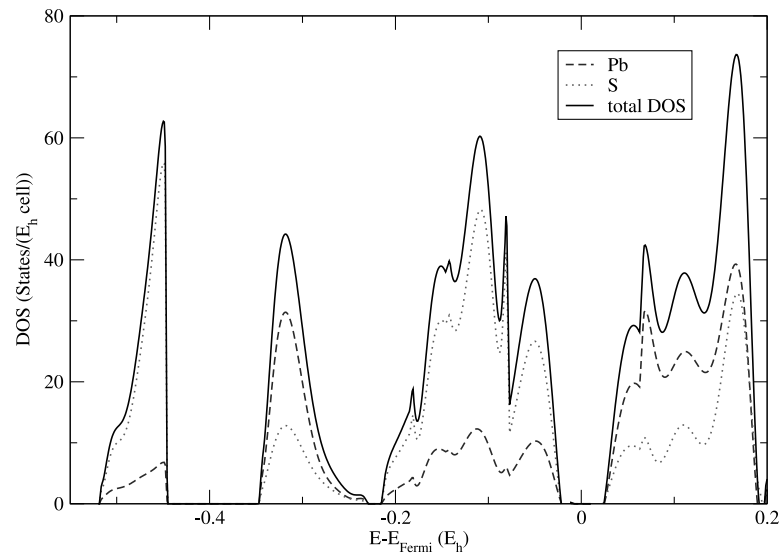


**Figure 8.11: Electronic density of states (DOS) in the NaCl type of structure at equilibrium volume ( $V = 50.30 \text{ \AA}^3$ ,  $a = 5.86 \text{ \AA}$ ) - Calculation performed in the PbS system using the LDA functional.**

## 8. INVESTIGATION OF KINETIC STABILITY, ELECTRONIC AND VIBRATIONAL PROPERTIES OF PBS AND BAS AS A FUNCTION OF PRESSURE

---

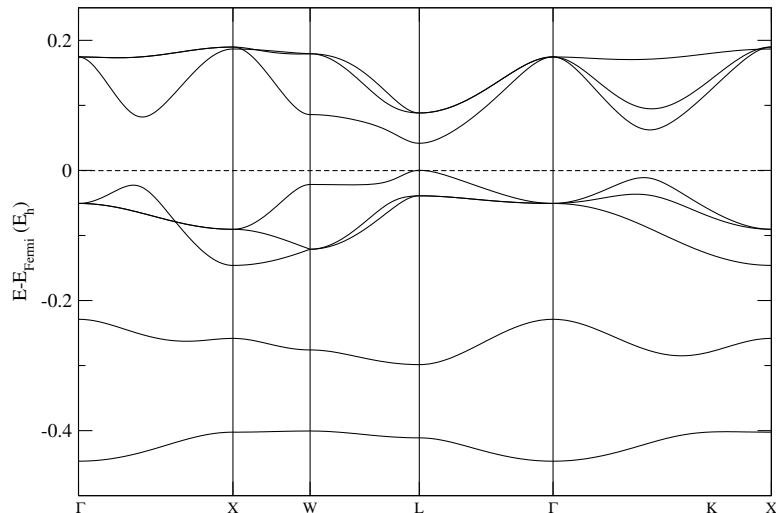


**Figure 8.12:** Band structure calculation performed using the LDA functional in the NaCl type of structure at expanded volume ( $V = 61.48 \text{ \AA}^3$ ,  $a = 6.24 \text{ \AA}$  in the PbS sytem), which corresponds to the pressure greater then 10GPa - Note that the labels of the special points correspond to a face-centered cubic lattice, respectively (notation according to [232]).

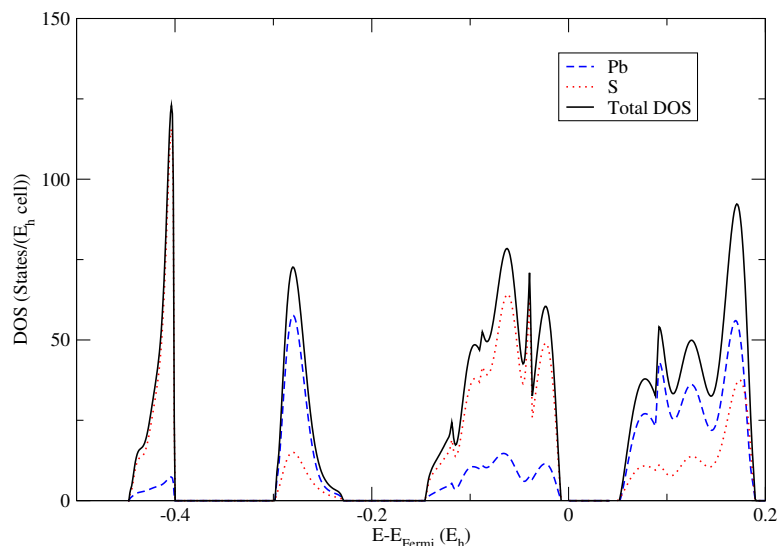


**Figure 8.13:** Electronic density of states (DOS) in the NaCl type of structure at expanded volume ( $V = 61.48 \text{ \AA}^3$ ,  $a = 6.24 \text{ \AA}$ ), which corresponds to the pressure greater then 10GPa - Calculation performed in the PbS system using the LDA functional.



existence of a weakly interacting lone pair of electrons associated with Pb, exhibiting an approximately spherical charge distribution. These observations are consistent with earlier calculations where it was argued that the lone pair in PbS has essentially  $s$ -character due to the small overlap between the Pb  $6s$  lone pair and the S  $p$ -levels. [325] Furthermore, the position of the unoccupied Pb  $6p$  band also plays a role [299, 326]. In addition, we have calculated the DOS projected on Pb  $s$ - and Pb  $p$ -, and S  $s$ - and  $p$ -orbitals separately (see Appendix).

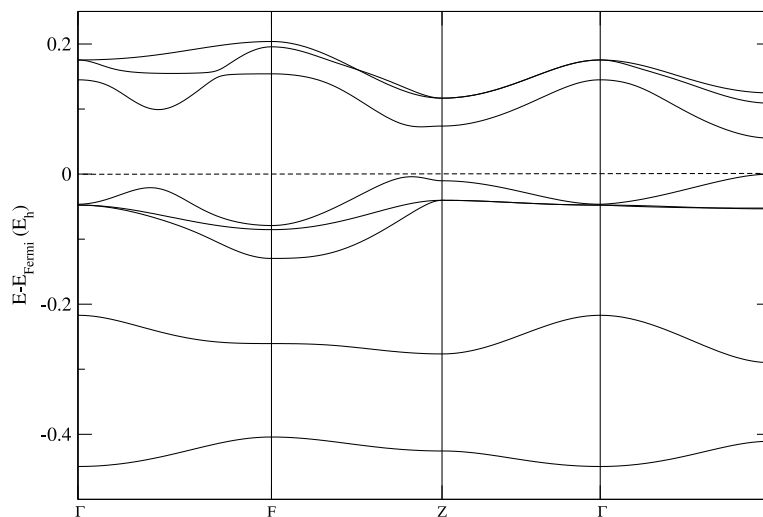


**Figure 8.14:** Band structure calculation performed using the LDA functional in the  $\alpha$ -GeTe type of structure at expanded volume ( $V = 61.48 \text{ \AA}^3$ ,  $a=4.56 \text{ \AA}$ ,  $\alpha = 56.32^\circ$ ) in the PbS system, which corresponds to the pressure greater than 10GPa - Note that the labels of the special points correspond to a rhombohedral lattice, respectively (notation according to [232]).

Finally we have compared the rock salt band structures and DOS in the PbS system and in the BaS system, and we note that the band is missing in BaS (see figure 8.18 and refs. [313–315]). Nevertheless, when comparing the NaCl band structure in the lead sulfide system [262, 267] and  $\alpha$ -GeTe type band structure in the germanium telluride system [321], one would conclude that the band structure by itself does not produce any strong evidence that the Pb lone pair is sterically active, as it does not show any interaction with the  $3s$  and  $3p$  bands of sulphur.

## 8. INVESTIGATION OF KINETIC STABILITY, ELECTRONIC AND VIBRATIONAL PROPERTIES OF PBS AND BAS AS A FUNCTION OF PRESSURE

---

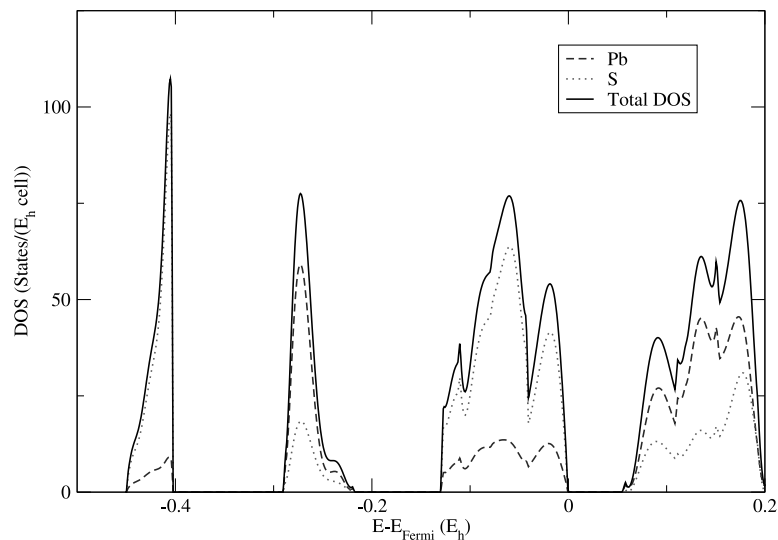


**Figure 8.15:** Electronic density of states (DOS) performed in the  $\alpha$ -GeTe type of structure at expanded volume ( $V = 61.48 \text{ \AA}^3$ ,  $a=4.56 \text{ \AA}$ ,  $\alpha = 56.32^\circ$ ), which corresponds to the pressure greater than 10GPa - Calculation performed in the PbS system using the LDA functional.

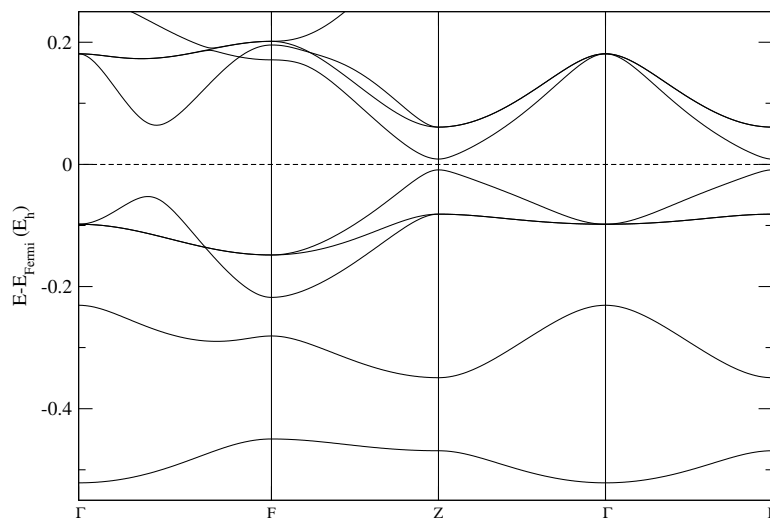


**Figure 8.16:** Band structure calculation performed using the LDA functional in the  $\alpha$ -GeTe type of structure at equilibrium volume ( $V = 50.30 \text{ \AA}^3$ ,  $a = 4.13 \text{ \AA}$ ,  $\alpha = 60^\circ$ ), in the PbS system - Note that the labels of the special points correspond to a rhombohedral lattice, respectively (notation according to [232]).

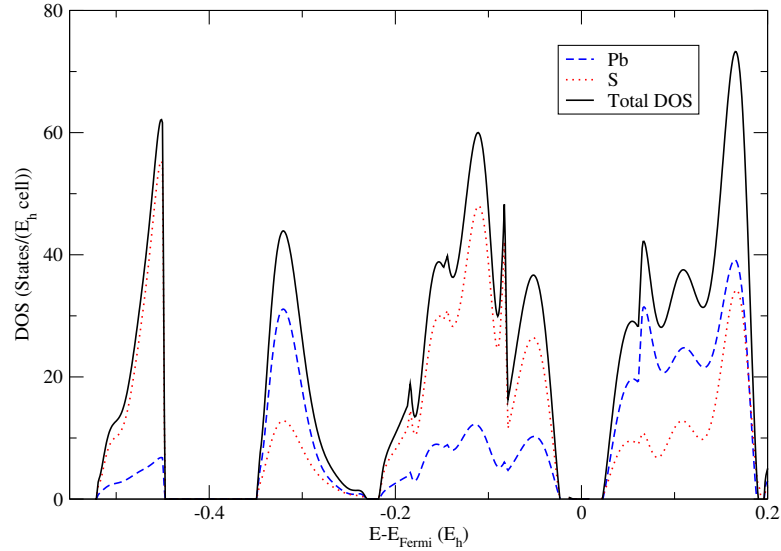


**Figure 8.17:** Electronic density of states (DOS) performed using the LDA functional in the  $\alpha$ -GeTe type of structure at equilibrium volume ( $V = 50.30 \text{ \AA}^3$ ,  $a = 4.13 \text{ \AA}$ ,  $\alpha = 60^\circ$ ) - Calculation performed in the PbS system using the LDA functional.

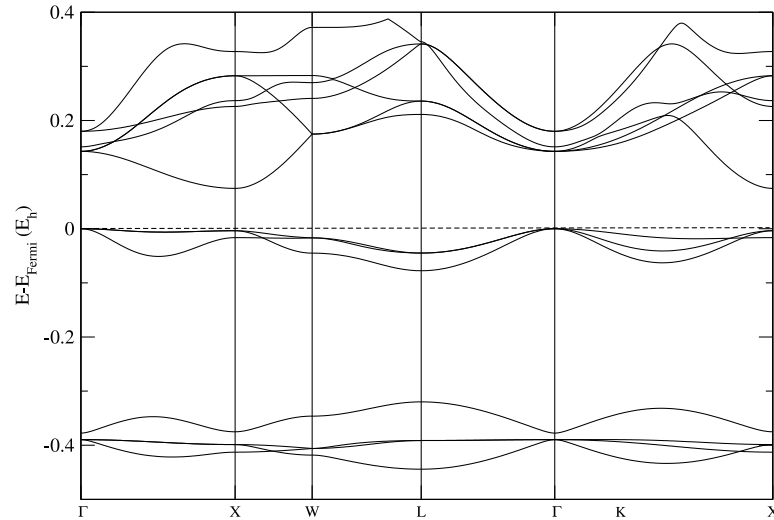


**Figure 8.18:** Band structure calculation performed using the LDA functional in the NaCl type of structure at equilibrium volume in barium sulfide system - Note that the labels of the special points correspond to a face-centered cubic lattice, respectively (notation according to [232]).

## 8. INVESTIGATION OF KINETIC STABILITY, ELECTRONIC AND VIBRATIONAL PROPERTIES OF PBS AND BAS AS A FUNCTION OF PRESSURE

---

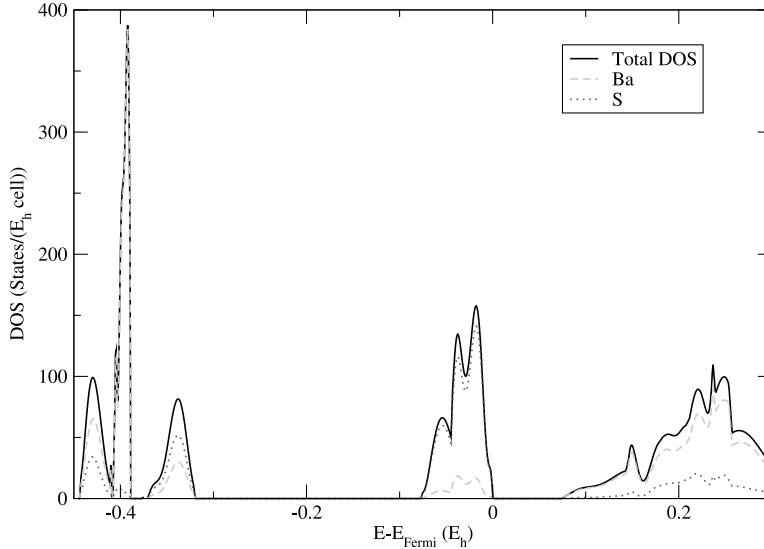


**Figure 8.19: Electronic density of states (DOS) calculation performed in the NaCl type of structure at equilibrium volume** - Calculation performed in the BaS system using the LDA functional.

### 8.3.2 Vibrational properties

The effect of the two excess electrons in the lead sulfide system might be more subtle and lead to a dynamical instability of the experimentally observed NaCl type modification. Thus, we have computed the phonon spectrum for the NaCl type structure, using the Hartree-Fock approximation (HF), and density functional theory (B3LYP- and LDA-functionals). We recall that the  $E(V)$  and  $H(p)$  curves [252] (see also **chapter 7**) show that when using the LDA functional, the NaCl modification is most stable at standard pressure (corresponding to  $a = 5.86 \text{ \AA}$ ), while the  $\alpha$ -GeTe type becomes kinetically stable at negative pressures of about -6 GPa ( $a = 6.03 \text{ \AA}$ ). For the B3LYP functional, the NaCl and the  $\alpha$ -GeTe modification have nearly equal energies (transition at about -7 GPa, i.e. for  $a = 6.08 \text{ \AA}$ ), and with the Hartree-Fock approximation, the  $\alpha$ -GeTe type is the lowest in energy already at standard pressure (see **chapter 7**).

Final results of our calculations are shown in the next figures: the phonon spectrum of the NaCl modification computed using LDA in the PbS system at equilibrium (figure 8.20), the phonon spectra in the PbS system at expanded volumes (see figures 8.21 and 8.22) and the phonon spectrum in the BaS system at equilibrium (see figure 8.23).

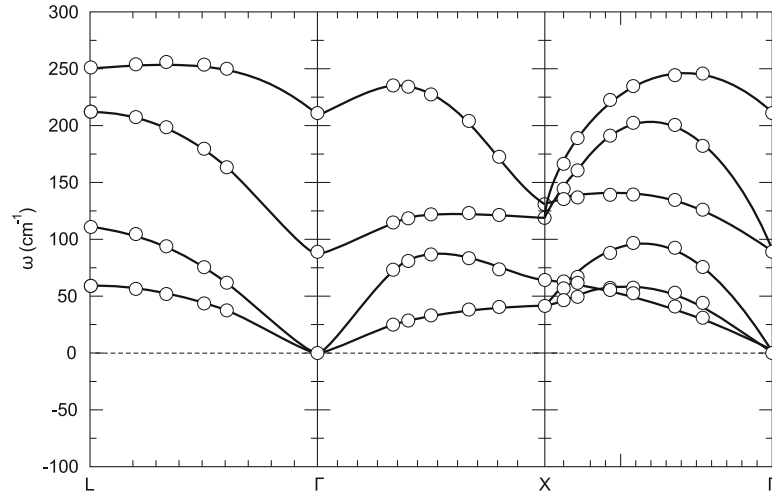


**Figure 8.20: Phonon-dispersion relation of the NaCl type modification using the LDA functional** - The NaCl modification is stable in the PbS system at equilibrium ( $V = 50.30 \text{ \AA}^3$ ,  $a = 5.86 \text{ \AA}$ ). The lines are meant to guide the eye.

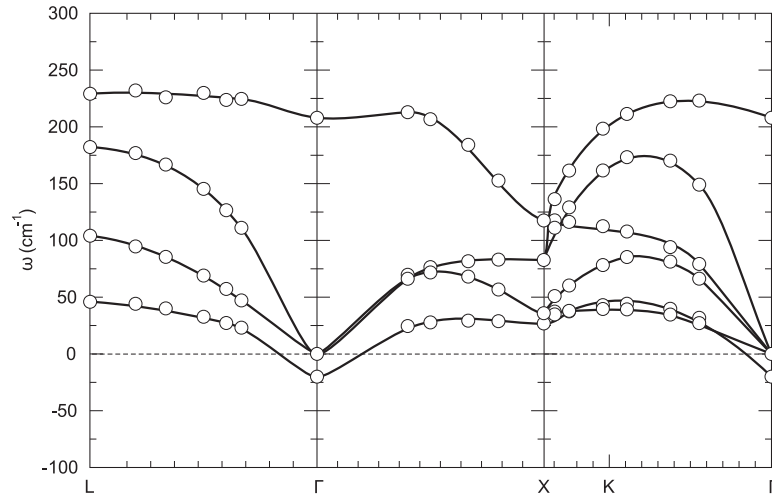


**Figure 8.21: Phonon-dispersion relation of the NaCl type modification using the LDA functional** - The NaCl modification becomes unstable at the  $\Gamma$ -point in the PbS system at a transition pressure of  $\approx 6 \text{ GPa}$  ( $V = 54.81 \text{ \AA}^3$ ,  $a = 6.03 \text{ \AA}$ ). The lines are meant to guide the eye.

## 8. INVESTIGATION OF KINETIC STABILITY, ELECTRONIC AND VIBRATIONAL PROPERTIES OF PBS AND BAS AS A FUNCTION OF PRESSURE

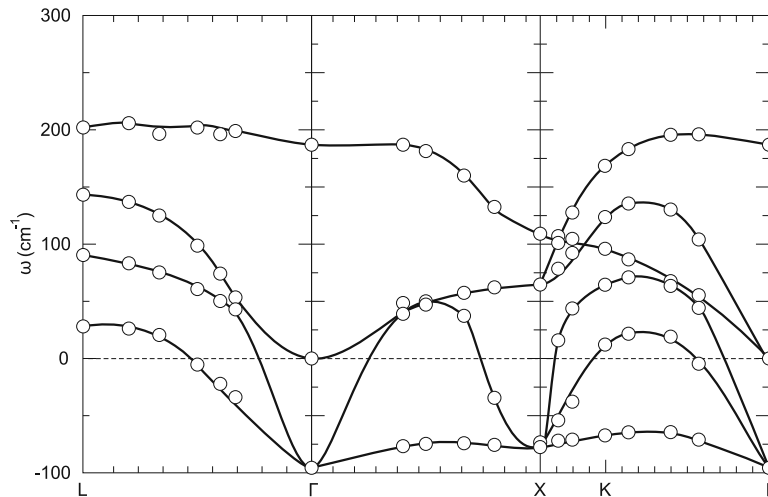


**Figure 8.22: Phonon-dispersion relation of the NaCl type modification using the LDA functional** - In the PbS system in the low density region ( $V = 61.48 \text{ \AA}^3$ ,  $a = 6.24 \text{ \AA}$ ), which corresponds to the pressures greater than 10GPa, imaginary frequencies occur in all directions of the Brillouin zone. Note that the negative values in PbS indicate imaginary values of the frequency. The lines are meant to guide the eye.

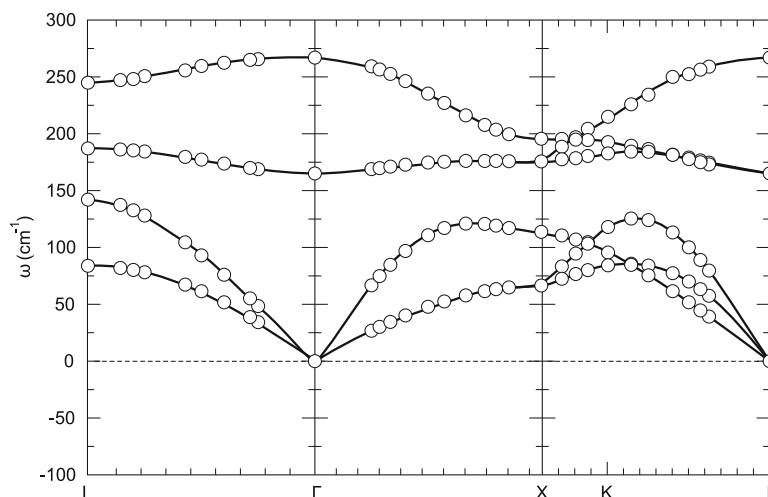


**Figure 8.23: Phonon-dispersion relation of BaS (NaCl structure) using the LDA functional** - In the BaS system at equilibrium volume, the NaCl structure appears to be stable (and also at large negative pressures). A similar result is observed with Hartree-Fock and B3LYP in BaS. Clearly, the  $\alpha$ -GeTe type of structure is not a separate minimum in BaS, but a part of the big basin of the NaCl modification. The lines are meant to guide the eye.

First, we discuss our results in the lead sulfide system and then we compare them to the corresponding ones for the barium sulfide system. Our calculations performed in PbS are in good agreement with experiment [285] and earlier calculations [286, 287, 324]. Since all the frequencies are real, the structure is kinetically stable. However, when we repeat the calculation for negative pressures, the lowest optical frequency at the  $\Gamma$ -point decreases and becomes imaginary at  $a = 6.03 \text{ \AA}$ , indicating a loss of stability.

Since the NaCl modification in the PbS system has cubic symmetry, the three modes as a whole displace the atoms along the  $[111]$  direction at the  $\Gamma$ -point (see figures 8.3 and 8.4). This just corresponds to the displacement mechanism required for the NaCl to  $\alpha$ -GeTe transition, see e.g. refs. [308, 319, 321]. For even larger values of  $a$ , whole branches of the phonon spectrum (first the ones along  $[111]$  and equivalent directions,  $\Gamma$ -L) become imaginary resulting in a complete breakdown of the structure. When using the B3LYP functional and HF, the instability is also observed for  $a > 6.13 \text{ \AA}$  and  $a > 6.18 \text{ \AA}$ , respectively (see figures 8.24, 8.25 and 8.26).

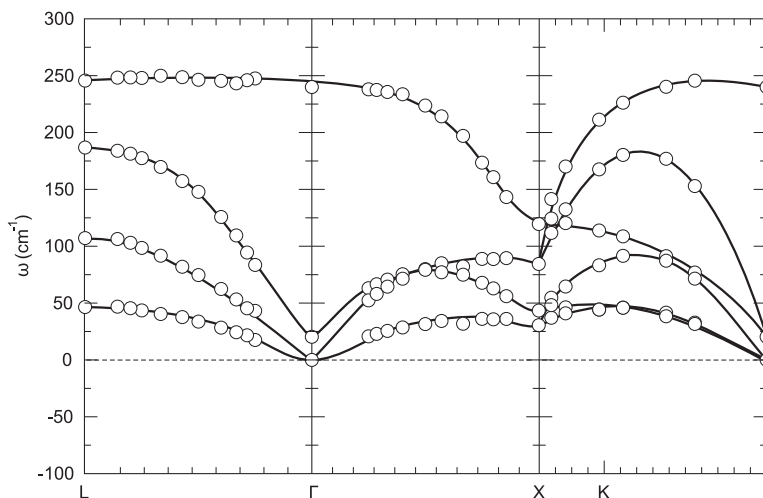


**Figure 8.24: Phonon-dispersion relation of the NaCl type modification in PbS using the B3LYP functional** - At equilibrium ( $a = 6.08 \text{ \AA}$ ), the optical frequencies are lower at the  $\Gamma$  point than calculated with LDA, which indicates a lower stability of the NaCl-type and a much closer transition to the  $\alpha$ -GeTe type. The lines are meant to guide the eye.

Conversely, the  $\alpha$ -GeTe modification shows no imaginary frequencies at the  $\Gamma$ -point for negative pressures, while the structure transforms to the NaCl modification at standard pressure at LDA-level (see figures 8.27 and 8.28). In the case of the B3LYP and the

## 8. INVESTIGATION OF KINETIC STABILITY, ELECTRONIC AND VIBRATIONAL PROPERTIES OF PBS AND BAS AS A FUNCTION OF PRESSURE

---

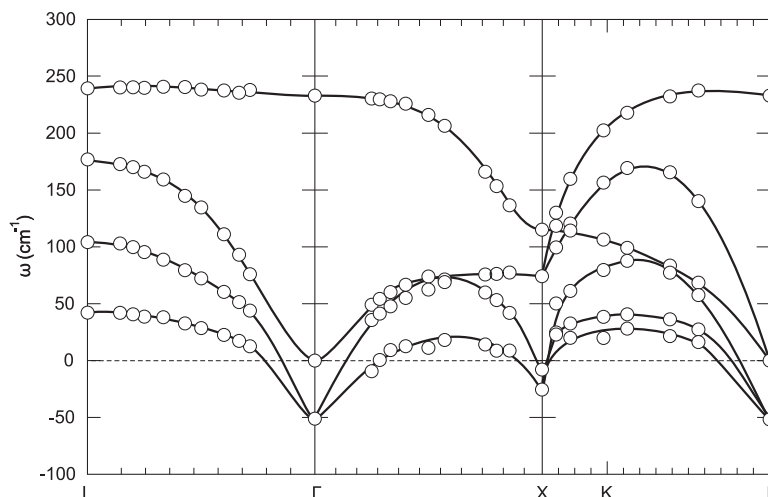


**Figure 8.25: Phonon-dispersion relation of the NaCl type modification in PbS using the B3LYP functional** - In the low density region, already at  $a = 6.13 \text{ \AA}$ , imaginary frequencies occur in all directions of the Brillouin zone. The lines are meant to guide the eye.

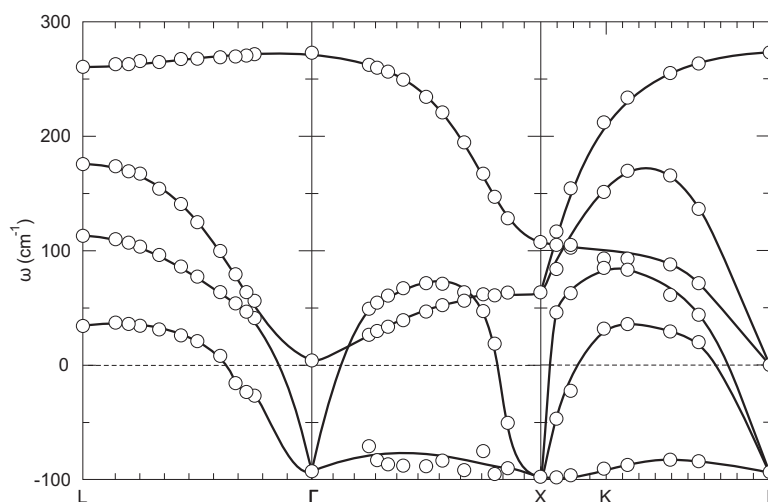


**Figure 8.26: Phonon-dispersion relation of the NaCl-type modification in PbS using the Hartree-Fock approximation** - The NaCl-modification appears to be unstable already at equilibrium volume (cell parameters of  $a = 6.18 \text{ \AA}$ ). The  $\alpha$ -GeTe-phase appears to be the stable form according to the  $E(V)$  and  $H(p)$  curves, phonon and band structure calculation already at equilibrium in the Hartree-Fock approximation. The lines are meant to guide the eye



HF based calculations, the  $\alpha$ -GeTe type is stable at standard pressure. [252] Clearly, on the LDA level, the NaCl modification of PbS is only marginally stable at standard pressure, and will transform to the  $\alpha$ -GeTe type at moderately large negative pressures. [62]

Regarding the influence of the steric electron pair on the comparatively low structural stability of PbS in the NaCl type, we turn to the main group analogue BaS, which also crystallizes in the NaCl type at standard pressure. If we now compare the phonon spectrum for PbS with the one for BaS (see figure 8.23 and ref. [323]), we note that: a) there is a marked dip of the lowest optical frequency at the  $\Gamma$ -point in PbS compared to BaS already at standard pressure, and b) the BaS rock salt modification remains stable also for large negative pressures. [62]

We have concluded that the  $\alpha$ -GeTe type modification is not a separate minimum in the barium sulfide system. When started the calculation from such a distorted NaCl structure, after relaxation it was found as the NaCl structure even at large negative pressures. Therefore, we conclude that the two excess electrons present in PbS, while not directly sterically active, make their presence felt in the reduction of the mechanical stability of the NaCl modification and in the existence of a competing  $\alpha$ -GeTe modification on the enthalpy landscape of PbS. This new metastable modification of PbS might be accessible in experiments, e.g. the low-temperature atom beam deposition method. [47] Recent experiments in PbS confirm the instability of the rock salt modification at high temperatures [327], although the directions suggested there, are not necessarily connected to the soft modes at the  $\Gamma$ -point.

## 8.4 Conclusion

According to our calculations, both the NaCl-type and the  $\alpha$ -GeTe type band structure show a clearly separated  $6s^2(\text{Pb})$ -band. This might suggest the existence of a weakly interacting lone pair of electrons associated with Pb, exhibiting an approximately spherical charge distribution, and, in addition, the position of the unoccupied Pb  $6p$  band also plays a role. The phonon spectrum of the NaCl and  $\alpha$ -GeTe type modifications is computed using Hartree-Fock and DFT (LDA and B3LYP). The results for the NaCl modification are in good agreement with experiment and previous calculations. While the NaCl structure is kinetically stable at equilibrium, it is unstable at negative pressures

## 8. INVESTIGATION OF KINETIC STABILITY, ELECTRONIC AND VIBRATIONAL PROPERTIES OF PBS AND BAS AS A FUNCTION OF PRESSURE

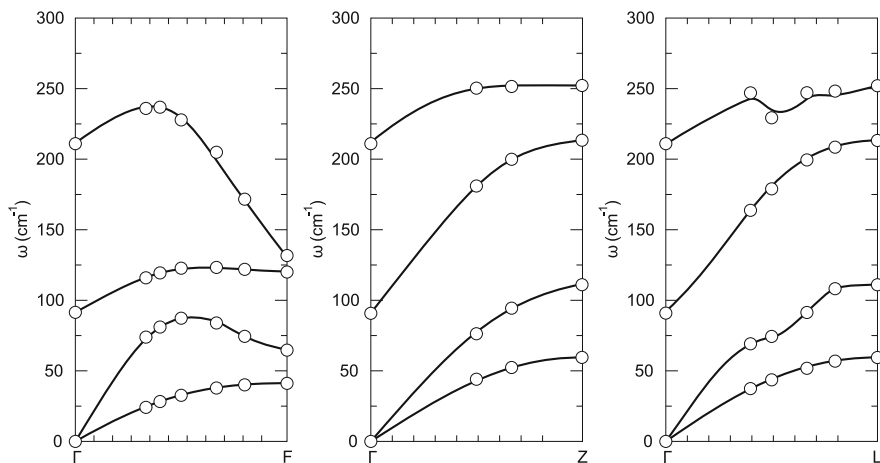


**Figure 8.27: Phonon-dispersion relation of the  $\alpha$ -GeTe type modification using the LDA functional** - At equilibrium volume ( $V = 50.30 \text{ \AA}^3$ ,  $a = 4.13 \text{ \AA}$ ,  $\alpha = 60^\circ$ ), the modification is identical to the NaCl type of structure. The lines are meant to guide the eye.

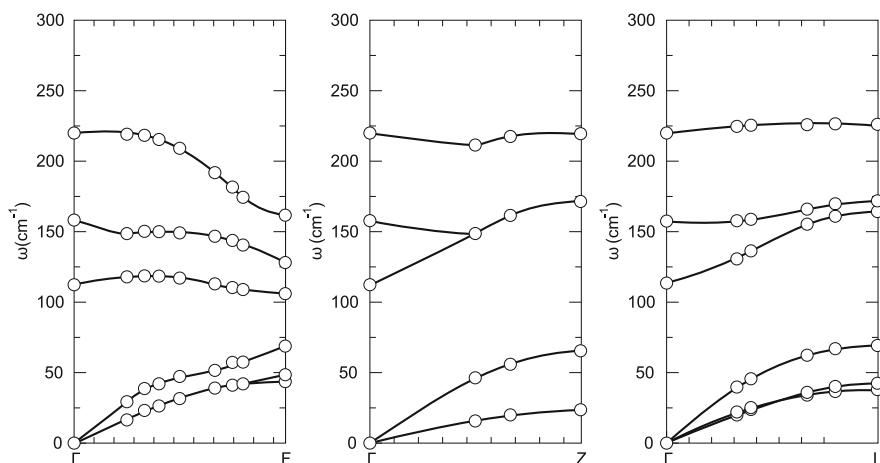


**Figure 8.28: Phonon-dispersion relation of the  $\alpha$ -GeTe type modification using the LDA functional** - In the low density region ( $V = 61.48 \text{ \AA}^3$ ,  $a = 4.56 \text{ \AA}$ ,  $\alpha = 56.32^\circ$ ), the modification appears to be stable. The lines are meant to guide the eye.

at the LDA level of theory. Conversely, the  $\alpha$ -GeTe modification shows no imaginary frequencies at the  $\Gamma$ -point for negative pressures, while the structure transforms to the NaCl modification at standard pressure on LDA level. In the case of the B3LYP and HF based calculations, the  $\alpha$ -GeTe type is stable at standard pressure. Clearly, the NaCl modification of PbS is only marginally stable at standard pressure, and will transform to the  $\alpha$ -GeTe type at moderately large negative pressures.

Finally, the results were compared with the BaS system, where a lone-pair effect is not expected. Local optimizations performed here, using Hartree-Fock and DFT (LDA and B3LYP), showed only the NaCl modification as a stable form, and no separate minimum for the  $\alpha$ -GeTe modification exists. Similarly, the phonon spectrum for the NaCl modification shows stability for a wide range of pressure independent of calculation method employed. We can conclude that the two excess electrons present in PbS, while not directly sterically active as such, make their presence felt in the reduction of the mechanical stability of the experimentally observed NaCl modification of PbS and in the existence of a competing  $\alpha$ -GeTe modification on the energy landscape of PbS. This new metastable modification might be accessible in experiments that involve effective negative pressures such as the low-temperature atom beam deposition method.

**8. INVESTIGATION OF KINETIC STABILITY, ELECTRONIC AND VIBRATIONAL PROPERTIES OF PBS AND BAS AS A FUNCTION OF PRESSURE**

---

## 9

# Structure prediction in the zinc oxide (ZnO) system for various pressures

*"The future will show whether my foresight is as accurate now as it has proved heretofore."*

(Nikola Tesla (1856-1943), Serbian-Croatian inventor and engineer)

### 9.1 Introduction

In condensed matter physics and solid state chemistry, zinc oxide is known as a II-VI semiconductor with a wide band gap of about 3.3 eV at room temperature, exhibiting a variety of desirable properties, e.g. transparency, electron mobility, luminescence, etc. Therefore, ZnO is frequently used in industrial applications, e.g. for transparent electrodes (in LCD television screens), energy-saving or heat-protecting windows, etc. Furthermore, ZnO powder is widely used as an additive to numerous materials and products including plastics, ceramics, glass, cement, rubber, oil lubricants, paints, adhesives, sealants, pigments, foods, batteries, electronics, etc. [328, 329]

The physical properties of porous semiconducting zinc oxide depend on the amount and nature of chemisorbed oxygen, while the excitonic photoluminescence of ZnO is very sensitive to the quality of the crystal and to the presence of defects. [330] However, there is no clear understanding so far of the defect related luminescence phenomena in

## 9. STRUCTURE PREDICTION IN THE ZINC OXIDE (ZNO) SYSTEM FOR VARIOUS PRESSURES

---

ZnO. [331] Similarly, there are strong effects of impurities and dopants on the physical properties of zinc oxide. [328, 332, 333]

Zincite is the natural mineral form of zinc oxide (ZnO), although crystal forms of ZnO are rare in nature (see figures 9.1 and 9.2).<sup>1</sup> Zincite has a hexagonal crystal structure and its color depends on the presence of impurities. Usual impurities in the zincite mineral are MnO, FeO and SiO<sub>2</sub>, but their presence is less than 1%.<sup>2</sup> This makes ZnO translucent, transparent in thin fragments with color ranging from yellow-orange to deep red, and rarely yellow, green, or colorless. Zincite crystals can also be grown artificially, and synthetic zincite crystals are available as a by-product of zinc smelting. [253–256]



**Figure 9.1: Zincite mineral (ZnO) from Franklin Hill Mine in New Jersey, USA**  
- The picture shows the vein "in situ" in the granular ore of zincite. The mineral size is 8 x 5.3 cm<sup>2</sup>. [256]

Zinc oxide is one of the most studied systems, both experimentally [328, 334–336] and theoretically [337–340]. Although in nature ZnO appears as the mineral zincite (with impurities of Fe and Mn), an ideal bulk zinc oxide adopts the hexagonal wurtzite type of structure at ambient conditions (see figure 9.3). [341, 342] There is a transition to the rocksalt modification under pressure (see figure 9.3) and the coexistence of the two phases has been investigated. [328, 341, 343] The sphalerite modification

---

<sup>1</sup>An exception to this rule is at the Franklin and Sterling Hill Mines in New Jersey, USA.

<sup>2</sup>The zincite from the Franklin and Sterling Hill Mines is red-colored, mostly due to iron and manganese impurity, and it is associated with willemite and franklinite.

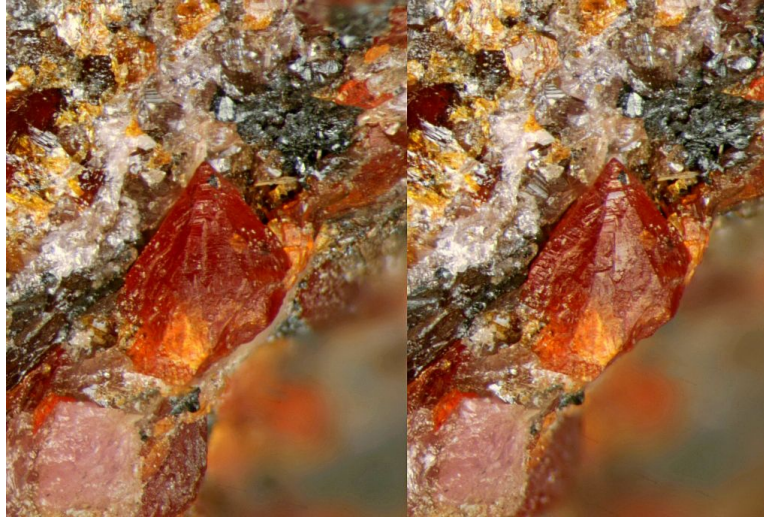


**Figure 9.2: Small embedded zincite mineral (ZnO) from Franklin Hill Mine in New Jersey, USA** - The picture shows mineral association of zincite (red color), leucophoenicite (pink color), and franklinite ore (black color). One can see nice tetrahedral crystals of ZnO in the so-called "stereo child photos" of zincite. The mineral size is  $2.2 \times 2.9 \text{ mm}^2$ . [256]

can be stabilized by growing ZnO on substrates with cubic lattice structure resulting in nanocrystalline ZnO thin films. [344–347] Since there are only three experimentally known modifications of ZnO, finding possible new polymorphs and understanding transitions among them would be very important.

## 9.2 Optimization procedure

In this study, we have globally explored the zinc oxide system with an empirical potential (Lennard-Jones potential + Coulomb potential) employing simulated annealing, both at standard and elevated pressure (up to 100 GPa) using up to 5 formula units ( $Z = 5$ ) per simulation cell. The local optimization was performed on the *ab initio* level using Hartree-Fock and various density functionals (LDA and B3LYP). Both the atom positions (70% of all Monte Carlo steps move an individual atom, 10% swap the positions of two atoms) and the parameters of the periodically repeated simulation cell (20% of all Monte Carlo steps) were freely varied during the random walks. Each simulated annealing run consisted of 4000 steps, followed by 10000 quench steps.

Local optimizations were performed at the *ab initio* level with the program **CRY-**

## 9. STRUCTURE PREDICTION IN THE ZINC OXIDE (ZNO) SYSTEM FOR VARIOUS PRESSURES

---

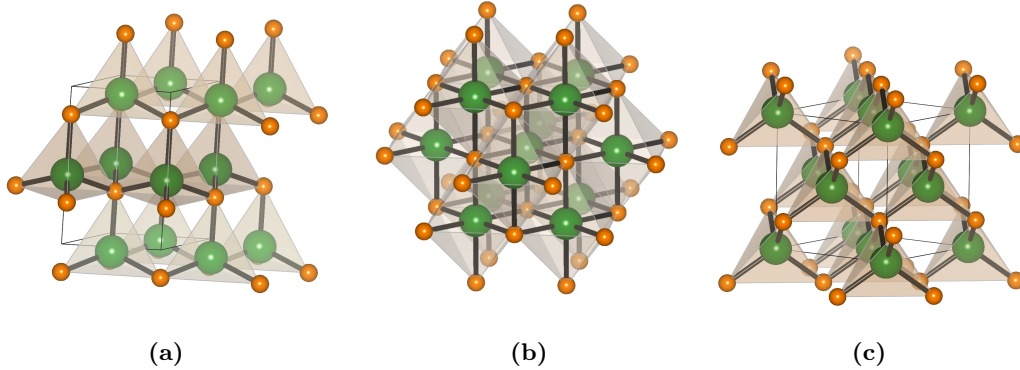


**Figure 9.3:** Visualization of the experimentally observed structure types in the ZnO system: a) wurtzite ( $B4$ ) type; b) rock salt ( $B1$ ) type; c) sphalerite ( $B3$ ) type. Note that the small light spheres and large dark spheres correspond to O and Zn atoms, respectively.

**TAL09.** [191, 192] For Zn we used an "86–411 $d31G$ " basis set as in refs. [190, 348, 349], and for O we used an "8–411" basis set (modified by Muscat) as in refs. [190, 350, 351]. A  $8 \times 8 \times 8$  k-point sampling net was employed and a smearing temperature of  $0.01 E_h$  was applied during the local optimization and the calculation of the  $E(V)$  curves, in order to facilitate the numerical integration.

### 9.3 Results and Discussion

#### 9.3.1 Statistical analysis of the optimization process

At the first stage of the energy landscape investigation of ZnO, we performed several global optimizations for different numbers of formula units and various pressures. This was followed by the full structural analysis of the landscape, elimination of the duplicate structures and identification of the most important minima. Afterwards, these structural candidates were chosen as the starting point for the following calculations.

In table 9.1 we show the results of the global optimization in the zinc oxide system where the radius scale factor  $R$  [15] was varied for the  $Zn^{2+}$  and the  $O^{2-}$  ion, and the number of atoms in the simulation cell  $Z$ . In the first round of calculations, the pressure was set to  $p = 0$  GPa. Finally, we have performed a structural and crystallographic analysis of the calculated landscape. We observe that for 1 formula unit ( $Z = 1$ ), besides the sphalerite and the NaCl type of structures and their distortions, only the unknown structures in space group  $Cm$  (no. 8) appeared. With  $Z = 2$ , wurtzite was the most



dominant structure type, showing space group  $P6_3mc$  (no. 186), although there was a radius setting of  $Zn$  and  $O$  ions, where the NaCl ( $Fm - 3m$ , no. 225) and the 5-5 ( $P6_3/mmc$ , no. 194) structure type appeared more time than the wurtzite structure on the energy landscape of ZnO, and therefore had a higher probability to be found than the wurtzite structure. With calculations performed for 3 formula units, the sphalerite structure type, showing the  $F - 43m$  (no. 216) space group, was the most observed minimum. Again, there was a setting of the radius scale factors ( $R_{Zn} = 0.8$ ,  $R_O = 1.2$ ), similarly to the previous case, which favored the GeP structure type ( $I4mm$ , no. 107). With  $Z = 4$ , in most of the calculations we have found the  $\beta$ -BeO structure type, exhibiting space group ( $P4_2/mnm$ , no. 136), although there were again radius settings of the  $Zn$  and  $O$  ions where the NaCl type ( $Fm - 3m$ , no. 225) was the most dominant on the landscape. When we performed calculations for 5 formula units, we observed only distortions of all the structure types mentioned, mostly in the space group  $Amm2$  (no. 38) or  $P1$  (no. 1).

$R_{Zn}$	$R_O$	<b>Z=1</b>	<b>Z=2</b>	<b>Z=3</b>	<b>Z=4</b>	<b>Z=5</b>
0.7	1.2	8	186	216	136	38
0.7	1.3	8	186	216	136	38
0.8	1.2	8	225	107	225	1
0.8	1.3	8	194	216	136	38
0.8	1.4	8	186	216	136	38

**Table 9.1: Results of the crystallographic analysis of the global optimization calculations in ZnO for different number of formula unit  $Z$  and radius  $R$  -** The pressure during calculations was set to  $p = 0$  GPa, and the numbers show predominately found space groups.

Next, we performed a series of high pressure calculations for  $p = 0.1$  MPa, 1 MPa, 10 MPa, 100 MPa, 1 GPa, 10 GPa, 100 GPa, besides the variation of the radius scale factor  $R$  of  $Zn^{2+}$  and  $O^{2-}$  atom, and the number of formula units  $Z$  (see table 9.2).

We observe that the most frequent minimum on the high pressure landscape of ZnO is the NaCl structure type, exhibiting space group  $Fm - 3m$  (no. 225). Again, with different  $Z$  and  $R$  values, [15] we observe different distortions of the NaCl structure type, e.g. in the space group  $Cm$  (no. 8) or  $P2_1/m$  (no. 11), or structures which are close to perfect NaCl, e.g. the 5-5 structure ( $P6_3/mmc$ , no. 194) or the GeP structure type ( $I4mm$ , no. 107). If we increase the number of formula units to  $Z = 5$ , then in the most cases we observe "amorphous" structures ( $P1$ , no. 1). Finally, the structure

## 9. STRUCTURE PREDICTION IN THE ZINC OXIDE (ZNO) SYSTEM FOR VARIOUS PRESSURES

---

candidates which were obtained with the radius scale factors of  $R_{Zn} = 0.8$  and  $R_O = 1.4$  in the global and local optimizations, were chosen for the next level of calculations using the threshold and the prescribed path algorithm.

$R_{Zn}$	$R_O$	<b>Z=1</b>	<b>Z=2</b>	<b>Z=3</b>	<b>Z=4</b>	<b>Z=5</b>
0.7	1.2	225	194	225	225	1
0.7	1.3	225	225	1	225	38
0.8	1.2	225	225	107	225	1
0.8	1.3	8	11	107	225	1
0.8	1.4	8	225	225	225	1

**Table 9.2: Overview of the crystallographic analysis of the global optimization calculations performed at various pressures in ZnO for different number of formula unit  $Z$  and radius  $R$  -** The pressure during calculations was set to  $p = 0.1$  MPa, 1 MPa, 10 MPa, 100 MPa, 1 GPa, 10 GPa, 100 GPa. Note that the numbers show predominately found space groups.

### 9.3.2 Phase transitions and modifications found in the high pressure region

Our final local optimizations show that the experimentally observed polymorphs of zinc oxide are the energetically lowest and thermodynamically most stable ones, which is in agreement with experiment [328, 334–336, 341, 342] and previous calculations [337–340].

The wurtzite type together with the sphalerite type (see figures 9.3 and 9.4) are the stable modifications at ambient conditions. With calculations performed on LDA and B3LYP level, these two minima are part of one big wurtzite-sphalerite basin. However, with calculations performed on the Hartree-Fock level, these minima are separated. Both modifications are known in the zinc/iron sulfides with the analogous formula, (Zn, Fe)S. Wurtzite ( $B4$ ) exhibits space group  $P6_3mc$  and its structure is composed of  $ZnO_4$  tetrahedra that are stacked in a hexagonal sequence  $ABABAB\dots$  (*hcp*-packing). Sphalerite ( $B3$ ) exhibits space group  $F - 43m$ , and its structure can be visualized as an  $ABCABCABC\dots$  cubic sequence of  $ZnO_4$  tetrahedra (*fcc*-packing).

In the ZnO system at pressures above 10 GPa, the rock-salt modification (see figure 9.3) is observed as the most stable form. [328, 341, 343] We have calculated the transition pressure from the  $H(p)$  curves using different functionals. With the calculations performed using Hartree-Fock we observe a transition from wurtzite to NaCl at about 9 GPa, and with B3LYP at about 12.5 GPa (see figures 9.7 and 9.8). When

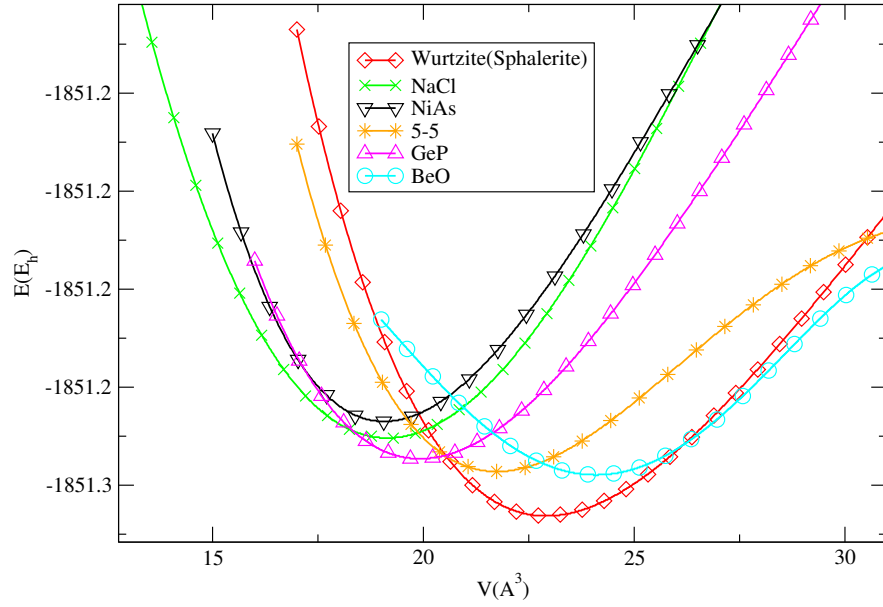


**Figure 9.4:**  $E(V)$  curves at LDA level for the most relevant structure types in ZnO - Energies per formula unit are given in hartrees ( $E_h$ ).

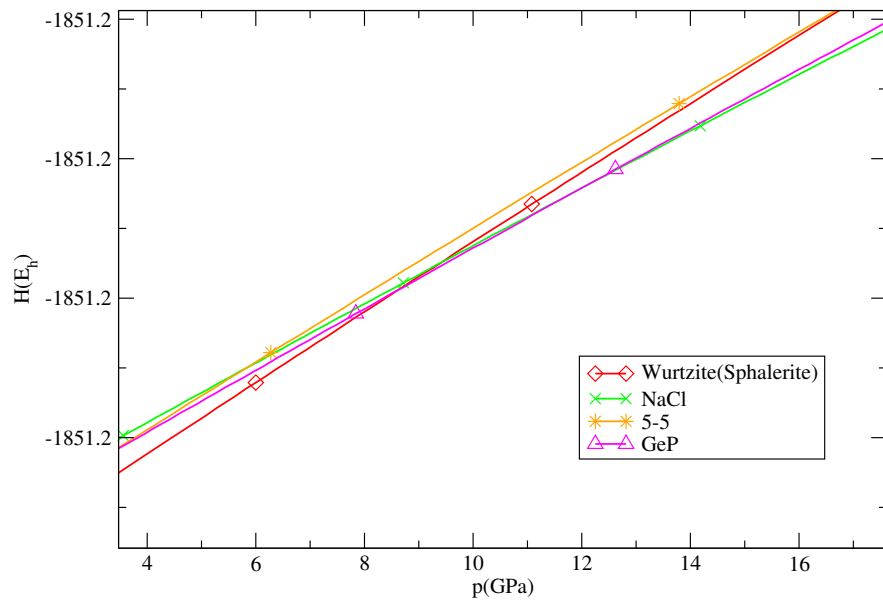


**Figure 9.5:**  $H(p)$  curves at LDA level in the ZnO system - The figure shows relevant modifications participating in high pressure region. Enthalpies per formula unit are given in hartrees ( $E_h$ ).

## 9. STRUCTURE PREDICTION IN THE ZINC OXIDE (ZNO) SYSTEM FOR VARIOUS PRESSURES

---

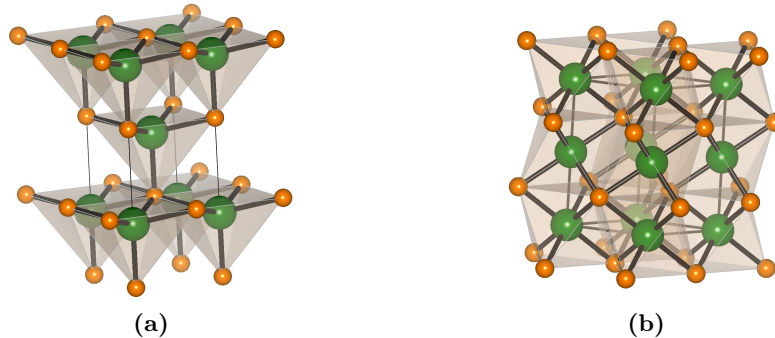


**Figure 9.6:** Visualization of the calculated structure types in the ZnO system participating in the high-pressure region: a) germanium phosphide (GeP); and b) nickel arsenide (NiAs) structure types. Note that the small light spheres and large dark spheres correspond to O and Zn atoms, respectively.

using the LDA functional, we observe this transition at  $\approx 9.5$  GPa (see figure 9.5). All of these results are in good agreement with experimental observations. However, with calculations performed using LDA functional, we observe an earlier transition from the wurtzite to the new GeP structure type at about 8.5 GPa, and then later a transition from the GeP to the NaCl structure type at  $\approx 12$  GPa (see figure 9.5).

The germanium phosphide (GeP) structure type can be described as a distorted variant of the rock salt type, which has 5+1 coordination number (CN) and exhibits space group  $I4mm$  (no. 107) (see figure 9.6). In addition, we have found several new hypothetical modifications in the ZnO system. One of them is the NiAs ( $B8_1$ ) structure type that appeared as a meta-stable modification at standard conditions (see figure 9.6) and also at extremely high pressures (see figure 9.4). According to our calculations, this modification is meta-stable even with an increase of temperature and/or pressure; thus it would be very hard to synthesize, although its coordination number suggests that it might be a metastable phase at high pressures in the ZnO system.

### 9.3.3 Investigations of the new stacking variants of ZnO

Our searches also resulted in many interesting candidates which exhibit different stacking orders similar to the many polytypes in the ZnS system, while varying the numbers of formula units per simulation cell. There have been many examples in various systems where different stacking orders, based on mixing the *hcp* and the *fcc* stacking, produce different polytypes. [99, 100, 352] We could relate our polytype structures to the ZnS

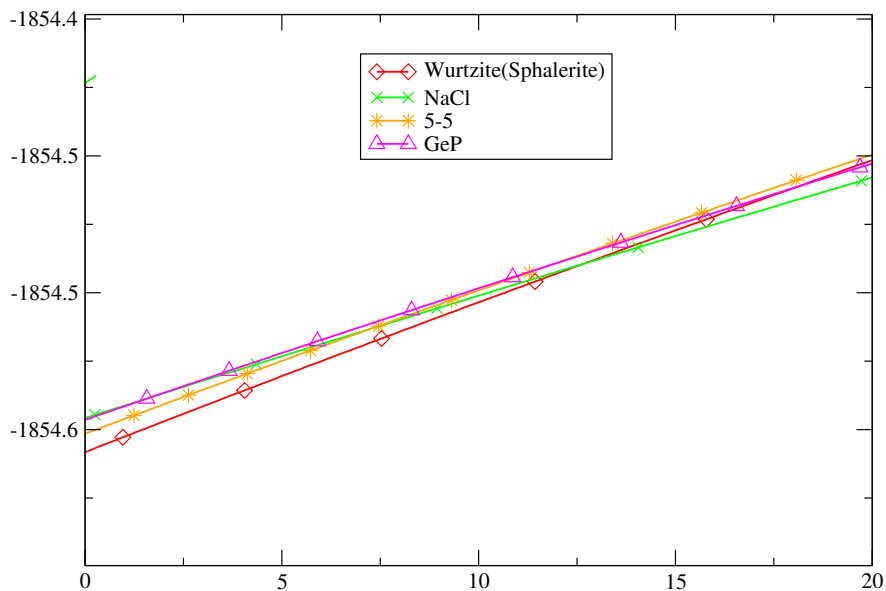


**Figure 9.7:**  $H(p)$  curves at B3LYP level in the ZnO system - The figure shows relevant modifications participating in high pressure region. Enthalpies per formula unit are given in hartrees ( $E_h$ ).

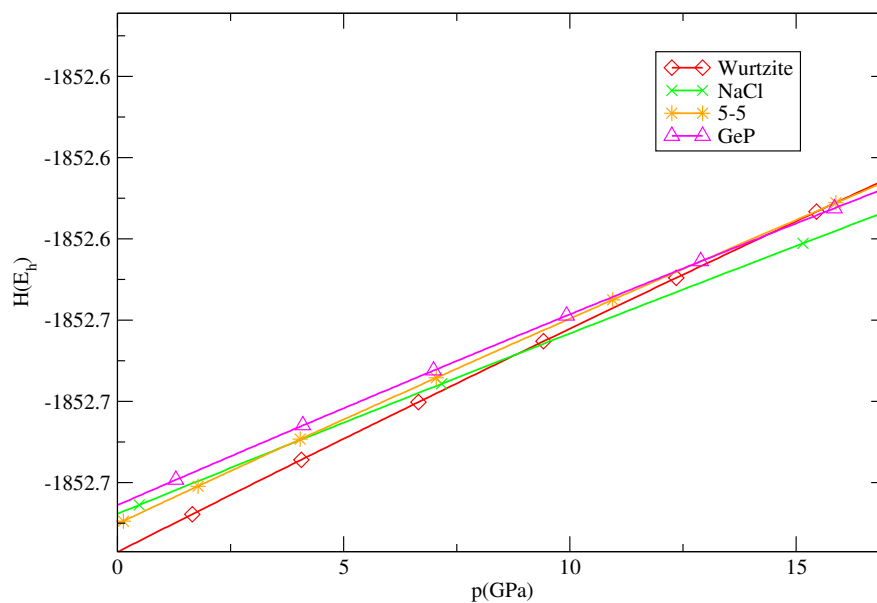


**Figure 9.8:**  $H(p)$  curves at Hartree-Fock level in the ZnO system - The figure shows relevant modifications participating in high pressure region. Enthalpies per formula unit are given in hartrees ( $E_h$ ).

## 9. STRUCTURE PREDICTION IN THE ZINC OXIDE (ZNO) SYSTEM FOR VARIOUS PRESSURES

---

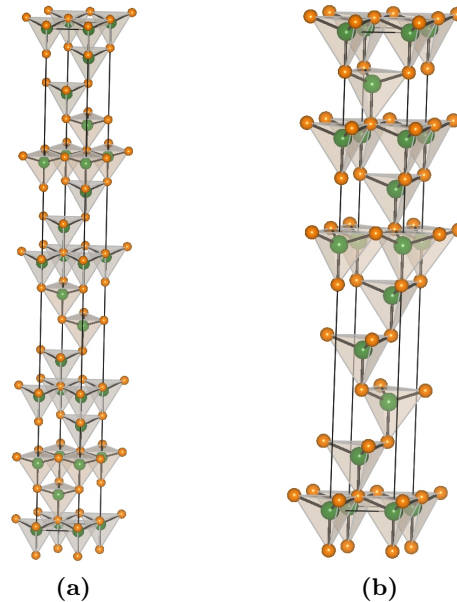


**Figure 9.9:** Visualization of the new stacking variants of ZnO: a) 5H ; and b) 9R polytypes. Note that the small light spheres and large dark spheres correspond to O and Zn atoms, respectively.

system, due to some resemblance to the matraite structure in trigonal ( $R3m$ ) symmetry [353], or to the structures in the SiC system [354], where different polytypes have also been observed [355].

The appearance of a 9R stacking polytype in the global search and threshold runs could be an indication of many other similar structures in the ZnO system, and therefore we performed a series of local optimizations on ZnS polytypes 4H, 5H, 6H, 8H, 9R, and 12R. [352, 356, 357] With the calculation performed using DFT (LDA and B3LYP), we observe that several polytypes (4H, 6H, 8H and 12R) are part of the big wurtzite-sphalerite basin (see figures 9.10 and 9.11). Two polytypes were different at this level of calculations : 9R and distorted 5H. The 9R polytype was metastable, but a good candidate, when energies are compared. The 5H stacking variant could only be optimized as distorted version, and was high in energy on DFT level (see figures 9.10 and 9.11). However, with the calculation performed using Hartree-Fock, we observe the 12R polytype as separate minimum, while the 9R became part of the wurtzite basin. The distorted 5H polytype, together with the 4H, 6H and 8H variants, were found as

minima close-by to sphalerite (see figure 9.12).

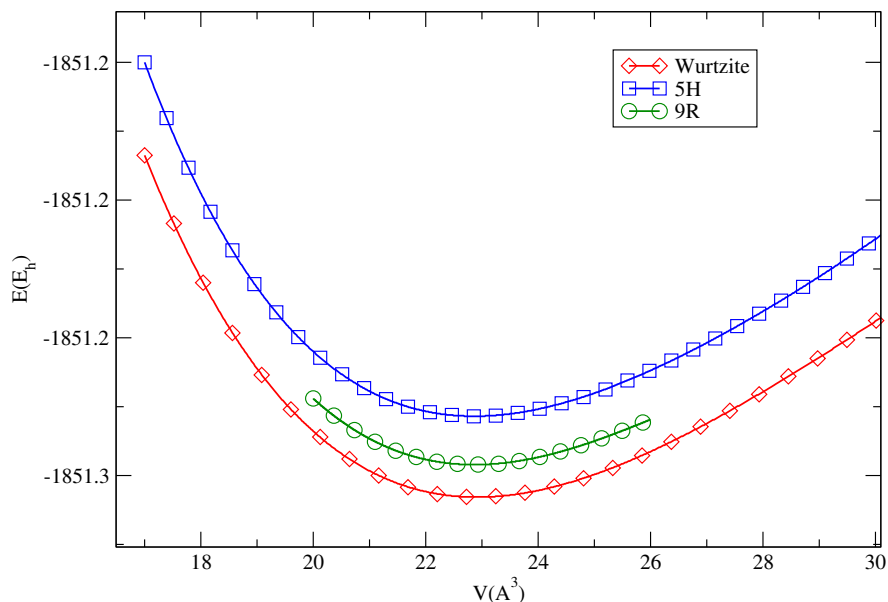


**Figure 9.10:**  $E(V)$  curves at LDA level for the new stacking variants of ZnO - Energies per formula unit are given in hartrees ( $E_h$ ).

### 9.3.4 Negative pressure region and low-density modifications

At effective negative pressures, we observed the  $\beta$ -BeO-type in the ZnO system (see figure 9.13). In the beryllium oxide (BeO) system, two known modifications occur:  $\alpha$ -BeO [358], which adopts the hexagonal wurtzite structure form and  $\beta$ -BeO, a high temperature form which shows tetragonal symmetry. [359] The  $\beta$ -BeO type exhibits space group  $P4_2/mnm$  and is hexagonal close packed (*hcp*). Be-atoms are located in tetrahedral interstices resulting in pairs of edge connected tetrahedrons. The  $\beta$ -BeO-type of structure is closely related to the wurtzite type, with 4-fold coordination of the Be-atoms by O-atoms. [359] Analogously, one can expect a similar relation in the ZnO system, which would mean that with an increase of temperature one might be able to synthesize the  $\beta$ -BeO-type modification as a metastable phase in the ZnO system.

In our calculations performed using Hartree-Fock we observed the transition from the wurtzite to the  $\beta$ -BeO modification at about -4 GPa, while using B3LYP this occurred at about -7 GPa (see figure 9.14). When using the LDA functional, we observed

## 9. STRUCTURE PREDICTION IN THE ZINC OXIDE (ZNO) SYSTEM FOR VARIOUS PRESSURES

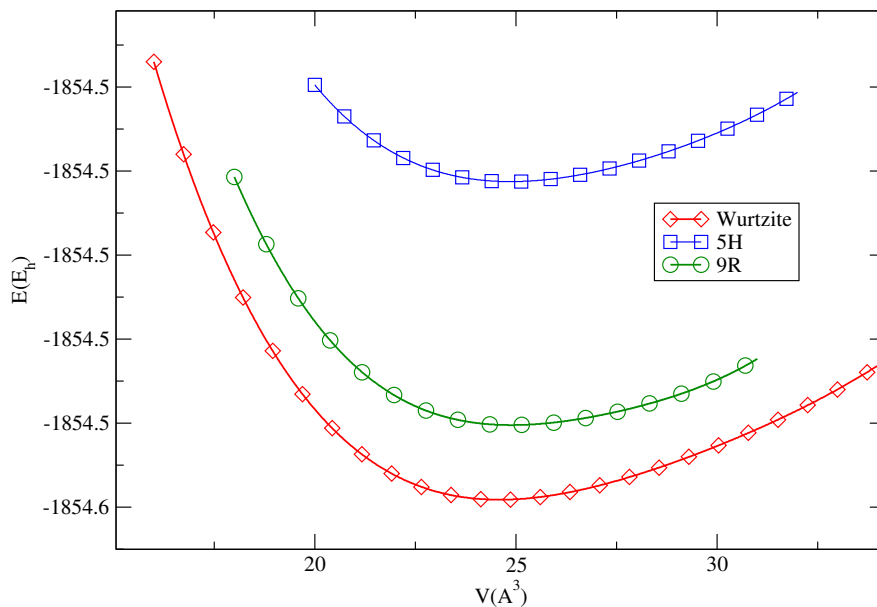


**Figure 9.11:**  $E(V)$  curves at B3LYP level for the new stacking variants of ZnO - Energies per formula unit are given in hartrees ( $E_h$ ).

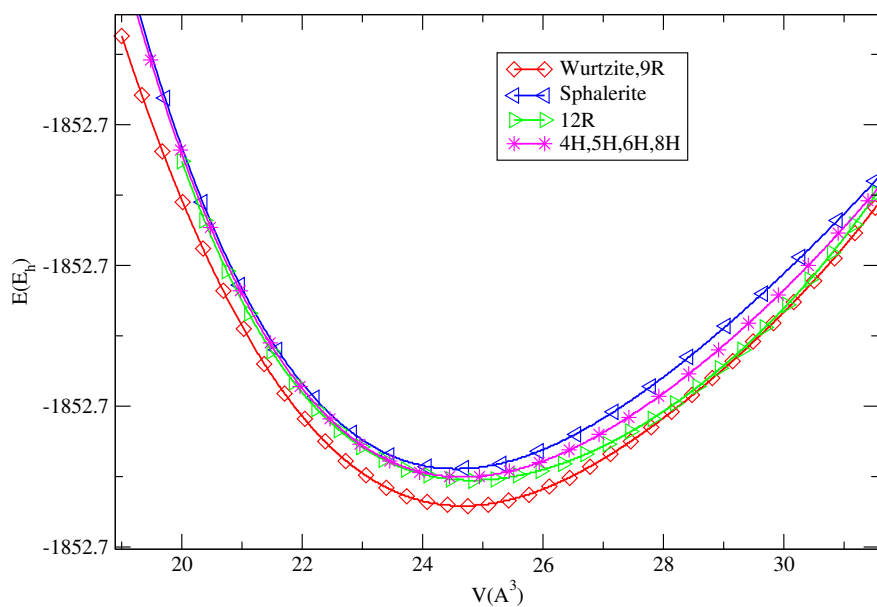


**Figure 9.12:**  $E(V)$  curves at Hartree-Fock level for the for the new stacking variants of ZnO - Energies per formula unit are given in hartrees ( $E_h$ ).



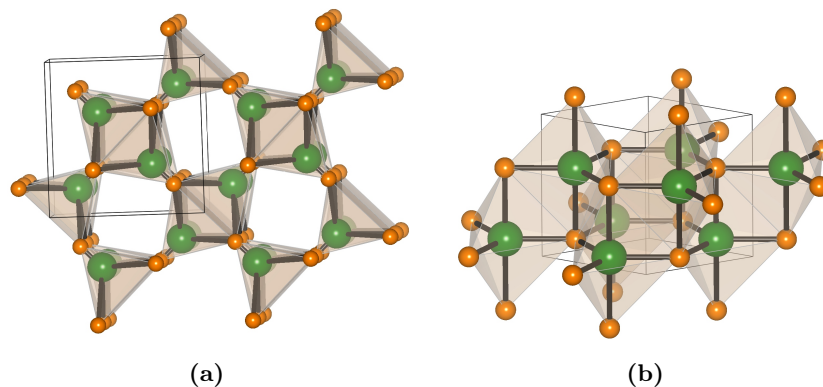


**Figure 9.13:** Visualization of the calculated structure types in the ZnO system participating in negative pressure region: a)  $\beta$ -beryllium oxide (BeO); and b) "5-5" structure types. Note that the small light spheres and large dark spheres correspond to O and Zn atoms, respectively.

this transition beyond -10 GPa, and even prior to this transition we observe another metastable phase - the "5-5" structure.

One further interesting structure candidate, which we found as a metastable phase along the route of the wurtzite(sphalerite) -  $\beta$ -BeO transition, is the so-called "5-5"-type (see figure 9.13). This structure type has been found on the energy landscapes of many  $AB$  compounds [15, 360], and furthermore its existence in the ZnO system has been proposed in some recent experiments. [361, 362] We can describe this structure type as a fivefold coordination of Zn by O in a hexagonal lattice ( $P6_3/mmc$ ) with  $ABAB$  stacking. The O- and Zn-atoms form trigonal bipyramids around Zn and O, respectively. The 5-5 structure can be derived from the BN-structure by requiring that the bond length in the  $c$ -direction must be (nearly) identical to the one within the planar hexagons. Therefore, this modification appears to be a very good candidate for a synthesis of nanocrystalline structures.

## 9.4 Conclusion

In order to gain new insights in the ZnO system, we have performed global explorations of the energy landscape using simulated annealing with an empirical potential, both at standard and elevated pressure (up to 100 GPa), for different numbers of atoms (up to  $Z = 5$ ) and radius scale factor ( $R$ ), in order to identify possible new ZnO modifications, while the local optimizations were performed on *ab initio* level, using

## 9. STRUCTURE PREDICTION IN THE ZINC OXIDE (ZNO) SYSTEM FOR VARIOUS PRESSURES

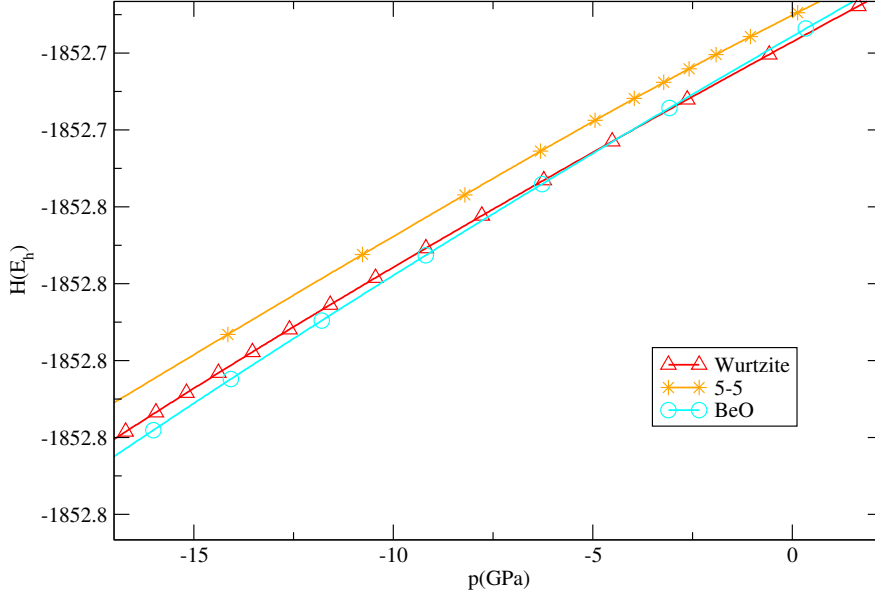


**Figure 9.14:**  $H(p)$  curves at Hartree-Fock level in the ZnO system - The figure shows relevant modifications participating in the low pressure region. Enthalpies per formula unit are given in hartrees ( $E_h$ ).

Hartree-Fock and DFT (LDA and B3LYP). This was followed by the full structural analysis of the landscape, elimination of the duplicate structures and identification of the most important minima. We have found that different numbers of atoms in the simulation cell ( $Z$ ), and different radius scale factors ( $R$ ), can strongly influence the structural distribution on the energy landscape. Furthermore, when performing calculations at different pressure, we observe this influence even more pronounced.

We have found the known structure types (wurtzite, sphalerite and rock-salt), in agreement with experiment. In addition, many new interesting modifications were identified in different regions of the energy landscape. We have found the GeP type as a high pressure candidate and the nickel arsenide ( $B8_1$ ) type as a metastable modification at standard conditions. At effective negative pressures we have observed the  $\beta$ -BeO-type, while with increase/decrease of pressure, we also find the so-called "5-5" type, which should be possible to be synthesized as a metastable phase. Finally, we observe stacking variants of the wurtzite and the sphalerite modifications, which also should be accessible to the experiment.

# 10

## Energy landscape investigation in ZnO

*"We build too many walls and not enough bridges."*

(Isaac Newton (1642-1727), English mathematician and physicist)

### 10.1 Introduction

In order to investigate the energy landscape of zinc oxide, we performed several sets of calculations using different methods. First, we performed several global (followed by local) optimizations (for details see **part III** and **chapter 9**) for different numbers of atoms (formula units) and pressures. The full analysis of the landscape was performed and important minima were identified.

An important aspect beyond the identification of local minima is the analysis of the barrier structure of the landscape surrounding the minima, and of the possible transition paths connecting the major locally ergodic regions. Therefore, in the next step we have performed threshold algorithm calculations (for details see **part III**) for different numbers of formula units. Structure candidates which we had obtained previously were used as starting points for the threshold runs. Then, the complete energy landscape was analysed lid by lid, for each specific structure. Also, we performed the TA runs for different shapes of the primitive cell for a given structure. With a new lid-by-lid analysis, we have gained new insights into the influence of increasing the number of atoms in the simulation cell on the energy landscape of a periodic system. Finally,

we performed prescribed path calculations (for details see **part III**), which allows us to explore transition routes and barriers between even distant minima, as well as gain more insights into the temperature dependence of the synthesis and transformation processes in the system.

### 10.2 Optimization procedure

Our general approach to the exploration of energy landscapes and the determination of structure candidates has been given in detail in **part III** and specific to ZnO investigations in **chapter 9**. The energy barriers are determined using the threshold algorithm, where the landscape accessible from a local minimum below a sequence of energy barriers (thresholds) is systematically explored for all important local minima. In particular, we can measure the transition probability among the minima as a function of the threshold value. Each TA run consisted of 50000 steps, followed by a triple quench, each having 20000 quench steps. The number of atoms are varied in the calculation, ranging from 1 Zn and 1 O atom ( $Z = 1$ ) to 6 Zn and 6 O atoms ( $Z = 6$ ).

The final aspect of the landscape investigations is the study of possible transformation paths using the prescribed path algorithm. Several procedures were used in the prescribed path explorations. In procedure I, a standard stochastic quench was used along the prescribed path at 100 points between two distant minima on the energy landscape. In each run, 8 atoms (4 Zn, 4 O) per cell were used. The path between structure 1 and 2 was defined by varying the cell parameters from the ones of structure 1 to those of structure 2, keeping the relative atom coordinates as those of structure 1. This corresponds to a shear force deforming the unit cell towards the one of the target structure, followed by restricted (keeping cell parameters fixed) and full free minimizations.

During the quenches, first only the atom positions were free to vary (30000 steps), and subsequently both atom positions and cell parameters (20000 steps). Here we observe that using stochastic quenches along the prescribed path, different transition routes are identified depending on the direction of the path, e.g. different transition routes are found going from the wurtzite to the sphalerite structure than going from the sphalerite to the wurtzite structure. This way, we obtain a good overview over the range of possible transition routes between two structures. [57]

Procedure II is an extension of procedure I, as far as the initial prescribed path is generated in the same way as in procedure I by variation of only the cell parameters. The main difference to the previous procedure is in the relaxation/local exploration part, where in case of procedure I a standard stochastic quench (i.e.  $T = 0$  K) was used, and in procedure II constant temperature Monte Carlo simulations. In each run, 8 atoms (4 Zn, 4 O) per cell were used. Again, we observe that when using procedure II of the prescribed path, different transition routes are calculated depending on the direction of the path. Thus, in this calculation, the cell parameters were adjusted while the atom positions were kept fixed (at the same position as in the initial configuration), in order to generate 100 points along the prescribed path as in procedure I. Then, we performed constant temperature Monte Carlo runs keeping the cell parameters fixed. The temperatures selected varied from 50 - 1000 K, and for each temperature and starting structure, one run consisting of 30000 Monte Carlo steps at the given temperature followed by 20000 quench steps. During these runs, the cell vectors were free to vary. The set of constant temperatures consisted of: 50 K, 100 K, 150 K, 200 K, 250 K, 273 K, 300 K, 400 K, 500 K, 800 K and 1000 K. [57]

In procedure III, prescribed path calculations were performed as follows: the initial structure was connected to the target structure via a straight line, followed by minimizations and constant temperature Monte Carlo runs in the orthogonal plane, which is defined by the cell parameters and the atom position of the configurations that are orthogonal to the line connecting the initial with the target structure. Again, 100 points were chosen along each prescribed path as starting points for the explorations and in each run 8 atoms (4 Zn, 4 O) per cell were used. In procedure III, the prescribed path between two minima is unique, although the transition routes obtained will most likely differ because of the stochastic nature of the explorations in the orthogonal plane. [57]

The temperatures selected varied from 50 - 1000 K, and for each temperature and starting point, one exploration consisting of 10000 MC steps at the given temperature followed by 5000 quench steps. Both the atom positions (90% of all Monte Carlo steps shift an individual atom, 5% swap the positions of two atoms) and the parameters of the periodically repeated simulation cell (5% of all Monte Carlo steps) were freely varied during the random walks. The constant temperatures selected were: 50 K, 100 K, 150 K, 200 K, 250 K, 273 K, 300 K, 400 K, 500 K, 800 K and 1000 K. [57]

### 10.2.1 Analysis methods in the prescribed path explorations

Once the prescribed path runs are finished, we have obtained a large set of configurations associated with the points along the path. Therefore, a fast analysis of their structure types, their symmetries, and their structural relationship with the starting points along the path, in particular the two end points, is needed. As a first step, we perform an automated determination of the symmetries and space groups of the structures using the LOAD program, and eliminate duplicate structures using the FILTER program (for details see section 5.9).

Quite generally, when investigating relationships between structures, a frequent problem is the search for a sequence of transitions from one space group (supergroup) to a different space group (subgroup), which is not a maximal non-isomorphic subgroup. Such a crystallographic analysis of the various structures and their group-subgroup relations down to the "amorphous" state ( $P1$ ) is performed using the SPUG algorithm implemented in the KPLOT program, which computes the possible sequences of maximal non-isomorphic subgroups between two given space groups in a non-complex manner using the minimal number of indices. In order to perform additional more complex crystallographic analysis, the Bilbao Crystallographic Server [105] and especially the SUBGROUPGRAPH program [363] were used (for more information see Appendix). [57]

## 10.3 Results and Discussion

### 10.3.1 The threshold algorithm calculations

At the second stage of the energy landscape investigation in the zinc oxide system, we performed several calculations using the threshold algorithm. During these calculations the number of formula units  $Z$  and the initial structure were varied. Each calculation consisted of 28 lids, ranging from -6.3 to -3.9 eV, with the step size of 0.1 eV.

#### 10.3.1.1 Energy landscape of ZnO for different number of formula units

In this research we performed a large number of calculations using the threshold algorithm, where the number of atoms in the simulation cell ( $Z$ ) was varied from 1 Zn and 1 O atom to 6 Zn and 6 O atoms, and all the relevant structures found after global

and local optimization were used as the starting points of the TA runs. In this way we obtained a large number of calculated data and in the following text, we will show only the highlights of the results, while the rest will be presented in the form of tables in the appendix.

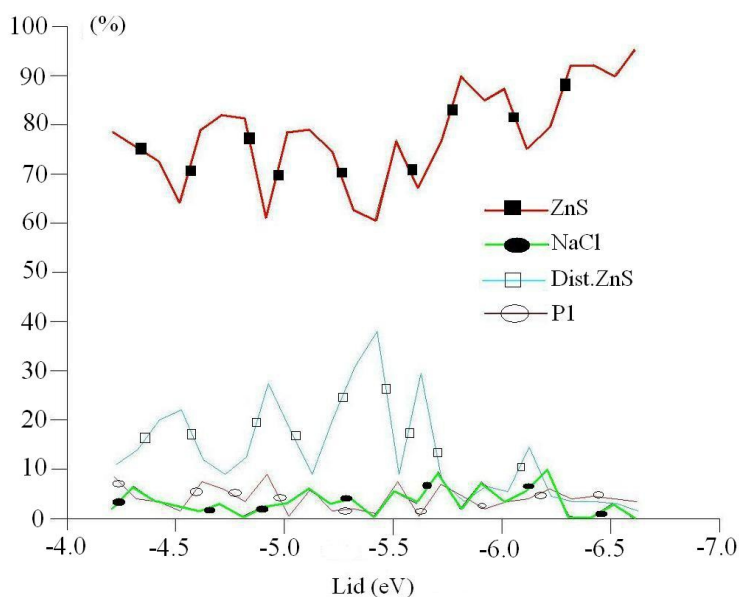


**Figure 10.1:** TA probability graph in ZnO system with 1 formula unit per simulation cell with sphalerite structure as a starting point - We observe low probability of sphalerite transforming into NaCl structure at the low energy lids, but with an energy increase, the probability of sphalerite distortions increases.

In figure 10.1, we show the results of the threshold algorithm calculations in the zinc oxide system for 1 Zn and 1 O atom in the simulation cell ( $Z = 1$ ). Since only the NaCl and the sphalerite structure can be transformed to 1 formula unit, the calculation was performed only for these two types as the starting point of the calculation. In figure 10.1, the sphalerite structure is used as the starting point. We observe that the sphalerite type is appearing most of the time on this constrained landscape. In very few cases we observe the NaCl type or an amorphous structures ( $P1$ ), a slightly more often, we see a distorted version of the sphalerite structure. We note that with an increase in lid value, this sphalerite distortion appear more frequently, and conversely the perfect sphalerite structure appears less. A similar distribution of structures is observed for the energy landscape of ZnO with  $Z = 1$  when the starting point is NaCl, indicating that

## 10. ENERGY LANDSCAPE INVESTIGATION IN ZNO

---

only few minima are present under these conditions.

Structure type	Times found (%)	Cell parameters	Times found (%)
NaCl	185 (11.45)	a=9 Å, b=6 Å, c=3 Å	100
Sphalerite	633 (39.20)	a=9.5 Å, b=6.4 Å, c=3.2 Å	54
		a=13.5 Å, b=6.4 Å, c=3.2 Å	46
SG 107 (dist.NaCl)	433 (26.81)	a=9 Å, b=6.2 Å, c=3.1 Å	100
Wurtzite	60 (3.71)	a=9.6 Å, b=7.6 Å, c=3.2 Å	100
SG 160 (new)	77 (4.77)	a=13 Å, b=6.3 Å, c=3.2 Å	2.6
		a=10.2 Å, b=6.3 Å, c=3.2 Å	1.3
		a=9.2 Å, b=6.4 Å, c=3.2 Å	96.1
SG 8 (new)	6 (0.37)	a=9.5 Å, b=6.4 Å, c=3.2 Å	50
		a=10.3 Å, b=6.2 Å, c=3.2 Å	50
P1/bad str.can.	221 (13.68)	-	-

**Table 10.1: Structural analysis of the energy landscape of ZnO with  $Z = 6$  and NaCl structure as a starting point of the TA calculations Part I** - Here we present the results of the first 5 lids (from -6.3 till -5.9 eV, with the step of 0.1 eV), where in total 1615 structure candidates were analyzed

With  $Z = 2$ , we observe that the wurtzite ( $P6_3mc$ , no. 186) and the sphalerite ( $F-43m$ , no. 216) type are the most dominant structures on the landscape, no matter which structure is taken as the starting point (see Appendix). However, with the high energy lids, we frequently observe a distorted variant of the wurtzite structure, exhibiting the space group  $I-4m2$  (no. 119). For the calculations performed with 3 formula units, again only two possible starting points are chosen: the sphalerite and the rock salt structure type. When starting from the NaCl type, we observe that the most frequent



minimum is the sphalerite structure (see Appendix). When starting from sphalerite structure type, most frequently we observe the distortions of sphalerite in space group  $Cm$  (no. 8) or the trigonal polytype 6H in space group  $R3m$  (no. 160), while at high energy lids mostly the sphalerite structure appears. With  $Z = 4$  most frequently found minima are the wurtzite ( $P6_3mc$ , no. 186) and the sphalerite ( $F-43m$ , no. 216) structure type. However, when starting from the  $\beta$ -BeO or "5-5" structure type, most of the times we observe the  $\beta$ -BeO type at low energy lids, and when starting from NaCl structure, besides the sphalerite modification, we observe a high percentage of the rock salt structure. With an increase of energy lids, the structures found become more distorted and finally "amorphous" ( $P1$ ). Since previous calculations produced "bad" structure candidates for  $Z = 5$ , we performed TA calculations for 6 formula units (see Appendix). The energy landscape becomes more diverse, dominated overall by the new trigonal polytype 6H in space group  $R3m$  (no. 160), while with higher energy lids, most of time we observe "amorphous" ( $P1$ ) structures, independent of the starting point.

Next, we performed a structural analysis of the energy landscape of ZnO with  $Z = 6$ , using different starting points for the calculations. The aim of this investigation is to study the distribution of structure candidates on the energy landscape as well as a change of the cell parameters (see tables 10.1 and 10.2). For one starting structure, we have analyzed more than 7000 structure candidates. Since this means a very large number of calculated data, here we will just present an excerpt of the investigations, which also depicts the amount of work invested in this study. With the calculations set for the first five lids (see table 10.1), we observe the sphalerite and the NaCl (including distortions) structures as the most dominant structure types.<sup>1</sup> Furthermore, we observe two different variants of the sphalerite structure, appearing in equal amounts on the landscape. Other structure types appear in small numbers at these low energy lids.

With an increase of the energy lids to -5.4 eV, we observed a big change on the landscape. The most frequent structure was a new trigonal polytype 6H in space group  $R3m$  (no. 160), while the NaCl structure rarely appeared. This 6H polytype is also exhibiting a diverse set of cell parameters, showing that it is easily accessible, at least at these energy lids. The sphalerite structure also shows a variety of unit cells, having different cell parameters. We note that the number of the wurtzite structure is increased, with an increased number of the cell variants.

<sup>1</sup>The cell parameters in the table are enlarged to fit the cell containing 6 formula units.

## 10. ENERGY LANDSCAPE INVESTIGATION IN ZNO

Structure type	Times found (%)	Cell parameters	Times found (%)
NaCl	10 (0.61)	a=9 Å, b=6 Å, c=3 Å	100
Sphalerite	423 (25.62)	a=8.5 Å, b=6.4 Å, c=3.2 Å	15.84
		a=9.6 Å, b=7.5 Å, c=3.2 Å	60.75
		a=10.1 Å, b=5.6 Å, c=3.2 Å	4.96
		a=11.5 Å, b=6.4 Å, c=3.2 Å	13.24
		a=12.4 Å, b=5.6 Å, c=3.2 Å	4.49
		a=13.6 Å, b=6.4 Å, c=3.2 Å	0.7
Wurtzite	161 (9.75)	a=8.3 Å, b=6.1 Å, c=3.2 Å	39.75
		a=9.7 Å, b=6.1 Å, c=3.2 Å	47.82
		a=11.65 Å, b=6.1 Å, c=3.2 Å	12.42
SG 160 (new)	644 (39.01)	a=8.6 Å, b=5.6 Å, c=3.2 Å	26.71
		a=9.2 Å, b=5.6 Å, c=3.2 Å	51.7
		a=10.3 Å, b=6.6 Å, c=3.2 Å	12.73
		a=11.2 Å, b=5.6 Å, c=3.2 Å	5.59
		a=12.2 Å, b=6.4 Å, c=3.2 Å	3.26
SG 8 (new)	80 (4.85)	a=9.5 Å, b=5.9 Å, c=3.2 Å	45
		a=10.3 Å, b=6.3 Å, c=3.1 Å	1.25
		a=11.2 Å, b=5.3 Å, c=3.3 Å	21.25
		a=12.3 Å, b=6.5 Å, c=3.2 Å	22.5
P1	260 (15.75)	Distortion/ bad str.can	4.5

**Table 10.2: Structural analysis of the energy landscape of ZnO with  $Z = 6$  and NaCl structure as a starting point of the TA calculations Part II** - Here we present the results of the next 5 lids (from -5.8 till -5.4 eV, with the step of 0.1 eV), where in total 1578 structure candidates were analyzed.

### 10.3.2 The Prescribed Path Algorithm calculations

In this section, we describe and employ the prescribed path method at the example of the energy landscape of ZnO. The focus is on the influence of the temperature on the stability of the various predicted structures in the ZnO system, the wurtzite, the sphalerite, the rock-salt, the 5-5, the nickel-arsenide, and the  $\beta$ -beryllium oxide type modifications found after global search and confirmed with local optimization and the threshold algorithm in the ZnO system. Every pair of local minima as initial/final configuration was separately analyzed. First, a stochastic quench was used along the path in order to investigate transition states and barriers separating minima. This was followed by constant temperature Monte Carlo simulations, in order to explore the regions beyond the barriers, as well as to investigate the temperature influence on the stability of the structures and their synthesis probability. Due to the large amount of results, only the most relevant ones are presented, i.e. for procedure II and III we only show the path analysis for the prescribed path connecting the experimentally observed structures wurtzite, sphalerite and rock salt. The results of our calculations are in good agreement with the experimental data, and represent a first attempt to connect predicted modifications to actual synthesis routes. [57]

#### 10.3.2.1 Energy landscape of ZnO for different temperatures (0 - 1000 K)

#### 10.3.2.2 Procedure I

We observed small energy barriers between the wurtzite, the sphalerite and the rock-salt-type structure, which is in agreement with experimental data. However, we observe much higher barriers between the 5-5, the NiAs and the  $\beta$ -BeO type, as well as in the case when these meta-stable types are connected to the sphalerite, the wurtzite and the NaCl structure types. This is plotted in a 2D-model of the energy landscape of the ZnO system, where all relevant local minima, which were used as initial/final configuration, are presented (see figure 10.2 and ref. [56]).

The model landscape was generated using the prescribed path algorithm with free stochastic quenches, where the paths were defined by variation of the size and shape of the unit cell from initial to final structure. The  $x$ -coordinate corresponds to the volume per 4 formula units and the  $y$ -coordinate is the cell parameter  $a$ . The projected

## 10. ENERGY LANDSCAPE INVESTIGATION IN ZNO

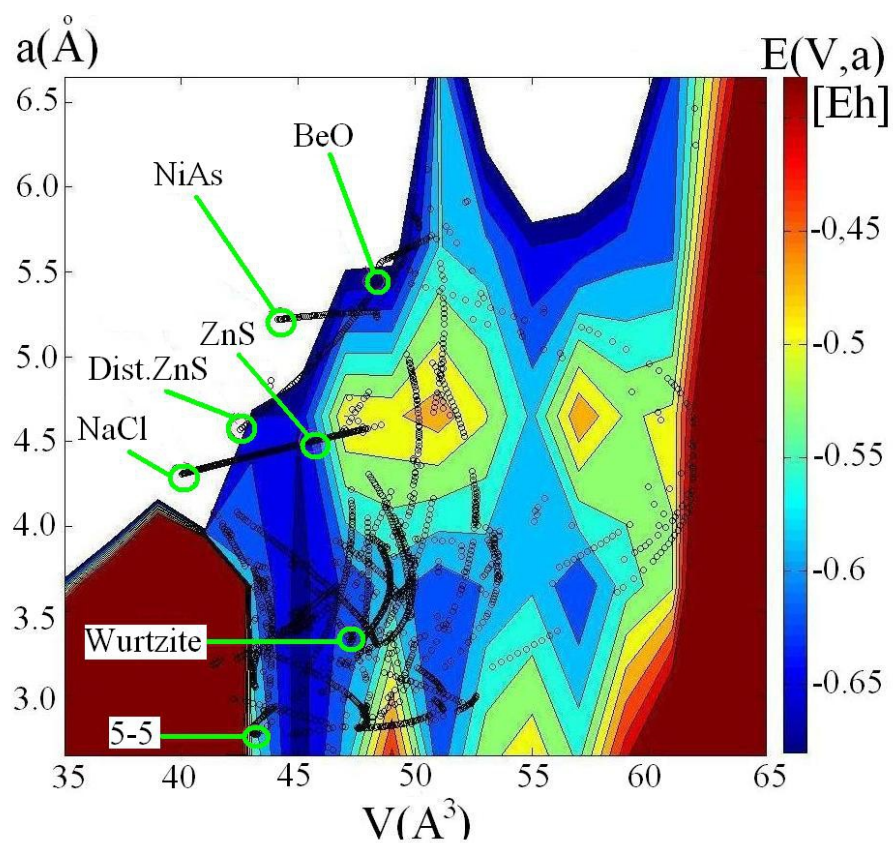


**Figure 10.2:** Model using all relevant local minima as initial/final configuration (the sphalerite, the wurtzite, the "5-5", the NaCl, the NiAs and the  $\beta$ -BeO type) - Points correspond to the restricted minima (for given Volume  $V(\text{\AA}^3)$  and cell parameter  $a(\text{\AA})$ ) found on the energy landscape of ZnO using the prescribed path algorithm procedure I.

landscape between these points has been interpolated using a special topological MatLab tool (biharmonic spline interpolation). [56]

### 10.3.2.3 Procedure II

Next, we used Monte Carlo walks at different temperature in order to investigate the height of the (generalized) barriers between two connected minima and the effect of the increased temperature. In this study we will present the part of the investigation which can be compared to the experimental observations: first, the prescribed path between the wurtzite and the sphalerite structure type, and second, the prescribed path between the wurtzite and the NaCl structure type, with temperatures varied from 50-1000 K. [57]

In figure 10.3 we show the crystallographic analysis of the prescribed path between the wurtzite and the sphalerite structure in the ZnO system with 4 formula units using procedure II. It appears that the wurtzite-sphalerite transition at extremely low temperatures (see figure 10.3) favors a more symmetric transformation route. With heating the system to 250 K, it loses a noticeable amount of symmetry along the path, where we cannot find wurtzite and sphalerite as the initial/final structure, and in-between, the minima which appeared along the prescribed path correspond to an "amorphous" state ( $P1$ ). With a further increase of temperature (see figure 10.4) to 500 K the only "non-amorphous" part of the transition path is close to the sphalerite region, where the system only manages to reach a distorted structure of sphalerite (space group  $I-4m2$ , no. 119). Increasing the temperature to 1000 K, we depart so far from the wurtzite/sphalerite basin, that every minimum reached corresponds to an "amorphous" state ( $P1$ ).

Furthermore, we performed the structure analysis of the prescribed path in order to determine the possible structures in the transition region between wurtzite and sphalerite using procedure II. The transition route at low temperatures is complex, but it could be approximated as wurtzite type ( $P6_3mc$ , no. 186) - distorted 5-5 structure type ( $Cmc2_1$ , no. 36 and  $Cmcm$ , no. 63) - mixed wurtzite and 5-5 structure type ( $C2/m$ , no. 12) - distorted 5-5 structure type ( $Pm$ , no.6,  $C2/c$ , no.15, and  $Cmcm$ , no. 63) - highly distorted sphalerite type ( $Pm$ , no. 6,  $Cm$ , no. 8, and  $P2_1/m$ , no.11) - distorted sphalerite ( $I-4m2$ , no. 119 and  $P4_2/mmc$ , no. 131) - distorted 5-5 structure type ( $P4/nmm$ , no.129) - NaCl type ( $Fm-3m$ , no. 225) - sphalerite type ( $F-43m$ , no. 216). A further increase of temperature, even to 250 K, is reflected in producing more

## 10. ENERGY LANDSCAPE INVESTIGATION IN ZNO

distortions in the minima along the prescribed path, and the wurtzite and sphalerite structure type cannot be found as undistorted anymore. The transition route at 500 K is largely changed by the effect of high temperatures: "amorphous" state ( $P1$ , no. 1) - distorted 5-5 structure type ( $P1$ , no. 1) - mixed wurtzite and 5-5 structure type ( $Pc$ , no. 7) - distorted 5-5 structure type ( $P4/nmm$ , no.129) - distorted sphalerite ( $I-4m2$ , no. 119). With a further increase of temperature to 1000 K, all calculated structures are associated with an "amorphous" state ( $P1$ ). Furthermore, note that application of a shear force sometimes results in reaching the NaCl instead of the sphalerite modification after the final unrestricted quench minimization. [57]

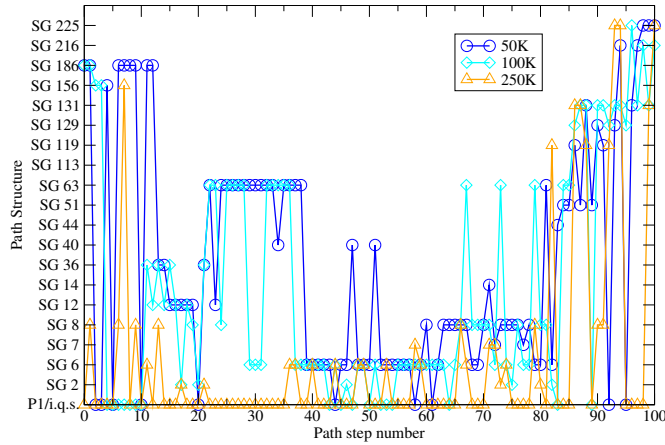


**Figure 10.3: Results of the crystallographic analysis in the prescribed path runs using the wurtzite type as initial configuration ( $x = 0$ ) and the sphalerite type cell as final configuration ( $x = 100$ ), performed with constant temperature Monte Carlo simulations within the prescribed path procedure II - Calculations performed at low temperatures (comparing results from 50 K, 100 K, and 250 K). Note that when the prescribed path is calculated from the sphalerite type to the wurtzite type cell using the procedure II, we observe different results, indicating the broadness of the transition path bundle. Note that  $P1$  (amorphous) phases are drawn together with several i.q.s. (incomplete quench structures), which are equally bad in symmetry and energy.**

In a short summary of these investigations we could say that the wurtzite - sphalerite transition prefers more symmetric route at low temperatures, which could be an indication of a low-temperature synthesis preference, and we could simplify the transition route as wurtzite - "5-5" - sphalerite type of modification. We compared our calculations to the available experimental data, and confirmed the conclusion that it would be easier to synthesize bulk sphalerite from wurtzite at low temperatures. [344, 345] As one can see from figure 10.4, there is a certain indication of the accessibility of the

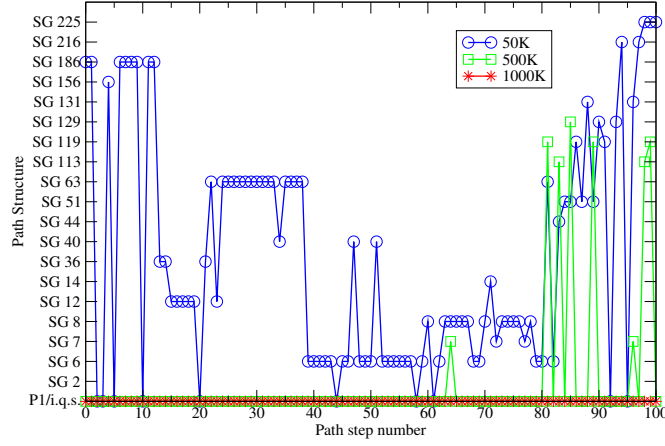


**Figure 10.4: Results of the crystallographic analysis in the prescribed path runs using the wurtzite type as initial configuration ( $x = 0$ ) and the sphalerite type cell as final configuration ( $x = 100$ ), performed with constant temperature Monte Carlo simulations within the prescribed path procedure II - Calculations performed at high temperatures (comparing results from 50 K, 500 K, and 1000 K).**

sphalerite modification at high temperatures, as it was observed in thin film synthesis at high temperatures [346, 347], but since this was not a unique path, procedure III of the prescribed path calculations was performed.

In the next step, we performed the crystallographic analysis of the prescribed path between the wurtzite and the rock salt structure in the ZnO system with 4 formula units using procedure II. Again we observe that the wurtzite - rock salt transition at low temperatures (see figure 10.5) favors a more symmetric transformation route. Although we note that the increase of heat reduces symmetry along the prescribed path, it is not so much affected as along the wurtzite - sphalerite path. Although with an increase of temperature to 500 K (see figure 10.6), most of the prescribed path explorations result in "amorphous" configurations, it is interesting that the wurtzite and the NaCl type could still be found as initial and final structures, as well as some symmetric modifications along the path. As in the wurtzite - sphalerite investigation, with an increase to 1000 K all the configurations found correspond to amorphous states ( $P1$ ). [57]

When the structure analysis is performed for the wurtzite - rock salt prescribed path, we observed a larger influence of temperature on the transition route. With calculations performed for the 50 K, the transition route corresponded to the wurtzite type ( $P6_3mc$ , no. 186) - highly or slightly distorted 5-5 structure type ( $Pm$ , no. 6,  $C2/m$ , no. 12,  $Cmc2_1$ , no. 36,  $Ama2$ , no. 40, and  $Cmcm$ , no.63) - distorted wurtzite ( $Cm$ , no. 8) -

## 10. ENERGY LANDSCAPE INVESTIGATION IN ZNO

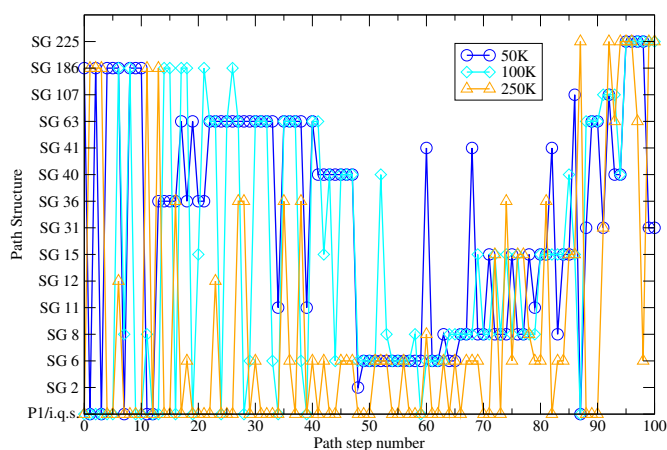


**Figure 10.5:** Results of the crystallographic analysis in the prescribed path runs using the wurtzite type as initial configuration ( $x = 0$ ) and the NaCl type cell as final configuration ( $x = 100$ ), performed with constant temperature Monte Carlo simulations within the prescribed path procedure II - Calculations performed at low temperatures (comparing results from 50 K, 100 K, and 250 K). Note that  $P1$  (amorphous) phases are drawn together with several i.q.s. (incomplete quench structures), which are equally bad in symmetry and energy.

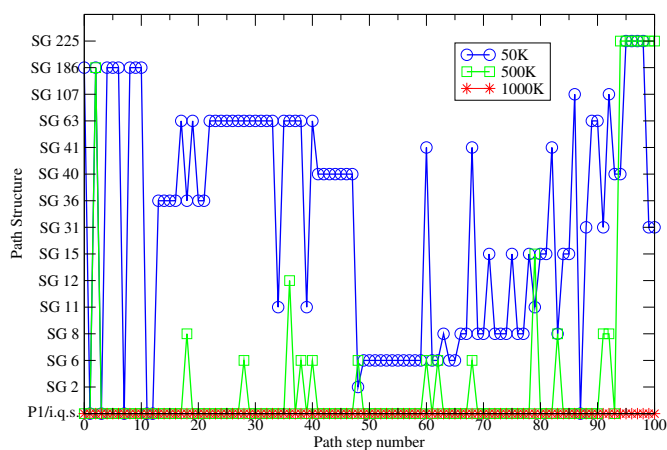


**Figure 10.6:** Results of the crystallographic analysis in the prescribed path runs using the wurtzite type as initial configuration ( $x = 0$ ) and the NaCl type cell as final configuration ( $x = 100$ ), performed with constant temperature Monte Carlo simulations within the prescribed path procedure II - Calculations performed at high temperatures (comparing results from 50 K, 500 K, and 1000 K).



highly or slightly distorted 5-5 structure type ( $Pm$ , no. 6 and  $C2/c$ , no. 15) - mixture of 5-5 and GeP type ( $Cm$ , no. 8) - distorted GeP type ( $Pmn2_1$ , no. 31, and  $Cmcm$ , no. 63) - GeP type ( $I4mm$ , no. 107) - NaCl ( $Fm - 3m$  - no. 225) - distorted GeP type ( $Pmn2_1$ , no. 31). With an increase to 100 K the starting structure is distorted, the structures along the middle part of the transition path are similar, but the prescribed path finishes at rock salt type of structure. Upon a further increase to 250 K, we observe a similar transition route as with 50 K. Again, the transition route at 500 K is largely changed by the effect of high temperatures: "amorphous" state ( $P1$ , no. 1) - wurtzite type ( $P6_3mc$ , no.186) - distorted wurtzite structure type ( $Pm$ , no. 6, and  $Cm$ , no. 8) - highly or slightly distorted 5-5 structure type ( $Pm$ , no. 6 and  $C2/m$ , no. 12) - highly distorted NaCl structure type ( $Pm$ , no. 6, and  $Cm$ , no. 8) - NaCl ( $Fm - 3m$ , no. 225). With a further increase of the temperature to 1000 K, we depart so far from the wurtzite/rock salt basin, that every minimum reached, corresponds to an "amorphous" state ( $P1$ ). [57]

We can conclude that there is a similar effect of heat on the symmetry during the prescribed path between the wurtzite and the rock salt structure, as in the previous case. The low temperature transition route we could simple write as wurtzite - "5-5" - GeP - NaCl structure type. Our calculations are in agreement with the available experimental observations, where the wurtzite - rock-salt transition is observed at high pressures and at low temperatures. [328, 341, 343, 364, 365]

#### 10.3.2.4 Procedure III

Additionally to the calculations above, where the random walks at various temperatures were essentially unrestricted and thus could yield a measure of the effective size of the basins involved, we performed calculations using procedure III of the prescribed path method. These calculations are a natural extension of the previous investigation; by including the option of orthogonal optimization at each point along the path, we explore the transition structures and the influence of temperature in more detail. Again, each pair of local minima as initial/final configuration was separately analyzed. [57]

In order to further analyze the prescribed path between the wurtzite and the spherulite type of structure (using procedure III), we performed several complex analyses:

## 10. ENERGY LANDSCAPE INVESTIGATION IN ZNO

---

the energy landscape analysis (of the calculated energies, see figures 10.7 and 10.9), crystallographic analysis (see figures 10.8 and 10.10) and group-subgroup relation analysis (see figures 10.11 and 10.12).

Figures 10.7, 10.9, 10.8 and 10.10 show the results of the prescribed path explorations using procedure III between the wurtzite and the sphalerite structure in the ZnO system with 4 formula units. At this level of calculation it is clear that no matter how high we heat the system, most of the actual transition path will be complicated and "amorphous" ( $P1$ ), since we are required to remain in the orthogonal plane. These results of crystallographic analysis also underline that there do not appear to be high-symmetry transition routes between the two structures that are accessible at low energies/temperatures. Still, we could conclude that the wurtzite - sphalerite transition prefers more symmetric route at low temperatures, which could be an indication of low temperature synthesis preference. The transition route can be approximated as wurtzite - "5-5" - sphalerite type of modification, as we observe in previous calculation with procedure II. We note that according to the investigations so far, the intermediate "5-5" structure is a meta-stable phase, which would appear in the wurtzite - sphalerite transition as a distorted variant at low temperatures. [57]

In the energy landscape analysis, we observe noticeable smaller barriers at low temperatures than at calculations performed at high temperatures. Maybe the way to bypass the high barrier at low temperature is structure S1 or at high temperatures structures S2 and S3. These structures are low in energy, but they exhibit  $P1$  symmetry and represent highly distorted variants of the sphalerite and 5-5 structure type, indicating the transition route explained above. [57]

We can conclude that at low temperatures (see figures 10.7 and 10.8), both the wurtzite and the sphalerite type appear to be more stable than at high temperatures (see figures 10.9 and 10.10). A consequence of this is that it would be easier to synthesize bulk sphalerite from wurtzite at low temperatures. [344, 345] Furthermore, we also observe, similarly as in figure 10.4, that there should be a possibility of synthesizing sphalerite at high temperatures, as it has been observed in thin film synthesis at high temperatures. [346, 347]

In order to further analyze our calculations, we performed a group - subgroup relation analysis for space groups  $P6_3mc$  (no. 186), where the ideal wurtzite structure appears, and  $F - 43m$  (no. 216), where the ideal sphalerite structure appears, to the

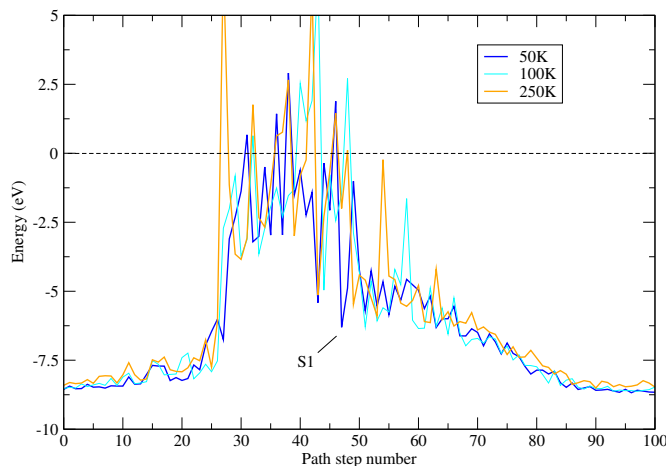


**Figure 10.7:** Results of the energy landscape analysis in the prescribed path runs between the wurtzite ( $x = 0$ ) and the sphalerite type ( $x = 100$ ), performed with constant temperature MC simulations within the prescribed path procedure III at low temperatures (comparing results from 50 K, 100 K, and 250 K) - Note that transition structure S1, represented in the middle part of the prescribed path at low temperatures, can be described as a distorted mixture of sphalerite and 5-5 structure type.

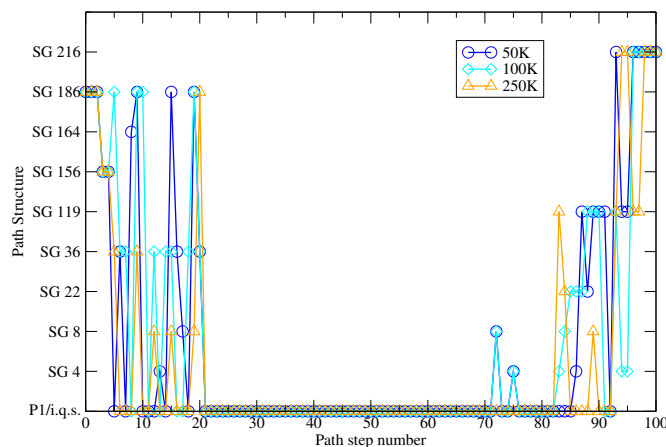


**Figure 10.8:** Results of the crystallographic analysis in the prescribed path runs using the wurtzite type as initial configuration ( $x = 0$ ) and the sphalerite type cell as final configuration ( $x = 100$ ), performed with constant temperature Monte Carlo simulations within the prescribed path procedure III - Crystallographic analysis performed at low temperatures (comparing results from 50 K, 100 K, and 250 K). Note that *P1* (amorphous) phases are drawn together with several i.q.s. (incomplete quench structures), which are equally bad in symmetry and energy.

## 10. ENERGY LANDSCAPE INVESTIGATION IN ZNO

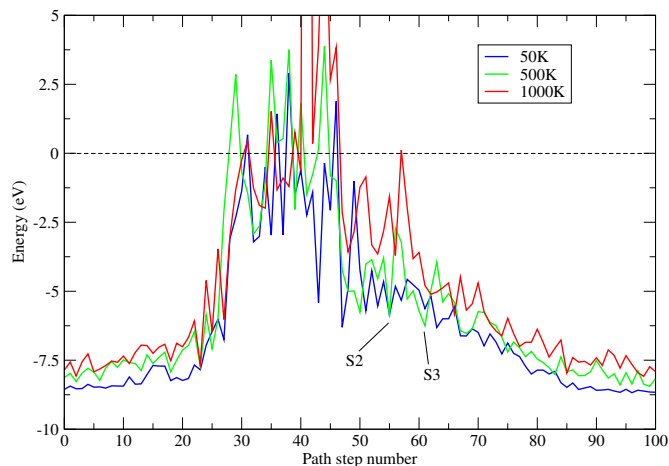


**Figure 10.9:** Results of the energy landscape analysis in the prescribed path runs using the wurtzite type as initial configuration ( $x = 0$ ) and the sphalerite type cell as final configuration ( $x = 100$ ), performed with constant temperature Monte Carlo simulations within the prescribed path procedure III at high temperatures (comparing results from 50 K, 500 K, and 1000 K) - Here, we note two structures, S2, which can be described as a highly distorted 5-5 type, and S3, which can be described as different mixture of the sphalerite and the 5-5 structure type.

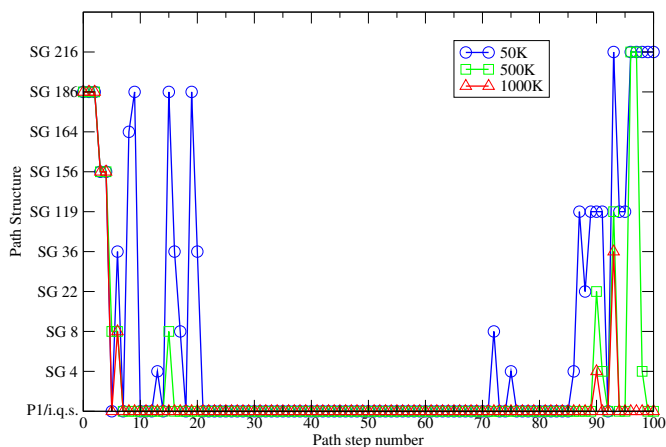


**Figure 10.10:** Results of the crystallographic analysis in the prescribed path runs using the wurtzite type as initial configuration ( $x = 0$ ) and the sphalerite type cell as final configuration ( $x = 100$ ), performed with constant temperature Monte Carlo simulations within the prescribed path procedure III at high temperatures (comparing results from 50 K, 500 K, and 1000 K) - Note that P1 (amorphous) phases are drawn together with several i.q.s. (incomplete quench structures), which are equally bad in symmetry and energy.

"amorphous" state ( $P1$ ), which was the most frequently found minimum along the transition path (see figures 10.11 and 10.12). Furthermore complex crystallographic and group - subgroup relation analysis was performed using higher indices as explained in the supporting information. [57]

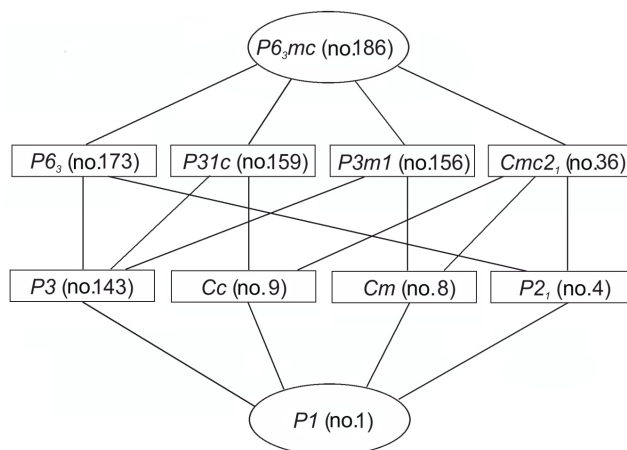


**Figure 10.11: Group-subgroup relation graph of subgroups for the group-subgroup pair** - The starting group is  $P6_3mc$ , where the ideal wurtzite ( $B4$ ) structure appears, and the final subgroup is  $P1$ , where the "amorphous" phases appear. Note that minimal indices were used in the graph, and the complex graphs, with higher indices, are presented in the Appendix.

As a result of our group-subgroup relation analysis, one can see that the variety of the space groups, which we observe in our calculations along the wurtzite-sphalerite prescribed path, matches the subgroup transformation of wurtzite and sphalerite as supergroup down to the "amorphous" state ( $P1$ ) as the final subgroup.

As in the previous case, we have performed a set of analyses in order to further investigate a prescribed path between the wurtzite and the NaCl (see figures 10.13, 10.15, 10.14, and 10.16). The results of the crystallographic analysis shows that the most of the transition paths will be complicated and pass through the amorphous ( $P1$ ) regions, independent of the specific temperature used. We can conclude that with the calculation performed at low temperatures (see figure 10.13), both the wurtzite and the NaCl structure appear to be stable, while with calculations performed at high temperatures, both structures become quite unstable (see figure 10.15). We could approximate the low temperature transition route as the wurtzite - "5-5" - GeP - NaCl structure type. The wurtzite - rock salt path is a pressure induced transition route, which at lower

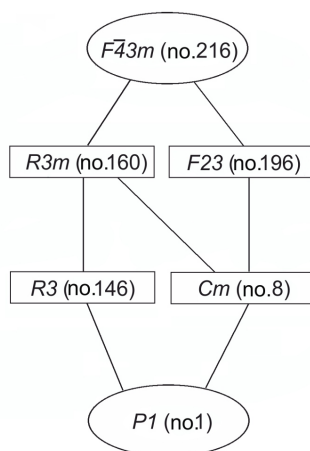


**Figure 10.12: Group-subgroup relation graph of subgroups for the group-subgroup pair** - The starting group is  $F-43m$ , where the ideal sphalerite ( $B3$ ) structure appears, and the final subgroup is  $P1$ , where the "amorphous" phases appear. Note that minimal indices were used in the graph, and the complex graphs, with higher indices, are presented in the Appendix.

temperatures at high pressures can follow the logical coordination number (CN) line: wurtzite (CN = 4) - "5-5" (CN = 5) - GeP (CN = 5+1) - rock salt (CN = 6) structure type. [57]

In the energy landscape analysis we observe the smallest barriers in the whole prescribed path investigation at low temperatures (see figure 10.13). With the calculation performed at high temperatures, the height of the barriers becomes so big, that it is highly unlikely to bypass them and perform a synthesis (see figure 10.15). However, if one would like to bypass the energy barriers at low temperatures, maybe the right way is to choose the structures S4 and S5. These are highly distorted variants of the 5-5 modification and they are low in energy, but they exhibit only  $P1$  symmetry. [57]

Our calculations are in agreement with the available experimental observations, where the wurtzite - rock salt transition is observed at high pressures and at low temperatures. [328, 341, 343, 364, 365] We would like to note that the intermediate 5-5 structure is observed at low temperatures (see figure 10.14), but also it appears stable at very high temperatures (see figure 10.16). This is in agreement with recent experimental observations where the existence of 5-5 structure has been suggested in thin films both at low and high temperatures. [361, 362, 366]

In order to further analyze our calculations, we performed a group-subgroup relation

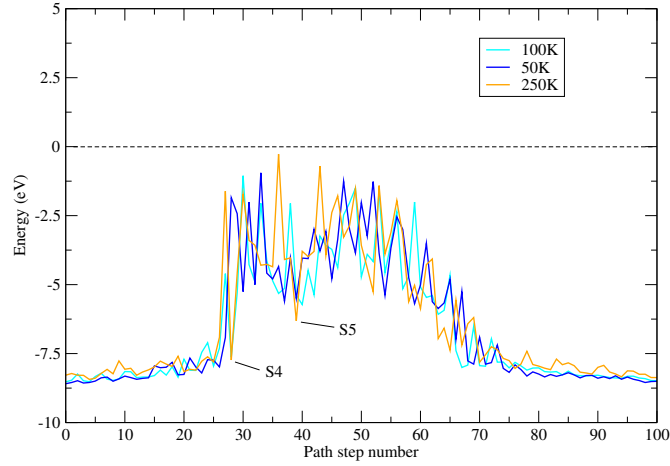


**Figure 10.13:** Results of the energy landscape analysis in the prescribed path runs using the wurtzite type as initial configuration ( $x = 0$ ) and the rock salt (NaCl) type cell as final configuration ( $x = 100$ ), performed with constant temperature Monte Carlo simulations within the prescribed path procedure III at low temperatures (comparing results from 50 K, 100 K, and 250 K) - Note that transition structures S4 and S5, observed in the middle part of the prescribed path, exhibit a highly distorted 5-5 structure type.

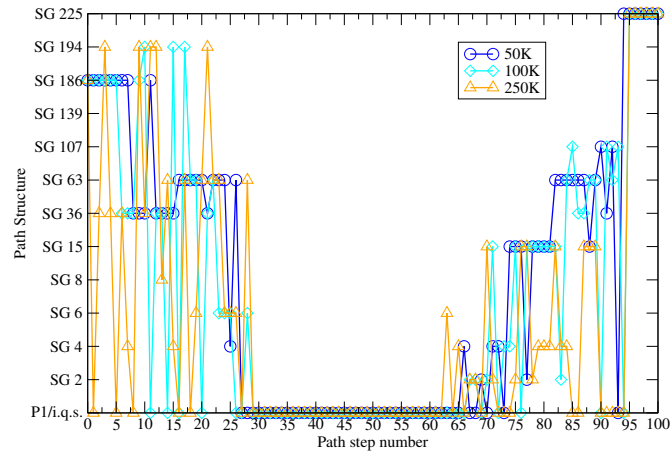


**Figure 10.14:** Results of the crystallographic analysis in the prescribed path runs using the wurtzite type as initial configuration ( $x = 0$ ) and the rock salt (NaCl) type cell as final configuration ( $x = 100$ ), performed with constant temperature Monte Carlo simulations within the prescribed path procedure III - Crystallographic analysis performed at low temperatures (comparing results from 50 K, 100 K, and 250 K). Note that  $P1$  (amorphous) phases are drawn together with several i.q.s. (incomplete quench structures), which are equally bad in symmetry and energy.

## 10. ENERGY LANDSCAPE INVESTIGATION IN ZNO

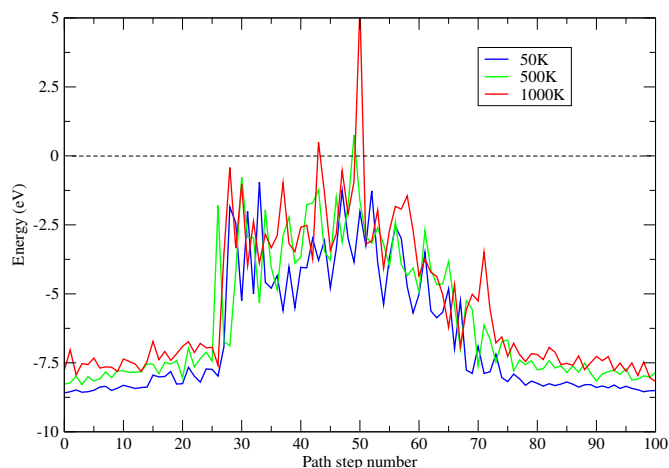


**Figure 10.15:** Results of the energy landscape analysis in the prescribed path runs using the wurtzite type as initial configuration ( $x = 0$ ) and the rock salt (NaCl) type cell as final configuration ( $x = 100$ ), performed with constant temperature Monte Carlo simulations within the prescribed path procedure III at high temperatures (comparing results from 50 K, 500 K, and 1000 K) - Note that  $P1$  (amorphous) phases are drawn together with several i.q.s. (incomplete quench structures), which are equally bad in symmetry and energy.

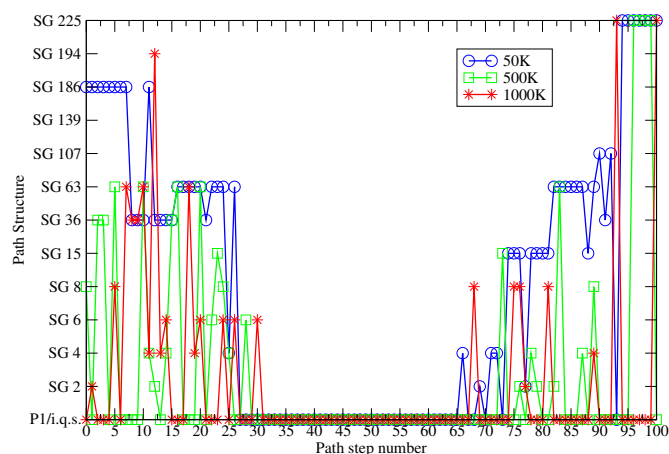


**Figure 10.16:** Results of the crystallographic analysis in the prescribed path runs using the wurtzite type as initial configuration ( $x = 0$ ) and the rock salt (NaCl) type cell as final configuration ( $x = 100$ ), performed with constant temperature Monte Carlo simulations within the prescribed path procedure III at high temperatures (comparing results from 50 K, 500 K, and 1000 K) - Note that  $P1$  (amorphous) phases are drawn together with several i.q.s. (incomplete quench structures), which are equally bad in symmetry and energy.



analysis for the wurtzite and the rock salt structure to the "amorphous" state ( $P1$ ) (see figure 10.11 and 10.17). Further complex crystallographic and group - subgroup relation analysis was performed using higher indices as explained in the supporting information. The results of the group-subgroup relation analysis show that the variety of space groups observed in our calculations matches the crystallographic results. [57]

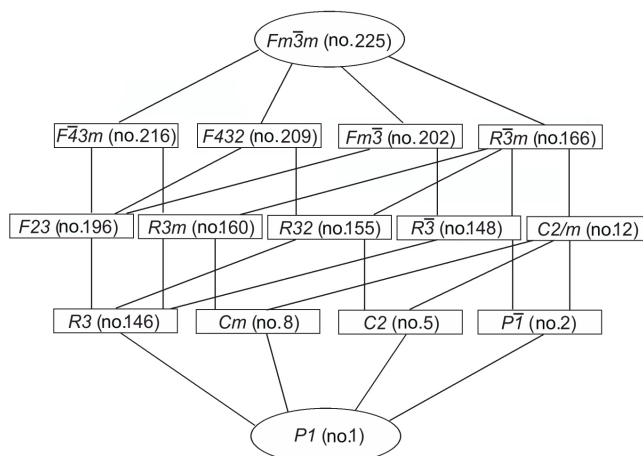


**Figure 10.17: Group-subgroup relation graph of subgroups for the group-subgroup pair** - The starting group is  $Fm - 3m$ , where the ideal rock salt ( $B1$ ) structure appears, and the final subgroup is  $P1$ , where the "amorphous phases" appear. Note that minimal indices were used in the graph, and the complex graphs, with higher indices, are presented in the Appendix.

Finally, we have analyzed the prescribed path between the sphalerite and the NaCl structure type using procedure III. Since we observed extremely high barriers within this prescribed path (see figures 10.18 and 10.20), even at low temperatures, we have concluded that a direct transition between the sphalerite and the rock salt type of structure is very unlikely. However, when we performed a crystallographic and group-subgroup analysis (see figures 10.12, 10.17, 10.19 and 10.21), we note two interesting observations: first, that preferred transition space group is  $Cm$  (no. 8), which we have observed in previous calculations and which is analyzed in more detail in the Appendix, and second, that this particular path produces one unusual distortion of the rock salt structure type, exhibiting space group  $R3m$  (no. 160) and has sevenfold coordination of the Zn atom by O atoms. A short summary of our prescribed path investigations is presented in figure 10.22. [57]

## 10. ENERGY LANDSCAPE INVESTIGATION IN ZNO

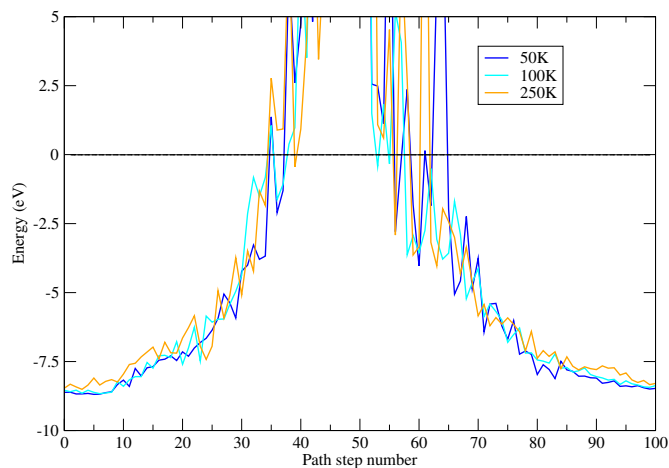


**Figure 10.18:** Results of the energy landscape analysis in the prescribed path runs using the sphalerite type as initial configuration ( $x = 0$ ) and the rock salt (NaCl) type cell as final configuration ( $x = 100$ ), performed with constant temperature Monte Carlo simulations within the prescribed path procedure III at low temperatures (comparing results from 50 K, 100 K, and 250 K) - We note that the size of the barriers are extremely high even at low temperatures.

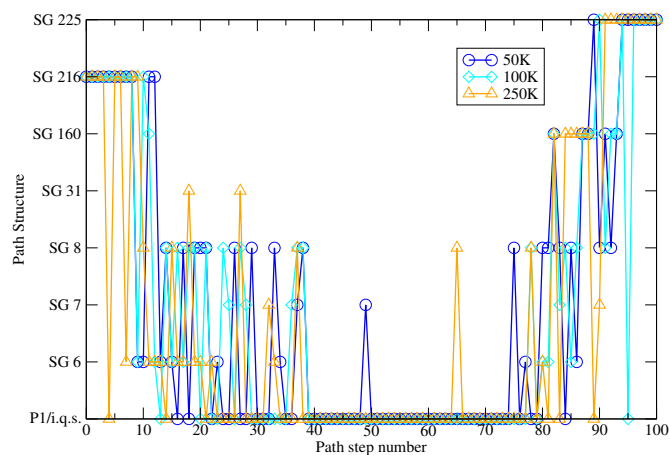


**Figure 10.19:** Results of the crystallographic analysis in the prescribed path runs using the sphalerite type as initial configuration ( $x = 0$ ) and the rock salt (NaCl) type cell as final configuration ( $x = 100$ ), performed with constant temperature Monte Carlo simulations within the prescribed path procedure III - Crystallographic analysis performed at low temperatures (comparing results from 50 K, 100 K, and 250 K). Note that  $P1$  (amorphous) phases are drawn together with several i.q.s. (incomplete quench structures), which are equally bad in symmetry and energy.

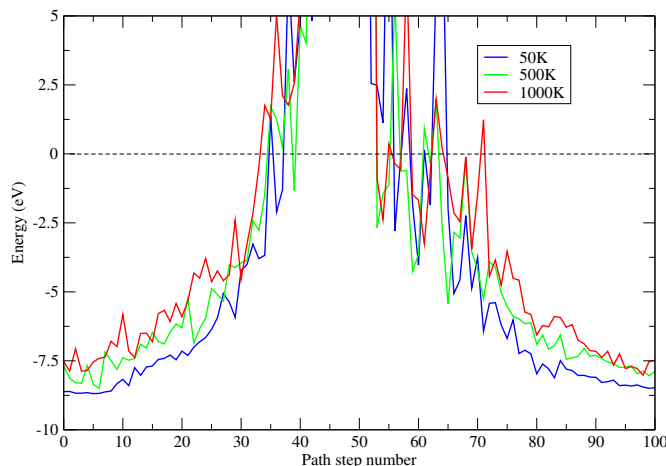


**Figure 10.20:** Results of the energy landscape analysis in the prescribed path runs using the sphalerite type as initial configuration ( $x = 0$ ) and the rock salt (NaCl) type cell as final configuration ( $x = 100$ ), performed with constant temperature Monte Carlo simulations within the prescribed path procedure III at high temperatures (comparing results from 50 K, 500 K, and 1000 K) - Note that  $P1$  (amorphous) phases are drawn together with several i.q.s. (incomplete quench structures), which are equally bad in symmetry and energy.

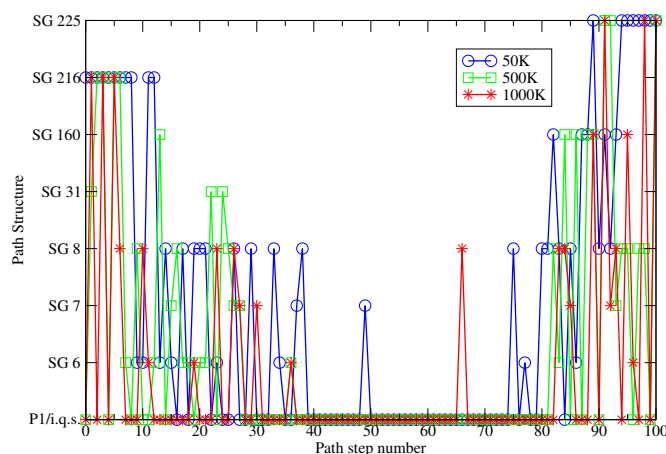


**Figure 10.21:** Results of the crystallographic analysis in the prescribed path runs using the sphalerite type as initial configuration ( $x = 0$ ) and the rock salt (NaCl) type cell as final configuration ( $x = 100$ ), performed with constant temperature Monte Carlo simulations within the prescribed path procedure III at high temperatures (comparing results from 50 K, 500 K, and 1000 K) - Note that  $P1$  (amorphous) phases are drawn together with several i.q.s. (incomplete quench structures), which are equally bad in symmetry and energy.

## 10. ENERGY LANDSCAPE INVESTIGATION IN ZNO

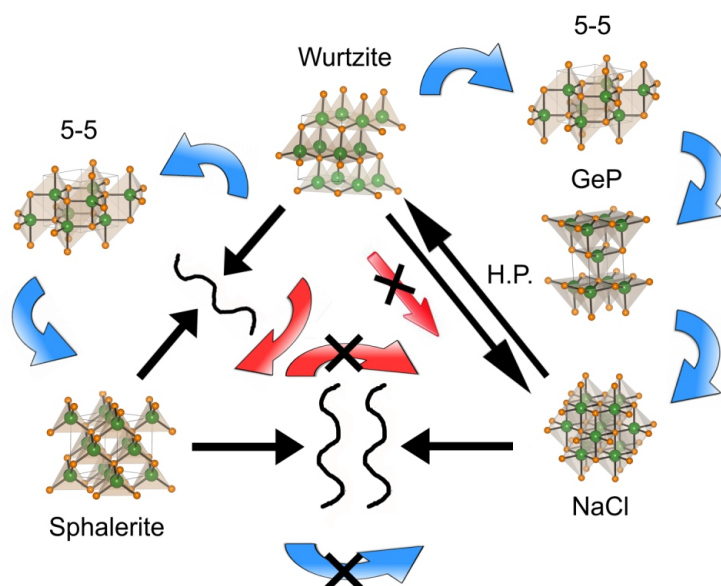


**Figure 10.22: A short summary of our prescribed path investigations in the ZnO system** - Black arrows represent prescribed paths between experimentally observed structures in the ZnO system: the wurtzite, the sphalerite and the rock salt type. The wavy black lines indicate the size of the barrier along the prescribed path in comparison to other paths. The blue arrows represent low temperature transition routes and the red arrows represent high temperature transition routes, respectively. A stable form of ZnO at ambient conditions is the wurtzite (B4) modification. Within a prescribed path between the wurtzite and the rock salt (B1) structure, essentially no barriers are observed if high pressure is used. With calculations performed at low temperatures, small barriers are observed, which can possibly be bypassed via two intermediate structures of the 5-5 and the GeP type. With a further increase of temperature, generalized barriers become very high and a synthesis/transformation becomes highly unlikely. Similarly, if the wurtzite (B4) and the sphalerite (B3) structure are connected, small barriers are observed at low temperatures. However, it could be possible to make a low-temperature phase transition via the 5-5 structure. There are some indications that this could be possible even at higher temperatures. In the case the of prescribed path runs between the sphalerite and the rock salt type, we observe extremely high barriers, regardless of any temperature employed; so we conclude that a direct transformation in bulk from the sphalerite to the NaCl modification is highly unlikely.

### 10.3.2.5 Thermal stability analysis (TSA) via constant temperature Monte Carlo simulations

Finally, in order to test the thermal stability of the structures involved in the prescribed path calculations, we performed short constant-temperature Monte Carlo simulations for the wurtzite, sphalerite and rock-salt structure, separately. In each MC run, 8 atoms (4 Zn, 4 O) per cell were used. The results are presented in the tables 10.1, 10.2, 10.3 and 10.4.

Temperature (K)	Wurtzite ( $P6_3mc$ ) (%)	ZnO d-I ( $P3m1$ ) (%)	ZnO d-dII ( $Cmc2_1$ ) (%)
50	100	-	-
100	100	-	-
250	80	-	20
500	99	1	-
1000	100	-	-

**Table 10.1: Thermal stability analysis (TSA) for the wurtzite type of structure in the ZnO system** - TSA Calculations performed via constant temperature Monte Carlo simulations.

In table 10.1 we have studied the wurtzite type ( $P6_3mc$ ) of structure, for the whole range of temperatures using the TSA method. It appears to be stable regardless of the heating effect, which is in agreement with the experiment, [367, 368] although a certain instability is observed at 250K with about 20% of all runs showing a distortion of wurtzite, marked as ZnO d-II ( $Cmc2_1$ , no. 36). However this unusual behavior we can relate to the features of the energy landscape of ZnO e.g. shallow neighboring minima (distorted wurtzite) become accessible at this intermediate temperature range (e.g. similar features are observed in the  $MgF_2$  system [369, 370]). At higher temperatures of about 500 K, we observe a structure, marked as ZnO d-I ( $P3m1$ , no. 156), which shows the structure of a highly distorted 4H polytype. This could be an indication that our predicted polytypes in ZnO, [57, 371] could be possibly synthesized at high temperatures. We also note that wurtzite tends to be quite stable at very high temperatures (about 1000 K), which is in agreement with experimental observations.

Table 10.2 shows the analogous results for the sphalerite type of structure ( $F-43m$ ), for the whole range of temperatures using the TSA method. It appears stable for both low and high temperatures, which is in agreement with the experiment. [344–347] It

## 10. ENERGY LANDSCAPE INVESTIGATION IN ZNO

---

Temperature (K)	Sphalerite ( $F-43m$ ) (%)	ZnO d-III ( $I-4m2$ ) (%)
50	100	-
100	100	-
250	100	-
500	100	-
1000	95	5

**Table 10.2: Thermal stability analysis (TSA) for the sphalerite type of structure in the ZnO system** - TSA Calculations performed via constant temperature Monte Carlo simulations.

starts to show instability at very high temperatures, close to 1000 K, where we observe a distortion of the sphalerite, marked as ZnO d-III ( $I-4m2$ , no. 119). [57]

The effect of the high temperature on the NaCl type of structure is easily observed through the presence of the highly distorted NaCl type, marked as ZnO d-VIII ( $Cmc2_1$ , no. 36) in tables 10.3 and 10.4. One should not confuse ZnO d-II and ZnO d-VIII type, which have the same symmetry ( $Cmc2_1$ , no. 36), but different structures; in the first case, we observe a large distortion of the wurtzite type and in second one, a large distortion of the NaCl type. This suggests a possibility of a (unique) transition structure, which partakes equally in both the initial and final structure, but with less symmetry. This structure perhaps could be found in space group  $Cm$  (no. 8), which is relatively frequently observed and consistent with the group-subgroup relations (for more details see Appendix). We also conclude that the NaCl type of structure in the ZnO system prefers low temperatures, which is in agreement with the experiment. [328, 341, 343, 364, 365]

Temperature (K)	NaCl ( $Fm-3m$ ) (%)	ZnO d-IV ( $P4_2/mnm$ ) (%)	ZnO d-V ( $Cmcm$ ) (%)
50	100	-	-
100	84	-	13
250	100	-	-
500	74	-	-
1000	64	1	1

**Table 10.3: Thermal stability analysis (TSA) for the rock salt (NaCl) type of structure in the ZnO system - Part I** - TSA Calculations performed via constant temperature Monte Carlo simulations.

The effect of the high temperature on the NaCl type of structure is easily observed through the presence of the highly distorted NaCl type, marked as ZnO d-VIII ( $Cmc2_1$ , no. 36) in tables 10.3 and 10.4. One should not confuse ZnO d-II and ZnO d-VIII type, which have the same symmetry ( $Cmc2_1$ , no. 36), but different structures; in the first case, we observe a large distortion of the wurtzite type and in second one, a large distortion of the NaCl type. This suggests a possibility of a (unique) transition structure, which partakes equally in both the initial and final structure, but with less symmetry. This structure perhaps could be found in space group  $Cm$  (no. 8), which is relatively frequently observed and consistent with the group-subgroup relations (for more details see Appendix). We also conclude that the NaCl type of structure in the ZnO system prefers low temperatures, which is in agreement with the experiment. [328, 341, 343, 364, 365]

Temperature (K)	NaCl ( $Fm-3m$ ) (%)	ZnO d-VI ( $P4_2/mnm$ ) (%)	ZnO d-VII ( $Cmcm$ ) (%)	ZnO d-VIII ( $P4_2/mnm$ ) (%)
50	100	-	-	-
100	84	1	-	-
250	100	-	-	-
500	74	10	3	13
1000	64	4	1	29

**Table 10.4: Thermal stability analysis (TSA) for the rock salt (NaCl) type of structure in the ZnO system - Part II** - TSA Calculations performed via constant temperature Monte Carlo simulations.

## 10.4 Conclusion

The energy landscape of the zinc oxide system was investigated by performing a number of calculations using the threshold algorithm, where the number of atoms in the simulation cell ( $Z$ ) was varied from 1 Zn and 1 O atom to 6 Zn and 6 O atoms. All the relevant structures found after global and local optimization, were used as the starting points of the TA runs and the calculations were performed for large numbers of energy lids. We observe that the energy landscape is highly influenced by the number of formula units, and the energy lid. We note that this influence has a strong effect on the structural

## 10. ENERGY LANDSCAPE INVESTIGATION IN ZNO

---

distribution, and also on the size of the structures, producing new variants inside the same structure type.

Starting from results of the global optimizations and threshold calculations in the ZnO system, we performed prescribed path explorations, in order to investigate the features of the energy landscape of ZnO that connect the major minimum basins of the system. We present here the prescribed path algorithm, a new method for exploring transition routes and barriers between even distant minima, as well as for learning about aspects of the structural stability and possible synthesis processes as function of temperature and pressure, and for making contact with experimental observations.

Several procedures were selected, from among the variety of modules available in the prescribed path algorithm, which explored the prescribed path between the most relevant minima (the wurtzite, the sphalerite, and the NaCl type of structure) in different ways. Our calculation showed that a stable form of ZnO at ambient conditions is the wurtzite (*B4*) modification. Within a prescribed path between the wurtzite and the rock salt (*B1*) structure, no barriers are observed at 0K if high pressure is used, which is in agreement with experimental results. With calculations performed at low temperatures, small barriers are observed, which can possibly be bypassed by intermediate structure of the GeP type. With further increase of temperature, barriers become very high and the synthesis becomes highly unlikely.

Similarly, if the wurtzite (*B4*) and the sphalerite (*B3*) structure are connected, small barriers are observed already at 0 K. However, it could be possible to make the low-temperature phase transition to the 5-5 structure type. There are some indications that this could be possible even at higher temperatures, which is in agreement with recent experimental observations. In the case of the prescribed path between the sphalerite and the rock salt type, we observe extremely high barriers, regardless to any temperature calculated, so we conclude that a direct synthesis in bulk from the sphalerite to the NaCl modification is highly unlikely. Each calculation was separately analyzed according to their energies, crystallographic and structural aspects.

Finally, for each relevant structure, the thermal stability was separately analyzed. Our calculations showed that the wurtzite (*B4*) structure should be stable over a wide range of temperatures. Similarly, the sphalerite (*B3*) structure in the ZnO system exhibits a wide range of temperatures where it is stable, although it should prefer low temperatures for its synthesis. The rock salt (*B1*) structure type is unstable at high



temperatures, which is in agreement with experimental results. Quite generally, the results of the prescribed path runs are in satisfying agreement with experimental information about the stability and synthesis conditions of the various ZnO modifications.

## 10. ENERGY LANDSCAPE INVESTIGATION IN ZNO

---

# 11

## Structure prediction as a guide in synthesis planning: investigation of systems exhibiting the 5-5 structure type

*"Employ your time in improving yourself by other men's writings, so that you shall gain easily what others have labored hard for."*

(Socrates (469-399 BC), Greek Athenian philosopher)

### 11.1 Introduction

Both of our previous investigations in the PbS and the ZnO system have produced the so-called 5-5 structure as an interesting structure candidate. Similarly, in many other previous theoretical [15, 337, 339, 340, 360, 372] and experimental studies [361, 362], the 5-5 structure has been observed. (Note that different scientific groups have rediscovered this structure in different contexts, and afterwards gave different names to this structure type). This structure type can be described as a mutual fivefold coordination of cation  $A$  by anion  $B$  in a hexagonal lattice ( $P6_3/mmc$ , no. 194) with  $ABAB$  stacking. [15]  $A$ -atoms form trigonal bipyramids around  $B$ -atoms, and conversely (see figure 11.1). The 5-5 structure can be derived from the  $h$ -BN structure by requiring that the bond length in the  $c$ -direction must be essentially identical to the one within the planar

## 11. STRUCTURE PREDICTION AS A GUIDE IN SYNTHESIS PLANNING: INVESTIGATION OF SYSTEMS EXHIBITING THE 5-5 STRUCTURE TYPE

---

hexagons (see figure 11.1). In order to find the best chemical system for the synthesis of a modification that exhibits the 5-5 structure type, we performed data mining based explorations in group V, IV - VI, and III - VII binary compounds. In each of the investigated systems, local optimizations on *ab initio* level were performed for the 5-5 and typical *AB*-structure types for comparison. [152, 372]

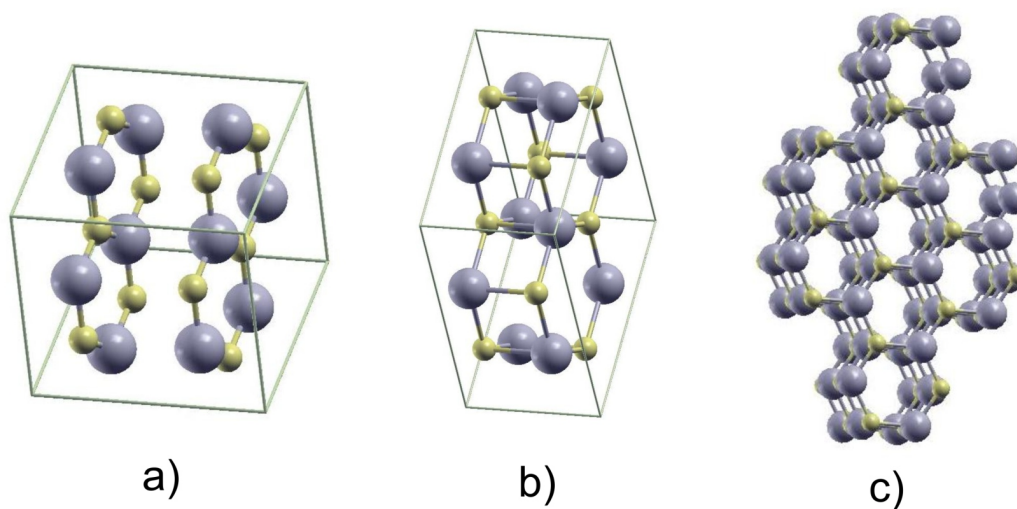


**Figure 11.1:** Visualization of the: a) *h*-BN-structure type. Note the 3-fold coordination of this structure and a longer bond length in *c*-direction, compared to the 5-5 type; b) and c) 5-5 structure type in a primitive and a periodically repeated cell. - Note the 5-fold coordination and a shorter bond length in *c*-direction. The smaller light spheres and larger dark spheres correspond to *A* and *B* atoms, respectively.

### 11.2 Optimization procedure

In order to find suitable *AB* compounds for a synthesis of the 5-5 structure type, we performed a data mining based exploration in group V, IV - VI, and III - VII compounds. [79–83] The guiding idea was to find *AB* compounds with ten valence electrons in total. This would formally allow the system to form *AB* compounds with five bonds per atom, leading in a natural way to a five-fold coordination. For every such combination of elements, we first performed a local minimization of the hypothetical compound on the *ab initio* level in the 5-5 structure type. If this resulted in a stable structure, we computed the  $E(V)$  curves for: the 5-5 modification, the experimentally observed structures if there were some known in the system, plus several important

*AB* structure types, which had been found in previous calculations and experiments for other *AB* systems.

The experimentally observed structures were taken from the ICSD [65, 66] and all the total energy calculations and energy minimizations were performed on the *ab initio* level with an LDA functional using the program **CRYSTAL09**. [191, 192] Furthermore, the symmetries and space groups of the related configurations are determined using the algorithms SFND [228] and RGS [229], and the CMPZ algorithm is used to confirm our results. [230]

The basis sets and optimization procedure in the lead sulfide (PbS) system is explained in the **chapter 7** and in the zinc oxide (ZnO) system is explained in the **chapter 9**. We observe a close relation between the known polytypes of ZnS and calculated polytypes in the ZnO system (see **chapter 9**). Therefore, we perform this local optimizations in the ZnS system, using the basis set for Zn as in the **chapter 9**, and for S as in **chapter 7**.

The GeS, GeSe, SnS and SnSe systems were chosen for local optimizations, although in these systems only the 6-fold coordination has been experimentally observed so far [373], and with an increase of pressure or temperature, one would expect even higher (7-fold) coordination (TII type in the case of the SnS and SnSe system as experimentally observed [374] and calculated in the GeS system [375]). However, we observed the same coordination in the PbS system, where both global and local search is performed, and the 5-5 structure was obtained in the negative pressure region [56, 252], which also might be possible in these systems. In the GeSe system, we used "ECP10MDF\_VDZ" basis set for Ge [193, 376], where we removed the *f* shell and used two diffuse *sp* shell (exponents 0.50 and 0.15). The "ECP10MDF\_VDZ" [193, 377] basis set was used for Se, with diffuse *sp* shells of 0.45 and 0.14. The same germanium basis set was used in the GeS system, with removed *f* shell, with two diffuse *sp* shell (exponents 0.67 and 0.17), and the S basis set was used as in the **chapter 7**. In the case of the SnS system, we used "ECP28MDF" basis set [193, 284] for Sn, with *sp* exponents 0.74 and 0.15 plus one *f* shell of 0.4. The S basis set was used as in the **chapter 7**. In the SnSe system, we used the same basis set for Sn as in the SnS system (ECP28MDF), and for Se, the one from the GeSe system (ECP10MDF\_VDZ).

In the case of PbO, SnO and TlF, experimental data was the main criteria for further research. In all of these systems, structures with 4-fold coordination are most

## 11. STRUCTURE PREDICTION AS A GUIDE IN SYNTHESIS PLANNING: INVESTIGATION OF SYSTEMS EXHIBITING THE 5-5 STRUCTURE TYPE

---

stable modifications at standard conditions. [378–380] With changes of pressure or temperature, the PbO system would keep the 4-fold coordination [381], TlF would gain a 5-fold coordination [380] and SnO should reach a 6-fold coordination [382]. We then expected the 5-5 structure type, which is 5-fold coordinated, to appear at the same intermediary level between the 4-fold and the 6-fold coordination in the calculations, and to possibly obtain some high-pressure candidate, which is usually easier to achieve than modifications at negative effective pressures. In the PbO system, we used the basis set for Pb as in **chapter 7**, and the basis set for O as in **chapter 9**. Similarly, in the SnO system we used the Sn basis set as in the SnS system (ECP28MDF), and the basis set for O as in **chapter 9**. In the case of the TlF system, we used the "ECP60MWB" basis set for the Tl atom [193, 383], and a 7 – 311G basis set for the F atom [190, 384].

### 11.3 Results and Discussion

All combinations among the elements of the group V brought no candidates for further research. Combining all the elements of the groups IV and VI and all the elements of the groups III and VII, we have found several candidate systems according to different criteria. Experimental data of the system was one of our main criteria, since we performed only local optimizations, and most of the AB systems had not yet been explored. As a result TlF, SnO, SnS, SnSe, GeS, GeSe, PbO, PbS, ZnO and ZnS were chosen as candidate systems.

Our results show that in most of the chosen systems, the 5-5 structure type appears in the negative pressure region. The best candidate for synthesis of the 5-5 type in this region appears to be germanium selenide. In the GeSe system we performed local optimizations with LDA starting from two experimentally known structures (GeS type, showing space group  $Pnma$ , and NaCl type, showing space group  $Fm-3m$ ) and three so far unknown types in this system (TII type, showing space group  $Cmcm$ , wurtzite, showing space group  $P6_3mc$ , and 5-5 type, showing space group  $P6_3/mmc$ ). The calculations were performed also with the B3LYP functional, resulting in slight changes of the  $E(V)$  curves. However, the order of predicted minima did not change: the TII-type was the high pressure phase and the 5-5 structure type was a transition structure on the route to the wurtzite type in the low-density region.

System	Cell parameters	Stability
SnS	a = 4.80 Å, c = 5.69 Å	Stable
SnSe	a = 4.94 Å, c = 5.83 Å	Stable
SnO	a = 4.11 Å, c = 4.98 Å	Metastable
GeS	a = 4.52 Å, c = 5.35 Å	Metastable
GeSe	a = 4.61 Å, c = 5.58 Å	Stable
PbO	a = 4.21 Å, c = 5.17 Å	Metastable
PbS	a = 4.88 Å, c = 5.84 Å	Stable
TlF	a = 4.51 Å, c = 5.38 Å	Metastable
ZnO	a = 3.53 Å, c = 4.76 Å	Stable
ZnS	a = 4.11 Å, c = 5.42 Å	Metastable

**Table 11.1: Stability and cell parameters of the 5-5 structure in different systems calculated with the LDA functional** - Note that 5-5 structure type has a hexagonal lattice ( $P6_3/mmc$ , no. 194) with atom positions:  $A(\frac{1}{3}\frac{2}{3}\frac{3}{4})$ ;  $B(\frac{1}{3}\frac{2}{3}\frac{1}{4})$ .

This procedure was followed in the GeS, SnS, SnSe, TlF, SnO and PbO systems. The results were similar, with the exception that the 5-5 type modification was higher in energy. In the PbS system there is a small possibility of finding the 5-5 type, as it looks like a very small minimum on the way to the wurtzite modification in the negative pressure region. Concerning the ZnO system the threshold algorithm and prescribed path algorithm studies in chapter 10 showed that the 5-5 type is a minimum that should be accessible via solid state synthesis. Similarly, in the ZnS system the 5-5 structure type was found at high pressure, but only as a metastable modification (after the wurtzite to the NaCl transition, and not in-between like in the ZnO system).

The results of all the calculations, performed on *ab initio* level (with LDA), are presented in table 11.1, including cell parameters of the 5-5 structure in different systems and their thermodynamical stability. We note here that the systems where the 5-5 structure type exists as a stable phase are those with a small pressure window between the 6-fold and the 4-fold-coordinated modifications in the negative pressure region. In systems where the 5-5 type is metastable, the 5-5 type is usually much worse regarding its energy than the other candidates, which suggests that the synthesis is less likely in these systems.

Furthermore, the results are compared with earlier theoretical work involving the 5-5 structure type in earth alkaline metal oxides [152] and alkali metal halides [372]. We investigated the correlation between the ration of ionic radii ( $R$ ) [99, 100] and transition pressure ( $p$ ) (see figure 11.2) for the systems investigated.

## 11. STRUCTURE PREDICTION AS A GUIDE IN SYNTHESIS PLANNING: INVESTIGATION OF SYSTEMS EXHIBITING THE 5-5 STRUCTURE TYPE

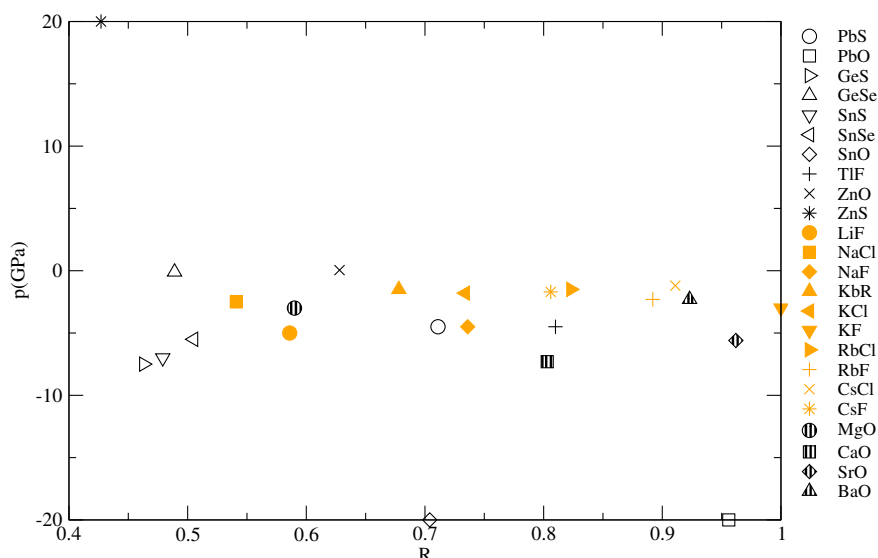


**Figure 11.2:** Correlation diagram for  $AB$  systems with the 5-5 structure type between the ratio of the ionic radii and the transition pressure - Note the extremes in the ZnS, SnO and PbO systems.

In this respect, we note that there are extremes, e.g. at pressures of about 20 GPa we observe the transition to the 5-5 structure in the ZnS system, which is not likely to happen.<sup>1</sup> Similarly, at extreme negative pressures of about -20 GPa, we have found the 5-5 modification in PbO and SnO, which is very far from other related systems and very hard to reach experimentally. Therefore, we excluded these three systems as unlikely for a synthesis of the 5-5 structure at this level of investigation. Within this investigation we find the ZnO and the GeSe systems to be the best candidates for synthesizing the 5-5 type structure in binary compounds, and as closest other possibilities the MgO and the NaCl system.

We performed a similar correlation investigation between the ratio of the ionic radii and the energy (see figure 11.3), which has been calculated as the difference between the minimum energy and the energy of the 5-5 structure in a specific system. In this investigation, the only system which should be discarded as being too high in energy, is SnO. ZnS shows a surprisingly good energy, and therefore, one could choose this system as a strong candidate for synthesis, but since this type would always be metastable, this would be very hard. We conclude that again the ZnO and the GeSe systems are

<sup>1</sup>In ZnS the transition appears at very high pressure, since the 5-5 type is metastable in this system, and this is just a hypothetical transition, since e.g. the sphalerite type transforms to the NaCl type already at lower pressures.



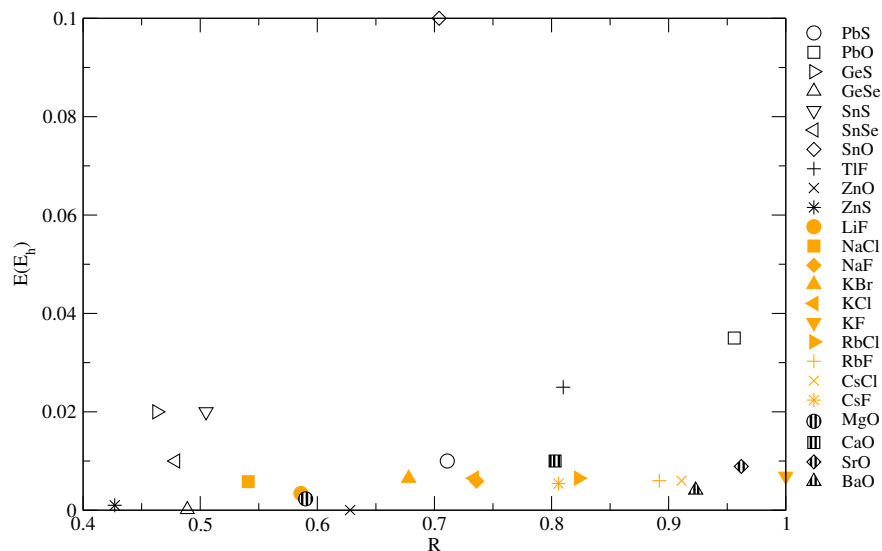


**Figure 11.3: Correlation diagram for  $AB$  systems with the 5-5 structure type between the ratio of the ionic radii and the energy** - Note that the energies are calculated as the difference between local minimum and 5-5 structure in the investigated system ( $E = E_{loc} - E_{5-5}$ ). Energies per formula unit are given in hartree ( $E_h$ ).

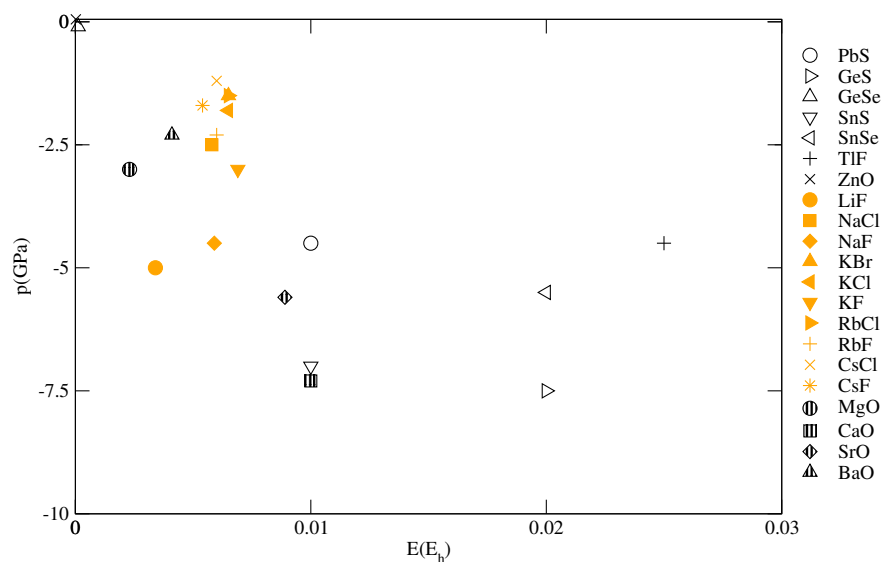


**Figure 11.4: Correlation diagram for the  $AB$  systems with the 5-5 structure type, using energies and transition pressures** - Note that the energies are calculated as the difference between the local minimum and the 5-5 structure in the investigated system ( $E = E_{loc} - E_{5-5}$ ). Energies per formula unit are given in hartree ( $E_h$ ).

## 11. STRUCTURE PREDICTION AS A GUIDE IN SYNTHESIS PLANNING: INVESTIGATION OF SYSTEMS EXHIBITING THE 5-5 STRUCTURE TYPE

---

even the energetically best candidates for synthesizing the 5-5 type, and as the closest alternatives, the MgO and the LiF system.

Finally, we investigate the correlation between the transition pressures and the energies in the specific system (see figure 11.4). In order to make such a correlation possible, we exclude the systems with extreme values (PbO, SnO and ZnS). From this correlation we can draw similar conclusions, i.e. that again the ZnO and the GeSe system are the best candidates for synthesizing the 5-5 type, while this time the closest alternatives (if we exclude the ionic ratio) would be the CsCl and the CsF system.

### 11.4 Conclusion

In order to find suitable  $AB$  compound for synthesis of the "5-5" structure type, we performed data exploration for binary compounds with elements from groups V, IV - VI, and III - VII. As a result TlF, SnO, SnS, SnSe, GeS, GeSe, PbO, PbS, ZnO and ZnS were chosen as candidate systems. Next, local optimizations on *ab initio* level with the LDA functional were performed. Furthermore, the results are compared with earlier theoretical work involving the 5-5 structure type in the earth alkaline metal oxides and the alkali metal halides. We suggest GeSe and ZnO as the most suitable systems for synthesizing the 5-5 structure type. In both cases, the possibility of synthesis of this 5-fold coordinated structure should exist in a small pressure range between the 6-fold coordinated NaCl and the 4-fold coordinated wurtzite structure type.

## Part V

# Summary



## 12

# Summary

*"Sapienti sat/A word to the wise is sufficient."*

(Plato (423-347 BC), Greek philosopher and mathematician) [93]

The search for new crystalline compounds is a central topic of theoretical chemistry and condensed matter physics. Scientists have successfully synthesized many new materials, with dimensions on the nanoscale to the atomic level, but the purely experimental approach is no longer the only route to discover new compounds. The theoretical prediction of new compounds and new (meta)stable crystalline modifications of already existing solids followed by their synthesis is fast becoming an alternative. Similarly, the properties of the materials are nowadays calculated with high precision and sometimes are the first or the only source of information about the compound. In this work, several systems were investigated using modern computational methods, which induced in many cases the development of new applications, methods and techniques, e.g. new modifications and applications of the prescribed path algorithm, phonon "supercell" technique in CRYSTAL09, new visualization techniques and scripts for structure analysis.

In the PbS system, which is known to be an important semiconductor, it would be of great interest to identify possible stable and metastable modifications, which might be possible to synthesize at standard and elevated pressures. To predict such structures, global optimizations on the energy landscape of lead sulfide were performed for various pressures, using simulated annealing followed by local optimization of the candidates found. In order to be able to take the effect of the non-bonding valence electrons of Pb into account, *ab initio* energies were employed. Besides the experimentally known

## 12. SUMMARY

---

modifications e.g. the NaCl (*B1*) structure type at standard pressure and the CsCl (*B2*) structure type at high pressure, we have found several additional promising structures. We have found the TII (*B33*) modification as a stable form at high pressures and the FeB (*B27*) modification as a metastable form at high pressures. In addition, we have found new structure candidates which have not yet been discussed theoretically or experimentally, in particular an additional modification exhibiting the  $\alpha$ -GeTe structure type, which might be stable at slightly negative pressures. Furthermore, we have investigated the electronic band structures of the most relevant structure types which appeared to be in good agreement with the experimental data.

Next, we have investigated the possible reasons for the existence of this metastable  $\alpha$ -GeTe modification, where the focus of the study was on whether the  $\alpha$ -GeTe type modification might be stabilized (and conversely the NaCl modification destabilized) by steric effects of the non-bonding electron pair. For this reason we have performed a detailed analysis of the electronic band structure of two competing modifications, which was followed by an investigation of their phonon spectra as a function of the volume. Finally, the results were compared with the BaS system, where a lone-pair effect was not expected. We have concluded that although the two excess electrons present in PbS were not directly observed as sterically active, their presence was felt in the reduction of the mechanical stability of the experimentally observed rock salt modification of PbS and in the existence of a competing  $\alpha$ -GeTe modification on the energy landscape of PbS. We suggest the possibility of accessing this new metastable modification in experiments that involve effective negative pressures, e.g. the low-temperature atom beam deposition method.

Similarly, we performed structure prediction in the zinc oxide system. We have performed global explorations of the energy landscape using simulated annealing with an empirical potential, both at standard and elevated pressure (up to 100 GPa), for different numbers of atoms (up to  $Z = 5$ ) and radius scale factor ( $R$ ), in order to identify possible new ZnO modifications, while the local optimizations were performed on *ab initio* level. We have found that different numbers of atoms in the simulation cell ( $Z$ ), and different radius scale factors ( $R$ ), can strongly influence the structure distribution on the energy landscape. Our calculations have found the experimentally observed structure types (wurtzite (*B4*), sphalerite (*B3*) and rock-salt (*B1*)). In addition, many new interesting modifications were calculated in different regions of the energy landscape. We have

---

found the GeP type as a high pressure candidate and the nickel arsenide ( $B8_1$ ) type as a metastable modification at standard conditions. At effective negative pressures we have observed the  $\beta$ -BeO-type, while with increase/decrease of pressure, we also find the so-called "5-5" type, which should be possible to be synthesized as a metastable phase. Finally, we observe stacking variants of the wurtzite and the sphalerite modifications, which also should be accessible to the experiment.

In addition, we explored the energy landscape of ZnO by using the threshold algorithm and prescribed path calculations. In the threshold algorithm runs, the number of atoms in the simulation cell ( $Z$ ) was varied from 1 Zn and 1 O atom to 6 Zn and 6 O atoms. All the relevant structures found after global and local optimization, were used as the starting points of the TA runs and the calculations were performed for large numbers of energy lids. Again, we observe that the energy landscape is highly influenced by the number of formula units. We note that this influence has strong effects on the structure distribution, but also on the size of the structures, producing new variants inside the same structure type. Next, prescribed path calculations were performed using different procedures, which explored the prescribed path between the most relevant minima (the wurtzite, the sphalerite, and the NaCl type of structure) in different ways. Our calculation showed that a stable form of ZnO at ambient conditions is the wurtzite ( $B4$ ) modification. Within a prescribed path between the wurtzite and the rock salt ( $B1$ ) structure, no barriers are observed at 0K if high pressure is used, which is in agreement with experimental results.

With calculations performed at low temperatures, small barriers are observed, which can possibly be bypassed via intermediate structures of the GeP type. With a further increase of temperature, the barriers become very high and a synthesis becomes highly unlikely. Similarly, if the wurtzite ( $B4$ ) and the sphalerite ( $B3$ ) structure are connected, small barriers are observed already at 0 K. However, it could be possible to follow the low-temperature phase transition to the 5-5 structure type. There are some indications that this could be possible even at higher temperatures, which is in agreement with recent experimental observation. In the case of the prescribed path between the sphalerite and the rock salt type, we observe extremely high barriers, regardless of any temperature employed, so we conclude that a direct transformation in bulk from the sphalerite to the NaCl modification is highly unlikely. Each calculation was separately analyzed according to their energies, crystallographic and structural aspects. Finally,

## 12. SUMMARY

---

for each relevant structure, its thermal stability was separately analyzed. The results of the prescribed path runs are in satisfying agreement with experimental information about the stability and synthesis conditions of the various ZnO modifications.

Furthermore, we used newly developed methods for the energy landscape representation. Energy landscapes are used to understand the behaviour of a chemical system, but problems exist with the visualization of high-dimensional spaces and the complexity of the structures. Therefore, finding low-dimensional representations of the energy landscape in order to analyze specific properties would be a significant step. Here, we present multidimensional representations of the energy landscapes of PbS and ZnO with various approximations.

Finally, we performed a model study of several binary systems combining data exploring and *ab initio* methods. In order to find suitable  $AB$  compound for the synthesis of the "5-5" structure type, we performed data exploring for binary compounds with elements from groups V, IV - VI, and III - VII. As a result TlF, SnO, SnS, SnSe, GeS, GeSe, PbO, PbS, ZnO and ZnS were chosen as a candidate systems. Next, local optimizations on *ab initio* level with LDA functional were performed. Furthermore, the results were compared with earlier theoretical work involving the 5-5 structure type in the earth alkaline metal oxides and the alkali metal halides. We suggest GeSe and ZnO as the most suitable systems for synthesizing the 5-5 structure type. In both cases, there should exist a possibility to synthesize this 5-fold coordinated structure in a small pressure range between the 6-fold coordinated NaCl and the 4-fold coordinated wurtzite structure type.



Part VI

Appendix



# 13

## Appendix A: Software available in the research group

### 13.1 Computational software

#### 13.1.1 G-42 program

The **G-42** program is an internally used program written by J. C. Schön. This computer program consists of a number of modules which can be used to explore the energy landscape of a chemical system of interest (molecule/cluster or periodic compound). Three basic exploration methods are used in the **G-42** program: stochastic walkers, gradient descent and prescribed path. The energy landscape of the system is defined via three features: the state space (e.g. atom positions plus the cell parameters), the moveclass (i.e. the neighborhood of the state space), and the energy function. [16, 17]

The available modules in the **G-42** program are: single energy calculation, simulated annealing, stochastic quench, threshold algorithm, shadow (or local) run, thermal cycling (or multi-quench), prescribed path, gradient decent, line search, POWELL, simplex, and findcell.

#### 13.1.2 CRYSTAL-program

The **CRYSTAL** program is used to compute the electronic structure of periodic systems within Hartree Fock (HF), density functional theory (DFT) or various hybrid approximations (e.g. B3LYP). The Bloch functions of the periodic systems are expanded as linear combinations of atom centred Gaussian functions (LCAO). Powerful screening

## 13. APPENDIX A: SOFTWARE AVAILABLE IN THE RESEARCH GROUP

---

techniques are used to exploit real space locality. The code may be used to perform consistent studies of the physical, electronic and magnetic structure of molecules, polymers, surfaces and crystalline solids.

**CRYSTAL** is one of the most popular general-purpose programs for the study of crystalline solids, and the first which has been distributed publicly. The first public version was released in 1988, and then the next versions have followed: **CRYSTAL92**, **95**, **98**, **03**, **06**. The currently released version is **CRYSTAL09**.

The **CRYSTAL** program is jointly developed by the Theoretical Chemistry Group (R. Dovesi, C. Roetti, R. Orlando, B. Civalleri ) at the University of Torino and the Computational Materials Science Group (V.R. Saunders, N.M. Harrison, I.J. Bush), in CLRC, with important contributions from researchers visiting the two laboratories (C.M. Zicovich-Wilson, K. Doll, Ph. D'Arco, M. Llunell). [191, 192, 385]. For more details, see the following link: (<http://www.crystal.unito.it/>)

### 13.1.3 VASP program

The Vienna *Ab initio* Simulation Package (**VASP**) is a computer code used in materials modelling, e.g. electronic structure calculations and quantum-mechanical molecular dynamics, from first principles. In **VASP**, central quantities, like the one-electron orbitals, the electronic charge density, and the local potential are expressed in plane wave (PW) basis sets. The interactions between the electrons and ions are described using norm-conserving or ultrasoft pseudopotentials, or the projector-augmented-wave method (PAW).

To determine the electronic groundstate, **VASP** makes use of efficient iterative matrix diagonalisation techniques, like the residual minimisation method with direct inversion of the iterative subspace (RMM-DIIS) or blocked Davidson algorithms. These are coupled to highly efficient Broyden and Pulay density mixing schemes to speed up the self-consistency cycle. For more details, see the following link: (<http://www.vasp.at/>)

### 13.1.4 GULP program

**GULP** is a program used for material simulation using boundary conditions of 0-D (molecules and clusters), 1-D (polymers), 2-D (surfaces, slabs and grain boundaries), or 3-D (periodic solids). The focus of the program is on analytical solutions, through the use of lattice dynamics, rather than on molecular dynamics (MD). A variety of force

fields can be used within **GULP** program, e.g. the shell model for ionic materials, molecular mechanics for organic systems, the embedded atom model for metals and the reactive REBO potential for hydrocarbons. Analytic derivatives are included up to at least second order for most force fields, and to third order for many. [205–207] For more details, see the following link: (<http://projects.ivec.org/gulp/>)

## 13.2 Visualizational software

### 13.2.1 KPLOT program

The program **KPLOT**, written by Rudolf Hundt (Institute for Inorganic Chemistry, University of Bonn, Germany), is designed to draw, construct, and analyze crystal structures. Starting from the first version in 1979 the software has been continuously improved and updated. It provides different possibilities of crystal structure models, tools for the comparison of two crystal structures, plotting of ball-and-stick models, thermal ellipsoids and coordination polyhedra, symmetry analysis and transformation, space group determination, calculation of interatomic distances, angles and torsion angles, and interfaces to other programs (e.g. SHELX, ORTEP, SCHAKAL, MISSYM, LAZY PULVERIX). [227, 386]

The **KPLOT** program is available free of charge and can be downloaded from the links below. (<http://www.crystalimpact.com/download/kplot.htm>.)

### 13.2.2 VESTA program

The **VESTA** program is a 3D visualization program for structural models, volumetric data such as electron/nuclear densities, and crystal morphologies. The **VESTA** program can visualize multiple structural models, unlimited number of objects such as atoms, bonds polyhedra, and polygons on isosurfaces. It provides high quality smooth rendering of isosurfaces and sections and can export high-resolution graphic images exceeding video card limitation. The **VESTA** program runs on Windows, Mac OS X, and Linux. It is contributed free of charge for non-commercial users. [317]

For more details, see the following link: (<http://jp-minerals.org/vesta/en/>)

## 13. APPENDIX A: SOFTWARE AVAILABLE IN THE RESEARCH GROUP

---

### 13.2.3 MATLAB program

The **MATLAB** program is a programming environment for algorithm development, data analysis, visualization, and numerical computation. Using **MATLAB** you can solve technical computing problems faster than with traditional programming languages. **MATLAB** has a wide range of applications, including signal and image processing, communications, control design, test and measurement, financial modeling and analysis, and computational biology. For a million engineers and scientists in industry and academia, **MATLAB** is the language of technical computing, and for more details follow the link: (<http://www.mathworks.com/products/matlab/>).

### 13.2.4 J-ICE program

The **J-ICE** program is a **Jmol** Interface for visualization of Crystallographic and Electronic Properties. Since **J-ICE** fully relies on Jmol and consequently Java, the user must have installed, on his operative system, the Java Virtual Machine (JVM). **J-ICE** is distributed under the General Public License [GNU]. [318] For more details follow the link: (<http://j-ice.sourceforge.net/index.html>).

### 13.2.5 XCrySDen program

**XCrySDen**, developed by Anton Kokalj, is a crystalline and molecular structure visualization program aiming at display of isosurfaces and contours, which can be superimposed on crystalline structures and interactively rotated and manipulated. It can run on most **UNIX/Linux** platforms, without any special hardware requirements, and can import a variety of files for further analysis (e.g. from **CRYSTAL**).

**XCrySDen** has also been ported to **MAC OSX** (requires **X11**) and **Windows** (requires **CYGWIN**). The name of the program stands for Crystalline Structures and Densities and X because it runs under the X-Window environment. [387] For more details please follow the link: (<http://www.xcrysden.org/>)

### 13.2.6 XMGRACE program

The **Xmgrace** program is free software under the terms of the GNU General Public License maintained by Evgeny Stambulchik. **Xmgrace** is a WYSIWYG 2D plotting tool for the X Window System and M\*tif, and practically runs on any version of Unix

## 13.2 Visualizational software

---

OS, as well, on VMS, OS/2, and Win9\*/NT/2000/XP. The **Xmgrace** program can export vector graphics, possesses great graphing and analysis flexibility, possibilities of curve fitting and of programming. For more details, please follow the link:  
(<http://plasma-gate.weizmann.ac.il/Grace/>)

## 13. APPENDIX A: SOFTWARE AVAILABLE IN THE RESEARCH GROUP

---



## Appendix B: Structure prediction for PbS at various pressures on *ab initio* level

In table I, the basis sets employed during the global search are displayed. In table II, the basis sets used in the final local optimization and for the calculation of the  $E(V)$  curves are given. In table III, the results of a basis set optimization for Pb are presented. For this purpose, the total energy of the NaCl structure at a lattice constant of 5.936 Å was computed, at the level of the generalized gradient correction, with the gradient corrected PBE (Perdew, Burke, Ernzerhof) functional [388].<sup>1</sup> The lowest energy is obtained with a *sp* shell with exponent 0.11. However, such a small exponent can easily lead to numerical instabilities. [191, 192] Indeed, the smaller the exponent, the earlier linear dependence sets in (and therefore the smaller the maximum pressure which can be applied). This may be resolved by applying very high integral selection thresholds. [191, 192] However, this makes the calculations computationally expensive, especially for structures with a low number of symmetry operators. Therefore, we have chosen a slightly larger exponent (0.17), in order to be able to compute the total energy of the various structures also at high pressure.

---

<sup>1</sup>An optimization on the LDA level gives similar results, but here PBE is employed, in order to compare with recent calculations as in ref [270].

## 14. APPENDIX B: STRUCTURE PREDICTION FOR PBS AT VARIOUS PRESSURES ON *AB INITIO* LEVEL

---

S -Pseudopotential ECP10MWB				Pb-Pseudopotential ECP78MWB			
Type	exponent	contraction coefficient		Type	exponent	contraction coefficient	
s	6.833518	-0.043875		s	1.3051750	1.0104020	
	2.077738	0.319894			1.1352820	-1.4023550	
	0.419121	-0.661233			0.2027710	0.7933720	
p	1.817139		-0.079227	p	1.4416840		0.1456260
	0.855070		0.263671		0.9771430		-0.3198630
	0.312053		0.580682				
sp	0.15	1.0(s)	1.0(p)	sp	0.15	1.0(s)	1.0(p)

TABLE I. A local Gaussian basis set was used in the global search, with a large core pseudopotential for Pb and for S, with a  $[2s2p]$  basis set. For an explanation of the acronyms of the effective core potentials (ECP), see the corresponding publications.

Pb $-sp$ exponent	Energy ( $E_h$ ) at lattice constant of 5.936 Å	Band gap (eV) at lattice constant of 5.936 Å	Equilibrium lattice constant (Å)	Bulk modulus (GPA)
0.07	-591.050046	0.41	6.01	56
0.08	-591.051899	0.40	6.01	56
0.09	-591.055282	0.41	6.01	56
0.10	-591.055400	0.42	6.01	56
0.11	-591.055758	0.42	6.01	56
0.12	-591.055604	0.46	6.02	56
0.15	-591.054814	0.65	6.02	56
0.17	-591.053842	0.78	6.00	57

TABLE III. Variation of the outermost diffuse Pb  $sp$  exponent of the basis set in table II, on the level of PBE, in order to calculate the effect of the basis set. The total energy and the gap refer to the experimental value of the lattice constant (5.936 Å).

S-all electron basis set				Pb-Pseudopotential ECP60MWB			
Type	exponent	contraction coefficient		Type	exponent	contraction coefficient	
s	109211.0	0.0002520		s	570.503390	0.000311	
	16235.206	0.0019934			38.320736	0.017429	
	3573.0286	0.0111177			28.178721	-0.002239	
	943.23811	0.0498945			20.873127	-0.284421	
	287.26179	0.1661455			15.364793	0.598047	
	99.914226	0.3627018			6.355062	-0.973219	
	38.602137	0.4108787			1.717877	0.914096	
	15.531224	0.1457875			0.865573	0.483431	
sp	281.22171	-0.0057780	0.0081427	s	570.503390	-0.000134	
	67.106575	-0.0665855	0.0565570		38.320736	-0.016619	
	21.794135	-0.1203552	0.2039582		28.178721	0.047065	
	8.2097646	0.2741310	0.3973328		20.873127	0.030029	
	3.4178289	0.6463829	0.3946313		15.364793	-0.184019	
	1.5452225	0.2925792	0.1544345		6.355062	0.414229	
					1.717877	-0.567254	
			0.865573	-0.386722			
sp	4.3752432	-0.1750000	-0.0613439	sp	0.37	1.0(s)	1.0(p)
	1.8096201	-0.5938952	0.1272251				
	0.6833985	0.8298996	1.2215893				
sp	0.2413	1.0(s)	1.0(p)	sp	0.17	1.0(s)	1.0(p)
sp	0.106	1.0(s)	1.0(p)	p	207.765387		0.000085
					27.782277		0.012232
					20.389950		-0.074032
					15.103619		0.148020
					6.719426		-0.357073
					2.241566		0.424306
					1.293078		0.484544
					0.725623		0.249634
d	0.383		1.0(d)	p	207.765387		-0.000038
					27.782277		-0.001336
					20.389950		0.013469
					15.103619		-0.034499
					6.719426		0.103362
					2.241566		-0.156889
					1.293078		-0.162116
					0.725623		-0.119988
				d	142.026523		0.000065
					42.053989		0.000450
					10.345556		0.035334
					7.663305		-0.090005
					2.183094		0.322991
					1.061022		0.465670
				d	0.486787		1.0(d)
				d	0.201584		1.0(d)
				f	0.3		1.0(f)

TABLE II. A small-core pseudopotential together with a  $[4s4p3d1f]$  basis set was used for Pb and a  $[5s4p1d]$  basis set for S in the local optimization, respectively.

## 14. APPENDIX B: STRUCTURE PREDICTION FOR PBS AT VARIOUS PRESSURES ON *AB INITIO* LEVEL

---

In table III, we also display results for the total energy, the equilibrium lattice constant, the bulk modulus, and the computed gap at 5.936 Å.<sup>1</sup> The following results are obtained: the optimal Pb *sp* exponent (0.11) gives an energy which is 2 millihartree (0.05 eV) lower than the one for the exponent 0.17 employed in the present calculations. The equilibrium lattice constant and the bulk modulus hardly change when varying the exponent, and are in good agreement with the literature. [270] The largest change is observed for the computed band gap ( $E_{gap} = 0.78$  eV, for an exponent of 0.17, and  $E_{gap} = 0.42$  eV for an exponent of 0.11, respectively). The latter value is in good agreement with the recently computed at the PBE level ( $E_{gap} = 0.37$  eV) [270] using a plane wave pseudopotential code and independently an APW code. Therefore, we conclude that the main error caused by a larger exponent appears when calculating the band gap. However, the total energy and bulk modulus are barely affected. Nevertheless, by carefully optimizing the exponents with respect to the energy, a good value of the gap is obtained. Finally, it should be noted that the diffuse Pb *sp* exponent is mainly responsible for the value of the gap. When re-optimizing or varying the other exponents (such as the Pb *d*, *f*, or the S *sp*, *d* exponents), the value of the gap virtually does not change.

---

<sup>1</sup>In order to be able to compare with recent calculations in the literature (e.g. ref [270]), a direct comparison is best feasible with the results labeled as FP-APW+LO PBE and PAW PBE in reference [270], as this is a similar level of theory, i.e. without spin-orbit coupling similar to the present calculations.

## Appendix C: Investigation of kinetic stability, electronic and vibrational properties of PbS and BaS as a function of pressure

The LO-TO splitting was computed employing the dielectric constant. The dielectric constant was computed with the CPKS technique, and obtained as in Table CI. The Born effective charge was obtained as in the Table CII and it is in reasonable agreement with previous calculations. The references in the tables corresponds to the references in the text in the following order:

[a] - [389, 390]; [b] - [390, 391]; [c] - [324];  
[d] - [287]; [e] - [392]; [f] - [324]; [g] - [287].

## 15. APPENDIX C: INVESTIGATION OF KINETIC STABILITY, ELECTRONIC AND VIBRATIONAL PROPERTIES OF PBS AND BAS AS A FUNCTION OF PRESSURE

Method		NaCl-type				$\alpha$ -GeTe-type			
		Equilibrium V		Expanded V		Equilibrium V		Expanded V	
		a (Å)	$\epsilon$	a (Å)	$\epsilon$	a (Å)	$\epsilon$	a (Å)	$\epsilon$
LDA	xx	5.86	18.66	6.24	12.51	4.13	19.02	4.56	9.69
	zz	-	-	-	-	4.13	18.97	4.56	8.46
B3LYP	xx	6.08	10.24	6.13	10.00	4.35	9.50	4.45	8.99
	zz	-	-	-	-	4.35	9.12	4.45	8.59
HF	xx	6.18	6.50	6.28	6.19	4.59	5.87	4.69	5.53
	zz	-	-	-	-	4.59	5.99	4.69	5.62
Experiment		5.93 <sup>[a]</sup>	18.4 <sup>[b]</sup>	-	-	-	-	-	-
Theory		5.81 <sup>[c]</sup> 7.12 <sup>[d]</sup>	19.6 <sup>[c]</sup> 16.42 <sup>[d]</sup>	-	-	-	-	-	-

Table CI. Dielectric constant ( $\epsilon$ ) calculated with Hartree-Fock (HF) and DFT methods at equilibrium and expanded lattice constants. Components labeled with xx are threefold degenerate in the case of the NaCl structure, and twofold degenerate in the case of the  $\alpha$ -GeTe structure. The component zz is thus not degenerate. Results are compared with experiment and previous calculations. The experimental dielectric constant  $\epsilon$  at equilibrium is derived at 77K.<sup>[a]</sup>

Method		NaCl-type				$\alpha$ -GeTe-type			
		Equilibrium V		Expanded V		Equilibrium V		Expanded V	
		a (Å)	Z(e)	a (Å)	Z(e)	a (Å)	Z(e)	a (Å)	Z(e)
LDA	xx	5.86	4.44	6.24	4.35	4.13	4.44	4.56	3.55
	zz	-	-	-	-	4.13	4.44	4.56	2.50
B3LYP	xx	6.08	4.37	6.13	4.36	4.35	4.12	4.45	4.08
	zz	-	-	-	-	4.35	3.77	4.45	3.73
HF	xx	6.18	4.21	6.28	4.14	4.59	3.81	4.69	3.72
	zz	-	-	-	-	4.59	3.93	4.69	3.83
Experiment		5.93 <sup>[e]</sup>	4.40 <sup>[e]</sup>	-	-	-	-	-	-
Theory		5.81 <sup>[f]</sup> 7.12 <sup>[g]</sup>	4.5 <sup>[f]</sup> 4.48 <sup>[g]</sup>	-	-	-	-	-	-

Table CII. The Pb effective charge (S: identical, with opposite sign) was obtained as in the Supporting Table 1. Components labeled with xx are threefold degenerate in the case of the NaCl structure, and twofold degenerate in the case of the  $\alpha$ -GeTe structure. The component zz is thus not degenerate. Results are compared with experiment and previous calculations. The experimental Born effective charges Z(e) are derived from the experimentally measured LO/TO splittings.<sup>[g]</sup>

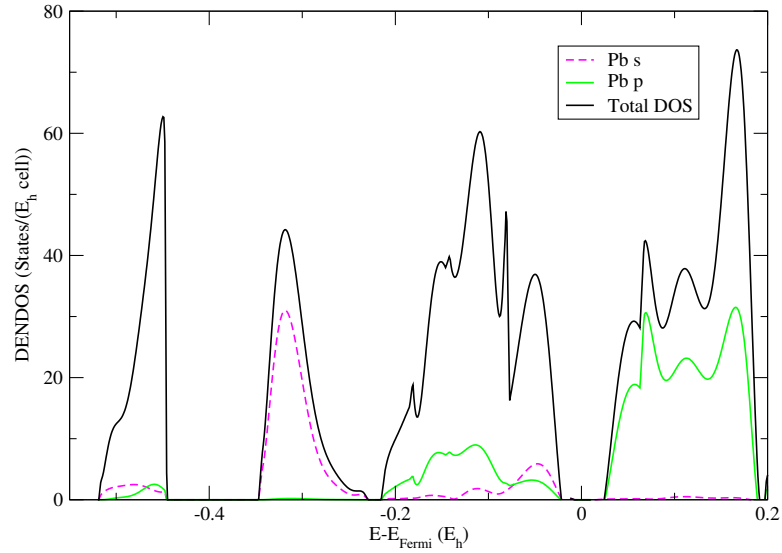


Figure 15.1: Projected density of states (DOS) performed using the LDA functional in the NaCl type of structure at equilibrium volume ( $V = 50.30 \text{ \AA}^3$ ,  $a = 5.86 \text{ \AA}$ ) - Density of states are projected on Pb  $s$ - and Pb  $p$ -orbitals.

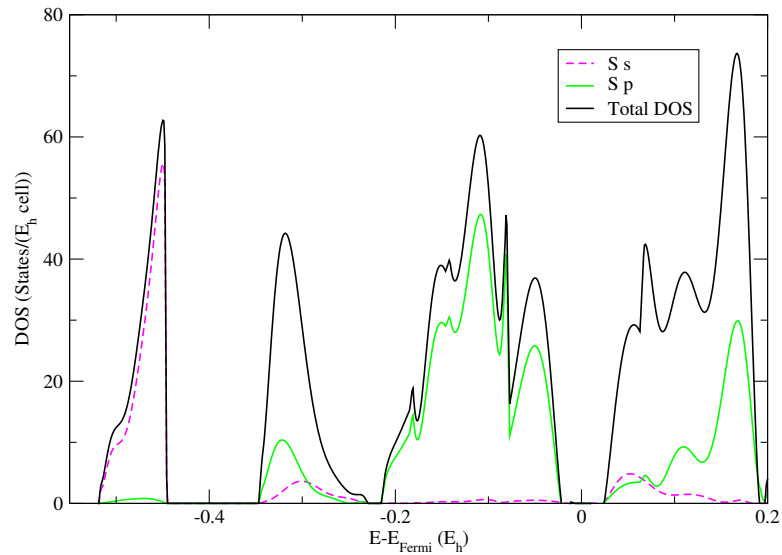
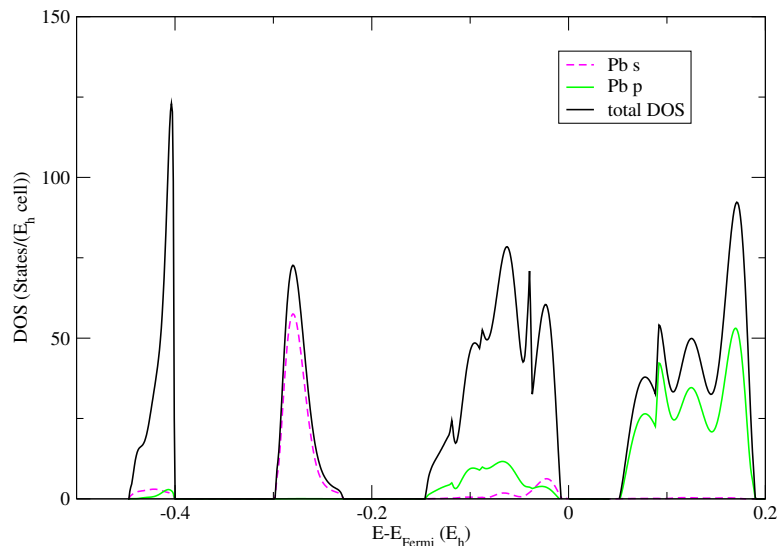


Figure 15.2: Projected density of states (DOS) performed using the LDA functional in the NaCl type of structure at equilibrium volume ( $V = 50.30 \text{ \AA}^3$ ,  $a = 5.86 \text{ \AA}$ ) - Density of states are projected on S  $s$ - and S  $p$ -orbitals.

## 15. APPENDIX C: INVESTIGATION OF KINETIC STABILITY, ELECTRONIC AND VIBRATIONAL PROPERTIES OF PBS AND BAS AS A FUNCTION OF PRESSURE

---



**Figure 15.3:** Projected density of states (DOS) performed using the LDA functional in the NaCl type of structure at expanded volume ( $V = 61.48 \text{ \AA}^3$ ,  $a = 6.24 \text{ \AA}$ ), which corresponds to the pressure greater than 10GPa. - Density of states are projected on Pb  $s$ - and Pb  $p$ -orbitals.

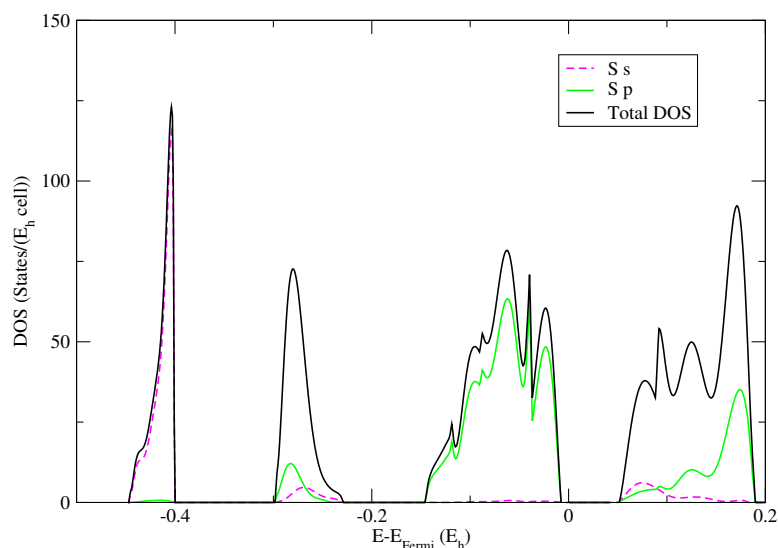


**Figure 15.4:** Projected density of states (DOS) performed using the LDA functional in the NaCl type of structure at expanded volume ( $V = 61.48 \text{ \AA}^3$ ,  $a = 6.24 \text{ \AA}$ ), which corresponds to the pressure greater than 10GPa. - Density of states are projected on S  $s$ - and S  $p$ -orbitals.



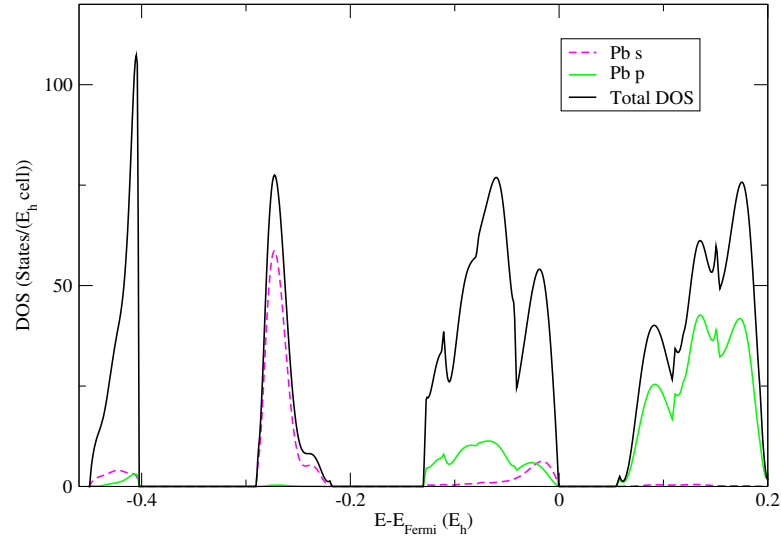


**Figure 15.5: Projected density of states (DOS) performed using the LDA functional in the  $\alpha$ -GeTe type of structure at expanded volume ( $V = 61.48 \text{ \AA}^3$ ,  $a=4.56 \text{ \AA}$ ,  $\alpha = 56.32^\circ$ ), which corresponds to the pressure greater than 10GPa. - Density of states are projected on Pb  $s$ - and Pb  $p$ -orbitals.**

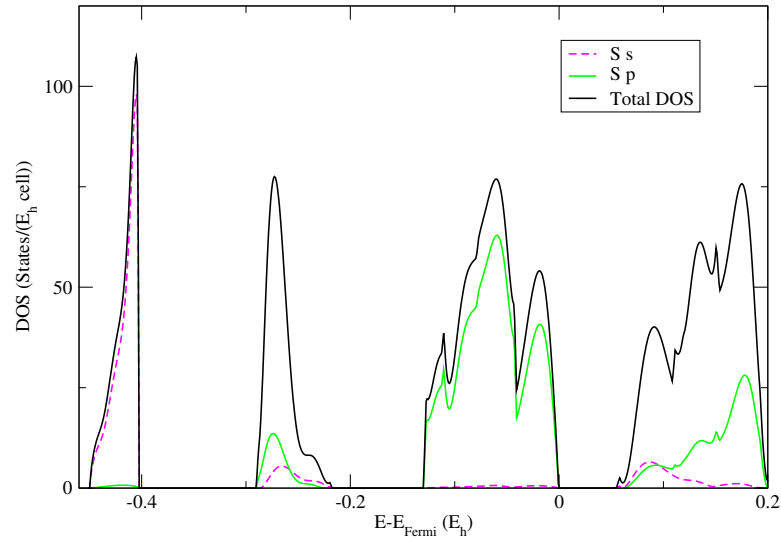


**Figure 15.6: Projected density of states (DOS) performed using the LDA functional in the  $\alpha$ -GeTe type of structure at expanded volume ( $V = 61.48 \text{ \AA}^3$ ,  $a=4.56 \text{ \AA}$ ,  $\alpha = 56.32^\circ$ ), which corresponds to the pressure greater than 10GPa. - Density of states are projected on S  $s$ - and S  $p$ -orbitals.**

**15. APPENDIX C: INVESTIGATION OF KINETIC STABILITY,  
ELECTRONIC AND VIBRATIONAL PROPERTIES OF PBS AND BAS  
AS A FUNCTION OF PRESSURE**

---

## Appendix D: Energy landscape investigation in ZnO

### 16.1 The threshold algorithm calculations

In this part we show the threshold algorithm calculations for  $Z = 2$  and  $Z = 4$  formula units per simulation cell (tables DI and DII), where we used all relevant structures as starting point: the wurtzite, the sphalerite, the rock salt, the nickel arsenide, the  $\beta$ -BeO and the 5-5 structure. In the case of the TA calculations for  $Z = 3$ , due to the restriction of the number of atom per simulation cell, only sphalerite and the NaCl structure were chosen as starting points. In this restricted energy landscape, we observed the sphalerite structure as most dominant, as well as polytypes exhibiting space group  $Cm$  (no. 8) and  $R3m$  (no. 160).

## 16. APPENDIX D: ENERGY LANDSCAPE INVESTIGATION IN ZNO

Lid (eV)	Structure candidate				
	NaCl	Sphalerite	5-5	Wurtzite	NiAs
-6.6	-	>Wurtzite,%Sphalerite	>Wurtzite,%Sphalerite	>Wurtzite,%Sphalerite	-
-6.5	-	>Wurtzite,%Sphalerite	>Wurtzite,%Sphalerite	>Wurtzite,%Sphalerite	-
-6.4	-	>Wurtzite,%Sphalerite	>Wurtzite,%Sphalerite	>Wurtzite,%Sphalerite	-
-6.3	>Sphalerite,%Wurtzite	>Wurtzite,%Sphalerite	>Wurtzite,%Sphalerite	>Wurtzite,%Sphalerite	-
-6.2	>Sphalerite,%Wurtzite	>Wurtzite,%Sphalerite	>Wurtzite,%Sphalerite	>Wurtzite,%Sphalerite	-
-6.1	>Sphalerite,%Wurtzite	Wurtzite =Sphalerite	Wurtzite =Sphalerite	Wurtzite =Sphalerite	-
-6.0	>Sphalerite,%Wurtzite	Wurtzite =Sphalerite	Wurtzite =Sphalerite	Wurtzite =Sphalerite	-
-5.9	>Sphalerite,%Wurtzite	Wurtzite =Sphalerite	Wurtzite =Sphalerite	Wurtzite =Sphalerite	-
-5.8	>Sphalerite,%Wurtzite	Wurtzite =Sphalerite	Wurtzite =Sphalerite	Wurtzite =Sphalerite	-
-5.7	>Sphalerite,%Wurtzite	Wurtzite =Sphalerite	Wurtzite =Sphalerite	Wurtzite =Sphalerite	-
-5.6	>Sphalerite,%Wurtzite	>Sphalerite,%Wurtzite, %SG9(BeO)	>Sphalerite,%Wurtzite	>Sphalerite,%Wurtzite	-
-5.5	>Sphalerite,%Wurtzite	>Sphalerite,%Wurtzite, %SG9(BeO)	>Sphalerite,%Wurtzite	>Sphalerite,%Wurtzite	-
-5.4	>Sphalerite,%Wurtzite	>Sphalerite,%Wurtzite, %SG9(BeO)	>Sphalerite,%Wurtzite	>Sphalerite,%Wurtzite	-
-5.3	>Sphalerite,%Wurtzite	>Sphalerite,%Wurtzite, %SG9(BeO)	>Sphalerite,%Wurtzite	>Sphalerite,%Wurtzite	>Sphalerite,%Wurtzite
-5.2	>Sphalerite,%Wurtzite	>Sphalerite,%Wurtzite, %SG9(BeO)	>Sphalerite,%Wurtzite	>Sphalerite,%Wurtzite	>Sphalerite,%Wurtzite
-5.1	>Sphalerite,%Wurtzite	>Sphalerite,%Wurtzite	>Sphalerite,%Wurtzite	>Sphalerite,%Wurtzite	>Sphalerite,%Wurtzite
-5.0	>Sphalerite,%Wurtzite	>Sphalerite,%Wurtzite	>Sphalerite,%Wurtzite	>Sphalerite,%Wurtzite	>Sphalerite,%Wurtzite
-4.9	>Sphalerite,%Wurtzite	>Sphalerite,%Wurtzite	>Sphalerite,%Wurtzite	>Sphalerite,%Wurtzite	>Sphalerite,%Wurtzite
-4.8	>Sphalerite,%Wurtzite	>Sphalerite,%Wurtzite	>Sphalerite,%Wurtzite	>Sphalerite,%Wurtzite	>Sphalerite,%Wurtzite
-4.7	>Sphalerite,%Wurtzite	>Sphalerite,%Wurtzite	>Sphalerite,%Wurtzite	>Sphalerite,%Wurtzite	>Sphalerite,%Wurtzite
-4.6	>Sphalerite,%Wurtzite	>Sphalerite,%Wurtzite	>Sphalerite,%Wurtzite	>Sphalerite,%Wurtzite	>Sphalerite,%Wurtzite
-4.5	>Sphalerite,%Wurtzite	>Sphalerite,%Wurtzite	>Sphalerite,%Wurtzite	>Sphalerite,%Wurtzite	>Sphalerite,%Wurtzite
-4.4	>Sphalerite,%Wurtzite	>Sphalerite,%Wurtzite	>Sphalerite,%Wurtzite	>Sphalerite,%Wurtzite	>Sphalerite,%Wurtzite
-4.3	>Sphalerite,%Wurtzite	>Sphalerite,%Wurtzite	>Sphalerite,%Wurtzite	>Sphalerite,%Wurtzite	>Sphalerite,%Wurtzite
-4.2	>Sphalerite,%Wurtzite, %SG119(Wur.)	>Sphalerite,%Wurtzite	>Sphalerite,%Wurtzite	>Sphalerite,%Wurtzite	>Sphalerite,%Wurtzite, %SG119(Wur.)
-4.1	>Sphalerite,%Wurtzite, %SG119(Wur.)	>Sphalerite,%Wurtzite	>Sphalerite,%Wurtzite	>Sphalerite,%Wurtzite	>Sphalerite,%Wurtzite, %SG119(Wur.)
-4.0	>Sphalerite,%Wurtzite, %SG119(Wur.)	>Sphalerite,%Wurtzite	>Sphalerite,%Wurtzite	>Sphalerite,%Wurtzite	>Sphalerite,%Wurtzite, %SG119(Wur.)
-3.9	>Sphalerite,%Wurtzite, %SG119(Wur.)	>Sphalerite,%Wurtzite	>Sphalerite,%Wurtzite	>Sphalerite,%Wurtzite	>Sphalerite,%Wurtzite, %SG119(Wur.)

Table D1: Structural analysis of the energy landscape of ZnO with Z = 2 and all relevant structures as a starting point of the TA calculations. Note that different starting structure can have different starting lid (e.g. for NaCl structure the lowest energy calculated is below -6.3 eV, while for the wurtzite or sphalerite structure, the energy lid was set to 6.6 eV, since there are lower in energy compared to NaCl at equilibrium). The special sign (>) is used for the structure most frequently found, and (%) sign mark the significant percentage of the structure/space group found during this search.

## 16.1 The threshold algorithm calculations

Lid (eV)	Structure candidate				
	NaCl	Sphalerite	5-5	BeO	NiAs
-6.6	-	sphalerite	BeO	BeO	-
-6.5	-	sphalerite	BeO	BeO	-
-6.4	-	sphalerite	BeO	BeO	-
-6.3	>Sphalerite,%NaCl	sphalerite	BeO	BeO	-
-6.2	>Sphalerite,%NaCl	sphalerite	BeO	BeO	-
-6.1	>Sphalerite,%NaCl	Wurtzite =Sphalerite	Wurtzite	Wurtzite	-
-6.0	>Sphalerite,%NaCl	Wurtzite =Sphalerite	Wurtzite	Wurtzite	-
-5.9	>Sphalerite,%NaCl	Wurtzite =Sphalerite	Wurtzite	Wurtzite	-
-5.8	>Wurtzite, %Sphaler.,%BeO	Wurtzite =Sphalerite	Wurtzite	Wurtzite	-
-5.7	>Wurtzite, %Sphaler.,%BeO	Wurtzite =Sphalerite	Wurtzite	Wurtzite	-
-5.6	>Wurtzite, %Sphaler.,%BeO	Wurtzite =Sphalerite	Wurtzite =Sphalerite	Wurtzite =Sphalerite	-
-5.5	>Wurtzite, %Sphaler.,%BeO	Wurtzite =Sphalerite	Wurtzite =Sphalerite	Wurtzite =Sphalerite	-
-5.4	>Wurtzite, %Sphaler.,%BeO	Wurtzite =Sphalerite	Wurtzite =Sphalerite	Wurtzite =Sphalerite	-
-5.3	Wurtzite =Sphalerite	Wurtzite =Sphalerite	Wurtzite =Sphalerite	Wurtzite =Sphalerite	>Sphalerite,%Wurtzite,
-5.2	Wurtzite =Sphalerite	Wurtzite =Sphalerite	Wurtzite =Sphalerite	Wurtzite =Sphalerite	>Sphalerite,%Wurtzite,
-5.1	Wurtzite =Sphalerite	Wurtzite =Sphalerite, %SG4	Wurtzite =Sphalerite, %SG4	Wurtzite =Sphalerite, %SG7	>Sphalerite,%Wurtzite,
-5.0	Wurtzite =Sphalerite	Wurtzite =Sphalerite, %SG4	Wurtzite =Sphalerite, %SG4	Wurtzite =Sphalerite, %SG7	>Sphalerite,%Wurtzite,
-4.9	Wurtzite =Sphalerite	Wurtzite =Sphalerite, %SG4	Wurtzite =Sphalerite, %SG4	Wurtzite =Sphalerite, %SG7	>Sphalerite,%Wurtzite,
-4.8	Wurtzite =Sphalerite, %SG4	Wurtzite =Sphalerite, %SG4	Wurtzite =Sphalerite, %SG4	Wurtzite =Sphalerite, %SG7	Wurtzite =Sphalerite, %SG4
-4.7	Wurtzite =Sphalerite, %SG4	Wurtzite =Sphalerite, %SG4	Wurtzite =Sphalerite, %SG4	Wurtzite =Sphalerite, %SG7	Wurtzite =Sphalerite, %SG4
-4.6	Wurtzite =Sphalerite, %SG4	Wurtzite =Sphalerite, %SG4	P1	P1	Wurtzite =Sphalerite, %SG4
-4.5	Wurtzite =Sphalerite, %SG4	Wurtzite =Sphalerite, %SG4	P1	P1	Wurtzite =Sphalerite, %SG4
-4.4	Wurtzite =Sphalerite, %SG4	Wurtzite =Sphalerite, %SG4	P1	P1	Wurtzite =Sphalerite, %SG4
-4.3	>Sphalerite,%Wurtzite, %SG 8	Wurtzite =Sphalerite, %SG4	P1	P1	Wurtzite =Sphalerite, %SG8
-4.2	>Sphalerite,%Wurtzite, %SG 8	Wurtzite =Sphalerite, %SG4	P1	P1	Wurtzite =Sphalerite, %SG8
-4.1	>Sphalerite,%Wurtzite, %SG 8	>P1,%Wurtzite, %Sphalerite	P1, %SG 8	P1, %SG 8	Wurtzite =Sphalerite, %SG8
-4.0	>Sphalerite,%Wurtzite, %SG 8	>P1,%Wurtzite, %Sphalerite	P1, %SG 8	P1, %SG 8	Wurtzite =Sphalerite, %SG8

Table DII: Structural analysis of the energy landscape of ZnO with Z = 4 and all relevant structures as a starting point of the TA calculations. The special sign (>) is used for the structure most frequently found, and (%) sign mark the significant percentage of the structure/space group found during this search.

## 16.2 The prescribed path calculations

When investigating relationships between structures, a frequent problem is the search for a sequence of transitions from one space group (supergroup) to a different space group (subgroup), which is not a maximal non-isomorphic subgroup. Such a crystallographic analysis of the various structures and their group-subgroup relations down to the "amorphous" state ( $P1$ ) is performed using the SPUG algorithm implemented in the KPLOT program [227], which computes the possible sequences of maximal non-isomorphic subgroups between two given space groups. However, the SPUG algorithm uses the search for a maximal non-isomorphic subgroup in 4 steps (as in refs [393–395]).

In order to gain more insights in the group - subgroup relations, it is possible to increase the step number in the KPLOT program to 8. Instead, we decided to use the Bilbao Crystallographic Server [105, 396] since it offers many options of crystallographic analysis. Especially the SUBGROUPGRAPH program [363] was used in order to produce the supplementary figures. The program is based on the data for the maximal subgroups of index 2, 3, and 4 of the space groups [393–395], while the KPLOT program uses only the first index available in the group (usually it is 2). This data is transformed into a graph with 230 vertices corresponding to the 230 space groups. If two vertices in the graph are connected by an edge, the corresponding space groups form a group - maximal-subgroup pair. Each one of these pairs is characterized by a group-subgroup index. The different maximal subgroups of the same space-group type are distinguished by the corresponding transformation matrices which describe the relations between the conventional bases of the group and the subgroup. The index and the set of transformation matrices are considered as attributes of the edge connecting the group with the subgroup. [105, 396]

In this section we present group - subgroup relation figures generated by the SUBGROUPGRAPH program. [363] In general, each figure consists of a group-subgroup pair, with the starting group  $G$  (e.g.  $Fm-3m$ ) and the final subgroup  $H$  (e.g.  $F-43m$ ), where  $G > H$  (e.g.  $Fm-3m > F-43m$ ), and corresponding group-subgroup indices  $i$  (e.g.  $i = [2]$ ) plotted in brackets. Two vertices in the graph are connected with an edge if there is a group-subgroup relation between the corresponding subgroups. If there are two edges connecting two groups then there is a group-subgroup relation between these groups in the two directions ( $G > H$ , and  $H > G$ ). If a group is connected with itself,

## 16.2 The prescribed path calculations

---

then this group has an isomorphic subgroup. Note that we do not show here the group - subgroup relation graph of maximal subgroups for the group-subgroup pair, where the starting group is  $Fm - 3m$  (where the ideal rock salt structure appears) and the final subgroup is  $Cm$ , where different distortions of experimentally observed structures appear, because of the high complexity of this graph.

## 16. APPENDIX D: ENERGY LANDSCAPE INVESTIGATION IN ZNO



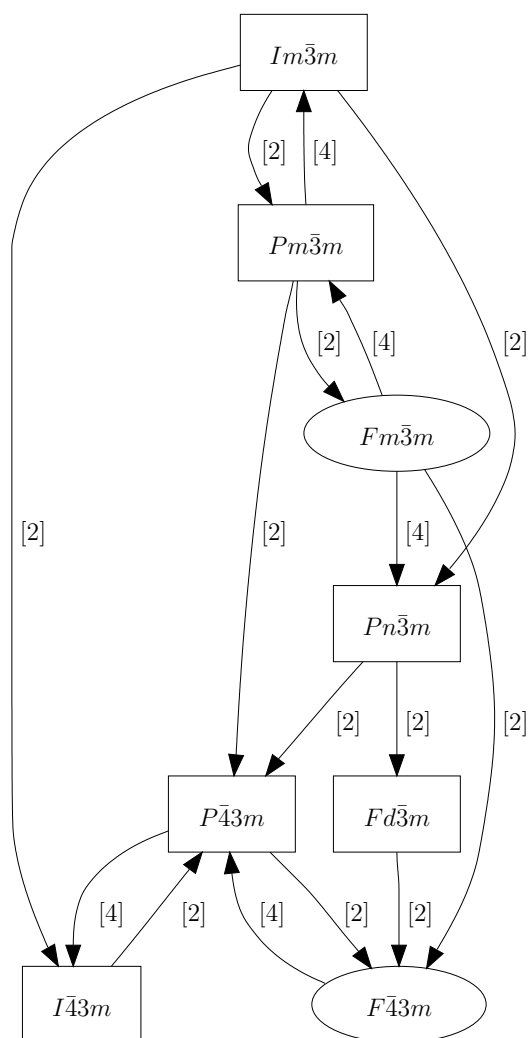


**Figure 16.1: Group - subgroup relation graph of maximal subgroups.** The starting group is  $Fm - 3m$  (no. 225), where the ideal rock salt ( $B1$ ) structure appears, and the final subgroup is  $F - 43m$  (no. 216), where the ideal sphalerite ( $B3$ ) structure appears - Although the crystallographic analysis gives us logical path between these two structures, the energy landscape analysis shows extremely high barriers and makes synthesis unlikely. The space group  $P6_3mc$  (no. 186), where wurtzite ( $B4$ ) structure appears, is even not possible to connect in group - subgroup relation with space groups  $Fm - 3m$  and  $F - 43m$ , where NaCl and sphalerite structure appear, but this is more likely way for synthesis, in respect to their calculated energies. Note that numbers in the brackets are corresponding indices of subgroup in a group ( $i$  is the index of  $H$  in  $G$ , see refs [105, 396]).

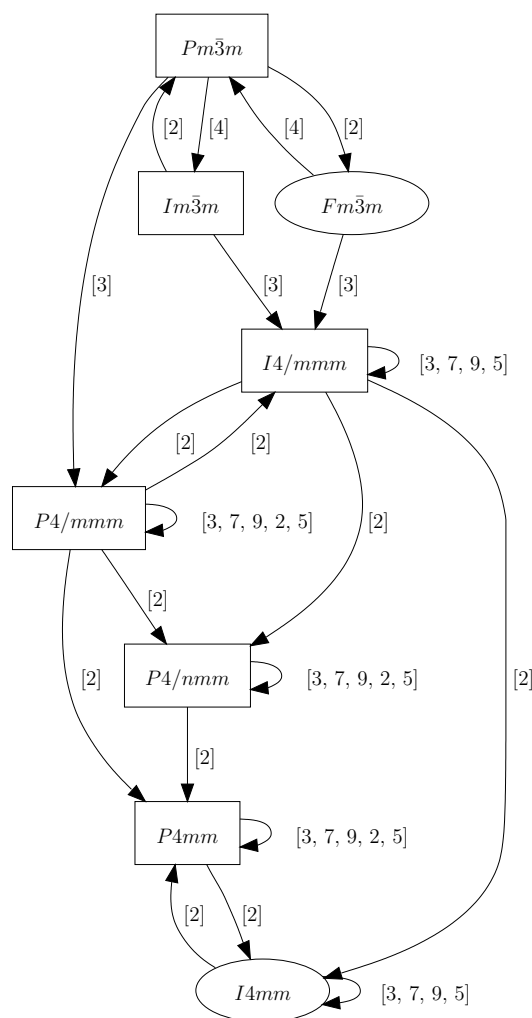


**Figure 16.2: Group - subgroup relation graph of maximal subgroups. The starting group is  $Fm\bar{3}m$  (no. 225), where the ideal rock salt ( $B1$ ) structure appears, and the final subgroup is  $I4mm$  (no. 107), where the ideal GeP structure appears - This is possible low-temperature and high pressure transition route in ZnO system, according to energy, structural and crystallographic analysis. Note that numbers in the brackets are corresponding indices of subgroup in a group ( $i$  is the index of  $H$  in  $G$ , see refs [105, 396]).**

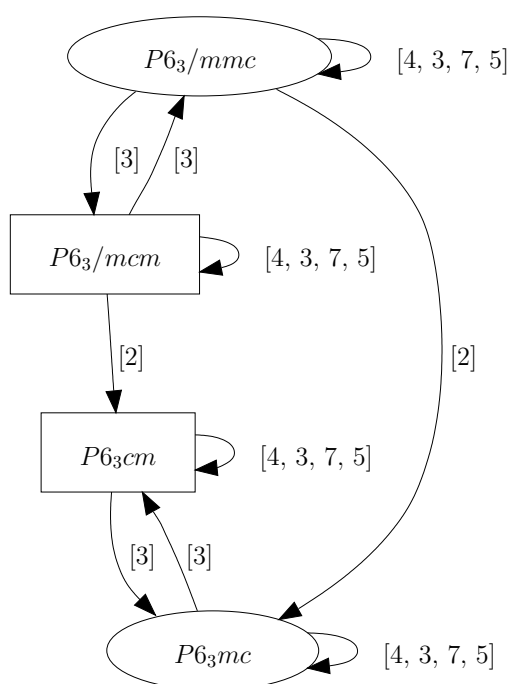


**Figure 16.3: Group - subgroup relation graph of maximal subgroups.** The starting group is  $P6_3/mmc$  (no. 194), where the ideal 5-5 structure appears, and the final subgroup is  $P6_3mc$  (no. 186), where the ideal wurtzite structure appears - This is a first order transition at low-temperature in ZnO system, according to energy, structural and crystallographic analysis. Note that numbers in the brackets are corresponding indices of subgroup in a group ( $i$  is the index of  $H$  in  $G$ , see refs [105, 396]).

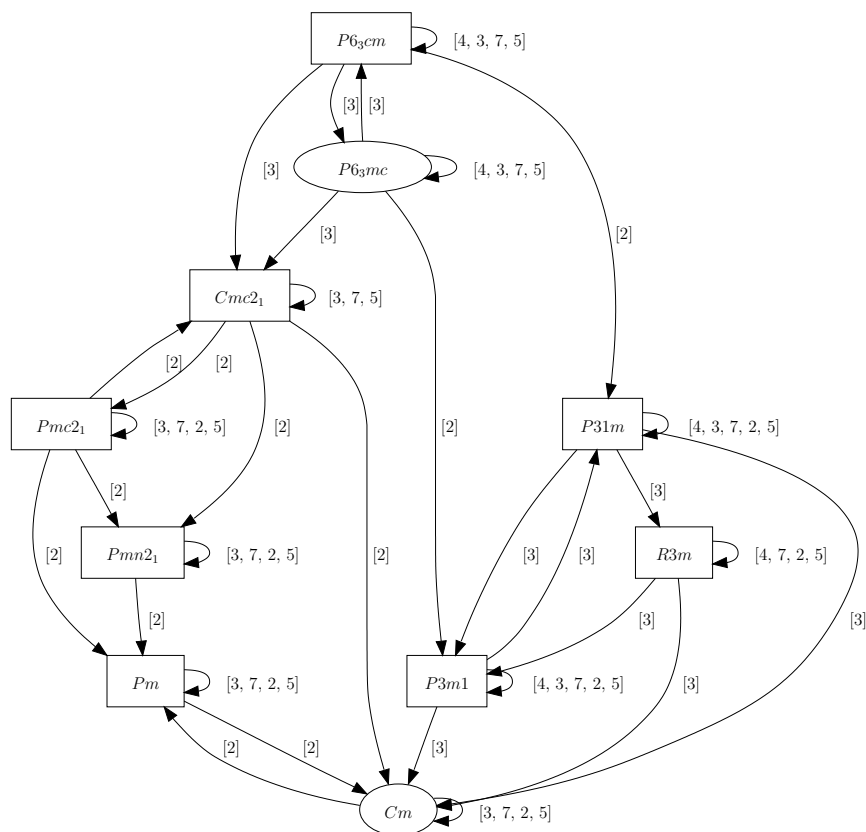
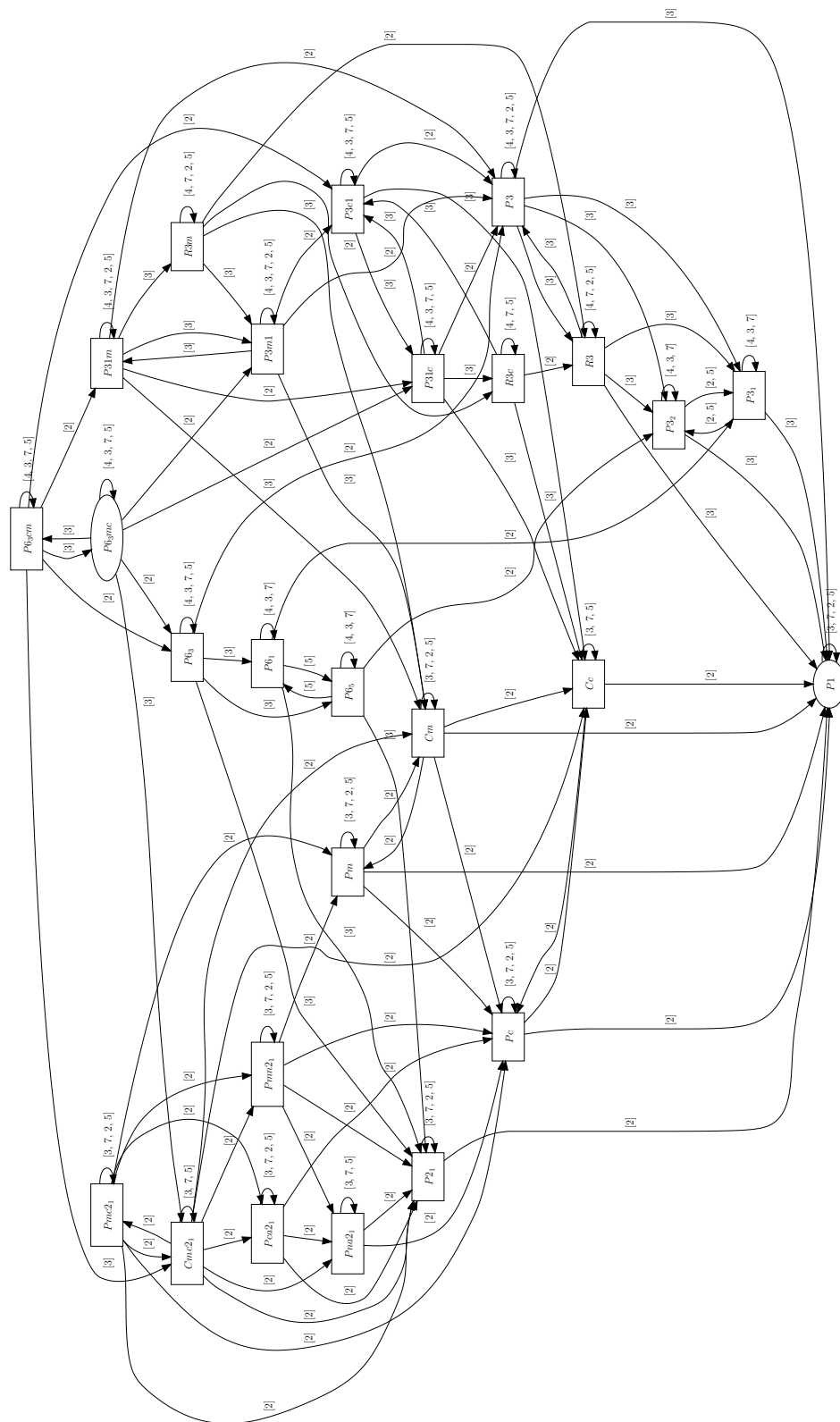
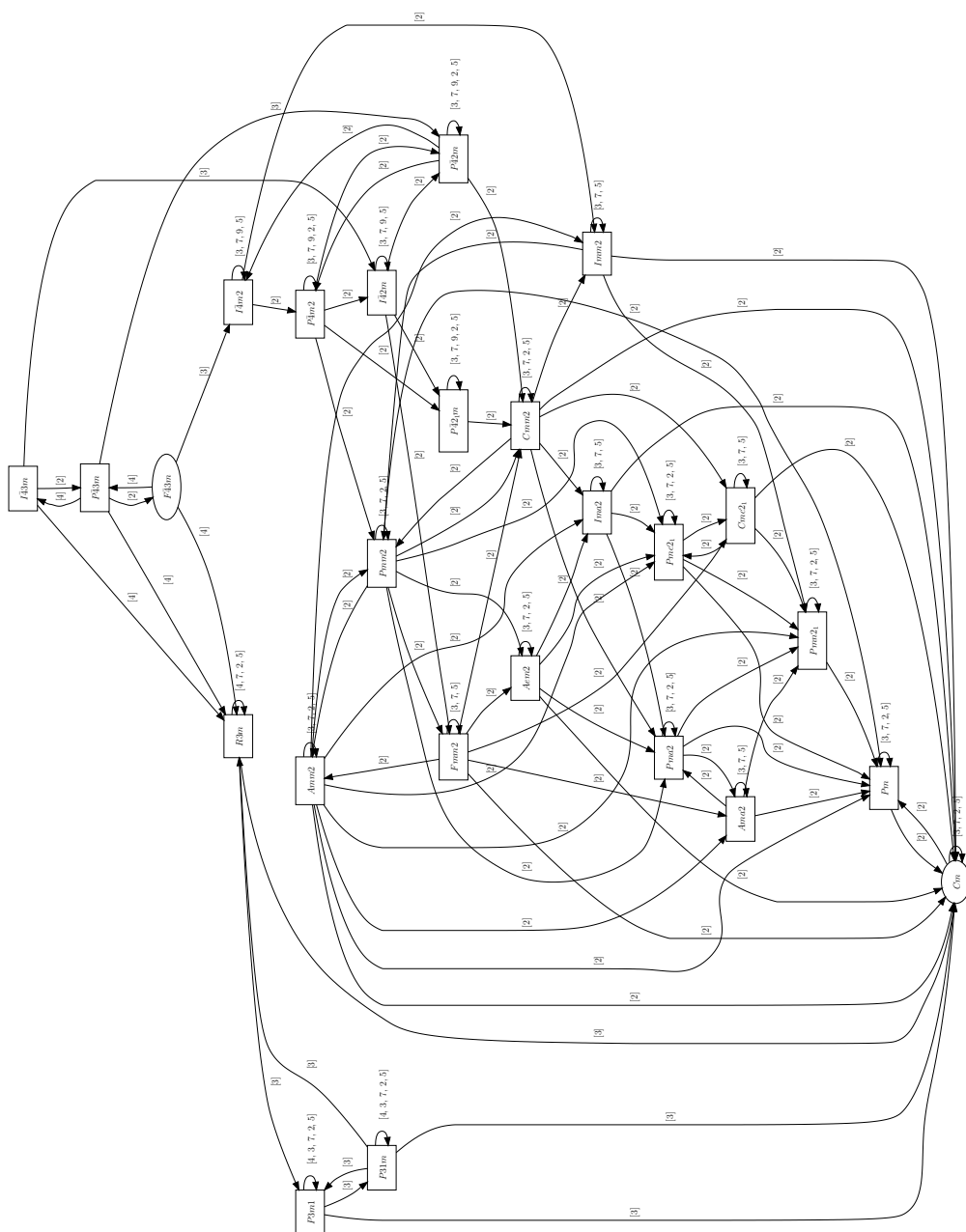


**Figure 16.4: Group - subgroup relation graph of maximal subgroups.** The starting group is  $P6_3mc$  (no. 186), where the ideal wurtzite structure appears, and the final subgroup is  $Cm$  (no. 8), where different distortions of experimentally observed structures appear - Space group  $Cm$  is a good candidate for transition structure space group, since it is possible to reduce all experimentally observed structure to  $Cm$  space group, and it is in a good agreement with energy, structural and crystallographic analysis. Note that numbers in the brackets are corresponding indices of subgroup in a group ( $i$  is the index of  $H$  in  $G$ , see refs [105, 396]).



Appendix Scheme D1. Group – subgroup relation graph of maximal subgroups. The starting group is  $P_{6gem}$ , where the ideal wurtzite structure appears, and the final subgroup is  $P_1$ , where the “amorphous phases” appear. The graph shows the complexity of the path, when it is reduced to the “amorphous state”. Note that numbers in the brackets are corresponding indices of subgroup in a group ( $i$  is the index of  $H$  in  $G$ ).

## 16. APPENDIX D: ENERGY LANDSCAPE INVESTIGATION IN ZNO



Appendix Scheme D2. Group – subgroup relation graph of maximal subgroups. The starting group is  $F-43m$ , where the ideal sphalerite structure appears, and the final subgroup is  $C_m$ , where different distortions of experimentally observed structures appear, which could be used in synthesis process as intermediate phase. Numbers in the brackets corresponds to indices of subgroup in a group ( $i$  is the index of  $H$  in  $G$ ).

# References

- [1] E. J. COREY. *Pure Appl. Chem.*, **14**:19, 1967.
- [2] E. J. COREY. *Angew. Chem. Int. Ed.*, **30**:455, 1991.
- [3] A. V. GUZZO. **Influence of Amino-Acid Sequence on Protein Structure.** *Biophys. J.*, **5**:809–822, 1965.
- [4] J. W. PROTHERO. **Correlation between Distribution of Amino Acids and Alpha Helices.** *Biophys. J.*, **6**:367–370, 1966.
- [5] G. D. FASMAN M. FROIMOWITZ. **Prediction of the secondary structure of proteins using the helix-coil transition theory.** *Macromolecules*, **7**:583–589, 1974.
- [6] R. L. JOHNSTON. *Atomic and Molecular Clusters.* Taylor and Francis, London, UK, 2002.
- [7] D. J. WALES. **Energy Landscapes with Applications to Clusters, Biomolecules and Glasses.** Cambridge University Press, 2003.
- [8] S. M. WOODLEY AND C. R. A. CATLOW. *Nature Mater.*, **7**:937, 2008.
- [9] M. JANSEN. *Syntheseplanung in der Festkörperchemie?* Presentation at the 30th anniversary of the Fonds der Chemie, Düsseldorf, 1980.
- [10] J. MADDOX. **Crystals From First Principles.** *Nature*, **335**:201–201, 1988.
- [11] C. R. A. CATLOW AND G. D. PRICE. **Computer Modeling of Solid-State Inorganic Materials.** *Nature*, **347**:243–248, 1990.
- [12] J. PANNETIER, J. BASSAS-ALSINA, J. RODRIGUEZ-CARVAJAL, AND V. CAIGNAERT. *Nature*, **346**:343, 1990.
- [13] C. M. FREEMAN, J. M. NEWSAM, S. M. LEVINE, AND C. R. A. CATLOW. *J. Mater. Chem.*, **3**:351, 1993.
- [14] J. C. SCHÖN AND M. JANSEN. *Ber. Bunsenges.*, **98**:1541–1544, 1994.
- [15] J. C. SCHÖN AND M. JANSEN. **Determination of candidate structures for simple ionic compounds through cell optimisation.** *Comp. Mater. Sci.*, **4**:43–58, 1995.
- [16] J. C. SCHÖN AND M. JANSEN. *Angew. Chem.*, **108**:1358, 1996.
- [17] J. C. SCHÖN AND M. JANSEN. **First step towards planning of syntheses in solid-state chemistry: Determination of promising structure candidates by global optimization.** *Angew. Chem. Int. Ed. Eng.*, **35**:1286–1304, 1996.
- [18] J. C. SCHÖN, K. DOLL, AND M. JANSEN. **Predicting solid compounds via global exploration of the energy landscape of solids on the ab initio level without recourse to experimental information.** *Phys. Stat. Sol. B*, **247**:23–39, 2010.
- [19] M. JANSEN, K. DOLL, AND J. C. SCHÖN. **Addressing chemical diversity by employing the energy landscape concept.** *Acta Cryst. A*, **66**:518–534, 2010.
- [20] Ž. ČANČAREVIĆ, J. C. SCHÖN, AND M. JANSEN. **Alkali metal carbonates at high pressure.** *Z. Anorg. Allg. Chem.*, **632**:1437–1448, 2006.
- [21] A. R. OGANOV, C. W. GLASS, AND S. ONO. **High-pressure phases of CaCO<sub>3</sub>: crystal structure prediction and experiment.** *Earth Planet. Sci. Lett.*, **241**:95–103, 2006.
- [22] S. M. WOODLEY, P. D. BATTLE, J. D. GALE, AND C. R. A. CATLOW. *Phys. Chem. Chem. Phys.*, **1**:2535–2542, 1999.
- [23] P. VERWER AND F. J. J. LEUSEN. *Reviews in Computational Chemistry*, edited K. B. Lipkowitz and D. B. Boyd. Wiley-VCH, New York, 1998.
- [24] J. C. SCHÖN AND M. JANSEN. *Z. Krist.*, **216**:307–325;361–383, 2001.
- [25] M. JANSEN. **A Concept of Synthesis Planning in Solid-State Chemistry.** *Angew. Chem. Int. Ed.*, **41**(20):3747–3766, 2002.
- [26] J. C. SCHÖN AND M. JANSEN. In J LI, N. E. BRESE, M. G. KANATZIDIS, AND M. JANSEN, editors, *Mat. Res. Soc. Symp. Proc. Vol 848: Solid State Chemistry of Inorganic Materials V.* MRS, Warrendale, 2005.
- [27] S. L. PRICE. **From crystal structure prediction to polymorph prediction: interpreting the crystal energy landscape.** *Phys. Chem. Chem. Phys.*, **10**:1996–2009, 2008.
- [28] G. J. ACKLAND. *Rep. Prog. Phys.*, **64**:483–516, 2001.
- [29] L. LIU AND W. A. BASSETT. *Elements, Oxides and Silicates. High-Pressure Phases with Implications for the Earth's Interior.* Oxford Univ. Press, New York, 1986.
- [30] R. J. HEMLEY, editor. *Ultra-high-Pressure Mineralogy: Physics and Chemistry of the Earth's Deep Interior*, **37** of *Reviews in Mineralogy*. The Mineralogical Society of America, Washington, DC, 1998.
- [31] M. T. YIN AND M. L. COHEN. **Will Diamond Transform under Megabar Pressures.** *Phys. Rev. Lett.*, **50**:2006–2009, 1983.
- [32] M. L. COHEN. **Prediction of New Materials and Properties of Solids.** *International Journal of Quantum Chemistry*, **29**:883–854, 1986.

## REFERENCES

---

- [33] R. E. COHEN. **Calculation of Elasticity and High Pressure Instabilities in Corundum and Stishovite with the Potential Induced Breathing Model.** *Geophys. Res. Lett.*, **14**:37–40, 1987.
- [34] H. CYNN, D. G. ISAAK, R. E. COHEN, M. F. NICOL, AND O. L. ANDERSON. **A High Pressure Phase Transition of Corundum Predicted by the Potential Induced Breathing Model.** *Amer. Mineral.*, **75**:439–442, 1990.
- [35] M. L. COHEN, Z. REUT, L. J. SHAM, P. B. ALLEN, N. W. ASHCROFT, AND V. HEINE. **Predicting New Solids and their Properties[and Discussion].** *Phil. Trans. Roy. Soc. London A*, **334**:501–513, 1991.
- [36] R. E. COHEN. **First-Principles Predictions of Elasticity and Phase Transitions in High Pressure SiO<sub>2</sub> and Geophysical Implications.** In M.H. MANGHNANI AND Y. SYONO, editors, *High Pressure Research in Mineral Physics: Application to Earth and Planetary Science*, pages 425–432. AGU, Washington, D.C., 1992.
- [37] F. C. MARTON AND R. E. COHEN. **Prediction of a High Pressure Phase Transition in Al<sub>2</sub>O<sub>3</sub>.** *Amer. Mineral.*, **79**:789–792, 1994.
- [38] K. T. THOMSON, R. M. WENTZCOVITCH, AND M. S. T. BUKOWINSKI. **Polymorphs of Alumina Predicted by First Principles: Putting Pressure on the Ruby Pressure Scale.** *Amer. Mineral.*, **79**:789–792, 1994.
- [39] B. WINKLER, C. J. PICKARD, V. MILMAN, W. E. KLEE, AND G. THIMM. **Prediction of a nanoporous sp<sup>2</sup>-carbon framework structure by combining graph theory with quantum mechanics.** *Chem. Phys. Lett.*, **312**:536–541, 1999.
- [40] J. C. SCHÖN, I. V. PENTIN, AND M. JANSEN. *Phys. Chem. Chem. Phys.*, **8**:1778, 2000.
- [41] J. C. SCHÖN, M. A. C. WEVERS, AND M. JANSEN. **Prediction of high pressure phases in the systems Li<sub>3</sub>N, Na<sub>3</sub>N, (Li,Na)<sub>3</sub>N, Li<sub>2</sub>S and Na<sub>2</sub>S.** *J. Mater. Chem.*, **11**:69–77, 2001.
- [42] B. WINKLER, C. J. PICKARD, V. MILMAN, AND G. THIMM. **Systematic prediction of crystal structures.** *Chem. Phys. Lett.*, **337**:36–42, 2001.
- [43] R. T. STRONG, C. J. PICKARD, V. MILMAN, G. THIMM, AND B. WINKLER. **Systematic prediction of crystal structures: An application to sp<sup>3</sup>-hybridized carbon polymorphs.** *Phys. Rev. B*, **70**:Art. No. 045101, 2004.
- [44] Ž. ČANČAREVIĆ, J. C. SCHÖN, AND M. JANSEN. **Prediction of possible high-pressure phases of Cu<sub>3</sub>N.** *Z. Anorg. Allgem. Chem.*, **631** : 1167 – 1171, 2005.
- [45] P. KROLL, T. SCHRÖTER, AND M. PETERS. **Prediction of Novel Phases of Tantalum(v) Nitride and Tungsten(VI) Nitride That Can Be Synthesized under High Pressure and High Temperature.** *Angew. Chem. Int. Ed.*, **44**:4249–4254, 2005.
- [46] D. FISCHER AND M. JANSEN. **Synthesis, structure of Na<sub>3</sub>N.** *Angew. Chem. Int. ed.*, **41**:1755–1756, 2002.
- [47] D. FISCHER AND M. JANSEN. **Low-Activation Solid-State Syntheses by Reducing Transport Lengths to Atomic Scales As Demonstrated by Case Studies on AgNO<sub>3</sub> and AgO.** *J. Am. Chem. Soc.*, **124**:3488, 2002.
- [48] D. FISCHER AND M. JANSEN. *Z. Anorg. Allg. Chem.*, **629**:1934, 2003.
- [49] D. FISCHER, Ž. ČANČAREVIĆ, J. C. SCHÖN, AND M. JANSEN. **Zur Synthese und Struktur von K<sub>3</sub>N.** *Z. Allgem. Anorg. Chem.*, **630**:156–160, 2004.
- [50] C. MELLOT-DRAZNIENKS, J. M. NEWSAM, A. M. GORMAN, C. M. FREEMAN, AND G. FERREY. *Angew. Chem. Int. Ed. Eng.*, **39**:2270–2275, 2000.
- [51] A. C. KAY. *at a 1971 meeting of PARC (Palo Alto Research Center).* <http://en.wikipedia.org/wiki/>, <http://www.smalltalk.org/>, 1971.
- [52] COMPILED BY A. D. MCNAUGHT AND A. WILKINSON. *IUPAC. Compendium of Chemical Terminology, 2nd ed. (the Gold Book)*, Blackwell Scientific Publications, Oxford, pages (<http://goldbook.iupac.org> (2006–)), 1997.
- [53] M. GOLDSTEIN. **Viscous Liquids and the Glass Transition: A Potential Energy Barrier Picture.** *J. Chem. Phys.*, **51**:3728–3740, 1969.
- [54] AND T. A. WEBER F. STILLINGER. *Phys. Rev. A*, **25**:978–989, 1982.
- [55] J. C. SCHÖN AND M. JANSEN. *Z. Krist.*, **216**:307–325, 2001.
- [56] D. ZAGORAC, J. C. SCHÖN, K. DOLL, AND M. JANSEN. **Structure Prediction for PbS and ZnO at Different Pressures and Visualization of the Energy Landscapes.** *Acta Phys. Pol. A*, **120**:215–220, 2011.
- [57] D. ZAGORAC, J. C. SCHÖN, AND M. JANSEN. **Energy landscape investigations using the prescribed path method in the ZnO system.** *submitted to J. Phys. Chem. C*, 2012.
- [58] J. C. SCHÖN AND P. SIBANI. *J. Phys. A: Math. Gen.*, **31**:8165–8178, 1998.
- [59] J. C. SCHÖN AND M. JANSEN. In Z. MAKSIC AND W. ORVILLE-THOMAS, editors, *Pauling's Legacy: Modern Modeling of the Chemical Bond*, pages 103–127. Elsevier, Amsterdam, 1999.
- [60] J. C. SCHÖN, M. A. C. WEVERS, AND M. JANSEN. **'Entropically' stabilized region on the energy landscape of an ionic solid.** *J. Phys.: Cond. Matter*, **15**:5479–5486, 2003.
- [61] J. C. SCHÖN AND M. JANSEN. *Z. Krist.*, **216**:361–383, 2001.
- [62] D. ZAGORAC, K. DOLL, J. C. SCHÖN, AND M. JANSEN. **Sterically active electron pairs in lead sulfide? An investigation of the electronic and vibrational properties of PbS in the transition region between the rock salt and the α-GeTe type modifications.** *accepted in Chem. Eur. J.*, 2012.



## REFERENCES

- [63] ED. BY A. R. OGANOV. *Modern Methods of Crystal Structure Prediction*. Wiley, Weinheim, 2011.
- [64] C. R. A. CATLOW, editor. *Computer Modeling in Inorganic Crystallography*. Academic Press, Sand Diego, 1997.
- [65] G. BERGERHOFF, R. HUNDT, R. SIEVERS, AND I. D. BROWN. *J. Chem. Inf. Comput. Sci.*, **23**:66, 1983.
- [66] ICSD-FIZ-KARLSRUHE. **Inorganic Crystal Structure Database**. <http://icsd.fiz-karlsruhe.de/>, 2012.
- [67] P. VILLARS AND K. CENZUAL. **Pearson's Crystal Data: Crystal Structure Database for Inorganic Compounds (on CD-ROM)**. ASM International, Materials Park, Ohio, USA, (<http://www.crystalimpact.com/pcd/>), Release 2011/12, 2011.
- [68] J. VAN DE STREEK. **Searching the Cambridge Structural Database for the 'best' representative of each unique polymorph**. *Acta Cryst. B*, **62**:567–579, 2006.
- [69] M.D. SHANNON, J.L. CASCI, P.A. COX, AND S.J. ANDREWS. **Structure of the two-dimensional medium-pore high-silica zeolite NU-87**. *Nature*, **353**:417–420, 1991.
- [70] S. KIRKPATRICK, C. D. GELATT JR., AND M. P. VECCHI. *Science*, **220**:671–680, 1983.
- [71] V. CZERNY. *J. Optim. Theo. Appl.*, **45**:41–51, 1985.
- [72] P. SALAMON, P. SIBANI, AND R. FROST. *Facts, Conjectures and Improvements for Simulated Annealing*. SIAM Monographs on Mathematical Modeling and Computation. Society for Industrial and Applied Mathematics, Philadelphia, USA, 2002.
- [73] J. H. HOLLAND. *Adaptation in Natural and Artificial Systems*. Univ. Mich. Press, Ann Arbor, 1975.
- [74] L. DAVIS. *Genetic Algorithms and Simulated Annealing*. Pitman, London, 1987.
- [75] D. A. COLEY. *An Introduction to Genetic Algorithms for Scientists and Engineers*. World Scientific, 1999.
- [76] D. J. WALES AND J. P. K. DOYE. **Global Optimization by Basin-Hopping and the Lowest Energy Structures of Lennard-Jones Clusters Containing up to 110 Atoms**. *J. Phys. Chem. A*, **101**:5111–5116, 1997.
- [77] A. MÖBIUS, A. NEKLIODOV, A. DIAZ-SANCHEZ, K. H. HOFFMANN, A. FACHAT, AND M. SCHREIBER. **Optimization by Thermal Cycling**. *Phys. Rev. Lett.*, **79**:4297–4301, 1997.
- [78] A. MÖBIUS, B. FREISLEBEN, P. MERZ, AND M. SCHREIBER. **Combinatorial optimization by iterative partial transcription**. *Phys. Rev. E*, **59**:4667–4674, 1999.
- [79] J. HAN AND M. KAMBER. **Data Mining: Concepts and Techniques**. 2nd ed, *The Morgan Kaufmann Series in Data Management Systems (Ed: Jim Gray)*, ISBN 1-55860-901-6, 2006.
- [80] M.M. GABER. **Scientific data mining and knowledge discovery: Principles and Foundation**. Springer, Berlin, Heidelberg, 2010.
- [81] P. VILLARS. **A three-dimensional structural stability diagram for 998 binary AB intermetallic compounds**. *J. Less Common Met.*, **92**:215–238, 1983.
- [82] D.G. PETTIFOR. **The structures of binary compounds: I. Phenomenological structure maps**. *J. Phys. C*, **19**:285–313, 1986.
- [83] G. L. W. HART. **Where are nature's missing structures?** *Nature Mat.*, **6**:941 – 945, 2007.
- [84] C. C. FISCHER, K. J. TIBBETTS, D. MORGAN, AND G. CEDER. **Predicting crystal structure by merging data mining with quantum mechanics**. *Nature Mat.*, **5**:641–646, 2006.
- [85] G. CEDER, D. MORGAN, C. FISCHER, AND K. TIBBETTS. **Data-Mining-Driven Quantum Mechanics for the Prediction of Structure**. *MRS Bull.*, **31**:981, 2006.
- [86] A. F. WELLS. **The geometrical basis of crystal chemistry. 1-4**. *Acta Crystallogr.*, **7**:535–554, 842–853, 1954.
- [87] J. V. SMITH. **Enumeration of 4-connected 3-dimensional nets and classification of framework silicates. I. Perpendicular linkage from simple hexagonal net**. *Am. Mineral.*, **62**:703–709, 1977.
- [88] M. M. J. TREACY AND ET AL. **Enumeration of periodic tetrahedral frameworks. II. Polynodal graphs**. *Micropor. Mesopor. Mater.*, **74**:121–132, 2004.
- [89] M. D. FOSTER AND ET AL. **Chemically feasible hypothetical crystalline networks**. *Nature Mater.*, **3**:234–238, 2004.
- [90] N. TAJIMA, S. TSUZUKI, K. TANABE, K. AOKI, AND T. HIRANO. **First principles prediction of crystal structures of CO<sub>2</sub> Electron**. *J. Theor. Chem.*, **2**:139–148, 1997.
- [91] P. RAITERI, R. MARTONAK, AND M. PARRINELLO. **Exploring polymorphism: The case of benzene**. *Angew. Chem. Int. Ed.*, **44**:3769–3773, 2005.
- [92] R. MARTONAK, A. LAIO, AND M. PARRINELLO. **Predicting crystal structures: The Parrinello-Rahman method revisited**. *Phys. Rev. Lett.*, **90**:75503, 2003.
- [93] PLATO. *Quote: A good decision is based on knowledge and not on numbers*. <http://www.brainyquote.com/quotes/authors/p/>, <http://en.wikipedia.org/wiki/>, 2012.
- [94] P. TRUCANO AND R. CHEN. **Structure of graphite by neutron diffraction**. *Nature*, **258**:136–137, 1975.
- [95] T. HOM, W. KISZENIK, AND B. POST. **Accurate lattice constants from multiple reflection measurements. Lattice constants of germanium, silicon and diamond**. *J. App. Crystal.*, **8**:457–458, 1975.

## REFERENCES

- [96] T.C. CHIANG AND F.J. HIMPSEL. *2.1.2 C (diamond phase)*. Goldmann, A., Koch, E.-E. (ed.). SpringerMaterials - The Landolt-Bornstein Database, (<http://www.springermaterials.com>). DOI:10.1007/103770197, 2012.
- [97] G. BERGERHOFF, M. BERNDT, K. BRANDENBURG, AND T. DEGEN. **Concerning inorganic crystal structure types**. *Acta Cryst. B*, **55**:147–156, 1999.
- [98] J.R. HOOK AND H.E. HAL. **Solid State Physics**. 2nd Edition, Manchester Physics Series, John Wiley Sons, 2001.
- [99] U. MÜLLER. *Anorganische Strukturchemie*. Teubner, Stuttgart, 1992.
- [100] U. MÜLLER. *Inorganic Structural Chemistry*. 2nd Ed., Wiley, Marburg, 2007.
- [101] N. W. ASHCROFT AND N. D. MERMIN. *Solid State Physics*. Thomson Learning Inc., Cornell University, 1976.
- [102] L. E. SMART AND E. A. MOORE. *Solid State Chemistry: An Introduction*. Taylor Francis Group, Boca Raton, London, New York, Singapore, 2005.
- [103] R. A. EVARESTOV. *Quantum Chemistry of Solids: The LCAO First Principles Treatment of Crystals*. Springer, Berlin Heidelberg New York, 2007.
- [104] CRYSTAL IMPACT. **Crystal impact - Software for Chemists and Material Scientists**. <http://www.crystalimpact.com/>, 2012.
- [105] M. I. AROYO, J. M. PEREZ-MATO, C. CAPILLAS, E. KROUMOVA, S. IVANTCHEV, G. MADARIAGA, A. KIROV, AND H. WONDRAUSCHKE. **Bilbao Crystallographic Server I: Databases and crystallographic computing programs**. *Z. Krist.*, **221**:15–27, 2006.
- [106] A. R. WEST. *Basic Solid State Chemistry*. 2nd edition, John Wiley and Sons, Ltd, Chichester, 2006.
- [107] R. ALLMANN AND R. HINEK. **The introduction of structure types into the Inorganic Crystal Structure Database ICSD**. *Acta Cryst. A*, **63**:412–417, 2007.
- [108] P. VILLARS. *New Series III/43A7*, DOI: 10.1007/978-3-540-69949-1<sub>1</sub>. SpringerMaterials - The Landolt - Bornstein Database, Berlin Heidelberg New York, 2009.
- [109] NRL. *Crystal Lattice Structures*. <http://cst-www.nrl.navy.mil/lattice/index.html>, 2008.
- [110] J. HAFNER, F. HULLIGER, W. B. JENSEN, J. A. MAJEWSKI, K. MATHIS, P. VILLARS, AND P. VOGL. *The Structures of Binary Compounds*. Elsevier, North Holland, Amsterdam, 1990.
- [111] P. D. HEDE AND S. P. BEIER. *Inorganic and Applied Chemistry*. Peter Dybdahl Hede, Soren Prip Beier Ventus Publishing Aps, ISBN 978-87-7681-221-9, 2007.
- [112] A. F. WELLS. *Structural Inorganic Chemistry*. Vol. 5, Clarendon Press, Oxford, 1995.
- [113] J.-M. RAULOT, G. BALDINOZZI, R. SESHADRI, AND P. CORTONA. *Solid State Sci.*, **4**:467–474, 2002.
- R. J. GILLESPIE AND E. A. ROBINSON. *Angew. Chem. Int. Ed. Engl.*, **35**:495–514, 1996.
- A. WALSH, D. J. PAYNE, R. G. EGDELL, AND G. W. WATSON. *Chem. Soc. Rev.*, **40**:4455–4463, 2011.
- Z.B. MAKSIC AND W. J. ORVILLE-THOMAS. *Pauling's Legacy: Modern Modelling of the Chemical Bond*. Elsevier, Amsterdam, The Netherlands, 1999.
- S. SCOUAR. *First Philosophy: The Theory of Everything*. <http://en.wikiquote.org/wiki/>, p. 89: quoted Niels Bohr, 2007.
- R. DOVESI, B. CIVALLERI, R. ORLANDO, C. ROETI, AND V. R. SONDERS. *Ab Initio Quantum Simulation in Solid State Chemistry*, **21** of *Reviews in Computational Chemistry*. Wiley-VCH, John Wiley & Sons, Inc., Weinheim, New York, 2005.
- A. SZABO AND N. S. OSTLUND. *Modern Quantum Chemistry: Introduction to Advanced Electronic Structure Theory*. Dover Publications, Mineola, New York, 1996.
- E. SCHROEDINGER. **An Undulatory Theory of the Mechanics of Atoms and Molecules**. *Physical Review*, **28**(6):1049–1070, 1926.
- M. BORN AND J. R. OPPENHEIMER. **Zur Quantentheorie der Molekeln / On the Quantum Theory of Molecules**. *Annalen der Physik*, **389**(20):457–484, 1926.
- C. ECKART. **The Kinetic Energy of Polyatomic Molecules**. *Physical Review*, **46**:383–387, 1935.
- <http://www.wikipedia.org/>, 2012.
- H. F. SCHAEFER III. *The Development of Ab Initio Methods in Molecular Electronic Structure Theory*. Second edition, Courier Dover Publications, Oxford, 2004.
- [125] J. SLATER AND H. C. VERMA. **The Theory of Complex Spectra**. *Phys. Rev.*, **34**:1293–1295, 1929.
- [126] D. R. HARTREE, W. HARTREE, AND B. SWIRLES. **Self-Consistent Field, Including Exchange and Superposition of Configurations, with Some Results for Oxygen**. *Phil. Trans. Roy. Soc. Lon. A*, **238**:229–247, 1939.
- V. FOCK, M. VESSELOW, AND M. PETRASHEN. *Zh. Exsp. Theor. Fiz.*, **10**:723, 1940.
- [128] C. C. J. Roothaan. **New Developments in Molecular Orbital Theory**. *Rev. Mod. Phys.*, **23**:69–89, 1951.
- [129] G. G. HALL. **The Molecular Orbital Theory of Chemical Valency. VIII. A Method of Calculating Ionization Potentials**. *Proc. Roy. Soc. Lon. A*, **205**:541–552, 1951.
- R. G. PARR AND W. YANG. *Density-Functional Theory of Atoms and Molecules*. Oxford University Press, New York, 1989.
- Ž. ČANČAREVIĆ. *Prediction of not-yet-synthesized solids at extreme pressures, and the development of algorithms for local optimization on ab-initio level*. Phd-thesis, University of Stuttgart, Fakultät 3: Chemie, University of Stuttgart, Stuttgart, Germany, September 2006.
- R. MARTIN. *Electronic Structure. Basic Theory and Practical Methods*. Cambridge University Press, Cambridge, 2004.

## REFERENCES

- [133] A. D. BECKE. *Phys. Rev. A*, **38**:3098, 1988.
- [134] A. D. BECKE. **Density Functional thermochemistry. III The role of exact exchange.** *J. Chem. Phys.*, **98**:5648, 1993.
- [135] L. H. THOMAS. *Proc. Camb. Philos. Soc.*, **23**:542, 1927.
- [136] E. FERMI. *Z. Phys.*, **48**:73, 1928.
- [137] P. HOHENBERG AND W. KOHN. **Inhomogeneous electro gas.** *Phys. Rev. B*, **136**:864–871, 1964.
- [138] W. KOHN AND L. J. SHAM. **Self-consistent equation including exchange and correlation effects.** *Phys. Rev. A*, **140**:1133–1138, 1965.
- [139] R. DOVESI. **Total Energy and Related Properties.** In C. PISANI, editor, *Quantum-Mechanical Ab-initio Calculation of the Properties of Crystalline Materials*, **67** of *Lecture Notes in Chemistry*. Springer-Verlag, Berlin Heidelberg New York, 1996.
- [140] C. PISANI, editor. *Quantum-Mechanical Ab-initio Calculation of the Properties of Crystalline Materials*, **67** of *Lecture Notes in Chemistry*. Springer-Verlag, Berlin Heidelberg New York, 1996.
- [141] R. DOVESI, R. ORLANDO, B. CIVALLERI, C. ROETI, V. R. SAUNDERS, AND C. M. ZICOVICH-WILSON. **CRYSTAL: a computational tool for the ab-initio study of the electronic properties of crystals.** *Z. Kristallogr.*, **220**:571–573, 2005.
- [142] C. LEE, W. YANG, AND R. G. PARR. *Phys. Rev. B*, **37**:785–789, 1988.
- [143] P. J. STEPHENS, F. J. DEVLIN, C. F. CHABALOWSKI, AND M. J. FRISCH. *J. Phys. Chem.*, **98**:11623, 1994.
- [144] F. BACON. *Meditationes Sacrae*. <http://en.wikipedia.org/wiki/>, 1597.
- [145] R. HORST, P. M. PARDALOS, AND N. V. THOAI. *Introduction to Global Optimization, Second Edition*. Kluwer Academic Publishers, 2000.
- [146] D. A. PIERRE. *Optimization Theory with Applications*. Dover, New York, 1986.
- [147] K. HAMACHER AND W. WENZEL. *Phys. Rev. E*, **59**(1):938–941, 1999.
- [148] W. WENZEL AND K. HAMACHER. *Phys. Rev. Lett.*, **82**(15):3003–3007, 1999.
- [149] P. Y. PAPALAMBROS AND D. J. WILDE. *Principles of Optimal Design: Modeling and Computation*. Cambridge University Press., Cambridge, 2000.
- [150] A. NEUMAIER. **Complete Search in Continuous Global Optimization and Constraint Satisfaction.** In A. ISERLES, editor, *Acta Numerica 2004*, pages 271–369. Cambridge University Press., Cambridge, 2004.
- [151] S. BOYD AND L. VANDENBERGHE. *Convex Optimization*. Cambridge University Press., Cambridge, 2004.
- [152] J. C. SCHÖN, A. HANNEMANN, AND M. JANSEN. *J. Phys. Chem. B*, **108**:2210–2217, 2004.
- [153] Ž. ČANGAREVIĆ, J. C. SCHÖN, AND M. JANSEN. *Progress in Materials Science and Processes (Mat. Sci. Forum)*, **453**:71–76, 2004.
- [154] K. DOLL, V. R. SAUNDERS, AND N. M. HARRISON. *Int. J. Quantum Chem.*, **82**:1–13, 2001.
- [155] K. DOLL. *Comput. Phys. Commun.*, **137**:74–88, 2001.
- [156] K. DOLL, R. DOVESI, AND R. ORLANDO. *Theor. Chem. Acc.*, **112**:394–402, 2004.
- [157] K. DOLL, R. DOVESI, AND R. ORLANDO. *Theor. Chem. Acc.*, **115**:354–360, 2006.
- [158] K. DOLL. *Mol. Phys.*, **108**:223–227, 2010.
- [159] R. A. BUCKINGHAM. *Proc. Roy. Soc. London A*, **168**:264, 1938.
- [160] M. BORN AND K. HUANG. *Dynamical Theory of Lattices*. Oxford University Press, London, 1954.
- [161] H. PUTZ, J. C. SCHÖN, AND M. JANSEN. *Comp. Mater. Sci.*, **11**:309–322, 1998.
- [162] H. PUTZ, J. C. SCHÖN, AND M. JANSEN. *Z. Anorg. Allg. Chem.*, **625**:1624–1630, 1999.
- [163] B. G. DICK AND A. W. OVERHAUSER. *Phys. Rev.*, **112**:90, 1958.
- [164] K. FISCHER, H. BLITZ, R. HABERNKORN, AND W. WEBER. *Phys. Status Solidi B*, **54**:285, 1972.
- [165] U. SCHRÖDER. *Solid State Commun.*, **4**:347, 1966.
- [166] V. NUSSLEIN AND U. SCHRÖDER. *Phys. Status Solidi B*, **21**:309, 1967.
- [167] R. G. GORDON AND Y. S. KIM. *J. Chem. Phys.*, **56**:3122, 1972.
- [168] A. J. COHEN AND R. G. GORDON. *Phys. Rev. B*, **14**:4593–4605, 1976.
- [169] C. MUHLHAUSER AND R. GORDON. *Phys. Rev. B*, **23**:900, 1981.
- [170] C. MUHLHAUSER AND R. GORDON. *Phys. Rev. B*, **24**:2147, 1981.
- [171] L. L. BOYER, M. J. MEHL, J. L. FELDMAN, J. R. HARDY, J. W. FLOCKEN, AND C. Y. FONG. **Beyond the rigid ion approximation with spherically symmetric ions.** *Phys. Rev. Lett.*, **54**:1940–1943, 1985.
- [172] M. J. MEHL, R. J. HEMLEY, AND L. L. BOYER. **Potential induced breathing model for the elastic moduli and high-pressure behaviour of the cubic alkaline-earth oxides.** *Phys. Rev. B*, **33**:8685–8696, 1986.
- [173] G. H. WOLF AND M. S. T. BUKOWINSKI. *Phys. Chem. Min.*, **15**:209–220, 1988.
- [174] M. D. JACKSON AND R. G. GORDON. *Phys. Chem. Min.*, **16**:212–220, 1988.
- [175] O. V. IVANOV AND E. G. MAKSIMOV. *Phys. Rev. Lett.*, **69**:108–111, 1992.

## REFERENCES

- [176] D. J. LACKS AND R. G. GORDON. **Crystal structure calculations with distorted ions.** *Phys. Rev. B*, **48**:2889–2908, 1993.
- [177] H. T. STOKES, L. L. BOYER, AND M. J. MEHL. **Spherical self-consistent atomic deformation model for first-principles energy calculations in ionic crystalline solids.** *Phys. Rev. B*, **54**:7729–7739, 1996.
- [178] L. L. BOYER, H. T. STOKES, AND M. J. MEHL. **Application of a Kohn-Sham like formulation of the self-consistent atomic deformation model.** *Ferroelec.*, **194**:1173–186, 1997.
- [179] R. E. COHEN. **First-principles theory of crystalline SiO<sub>2</sub>.** In P. J. HEANEY, C. T. PREWITT, AND G. V. GIBBS, editors, *MSA Reviews in Mineralogy; Silica: Physical Behavior, Geochemistry, and Materials Applications*, **29**, pages 369–402. Mineralogical Society of America, Washington, D.C., 1994.
- [180] L. STIXRUDE, R. E. COHEN, AND R. J. HEMLEY. **Theory of minerals at high pressures.** In R. J. HEMLEY, editor, *MSA Reviews in Mineralogy; Ultrahigh-Pressure Mineralogy*, **37**, pages 639–671. Mineralogical Society of America, Washington, D.C., 1998.
- [181] B. B. KARKI, L. STIXRUDE, AND R. M. WENTZCOVITCH. **High-pressure elastic properties of major materials of earth’s mantle from first principles.** *Reviews of Geophysics*, **39**:507–534, 2001.
- [182] S. W. DELEEUEW, J. W. PERRAM, AND E. R. SMITH. *Proc. Roy. Soc. A*, **373**:27–56;57–66, 1980.
- [183] B. CICHOCKI, B. U. FELDERHOF, AND K. HINSEN. **Electrostatic interactions in periodic Coulomb and dipolar systems.** *Phys. Rev. A*, **39**:5350–5358, 1989.
- [184] J. PILLARDY, R. J. WAWAK, Y. A. ARNAUTOVA, C. CZAPLEWSKI, AND H. A. SCHERAGA. **Crystal Structure Prediction by Global Optimization as a Tool for Evaluating Potentials: Role of the Dipole Moment Correction Term in Successful Predictions.** *J. Am. Chem. Soc.*, **122**:907–921, 2000.
- [185] W. A. HARRISON. *Electronic Structure and the Properties of Solids*. W. H. Freeman and Co., San Francisco, 1980.
- [186] J. EMSLEY. *The Elements*. Clarendon Press, Oxford, 1992.
- [187] J. A. POPLE AND R. K. NESBET. *Journal of Chemical Physics*, **22**:571, 1954.
- [188] M. D. TOWLER. **An introductory guide to Gaussian basis sets in solid-state electronic structure calculations.** European Summer School, Ab initio modeling in solid state chemistry, Torino, Italy, 2000.
- [189] V. R. SAUNDERS, R. DOVESI, C. ROETTI, M. CAUSA, N. M. HARRISON, R. ORLANDO, AND C. M. ZICOVICH-WILSON. *CRYSTAL2003*. Univ. Torino, Torino, 2003.
- [190] R. DOVESI, V. R. SAUNDERS, C. ROETTI, R. ORLANDO, C. M. ZICOVICH-WILSON, F. PASCALE, B. CIVALLERI, K. DOLL, N. M. HARRISON, I. J. BUSH, P. D’ARCO, AND M. LLUNELL. *Basis sets*. Univ. Torino, <http://www.crystal.unito.it/BasisSets/Ptable.html>, 2012.
- [191] R. DOVESI, V. R. SAUNDERS, C. ROETTI, R. ORLANDO, C. M. ZICOVICH-WILSON, F. PASCALE, B. CIVALLERI, K. DOLL, N. M. HARRISON, I. J. BUSH, P. D’ARCO, AND M. LLUNELL. *CRYSTAL09 User’s Manual*. Univ. Torino, Torino, 2009.
- [192] R. DOVESI, R. ORLANDO, B. CIVALLERI, C. ROETTI, V. R. SAUNDERS, AND C. M. ZICOVICH-WILSON. *Z. Kristallogr.*, **220**:571, 2005.
- [193] M. DOLG, K. A. PETERSON, P. SCHWERDTFEGER, AND H. STOLL. *Stuttgart/Köln (ab initio) Pseudopotentiale für Wellenfunktions- und Dichtefunktionalrechnungen*. Theoretical Chemistry (UNI Stuttgart), and University of Cologne, <http://www.tc.uni-koeln.de/PP/index.de.html>, 2012.
- [194] M. BURKATZKI, C. FILIPPI, AND M. DOLG. **Energy-consistent pseudopotentials for QMC calculations.** *J. Chem. Phys.*, **126**:234105, 2007.
- [195] M. BURKATZKI, C. FILIPPI, AND M. DOLG. **Energy-consistent small-core pseudopotentials for 3d-transition metals adapted to quantum Monte Carlo calculations.** *J. Chem. Phys.*, **129**:164115, 2008.
- [196] D. J. FELLER. *The Basis Set Exchange (BSE) software v.1.2.2 and the EMSL Basis Set Library*. <https://bse.pnl.gov/bse/portal>, 2012.
- [197] D. J. FELLER. **The Role of Databases in Support of Computational Chemistry Calculations.** *J. Comp. Chem.*, **17**(13):1571–1586, 1996.
- [198] K. L. SCHUCHARDT, B. T. DIDIER, T. ELSETHAGEN, L. SUN, V. GURUMOORTHY, J. CHASE, J. LI, AND T. L. WINDUS. **Basis Set Exchange: A Community Database for Computational Sciences.** *J. Chem. Inf. Model*, **47**(3):1045–1052, 2007.
- [199] N. METROPOLIS, A. W. ROSENBLUTH, M. N. ROSENBLUTH, A. H. TELLER, AND E. TELLER. *J. Chem. Phys.*, **21**:1087–1092, 1953.
- [200] P. E. BLOECHL. **Projector augmented-wave method.** *Phys. Rev. B*, **50**:17953, 1994.
- [201] G. KRESSE AND J. HAFNER. **Ab initio molecular dynamics for liquid metals.** *Phys. Rev. B*, **47**:558, 1993.
- [202] R. Y. RUBINSTEIN AND D. P. KROESE. *Simulation and the Monte Carlo method*. Second Edition, John Wiley Sons, Inc., Hoboken, New Jersey, 2008.
- [203] D. P. LANDAU AND K. BINDER. *A Guide to Monte Carlo Simulations in Statistical Physics*. Third Edition, Cambridge University Press, Cambridge, <http://www.cambridge.org/gb/knowledge/>, 2009.
- [204] R. MOTWANI AND P. RAGHAVAN. *Randomized Algorithms*. Cambridge University Press., Cambridge, 1995.
- [205] J. D. GALE. *GULP 4.0*. Nanochemistry Research Institute, Department of Chemistry, Curtin University, Perth, Western Australia, <http://projects.ivec.org/gulp/>, 2012.
- [206] J. D. GALE. **GULP - a computer program for the symmetry adapted simulation of solids.** *JCS Faraday Trans.*, **93**:629, 1997.
- [207] J. D. GALE. **GULP: Capabilities and prospects.** *Z. Krist.*, **220**:552–554, 2005.

## REFERENCES

- [208] D. E. GOLDBERG. *Genetic Algorithms in Search, Optimization, and Machine Learning*. Addison-Wesley Publishing Company, Reading, M.A., 1989.
- [209] G. DUECK. *J. Comput. Phys.*, **104**:86–92, 1993.
- [210] P. SIBANI, J. C. SCHOEN, P. SALAMON, AND J. O. ANDERSSON. *Europhys. Lett.*, **22**:479–485, 1993.
- [211] P. SIBANI AND P. SCHRIVER. *Phys. Rev. B*, **49**:6667–6671, 1994.
- [212] P. SIBANI, R. VAN DER PAS, AND J. C. SCHOEN. *Comput. Phys. Commun.*, **116**:17–27, 1999.
- [213] D. SHEPPARD, R. TERRELL, AND G. HENKELMAN. *J. Chem. Phys.*, **128**:134106, 2008.
- [214] G. HENKELMAN, B. P. UBERUAGA, AND H. JONSSON. *J. Chem. Phys.*, **113**:9901, 2000.
- [215] H. JONSSON, G. MILLS, AND K. W. JACOBSEN. *Nudged Elastic Band Method for Finding Minimum Energy Paths of Transitions, in Classical and Quantum Dynamics in Condensed Phase Simulations*. Ed. B. J. Berne, G. Ciccotti and D. F. Coker, World Scientific, 1998.
- [216] G. HENKELMAN AND H. JONSSON. *J. Chem. Phys.*, **111**:7010, 1999.
- [217] J. KAESTNER AND P. SHERWOOD. *J. Chem. Phys.*, **128**:014106, 2008.
- [218] L. XU AND G. HENKELMAN. *J. Chem. Phys.*, **129**:114104, 2008.
- [219] W. TANG, E. SANVILLE, AND G. HENKELMAN. *J. Phys.: Condens. Matter*, **21**:084204, 2009.
- [220] W. E. W. REN AND E. VANDEN-ELJNDEN. *Phys. Rev. B*, **66**:052301, 2002.
- [221] L. MARAGLIANO, A. FISCHER, E. VANDEN-ELJNDEN, AND G. CICCOTTI. *J. Chem. Phys.*, **125**:024106, 2006.
- [222] C. DELLAGO, P. BOLHUIS, F. S. CSAJKA, AND D. CHANDLER. *J. Chem. Phys.*, **108**:1964, 1998.
- [223] D. MORONI, P.G. BOLHUIS, AND T.S. VAN ERP. *J. Chem. Phys.*, **120**:4055, 2004.
- [224] F. NOE, D. KRACHTUS, J. C. SMITH, AND S. FISCHER. *J. Chem. Theory Comput.*, **2**:840, 2006.
- [225] R. A. OLSEN, G. J. KROES, G. HENKELMAN, A. ARNALDSSON, AND H. JONSSON. *J. Chem. Phys.*, **121**:9776, 2004.
- [226] G. HENKELMAN, G. JÄSHANNESSON, AND H. JONSSON. *Methods for Finding Saddle Points and Minimum Energy Paths, in Progress on Theoretical Chemistry and Physics*. Ed. S. D. Schwartz, Kluwer Academic Publishers, 2000.
- [227] R. HUNDT. KPL0T: A Program for Plotting and Investigation of Crystal Structures, 2010.
- [228] R. HUNDT, J. C. SCHÖN, A. HANNEMANN, AND M. JANSEN. *J. Appl. Cryst.*, **32**:413–416, 1999.
- [229] A. HANNEMANN, R. HUNDT, J. C. SCHÖN, AND M. JANSEN. *J. Appl. Cryst.*, **31**:922–928, 1998.
- [230] R. HUNDT, J. C. SCHÖN, AND M. JANSEN. **CMPZ - an algorithm for the efficient comparison of periodic structures**. *J. Appl. Cryst.*, **39**:6–16, 2006.
- [231] M. GIOVAGNOLI. *Angels in the workplace : stories and inspirations for creating a new world of work*. <http://en.wikiquote.org/wiki/>, 1999.
- [232] C. J. BRADLEY AND A. P. CRACKNELL. *The Mathematical Theory of Symmetry in Solids*. Clarendon Press, Oxford, UK, 1972.
- [233] E. R. TUFTE. *The Visual Display of Quantitative Information*. Graphic Press, 16th ed., Cheshire, Connecticut, USA, 1998.
- [234] E. R. TUFTE. *Beautiful evidence*. Graphic Press, 3rd ed., Cheshire, Connecticut, USA, 2010.
- [235] E. R. TUFTE. *Visual Explanations: Images and Quantities, Evidence and Narrative*. Graphic Press, 9th ed., Cheshire, Connecticut, USA, 2010.
- [236] N. TRINAJSTIC. *Chemical Graph Theory: Volume I*. CRC Press, Inc., Boca Raton, Florida, USA, 1983.
- [237] N. TRINAJSTIC. *Chemical Graph Theory: Volume II*. CRC Press, Inc., Boca Raton, Florida, USA, 1983.
- [238] N. TRINAJSTIC, S. NIKOLIC, J. V. KNOP, W. R. MULLER, AND K. SZYMANSKI. *Computational Chemical Graph Theory: Characterization, Enumeration, and Generation of Chemical Structures by Computer Methods*. Ellis Horwood Ltd, England, UK, 1991.
- [239] B. THALLER. *Visual Quantum Mechanics*. Springer-Verlag (<http://www.uni-graz.at/imawww/vqm/index.html>), New York, Heidelberg, 2000.
- [240] B. THALLER. *Advanced Visual Quantum Mechanics*. Springer-Verlag (<http://www.uni-graz.at/imawww/vqm/index.html>), New York, Heidelberg, 2004.
- [241] D. HEIDRICH, W. KLIESCH, AND W. QUAPP. *Properties of Chemically Interesting Potential Energy Landscapes*. Springer, Heidelberg, 1991.
- [242] K. PEARSON. **On lines and planes of closest fit to systems of points in space**. *Philosophical Magazine*, **2**:559–572, 1901.
- [243] J.C. GOWER. *Biometrika*, **53**:325, 1966.
- [244] H. ABDI AND L. J. WILLIAMS. **Principal component analysis**. *Wiley Interdisciplinary Reviews: Computational Statistics*, **2**:433–459, 2010.
- [245] I. T. JOLLIFFE. *Principal Component Analysis*. Springer Series in Statistics, 2nd ed, New York, 2002.
- [246] P. SIBANI K.H. HOFFMANN. *Phys. Rev. A*, **38**:4261, 1988.
- [247] J. C. SCHÖN, H. PUTZ, AND M. JANSEN. **Studying the energy hypersurface of continuous systems - the threshold algorithm**. *J. Phys.: Cond. Matt.*, **8**:143–156, 1996.
- [248] A. HEUER. *Phys. Rev. Lett.*, **78**:4051, 1997.

## REFERENCES

- [249] T. KOMATSUZAKI, K. HOSHINO, Y. MATSUNGA, G.J. RY-  
LANCE, R.L. JOHNSTON, AND D.J. WALES. *J. Chem. Phys.*,  
**122**:084714, 2005.
- [250] J.P.K. DOYE AND C.P. MASSEN. *Cond. Mat.*, **1**:0411144,  
2004.
- [251] M. A. C. WEVERS, J. C. SCHÖN, AND M. JANSEN. **Global  
aspects of the energy landscape of metastable crystal  
structures in ionic compounds.** *J. Phys.: Cond. Mat.*,  
**11**:6487–6499, 1999.
- [252] D. ZAGORAC, K. DOLL, J. C. SCHÖN, AND M. JANSEN. **Ab  
initio structure prediction for lead sulfide at standard  
and elevated pressures.** *Phys. Rev. B*, **84**:045206, 2011.
- [253] W. D. NESSE. *Introduction to Mineralogy*. Oxford Univer-  
sity Press, New York, 2000.
- [254] M. ALLABY. *A Dictionary of Earth Sciences*. Third Edi-  
tion, Oxford University Press, New York, 2008.
- [255] J. W. ANTHONY, R. A. BIDEAUX, K. W. BLADH,  
AND M. C. NICHOLS. *Handbook of Mineralogy*.  
Mineralogical Society of America, Chantilly, USA,  
<http://www.handbookofmineralogy.org/>, 2012.
- [256] <http://www.mindat.org/>.
- [257] X. LIU AND M. ZHANG. *Inter. J. Infra. Millim. Waves*,  
**21**:1697, 2000.
- [258] S. A. MCDONALD, G. KONSTANTATOS, S. ZHANG, P. W. CYR,  
E. J. D. KLEM, L. LEVINA, AND E. H. SARGENT. *Nature mat.*,  
**4**:138, 2005.
- [259] I. KANG AND F. W. WISE. *J. Opt. Soc. Am. B*, **14**:1632,  
1997.
- [260] A. G. EVERY AND A. K. MCCURDY. *Table 7.  
Cubic system. Binary compounds.* Nelson, D. F.  
(ed.). SpringerMaterials - The Landolt-Bornstein Database,  
<http://www.springermaterials.com>, 1992.
- [261] H. OVERHOF AND U. RÄUSSLER. *Phys. Stat. Sol.*, **37**:691,  
1970.
- [262] F. HERMAN, R. L. KORTUM, I. B. ORTENBURGER, AND  
J. P. VAN DYKE. *J. Phys. (Paris)*, **29**:c4, 1968.
- [263] M. MIAN, N. M. HARRISON, V. R. SAUNDERS, AND W. R.  
FLAVELL. *Chem. Phys. Lett.*, **257**:627, 1996.
- [264] G. U. VON OERTZEN, R. T. JONES, AND A. R. GERSON. *Phys.*  
*Chem. Minerals.*, **32**:255, 2005.
- [265] P.J. LIN AND K. KLEINMAN. *Phys. Rev.*, **142**:478, 1966.
- [266] R. L. BERNICK AND L. KLEINMAN. *Solid State Comm.*, **8**:569,  
1970.
- [267] M. LACH-HAB, D. A. PAPACONSTANTOPOULOS, AND M. J MEHL.  
*J. Phys. Chem. Sol.*, **63**:833, 2002.
- [268] S. RABII. *Phys. Rev.*, **167**:801, 1968.
- [269] S.-H. WEI AND A. ZUNGER. *Phys. Rev. B*, **55**:13605, 1997.
- [270] K. HUMMER, A. GRÄJNEIS, AND G. KRESSE. *Phys. Rev. B*,  
**75**:195211, 2007.
- [271] A. SVANE, N. E. CHRISTENSEN, M. CARDONA, A. N. CHAN-  
TIS, M. VAN SCHILFGAARDE, AND T. KOTANI. *Phys. Rev. B*,  
**81**:245120, 2010.
- [272] Y. NODA, K. MATSUMOTO, S. OHBA, Y. SAITO, K. TORIUMI,  
Y. IWATA, AND I. SHIBUYA. *Acta Crystallogr. C*, **43**:1443,  
1987.
- [273] S. S. KABALKINA, N. R. SEREBRYANAYA, AND L. F. VERESHCHA-  
GIN. *Sov. Phys., Solid State*, **10**:574, 1968.
- [274] A. N. MARIANO AND K. L. CHOPRA. *Appl. Phys. Lett.*,  
**10**:282, 1967.
- [275] T. K. CHATTOPADHYAY, H. G. VON SCHNERING, W. A.  
GROSSHANS, AND W. B. HOLZAPFEL. **High pressure X-ray  
diffraction study on the structural phase transitions  
in PbS, PbSe and PbTe with synchrotron radiation.**  
*Physica B and C*, **139**:356–360, 1986.
- [276] K. KNORR, L. EHM, B. WINKLER, AND W. DEPMEIER. *Eur.*  
*Phys. J. B*, **31**:297, 2003.
- [277] A. GRZECHNIK AND K. FRIESE. *J. Phys. Condens. Matter.*,  
**22**:095402, 2010.
- [278] S. I. SADOVNIKOV AND A. A. REMPEL. *Phys. Sol. Stat.*,  
**51**:2375, 2009.
- [279] S. I. SADOVNIKOV, N. S. KOZHEVNIKOVA, AND A. A. REMPEL.  
*Semiconductors*, **44**:1349, 2010.
- [280] W. KÜCHLE, M. DOLG, H. STOLL, AND H. PREUSS. *Mol. Phys.*,  
**74**:1245, 1991.
- [281] A. BERGNER, M. DOLG, W. KÜCHLE, H. STOLL, AND  
H. PREUSS. *Mol. Phys.*, **80**:1431, 1993.
- [282] K. DOLL, J. C. SCHÖN, AND M. JANSEN. *Phys. Chem. Chem.*  
*Phys.*, **9**:61281, 2007.
- [283] K. DOLL, J. C. SCHÖN, AND M. JANSEN. *Phys. Rev. B*,  
**78**:144110, 2008.
- [284] B. METZ, H. STOLL, AND M. DOLG. *J. Chem. Phys.*,  
**113**:2563, 2000.
- [285] M. M. ELCOMBE. *Proc. Roy. Soc. London, Ser. A*, **300**:210,  
1967.
- [286] A. H. ROMERO, M. CARDONA, R. K. KREMER, R. LAUCK,  
G. SIEGLE, J. SERRANO, AND X. C. GONZE. *Phys. Rev. B*,  
**78**:224302, 2008.
- [287] Y. ZHANG, X. KE, C. CHEN, J. YANG, AND P.R.C. KENT.  
*Phys. Rev. B*, **80**:024304, 2009.
- [288] A.V. MUDRING. *Eur. J. Inorg. Chem.*, **2007**:882, 2007.
- [289] R. P. LOWNDES AND C. H. PERRY. *J. Chem. Phys.*, **58**:271,  
1973.
- [290] G. ROUSSE, S. KLOTZ, A. M. SAITTA, J. RODRIGUEZ-CARVAJAL,  
M. I. McMAHON, B. COUZINET, AND M. MEZOUE. *Phys. Rev.*  
*B*, **71**:224116, 2005.
- [291] Y. S. PONOSOV, S. V. OVSYANNIKOV, S. V. STRELTSOV, V. V.  
SHCHENNIKOV, AND K. SYASSEN. *High Press. Res.*, **29**:224,  
2009.

## REFERENCES

- [292] S. V. OVSYANNIKOV, V. V. SHCHENNIKOV, A. Y. MANAKOV, A. Y. LIKHACHEVA, I. F. BERGER, A. I. ANCHAROV, AND M. A. SHEROMOV. *Phys. Stat. Sol. B*, **244**:279, 2007.
- [293] P. TOLEDANO, K. KNORR, L. EHM, AND W. DEPMEIER. *Phys. Rev. B*, **67**:144106, 2003.
- [294] S. V. STRELTSOV, A. Y. MANAKOV, A. P. VOKHMYANIN, S. V. OVSYANNIKOV, AND V. V. SHCHENNIKOV. *J. Phys.: Condens. Matter*, **21**:385501, 2009.
- [295] C. KAPFENBERGER, B. ALBERT, R. PÄÜTTGEN, AND H. HUPPERTZ. *Z. Kristallogr.*, **221**:477, 2006.
- [296] T. NONAKA, G. OHBAYASHI, Y. TORIUMI, Y. MORI, AND H. HASHIMOTO. *Thin Solid Films*, **370**:258, 2000.
- [297] J. Y. RATY, J. P. GASPARD, C. BICHARA, C. BERGMAN, R. BELLISSENT, AND R. CEOLIN. *Physica B*, **276**:473, 2000.
- [298] K. A. KHACHATURYAN. *Phys. Rev. B*, **36**:4222, 1987.
- [299] A. WALSH AND G. W. WATSON. *J. Sol. State Chem.*, **178**:1422, 2005.
- [300] D. V. SUETIN, I. R. SHEIN, AND A. L. IVANOVSKI. *J. Phys. Chem. Sol.*, **70**:64, 2009.
- [301] J. MACLEAN, P. D. HATTON, R. O. PILTZ, J. CRAIN, AND R. J. CERNIK. *Nucl. Instrum. Methods Phys. Res. B*, **97**:354, 1995.
- [302] J. MUSCAT AND C. KLAUBER. *Surf. Sci.*, **491**:226, 2001.
- [303] O. MADELUNG, U. RÄÜSSLER, AND M. SCHULZ. *Landolt-Börnstein, Semiconductors: Group IV Elements, IV-VI and III-IV Compounds, New Series, Group III, Vol. 41, Pt. A*. SpringerMaterials - The Landolt-Bornstein Database, Springer-Verlag, Berlin, 2005.
- [304] H. J. LIAN, A. YANG, M. L. W. THEWALT, R. LAUCK, AND M. CARDONA. *Phys. Rev. B*, **73**:233202, 2006.
- [305] A. M. JAMES AND M. P. LORD. *Macmillan's Chemical and Physical Data*. Macmillan, London, UK, 1992.
- [306] M. S. T. BUKOWINSKI AND J. AIDUN. *J. Geophys. Res.*, **90** (B2):1794–1800, 1985.
- [307] M. W. STOLTZFUS, P. M. WOODWARD, R. SESHADRI, J.-H. PARK-KLEPSIS, AND B. BURSTEN. *Inorg. Chem.*, **46**:3839–3850, 2007.
- [308] K. M. RABE AND J. D. JOANNOPOULOS. *Phys. Rev. B*, **36**:6631–6639, 1987.
- [309] B. CIVALLERI, P. D'ARCO, R. ORLANDO, V. R. SAUNDERS, AND R. DOVESI. *Chem. Phys. Lett.*, **348**:131–138, 2001.
- [310] F. PASCALE, C. M. ZICOVICH-WILSON, F. LÁŠPEZ-GEJO, B. CIVALLERI, R. ORLANDO, AND R. DOVESI. *J. Comput. Chem.*, **25**:888–897, 2004.
- [311] P. J. HAY AND W. R. WADT. *J. Chem. Phys.*, **82**:299–310, 1985.
- [312] S. PISKUNOV, E. HEIFETS, R. I. EGLITIS, AND G. BORSTEL. *Comp. Mat. Science*, **29**:165–178, 2004.
- [313] G. KALPANA, B. PALANIVEL, AND M. RAJAGOPALAN. *Phys. Rev. B*, **50**:12318–12325, 1994.
- [314] A. POURGHAZIA AND M. DADSETANI. *Physica B*, **370**:35–45, 2005.
- [315] K. C. MISHRA, K. H. JOHNSON, AND P. C. SCHMIDT. *Material. Sci. Eng. B*, **18**:214–219, 1993.
- [316] M. FERRERO, M. RERAT, R. ORLANDO, AND R. DOVESI I. J. BUSH. *J. of Phys.: Conf. Series*, **117**:012016, 2008.
- [317] K. MOMMA AND F. IZUMI. *J. Appl. Crystallogr.*, **41**:653, 2008.
- [318] P. CANEPA, R. M. HANSON, P. UGLIENGO, AND M. ALFREDSSON. *J. Appl. Cryst.*, **44**:225–229, 2011.
- [319] E. F. STEIGMEIER AND G. HARBEKE. *Sol. Stat. Comm.*, **8**:1275–1279, 1970.
- [320] P. FONS, A. V. KOBOLOV, M. KRBAL, J. TOMINAGA, K. S. ANDRIKOPOULOS, S. N. YANNOPOULOS, G. A. VOVIATZIS, AND T. URUGA. *Phys. Rev. B*, **82**:155209, 2010.
- [321] G.-S. DO, J. KIM, S.-H. JHI, C.-H. PARK, S. G. LOUIE, AND M. L. COHEN. *Phys. Rev. B*, **82**:054121, 2010.
- [322] EDS: H. BILZ, A. BUSSMANN-HOLDER, W. JANTSCH, AND P. VOGL. *Dynamical Properties of IV-VI Compounds*. Springer, Berlin, Heidelberg, New York, 1983.
- [323] G. GOKOGLU. *J. Phys. Chem. Solids*, **69**:2924–2927, 2008.
- [324] O. KILIAN, G. ALLAN, AND L. WIRTZ. *Phys. Rev. B*, **80**:024304, 2009.
- [325] R. SESHADRI. *Proc. Indian Acad. Sci. (Chem. Sci.)*, **113**:487–496, 2001.
- [326] U. V. WAGHMARE, N. A. SPALDIN, H. C. KANDPAL, AND R. SESHADRI. *Phys. Rev. B*, **67**:125111, 2003.
- [327] E. S. BOZIN, C. D. MALLIAKAS, P. SOUVATZIS, T. PROFFEN, N. A. SPALDIN, M. G. KANATZIDIS, AND S. J. L. BILLINGE. **Entropically Stabilized Local Dipole Formation in Lead Chalcogenides**. *Science*, **330**:1660–1663, 2010.
- [328] U. OZGUR, YA. I. ALIVOV, C. LIU, A. TEKE, M. A. RESHCHIKOV, S. DOGAN, V. AVRUTIN, S.-J. CHO, AND H. MORKOC. *J. Appl. Phys.*, **98**:041301, 2005.
- [329] A. HERNANDEZ-BATTEZ, R. GONZALEZ, J. L. VIESCA, J. E. FERNANDEZ, J. M. DÁDÁZ FERNANDEZ, A. MACHADO, R. CHOU, AND J. RIBA. *Wear*, **265**:422, 2008.
- [330] H. SAWADA, R. WANG, AND A. W. SLEIGHT. **An electron density residual study of zinc oxide**. *J. Solid State Chem.*, **122**:148–150, 1996.
- [331] T.-B. HUR, G. S. JEEN, Y.-H. HWANG, AND H.-K. KIM. **Photoluminescence of polycrystalline ZnO under different annealing conditions**. *J. Appl. Phys.*, **94**:5787–5791, 2003.
- [332] Z. ZHOU, K. KATO, T. KOMAKI, M. YOSHINO, H. YUKAWA, M. MORINAGA, AND K. MORITA. **Effects of dopants and hydrogen on the electrical conductivity of ZnO**. *J. Eur. Ceram. Soc.*, **24**:139–146, 2004.
- [333] I. V. MARKEVICH AND V. I. KUSHNIRENKO. **Photoluminescence of ZnO ceramics sintered with a flux**. *Sol. Stat. Com.*, **149**:866–868, 2009.

## REFERENCES

- [334] C. KLINGSHIRN. *ChemPhysChem*, **8**:782, 2007.
- [335] Y. W. HEO, D. P. NORTON, L. C. TIEN, Y. KWON, B. S. KANG, F. REN, S. J. PEARTON, AND J. R. LAROCHE. *Mater. Sci. Eng. R*, **47**:1, 2004.
- [336] A. RECNIK, N. DANEU, T. WALTHER, AND W. MADER. *J. Am. Ceram. Soc.*, **84**:2657, 2001.
- [337] C. R. A. CATLOW, S. A. FRENCH, A. A. SOKOL, A. A. AL-SUNALDI, AND S. M. WOODLEY. *J. Comput. Chem.*, **29**:2234, 2008.
- [338] P. ERHART, N. JUSLIN, O. GOY, K. NORDLUND, R. MULLER, AND K. ALBE. *J. Phys.: Condens. Matter*, **18**:6585, 2006.
- [339] A. J. KULKARNI, M. ZHOU, K. SARASAMAK, AND S. LIMPIJUNONG. *Phys. Rev. Lett.*, **97**:105502, 2006.
- [340] J. E. JAFFE, J. A. SNYDER, Z. LIN, AND A. C. HESS. *Phys. Rev. B*, **62**:1660, 2000.
- [341] B. PREDEL. *O-Zn (Oxygen-Zinc)*. O. Madelung, (ed.). SpringerMaterials - The Landolt-Bornstein Database, (<http://www.springermaterials.com>). DOI:10.1007/10542753\_2334, 2012.
- [342] H. SOWA AND H. AHSBAHS. *J. Appl. Cryst.*, **39**:169, 2006.
- [343] C. H. BATES, W. B. WHITE, AND R. ROY. *Science*, **137**:3534, 1962.
- [344] W. BRAGG AND J. A. DARBYSHIRE. *Trans. Farad. Soc.*, **28**:522, 1932.
- [345] T. KOGURE AND Y. BANDO. *J. Elec. Microscopy*, **47**:135, 1998.
- [346] S.-K KIM, S.-Y JEONG, AND C. R. CHO. *Appl Phys Lett*, **82**:562, 2003.
- [347] A. B. M. A. ASHRAFI, A. UETA, A. AVRAMESCU, H. KUMANO, I. SUEMUNE, Y. OK, AND T. SEONG. *Appl. Phys. Lett.*, **76**:550, 2000.
- [348] J. E. JAFFE AND A. C. HESS. **Hartree-Fock Study of Phase Changes in ZnO at High Pressure**. *Phys. Rev. B*, **48**:7903, 1993.
- [349] T. HOMANN, U. HOTJE, M. BINNEWIES, A. BORGER, K. D. BECKER, AND T. BREDOW. **Composition-dependent band gap in Zn<sub>S</sub>xSe<sub>1-x</sub>: a combined experimental and theoretical study**. *Sol. Stat. Sci.*, **8**:44-49, 2006.
- [350] M.D. TOWLER, N.L. ALLAN, N.M. HARRISON, V.R. SAUNDERS, W.C. MACKRODT, AND E. APRA. **An ab initio Hartree-Fock study of MnO and NiO**. *Phys. Rev. B*, **50**:5041-5054, 1994.
- [351] A.M. FERRARI AND C. PISANI. **An ab-initio periodic study of NiO supported at the Pd(100) surface: (A) the perfect epitaxial monolayer**. *J. Phys. Chem.*, **110**:7909, 2006.
- [352] S. MARDIX. **Polytypism: A controlled thermodynamic phenomenon**. *Phys. Rev. B*, **33**:8677-8684, 1986.
- [353] S. KOCH. **The associated occurrences of the three ZnS modifications in the Gyongyosoroszi**. *Acta Mineralogy. Petrog. Univ. Szegediensis*, **11**:11-22, 1958.
- [354] H. SCHULZ AND K.H. THIEMANN. **Structure parameters and polarity of the wurtzite type compounds SiC-2H and ZnO**. *Solid State Commun.*, **32**:783-785, 1979.
- [355] J-S. LEE, S-C. YU, S-F. TUNG, W-Ji BAI, J-S. YANG, Q-S FANG, AND Z. ZHANG. **The crystal structure of natural 33R moissanite from Tibet**. *Zeit. Kristallog.*, **221**:213-217, 2006.
- [356] S. HAUSSUEHL AND G. MUELLER. **Neue Zn S-Polytypen (9R, 12R und 21R) in mesozoischen Sedimenten NW-Deutschland**. *Beitraege zur Mineralogie und Petrographie*, **9**:28-39, 1963.
- [357] G.Y. CHAO AND R. A. GAULT. **The occurrence of two rare polytypes of wurtzite, 4H and 8H, at Mont Saint-Hilaire, Quebec**. *Canad. Mineralog.*, **36**:775-778, 1998.
- [358] N.N. GREENWOOD AND A. EARNSHAW. *Chemistry of the Elements 2nd ed*. Butterworth-Heinemann, Oxford, UK, 1997.
- [359] D.K. SMITH, C.F. CLINE, AND S.B. AUSTERMAN. **The crystal structure of  $\beta$  - beryllia**. *ActaCryst.*, **18** : 393, 1965.
- [360] J. C. SCHÖN. *Z. Allg. Anorg. Chem.*, **630**:2354-2366, 2004.
- [361] C.L. PUEYO ET AL. *Chem. Mater.*, **22**:4263, 2010.
- [362] C. TUSCHE, H.L.MEYERHEIM, AND J. KIRSCHNER. *Phys. Rev. Lett.*, **99**:026102, 2007.
- [363] S. IVANTCHEV, E. KROUMOVA, G. MADARIAGA, J. M. PEREZ-MATO, AND M. I. AROYO. **SUBGROUPGRAPH - a computer program for analysis of group-subgroup relations between space groups**. *J. Appl. Cryst.*, **33**:1190, 2000.
- [364] H. KARZEL, U. POTZEL, W. POTZEL, J. MOSER, C. SCHAEFER, M. STEINER, M. PETER, A. KRATZER, AND G. M. KALVIUS. *Mater. Sci. Forum*, **79**:419, 1991.
- [365] H. LIU, J. S. TSE, AND H.-K. MAO. *J. Appl. Phys.*, **100**:093509, 2006.
- [366] F. CLAEYSSSENS, C. L. FREEMAN, N. L. ALLAN, Y. SUN, M. N. R. ASHFOLD, AND J. H. HARDING. *J. Mater. Chem.*, **15**:139, 2005.
- [367] K. KIHARA AND G. DONNAY. *Canad. Mineral.*, **23**:647, 1985.
- [368] K. YOSHIO, A. ONODERA, H. SATOH, N. SAKAGAMI, AND H. YAMASHITA. *Ferroelectrics*, **264**:133, 2001.
- [369] J. C. SCHÖN, M. A. C. WEVERS, AND M. JANSEN. *J. Phys. A: Math. Gen.*, **34**:4041-4052, 2001.
- [370] S. NEELAMRAJU, J. C. SCHÖN, K. DOLL, AND M. JANSEN. *Phys. Chem. Chem. Phys.*, **14**:1223, 2012.
- [371] D. ZAGORAC, J. C. SCHÖN, I. V. PENTIN, AND M. JANSEN. **Structure prediction and energy landscape exploration in the zinc oxide system**. *Processing and Application of Ceramics*, **5**:73-78, 2011.
- [372] Ž. ČANČAREVIĆ, J. C. SCHÖN, AND M. JANSEN. *Chem Asian J.*, **3**:561, 2008.
- [373] H. WIEDEMEIER AND H. G. VON SCHNERING. *Zeit. fuer Kristallographie, Kristallgeometrie, Kristallphysik, Kristallchemie*, **148**:295, 1978.



## REFERENCES

- [374] T.K. CHATTOPADHYAY, J. PANNETIER, AND H.G. VON SCHNER-  
ING. *J. Phys. Chem. Sol.*, **47**:879, 1986.
- [375] M. DURANDURDU. *Phys. Rev. B*, **72**:144106, 2005.
- [376] K. A. PETERSON. *J. Chem. Phys.*, **119**:11099, 2003.
- [377] K. A. PETERSON, D. FIGGEN, E. GOLL, H. STOLL, AND  
M. DOLG. *J. Chem. Phys.*, **119**:11113, 2003.
- [378] J. LECIEJEWICZ. *Acta Cryst.*, **14**:1304, 1961.
- [379] J. PANNETIER AND G. DENES. *Acta Cryst. B*, **36**:2763, 1980.
- [380] P. BERASTEGUI AND S. HULL. *J. Sol. Stat. Chem.*, **150**:266,  
2000.
- [381] G. BALDINOZZI, J. M. RAULOT, AND V. PETRICEK. *Materials*  
*Research Society Symposia Proceedings*, **755**:465, 2003.
- [382] N.R. SEREBRANAJA, S.S. KABALKINA, AND L.F. VERESHCHA-  
GIN. *Doklady Akademii Nauk SSSR*, **187**:307, 1969.
- [383] T. LEININGER, A. BERNING, A. NICKLASS, H. STOLL, H.-J.  
WERNER, AND H.-J. FLAD. *Chem. Phys.*, **217**:19, 1997.
- [384] F R. NADA, C.R.A. CATLOW, C. PISANI, AND R. ORLANDO.  
**Ab initio Hartree-Fock perturbed-cluster study of neu-  
tral defects in LiF.** *Modelling. Simul. Mater. Sci. Eng.*,  
**1**:165–187, 1993.
- [385] <http://www.crystal.unito.it/>.
- [386] <http://www.crystalimpact.com/>.
- [387] A. KOKALJ. **Computer graphics and graphical user in-  
terfaces as tools in simulations of matter at the atomic  
scale.** *Com. Mat. Sci.*, **28**:155–168, 2003.
- [388] J. P. PERDEW, K. BURKE, AND M. ERNZERHOF. **Generalized  
gradient approximation made simple.** *Phys. Rev. Lett.*,  
**77**:3865–3868, 1996.
- [389] J. N. ZEMEL, J. D. JENSEN, AND R. B. SCHOOLAR. *Phys. Rev.*  
*A*, **140**:330, 1965.
- [390] O. MADELUNG, U. ROSSLER, AND M. SCHULZ. *Collabo-  
ration: Authors and editors of the volumes III/17E-  
17F-41C: Lead sulfide (PbS) optical properties, di-  
electric constants.* SpringerMaterials - The Landolt-  
Bornstein Database, (<http://www.springermaterials.com>).  
DOI: 10.1007/10681727\_81, 2012.
- [391] S. E. KOHN, P. Y. YU, Y. PETROFF, Y. R. SHEN, Y. TSANG,  
AND M. L. COHEN. *Phys. Rev. B*, **8**:1477, 1973.
- [392] N. M. RAVINDRA AND V. K. SRIVASTAVA. *Phys. Status Solidi*  
*A*, **58**:311, 1980.
- [393] T. HAHN (ED.). *International Tables for Crystallography*  
*Volume A: Space  $\hat{A}$  group symmetry.* Kluwer Academic  
Publisher, Dordrecht, Boston, London, 1989.
- [394] H. WONDRATSCHEK AND U. MULLER (ED.). *International*  
*Tables for Crystallography Volume A1: Symmetry re-  
lations between space groups.* First online edition,  
(<http://rd.springer.com/>), 2006.
- [395] H. WONDRATSCHEK AND U. MULLER (ED.). *International*  
*Tables for Crystallography Volume A1: Symmetry re-  
lations between space groups.* Second online edition,  
(<http://onlinelibrary.wiley.com/book>), 2011.
- [396] M. I. AROYO, A. KIROV, C. CAPILLAS, J. M. PEREZ-MATO,  
AND H. WONDRATSCHEK. **Bilbao Crystallographic Server**  
**II: Representations of crystallographic point groups**  
**and space groups.** *Acta Cryst. A*, **62**:115–128, 2006.

## REFERENCES

---

## Part VII

# Formalia



## **Declaration**

The work described in this thesis was carried out by the author in the Department of Prof. Jansen and in the Max Planck Institute for Solid State Research from December 2007 to June 2012. The contents are the original work of the author except where indicated otherwise and have not been previously submitted for any other degree or qualification at any academic institution.

Stuttgart, June 2012

Dejan Zagorac

## **Erklärung**

Die vorliegende Doktorarbeit wurde vom Autor selbst in der Abteilung von Prof. Jansen und am Max-Planck-Institut für Festkörperforschung, im Zeitraum von Dezember 2007 bis Juni 2012 angefertigt. Der Inhalt ist die eigene Arbeit des Autors, Ausnahmen sind gekennzeichnet, und wurde noch nicht zur Erlangung einer Qualifizierung oder eines Titels an einer akademischen Institution eingereicht.

Stuttgart, Juni 2012

Dejan Zagorac

---

## List of publications

1. D. Zagorac, K. Doll, J. C. Schön, and M. Jansen, “**Ab initio structure prediction for lead sulfide at standard and elevated pressures**”, *Phys. Rev. B* **84**, 045206 (2011).
2. D. Zagorac, J. C. Schön, K. Doll, and M. Jansen, “**Structure Prediction for PbS and ZnO at Different Pressures and Visualization of the Energy Landscape**”, *Acta Phys. Pol. A*, **120**, 2, (2011).
3. D. Zagorac, J. C. Schön, I. V. Pentin, and M. Jansen, “**Structure prediction and energy landscape exploration in the zinc oxide system**”, *Processing and Application of Ceramics*, **4**, 73 (2011).
4. D. Zagorac, K. Doll, J. C. Schön, and M. Jansen, “**Sterically active electron pairs in lead sulfide? An investigation of the electronic and vibrational properties of PbS in the transition region between the rock salt and the  $\alpha$ -GeTe type modifications**”, *Chem. Eur. J.*- accepted (2012).
5. D. Zagorac, J. C. Schön, and M. Jansen, “**Energy landscape investigations using the prescribed path method in the ZnO system**”, *J. Phys. Chem. C*, submitted (2012).
6. D. Zagorac, J. C. Schön, J. Zagorac and M. Jansen, “**Ab initio structure prediction for zinc oxide at various pressures**”, *to be submitted* (2012).
7. D. Zagorac, J. C. Schön, and M. Jansen, “**Energy landscape visualizations and investigations using the threshold algorithm in the ZnO system**”, *to be submitted* (2012).
8. D. Zagorac, J. C. Schön, and M. Jansen, “**Structure prediction as a guide in synthesis planning: investigation of systems exhibiting the 5-5 structure type**”, *to be submitted* (2012).

---

## Curriculum vitae

### *Personal information*

Name: Dejan Zagorac  
Date of birth: 13/02/1979  
Place of birth: Sisak, Croatia  
Marital status: Married and father of two children  
Nationality: Serbian and Croatian



### *Education:*

1985 – 1991 Elementary school “Jure Kaštelan (25. Maj)” in Zagreb, Croatia  
1991 – 1993 Elementary school “Jovan Jovanović Zmaj” in Kovin, Serbia  
1993 – 1997 Gymnasium “Branko Radičević” in Kovin, Serbia. Graduation work in geography: “*Water resources of Vojvodina*”.  
10/1997 – 03/2007 Dipl.-Ing.-M.sc. in Geology, Department of mineral deposits research, Faculty of Mining and Geology; the University of Belgrade, Serbia  
Title of the thesis: “*Geological - economical estimate of coal deposit Kovin – accessible part*”  
12/2007 – 07/2012 Ph.D. research in the group of prof. Dr. Martin Jansen, Max-Planck Institute for Solid State Research, Stuttgart, Germany, and Ph.D. Degree from the Department of Chemistry, University of Stuttgart, Germany.  
Title of the thesis: “*Energy Landscape Investigations and Structure Prediction of Binary Solids*”

### *Lectures, Conferences and Workshops:*

07/01/2008 - 09/01/2008 Workshop “*Magnetism in nanostructures and novel materials*”, IMPRS, Stuttgart, Germany.  
28/04/2008 - 02/05/2008 Conference “*Ringberg 2008*”, MPI-FKF, Ringberg, Germany, oral presentation: “*Energy landscape of ZnO*”.  
07/07/2008 - 08/07/2008 Workshop “*The physics of fluctuations*”, MPI-IS, Stuttgart, Germany.  
15/09/2008 - 19/09/2008 Workshop “*MSSC2008 – Ab initio Modelling in Solid State Chemistry*”, London, UK.  
30/08/2009 - 04/08/2009 Gordon research conference “*Solid State Chemistry – New frontiers in Materials, Synthesis and Characterization*”,

- 
- 06/11/2009 - 07/11/2009 Oxford, UK. Poster presented: "*Ab initio structure prediction for the PbS system at different pressures*".  
Symposium "*The Spectrum of Solid State Chemistry: From Basic Research to Application*", MPI-FKF, Stuttgart, Germany.
- 04/03/2010 - 06/03/2010 Workshop "*Hemdsärmelkolloquium 2010*", MPI-FKF, Stuttgart, Germany.
- 28/03/2010 - 01/04/2010 Conference "*Ringberg 2010*", MPI-FKF, Ringberg, Germany, oral presentation: "*Energy landscape investigation in PbS and ZnO system*".
- 23/06/2010 – 03/07/2010 Workshop "*Energy Landscapes 2010*", TU Chemnitz, Chemnitz, Germany. Oral presentation: "*Structure prediction and energy landscapes in solid state research*".
- 06/09/2010 – 10/09/2010 Conference "*YUCOMAT 2010*", MRS, Herceg Novi, Montenegro. Oral presentation: "*Structure Prediction for PbS and ZnO at Different Pressures and Visualization of the Energy Landscapes*".
- 15/03/2011 - 19/03/2011 Conference "*ICSCS-2011*", Serbian Ceramic Society, Belgrade, Serbia. Oral presentation: "*Structure prediction and energy landscape exploration in the zinc oxide system*".
- 25/07/2011 - 05/08/2011 Conference "*Exploring Energy Landscapes: From single molecules to mesoscopic models*", TSRC, Telluride, Colorado, USA. Oral presentation: "*Energy Landscape Investigation using the Prescribed Path Algorithm in the Zinc Oxide System*".
- 19/09/2011 - 22/09/2011 Workshop "Computer methods in crystal structure", MPI-FKF, Stuttgart, Germany.
- 01/01/2008 - 01/07/2012 Variety of specialized lectures organized by Max-Planck Institute and University of Stuttgart.